CONFERENCE SERIES

Contributions

16th Symposium on Atomic and Surface Physics and Related Topics (SASP 2008)

20.1. – 25.1.2008, Les Diablerets, Switzerland

Editors: R. D. Beck, M. Drabbels and T. R. Rizzo

innsbruck university press

CONFERENCE SERIES

Series Editors: K. Habitzel, T. D. Märk, S. Prock, B. Stehno

iup • innsbruck university press

www.uibk.ac.at/iup

innsbruck university press in Conference Series:
Series Editors: K. Habitzel, T. D. Märk, S. Prock, B. Stehno

Also available by *i*up in this series:

Contributions – 2nd International Conference on Proton Transfer Reaction
Mass Spectrometry and Its Applications, ISBN-10: 3-901249-78-8, ISBN-13: 978-3-901249-78-5
Editors: A. Hansel, T. D. Märk

41st Symposium on Theoretical Chemistry – Innsbruck, Austria September 5–7, 2005
ISBN-10: 3-901249-80-X, ISBN-13: 978-3-901249-80-8 – Editors: B. M. Rode, B. R. Randolf

Contributions – 15th Symposium on Atomic and Surface Physics and Related Topics
ISBN-10: 3-901249-82-6, ISBN-13: 978-3-901249-82-2 – Editors: V. Grill, T. D. Märk

Microlearning: Emerging Concepts, Practices and Technologies
Proceedings of Microlearning 2005: Learning & Working in New Media Environments
ISBN-10: 3-901249-83-4, ISBN-13: 978-3-901249-83-9 – Editors: T. Hug, M. Lindner, P. A. Bruck

Zukunftsplattform Obergurgl 2006:
Forschungsplattformen innerhalb der Leopold-Franzens-Universität Innsbruck
ISBN-10: 3-901249-86-9, ISBN-13: 978-3-901249-86-0 – Editors: M. Grumiller, T. D. Märk

Bildung schafft Zukunft
1. Innsbrucker Bildungstage, 17. – 18. November 2005
ISBN-10: 3-901249-87-7, ISBN-13: 978-3-901249-87-7 – Editor: Heidi Möller

Die Wiederentdeckung der Langsamkeit
Tagungsband zum gleichnamigen Symposion anlässlich des Tages der psychischen Gesundheit 2005
ISBN-10: 3-901249-88-5, ISBN-13: 978-3-901249-88-4 – Editors: Matthias A. Brüstle, Wolfgang Weber

Pangeo Austria 2006
ISBN-10: 3-901249-93-1, ISBN-13: 978-3-901249-93-8 – Editor: Monika Tessadri-Wackerle

Proceedings of the 7th International Workshop on Adjoint Applications in Dynamic Meteorology
ISBN-10: 3-901249-98-2, ISBN-13: 978-3-901249-98-3 – Editors: M. Ehrendorfer, R. M. Errico

Micromedia & e-Learning 2.0: Gaining the Big Picture
Proceedings of Microlearning Conference 2006
ISBN-10: 3-901249-99-0, ISBN-13: 978-3-901249-99-0 – Editors: T. Hug, M. Lindner, P. A. Bruck

Contributions – 3rd International Conference on Proton Transfer Reaction
Mass Spectrometry and Its Applications, ISBN-10: 3-902571-03-9, ISBN-13: 978-3-902571-03-8
Editors: A. Hansel, T. D. Märk

Micromedia and Corporate Learning
Proceedings of the 3rd International Microlearning 2007 Conference
ISBN: 978-3-902571-09-0 – Editors: M. Lindner, P. A. Bruck

Österreich, Spanien und die europäische Einheit – Austria, España y la unidad europea
ISBN: 978-3-902571-11-3 – Editors: P. Danler, K.-D. Ertler, W. Krömer, E. Pfeiffer, E. Rodrigues-Moura

XXV CILPR 2007 – Congrès International de Linguistique et de Philologie Romanes
Communications : Résumés
ISBN: 978-3-902571-15-1 – Editors: M. Iliescu, H. Siller-Runggaldier

Geomorphology for the Future
ISBN: 978-3-902571-18-2 – Editors: A. Kellerer-Pirklbauer, M. Keiler, Ch. Embleton-Hamann, J. Stötter

Zukunftsplattform Obergurgl 2007
Forschungskooperationen innerhalb der Leopold-Franzens-Universität Innsbruck
ISBN: 978-3-902571-21-2 – Editors: M. Grumiller, T. D. Märk

Competence development as workplace learning
ISBN: 978-3-902571-25-0 – Editors: L. Chisholm, H. Fennes, R. Spannring

innsbruck university press
Univ.-Prof. Dr. Dr.h.c.mult. Tilmann Märk
Universität Innsbruck
Christoph-Probst-Platz, Innrain 52
A-6020 Innsbruck
www.uibk.ac.at/iup

Book editors: R. D. Beck, M. Drabbels and T. R. Rizzo
Publishing staff: Carmen Drolshagen
Cover design: Carmen Drolshagen
Produced: Fred Steiner, Rinn – Book on Demand

ISBN: 978-3-902571-31-1

16th Symposium on Atomic and Surface Physics and Related Topics (SASP 2008)

Les Diablerets, Switzerland
20-25 January, 2008

Contributions

Editors:
Rainer D. Beck
Marcel Drabbels
Thomas R. Rizzo

Ecole Polytechnique Fédérale de Lausanne (EPFL)
Laboratoire de Chimie Physique Moléculaire
1015 Lausanne
Suisse

16th Symposium on Atomic and Surface Physics and Related Topics (SASP 2008)

Les Diablerets, Switzerland
20-25 January, 2008

International Scientific Committee:

Davide Bassi, Universita degli Studi di Trento
Tilmann D. Märk, Leopold Franzens Universität Innsbruck
Martin Quack, Eidgenössische Technische Hochschule Zürich
Thomas R. Rizzo, Ecole Polytechnique Fédérale de Lausanne

Local Organizing Committee:

Rainer D. Beck
Marcel Drabbels
Thomas R. Rizzo

Ecole Polytechnique Fédérale de Lausanne (EPFL)
Laboratoire de Chimie Physique Moléculaire (LCPM)

Sponsors:

Ecole Polytechnique Fédérale de Lausanne (EPFL)
Swiss Chemical Society (SCS)
Swiss National Science Foundations (SNSF)
Swiss Academy of Science (scnat)
Ciba, Merck-Serono, Novartis, Roche, Syngenta
DYNEOS AG, EKSPLA, Coherent
Newport - Spectra Physics
Extrel
Radiant Dyes
Pfeiffer Vacuum

We gratefully acknowledge the permission for the use of the cover photograph by the Tourist Office of Les Diablerets.

Foreword

In 1978, SASP was founded as a biennial winter conference by members of the Institute for Atomic Physics (formerly the Institute for Ion Physics, and since 2006 the Institute for Ion Physics and Applied Physics) of the Leopold Franzens University Innsbruck, Austria.

From the beginning, the format of SASP has been similar to that of a Gordon Conference, with invited lectures, poster presentations with ample time for discussion and indoor and outdoor activities. The attendance of the symposium has been kept to about 100 participants.

This international symposium seeks to promote the growth of scientific knowledge and effective exchange of information among scientists in the field of atomic, molecular, and surface physics. The symposium deals in particular with collisional interactions involving different types of collision partners, i.e. electrons, photons, molecules, clusters, and surfaces. A special emphasis of SASP 2008 will on the topics of gas-surface interactions, cold molecules and helium droplets, and bio-molecules. SASP conferences are usually held in Austria, but every other meeting may be held in another alpine country.

SASP conferences took place in the following locations:

1978	Zirog, I
1980	Maria Alm, A
1982	Maria Alm, A
1984	Maria Alm, A
1986	Obertraun, A
1988	La Plagne, F
1990	Obertraun, A
1992	Pampeago, I
1994	Maria Alm, A
1996	Engelberg, CH
1998	Going, A
2000	Folgaria, I
2002	Going, A
2004	La Thuile, I
2006	Obergurgl, A
2008	Les Diablerets, CH

SASP Erwin Schrödinger Gold Medal 2008

In 1992 the 'SASP Award for Outstanding Scientific Achievements' was initiated by the SASP International Scientific Committee. This award is granted each meeting to one or two scientists, who have made important contributions to SASP. In the past, the award was granted to:

1992	David Smith, Birmingham
1994	Herman Zdenek, Praha
1996	Werner Lindinger and Tilmann Märk, Innsbruck
1998	Eldon Ferguson, Boulder, and Chava Lifshitz, Jerusalem
2000	Jean H. Futrell, Richland
2002	Eugen Illenberger, Berlin
2004	Anna Giardini-Guidoni, Roma
2006	Davide Bassi, Trento, and Martin Quack, Zürich

The recipient of the SASP 2008 award – in form of the 'Erwin Schrödinger Gold Medal' designed by Zdenek Herman – will be:

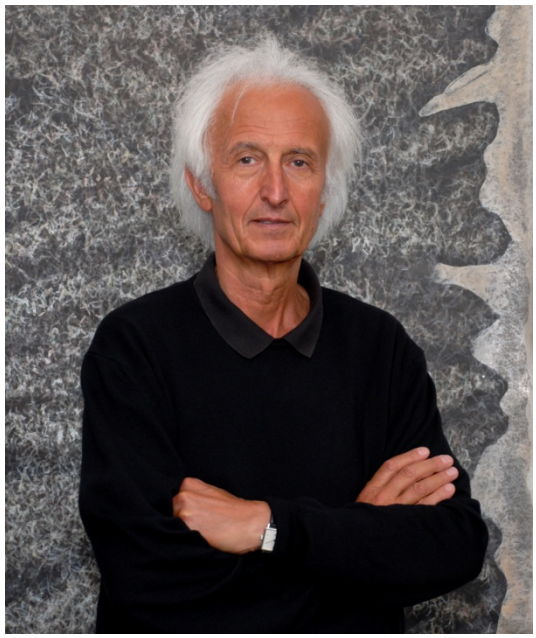

Helmut Schwarz, Berlin

Helmut Schwarz from TU Berlin, Germany, will receive the award for his exceptional achievements in the field of Mass Spectrometry, including fundamental contributions to the reaction dynamics of ions and gas phase catalysis, which are subjects that have been of key interest to SASP since its beginning. Helmut Schwarz also has had long-standing ties to SASP showing a continuous commitment to the goals of this conference.

Contents

Invited papers

Hot Topic Papers

Contributed papers

Poster session A

Contributed papers

Poster session B

Program SASP 2008

	Sunday January 20	Monday January 21	Tuesday January 22	Wednesday January 23	Thursday January 24	Friday January 25
7h00		Breakfast	Breakfast	Breakfast	Breakfast	Breakfast
8h30		Welcome				
8h45		Chair: Sibener	Chair: Rizzo	Chair: Märk	Chair: Ernst	Departure
9h00		Kroes	de Vries	Ptasińska	Neumark	
9h40		Sitz	Gabilica	Ingolfsson	Scheier	
10h20		Morris	Tsybin	Maier	Woell	
11h00		Price	Bald	Botschwina	Bisson	
11h20		Coffee break	Coffee break	Coffee break	Coffee break	
		Discussions	Discussions	Discussions	Discussions	
16h00	Registration	Coffee break	Coffee break	Coffee break	Coffee break	
16h15		Chair: Grant	Chair: Beck	Chair: Callegari	Chair: Schermann	
16h30		Meijer	Wodtke	Stienkemeier	Stearns	
17h10		Chandler	Hoefer	Halberstadt	Jouvet	
17h50		Wester	Saalfrank	Jaeger	Oomens	
18h30	Dinner	Even	Govers	Albert	Guyon	
19h00		Dinner	Dinner	Dinner	Conference Dinner	
20h30	Reception	Schrödinger Award (Chair: Quack)	Poster Session A	Poster Session B		

Invited papers

High dimensional dynamics studies of reaction of H_2 on Cu(111) and CH_4 on Ni(111): Symposium on Atomic, Cluster and Surface Physics

G.P. Krishnamohan, C. Díaz, R.A. Olsen, and G.J. Kroes
Leiden Institute of Chemistry, Gorlaeus Laboratories, P.O.Box 9502, 2300 RA Leiden, The Netherlands

New results will be presented on two paradigms of activated dissociative chemisorption: CH_4 + Ni(111) and H_2 + Cu(111).
A key question regarding CH_4 + Ni(111) concerns the role of excited molecular vibrational states: is the energy transfer among vibrational modes fast enough to make the reaction of the molecule statistical, as held in microcanonical unimolecular rate theory [1], or is the reaction mode-selective?
From experiments in which CH_4 is mode-selectively pre-excited it is now known that dissociative chemisorption of CH_4 on Ni is not a statistical process. Experiments on CH_4 + Ni(111) and Ni(100) have shown that the $1\nu_3$ excited antisymmetric C-H stretch state is significantly more effective at promoting reaction than the $3\nu_4$ excited bend state, even though $3\nu_4$ contains 30% more energy [2]. In an even more dramatic example, experiments on CH_4 + Ni(111) have shown that the $1\nu_1$ excited symmetric C-H stretch state is an order of magnitude more reactive than the $1\nu_3$ state, even though the $1\nu_3$ state contains more energy [3]. Before that, experiments on reaction of the isotopomer CH_2D_2 with Ni(100) had already shown that pre-excitation of the combination band ($\nu_1 + \nu_6$) containing one quantum each of symmetric and antisymmetric CH stretch vibration increases reactivity up to 5 times more than the antisymmetric stretch overtone ($2\nu_6$) [4].
Although experimentalists have speculated about the underlying reasons for vibrational mode-selectivity [2,3] of dissociative chemisorption of CH_4 on Ni surfaces, the actual underlying mechanisms remain unknown. From the present experiments it is also unknown how pre-excitation of the ν_2 symmetric bend mode (which is not infrared active) and of stretch-bend combination bands will affect the reactivity of CH_4. Our objectives are to provide answers to these questions by performing dynamics simulations.
We have performed density functional theory (DFT) calculations and normal mode analysis to model the energy flow among the methane vibrational energy states as the molecule adiabatically approaches a Ni(111) surface along the minimum energy reaction path. The model is in many ways similar to that used earlier by Halonen et al. [5], with, however, some crucial differences. Whereas the older work put restrictions on the approach orientation of methane and only modelled motion in the CH stretches, in our calculations we model all degrees of freedom of methane and put no restrictions on the orientation of the molecule. The energies of the vibrational states show avoided and non-avoided crossings, and an analysis of the change of the vibrational states along the reaction path allows one to assess whether these crossings should proceed mostly vibrationally adiabatically, or diabatically. This should provide insight in the vibrational mode-selectivity of the reaction. Results of the vibrational analysis will be presented at the meeting.
The H_2 + Cu(111) system is the most studied system in surface science. Many experimental measurements [6-10] and some theoretical calculations [11,12] have been carried out during the last

few decades, to determine the different dynamical parameters that play a role in this process. Experiments have been mainly focused on the different factors that influence the dissociative (associative) adsorption (desorption) of the molecule on (from) the surface, such as the molecule's initial translational energy or its initial quantum internal state. However rotationally inelastic and vibrationally inelastic scattering have also been studied in detail. From a theoretical point of view, some low and high dimensional calculations have been performed using analytical potential energy surfaces (PESs). But, as shown by us [12] these studies have been limited by the lack of an accurately fitted PES.

One goal of our research on H_2 + Cu(111) is to complete the picture regarding the applicability of the Born-Oppenheimer approximation to the scattering of H_2 from reactive metal surfaces. A concern for such studies is that the scattering (reactive or inelastic) may be accompanied by significant electron-hole pair excitation, and that the resulting dissipative energy loss would render results obtained with the Born-Oppenheimer approximation (which neglects electron-hole pair excitation) inaccurate. We have recently shown that calculations on H_2 + Pt(111) using a single PES could accurately describe both reaction and diffractive scattering [13]. This strongly suggests that the Born-Oppenheimer approximation allows an accurate description of reaction of hydrogen with metal surfaces. However, one could argue that the proof is incomplete to the extent that it has not yet been demonstrated that reaction as well as rotationally and vibrationally inelastic scattering can simultaneously be described accurately using a single PES, for a system with a significantly higher barrier (about 0.5 eV for H_2 + Cu(111)) than found for H_2 + Pt(111)) (0.06 eV). The H_2 + Cu(111) surface is ideally suited to answer this question. First of all, electron-hole pair excitation has been argued to be important to an accurate description of vibrationally inelastic scattering of H_2 from metal surfaces on the basis of calculations for the same system, H_2 + Cu(111), by Sitz and coworkers [14], though on the basis of a PES which fails to accurately describe vibrationally inelastic scattering in the adiabatic picture [12]. Secondly, as already mentioned, for H_2 + Cu(111) detailed experimental information is also available on rotationally [10] and vibrationally inelastic scattering [8]. It should be emphasized that the experimental information on reaction of H_2 on Cu(111) is also very detailed: the experiments of Hou et al. [6] effectively measure the simultaneous influence on the reaction of the molecule's orientation, its initial rovibrational state, and the collision energy.

We have already computed the 6D PES representing the electronic interaction for the system H_2/Cu(111). The ab initio data have been obtained using DFT with the use of the PW91 generalized gradient approximation [15] to take into account the exchange-correlation energy. The adsorbate/substrate system has been modeled using a four-layer slab and a 2x2 surface unit cell. The PES reproduces very well the main characteristics of the system, as the position (molecule on the bridge side) and the value (0.503 eV) of minimum reaction barrier, which are in excellent agreement with earlier DFT calculations [16].

The accuracy of our new PES has also been tested in a preliminary fashion through quasi-classical dynamics calculations. Quasi-classical calculations are very suitable to perform a quick test, because they are very 'cheap' from a computational point of view, and are expected to give a semi-quantitative description of activated reactions [17]. The dissociation probability and the rotational alignment as a function of the translational energy are shown in Figs. 1 and 2, respectively. From these two figures we see a good quantitative agreement between experiment and theory. The PES is currently being used in additional QCT and time-dependent wave packet calculations, results of which will be presented at the meeting.

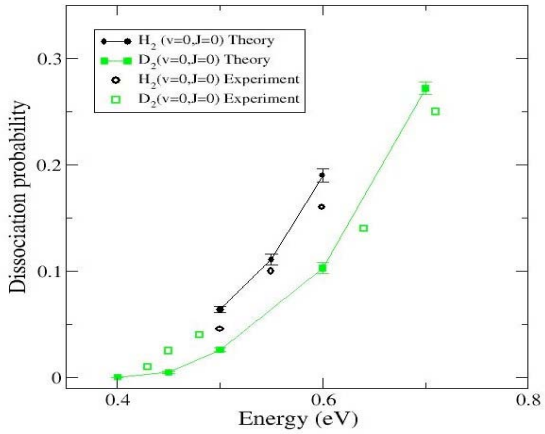

Figure 1: Dissociation probability as a function of the incidence translational energy. Black solid line with symbols: classical theoretical results for H_2; green solid line with symbols: classical theoretical results for D_2; black circles: experimental result for H_2 from [7]; green squares: experimental results for D_2 from [18].

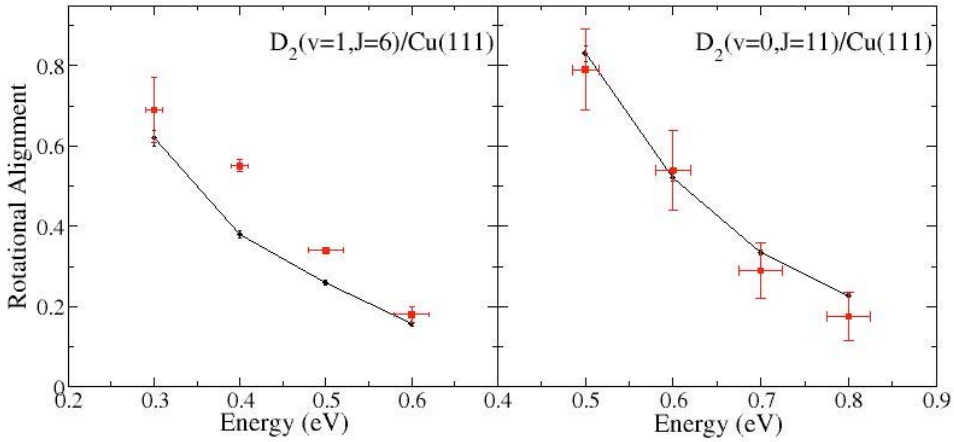

Figure 2: Rotational Alignment as a function of the incidence translational energy. Black solid line with symbols: classical theoretical results for H_2; Red squares: experimental results from [6].

[1] A. Bukoski and I. Harrison, J.Chem.Phys. **118**, 9762 (2003).

[2] L. B. F. Juurlink, P. R. McCabe, R. R. Smith, D. R. Killelea, and A. L. Utz, Phys.Rev.Lett. **94**, 208303 (2005).

[3] P. Maroni, D. C. Papageorgopoulos, M. Sacchi, T. T. Dang, R. D. Beck, and T. R. Rizzo, Phys. Rev. Lett. **94**, 246104 (2005).

[4] R. Beck, P. Maroni, D. C. Papageorgopoulos, T. T. Dang, M. P. Schmid, and T. R. Rizzo, Science **302**, 98 (2003).

[5] L. Halonen, S. L. Bernasek, and D. J. Nesbitt, J.Chem.Phys. **115**, 5611 (2001).

[6] H. Hou, S. J. Gulding, C. T. Rettner, A. M. Wodtke, and D. J. Auerbach, Science **277**, 80 (1997).

[7] C. T. Rettner, H. A. Michelsen, and D. J. Auerbach, J.Chem.Phys. **102**, 4625 (1995).

[8] C. T. Rettner, D. J. Auerbach, and H. A. Michelsen, Phys.Rev.Lett. **68**, 1164 (1992).
[9] C. T. Rettner, D. J. Auerbach, and H. A. Michelsen, Phys.Rev.Lett. **68**, 2547 (1992); A. Hodgson, J. Moryl, P. Traversaro, and H. Zhao, Nature **356**, 501 (1992).
[10] A. Hodgson, P. Samson, A. Wight, and C. Cottrell, Phys.Rev.Lett. **78**, 963 (1997).
[11] J. Dai and J. C. Light, J.Chem.Phys. **108**, 7816 (1998).
[12] S. Nave, D. Lemoine, M. F. Somers, S. M. Kingma, and G. J. Kroes, J.Chem.Phys. **122**, 214709 (2005).
[13] P. Nieto, E. Pijper, D. Barredo, G. Laurent, R. A. Olsen, E. J. Baerends, G. J. Kroes, and D. Farías, Science **312**, 86 (2006).
[14] A. C. Luntz, M. Persson, and G. O. Sitz, J.Chem.Phys. **124**, 091101 (2006).
[15] J. P. Perdew, J. A. Chevary, S. H. Vosko, K. A. Jackson, M. R. Pederson, D. J. Singh, and C. Fiolhais, Phys.Rev.B **46**, 6671 (1992).
[16] B. Hammer, M. Scheffler, K. W. Jacobsen, and J. K. Nørskov, Phys.Rev.Lett. **73**, 1400 (1994).
[17] G. J. Kroes and M. F. Somers, J. Theor.Comp.Chem. **4**, 493 (2005).
[18] H. A. Michelsen, C. T. Rettner, D. J. Auerbach, and R. N. Zare, J.Chem.Phys. **98**, 8294 (1993).

A comparison of the scattering of vibrationally excited H_2 and D_2 from copper and palladium surfaces.

A. Greg O. Sitz
Physics Department, The University of Texas at Austin

The interaction of hydrogen with metal surfaces is a paradigm for detailed studies of dissociative chemisorption [1, 2]. A key question is to what extent the internal degrees of freedom and translational energy of the molecules and the motions of the solid (both electronic and vibrational) have to be considered. We address such questions in our experiments by using nonlinear optical techniques to both prepare hydrogen molecules incident on a surface in selected internal states and to detect the scattered molecules in a quantum state specific manner. Results from studies of energy transfer between gas phase H_2 (D_2) and surface degrees-of-freedom are reported with an emphasis on phenomena which may be non-adiabatic, that is may involve surface *electronic* excitations, in origin. Recent experimental and theoretical work indicate that such non-adiabatic effects may be much more prevalent than has been previously thought. Current theoretical efforts are aimed at including non-adiabatic effects and need high quality data for comparison [3].

Specifically, measurements are reported comparing the reflectivity of Pd(111) and Cu(100) surfaces to vibrationally excited H_2 and D_2 molecules. Dissociation of hydrogen on Pd is not activated whereas on Cu there is an activation barrier of approximately 0.5 eV. This barrier is very nearly equal to the energy of one quanta of vibration in H_2. We report results of a search for dissociation of H_2(v=1) on Cu(100) using laser desorption to measure adsorbed hydrogen. We also report measurements of the translational energy loss accompanying collisions of H_2(v=1,J=1) with Cu(100) which are elastic with respect to the internal state; these results are difficult to interpret given the current knowledge of the H_2/Cu potential energy surface and the scattering dynamics.

[1] George R. Darling and Stephen Holloway. The dissociation of diatomic molecules at surfaces. *Report Prog. Phys.*, 58:1595–1672, 1995.

[2] Geert-Jan Kroes and M. F. Somers. Six-dimensional dynamics of dissociative chemisorption of H_2 on metal surfaces. *Journal of Theoretical & Computational Chemistry*, 4:493–581, 2005.

[3] A. C. Luntz and M. Persson. How adiabatic is activated adsorption/associative desorption. *J. Chem. Phys.*, 123:074704-01–074704-06, 2005.

Hydrogen Bonding Effects in the Dynamics of Polar Gases Colliding with Functionalized Organic Surfaces

William A. Alexander, Jessica Lu, Diego Troya, and John R. Morris
Department of Chemistry, Virginia Tech, Blacksburg Virginia, 24060

Molecular beam scattering experiments are used to explore how the structure, functionality, and hydrogen-bonding nature of an organic surface influence the dynamics of energy exchange in small molecule-surface collisions. Specifically, we explore collisions of 60 kJ/mol Ne, CD_4, ND_3, and D_2O with long-chain CH_3-, NH_2-, and OH-terminated self-assembled monolayers (SAMs). Time-of-flight measurements for the scattered gases reveal the extent of energy exchange and the propensity for each gas to thermally accommodate with the surface during a collision. Of the four gases studied, Ne transfers the least amount of translational energy into the monolayers. Neon atoms recoil from the OH-SAM with an average of 15±1 kJ/mol of energy, while D_2O retains only 6.5 ±1 kJ/mol of its 60 kJ/mol incident energy when scattering from the same surface. Overall, the trend in final translational energies follow the order Ne > CD_4 > ND_3 > D_2O for scattering from all three SAMs. The observed trend in the energy exchange is due to a combination of factors that include differences in the internal degrees of freedom and the gas-surface attractive forces. The thermal accommodation efficiencies of the four gases follow the opposite trend. Thermalization for the Ne atoms is nearly negligible for all three monolayers, whereas D_2O and ND_3 approach near complete accommodation on the OH- and NH_2-SAMs. Together, the results show that the extent of energy transfer depends on a balance between the rigidity of the surface, as affected by intra-surface hydrogen bonding, and the strength of the gas-surface attractive forces, as determined by dipole-dipole and dispersion interactions.

I. Introduction

The dissolution of gas phase molecules into a hydrocarbon liquid or the uptake of a vaporous species onto a solid organic surface depends on the physical and chemical properties of the interface that govern the motions of the molecules as they collide. Pioneering molecular beam scattering experiments by Saecker and Nathanson have provided detailed insight into the roles of gas-surface collision energy, dipole-dipole interactions, and surface free energy in determining the outcome of collisions of atomic and small polyatomic gases on liquid organic surfaces.[1] Their studies of Ne, CH_4, NH_3, and D_2O impinging on liquid glycerol and squalane show that the molecules recoil from the surfaces with energies that separate into two channels corresponding to impulsive scattering and trapping desorption. The final energy distributions of molecules that scatter impulsively from the surfaces of the two liquids are found to depend largely on the kinematics of the system. However, the extent of trapping

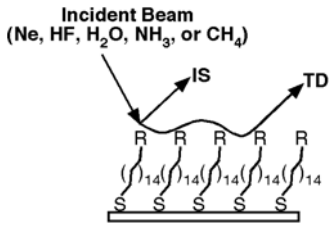

Figure 1. Schematic of our experimental objectives for scattering polar, nonpolar, and inert gases from SAMs where R = CH_3, OH, or NH_2.

on the surfaces depends markedly on the gas-surface attractive forces and the rigidity of the liquid. Overall, these studies have correlated the enthalpies and free energies of solvation with the final energy distributions of the gases to show that the "like dissolves like" principle can be used to predict the relative energy transfer and rate of approach to thermal equilibrium for gas-liquid collisions.[1] Our studies are designed to explore whether similar principles can be extended to understand the dynamics of gases colliding with solid organic materials where the interfacial region is more static, the microscopic structure is different, and the energetic degrees of freedom of the surface are altered significantly relative to those of a liquid.

The following studies examine collisions of the non-polar gases, Ne and CD_4, and polar gases, ND_3 and D_2O, with model organic surfaces composed of ω-functionalized alkanethiol self-assembled monolayers (SAMs) on gold. Alkanethiol SAMs on gold provide the opportunity to study gas-surface scattering dynamics on well-organized, atomically flat systems where the chemical groups of interest are located precisely at the gas-surface interface. Pure hydrocarbon surfaces are created by using long-chain CH_3-terminated SAMs and polar hydrogen-bonding groups are placed at the interface by employing NH_2 and OH-terminated SAMs.

II. Experimental

SAM preparation. The SAMs used in this study were prepared by spontaneous chemisorption of the alkanethiol of interest from a 1mM ethanolic solution onto a clean Au surface. For each monolayer, the clean gold slides were placed in the solutions for 48 hours, rinsed with copious amounts of ethanol, dried under a stream of ultrahigh purity nitrogen, and then immediately transferred to the main UHV chamber (base pressure < 5×10^{-10} Torr) via a load-lock system.

Molecular Beam Scattering. The experimental set-up has been described previously.[2] High-energy Ne, CD_4, and ND_3 beams are created by expanding ~2% mixtures of each gas in H_2 at approximately 700 Torr through a 0.05 mm diameter nozzle. After passing through a conical skimmer, the beam enters a differential pumping stage where it passes through a chopper wheel to provide 30 μs pulses. The peak energy of each beam was carefully tuned to 60 ± 1 kJ/mol (FWHM ~ 10 kJ/mol) by precisely controlling the mixing ratio.

The surface samples are aligned such that the normal is co-planar and at $\theta_i = 30°$ to the incident molecular beam. A fraction of the molecules that scatter from the surface is intercepted by a doubly differentially pumped mass spectrometer oriented at 60° to the incident beam such that $\theta_f = 30°$. The TOF distributions of each scattered gas are determined by monitoring the mass spectrometer signal at m/e = 20 as a function of time.

III. Results and Discussion

Figure 2 shows the final energy distributions, $P(E_f)$, for all four gases scattering from the OH-, NH_2-, and CH_3-terminated self-assembled monolayers. Within a two-channel model, the overall final energy distributions are a sum of a Boltzmann component (BC, dashed line) and an impulsive component (IC), with relative weighting, α, according to: $P(E_f) = \alpha P_{BC}(E_f) + (1-\alpha)P_{IC}(E_f)$.[1] For cases where the gas-surface potential energy well is sufficient to allow trapping after collision, α represents the trapping-desorption fraction. In addition to the BC fraction, the experimental data also reveals information about the fractional average energy transfer, $\langle \Delta E_f \rangle / E_i = (E_i - \langle E_f \rangle)/E_i$.

Neon Scattering. We find that the fractional energy transfer for Ne scattering from the CH_3-SAM is significantly greater than for the polar OH- and NH_2-SAMs. Previous experimental studies suggested that the hydrogen-bonding network that forms between alkane chains in polar protic SAMs creates a more rigid collision partner by restricting the types of low energy extended motions that facilitate energy transfer on non-hydrogen-bonding CH_3-SAMs.[2,3] The role of intra-monolayer hydrogen bonding in gas-surface collisions has also been explored through theoretical studies of Ar impinging on OH- and CH_3-SAMs.[4]

Methane Scattering. The overall dynamics governing CD_4 scattering from the CH_3-, NH_2-, and OH-SAMs mirror the dynamics for Ne scattering. The polar SAMs provide a more rigid collision partner than the non-polar SAM.[2,3] However, the overall energy transfer is much greater than for Ne scattering. In fact, the $P(E_f)$ distributions for scattering from each SAM display a maximum intensity close 2.5 kJ/mol, the peak of a Boltzmann distribution at the temperature of the surface. Potential energy calculations show that the CD_4-SAM energy minimum is approximately a factor of three deeper than the Ne-SAM potentials. The greater well leads to more efficient energy transfer and a significant amount of trapping, followed by thermal accommodation on the surfaces.

Ammonia and Water Scattering. The observed trends in the scattering dynamics for the polar gases, ND_3 and D_2O, are markedly different than the trends for Ne and CD_4. We find that nearly the entire $P(E_f)$ for the polar gases can be described by a Boltzmann distribution at the surface temperature. That is, very few molecules that collide with the CH_3, NH_2-, or OH-SAMs escape without first thermally equilibrating on the surface. For the NH_2- and OH-SAMs, the large thermal components are due to the significant attractive forces between the polar gases and the functional groups at the interface. It appears that the rigid nature of the intra-monolayer hydrogen-bonding network is countered by the strong attractive forces between the gas and the monolayer. Molecules that would otherwise skip impulsively off the rigid surfaces are instead

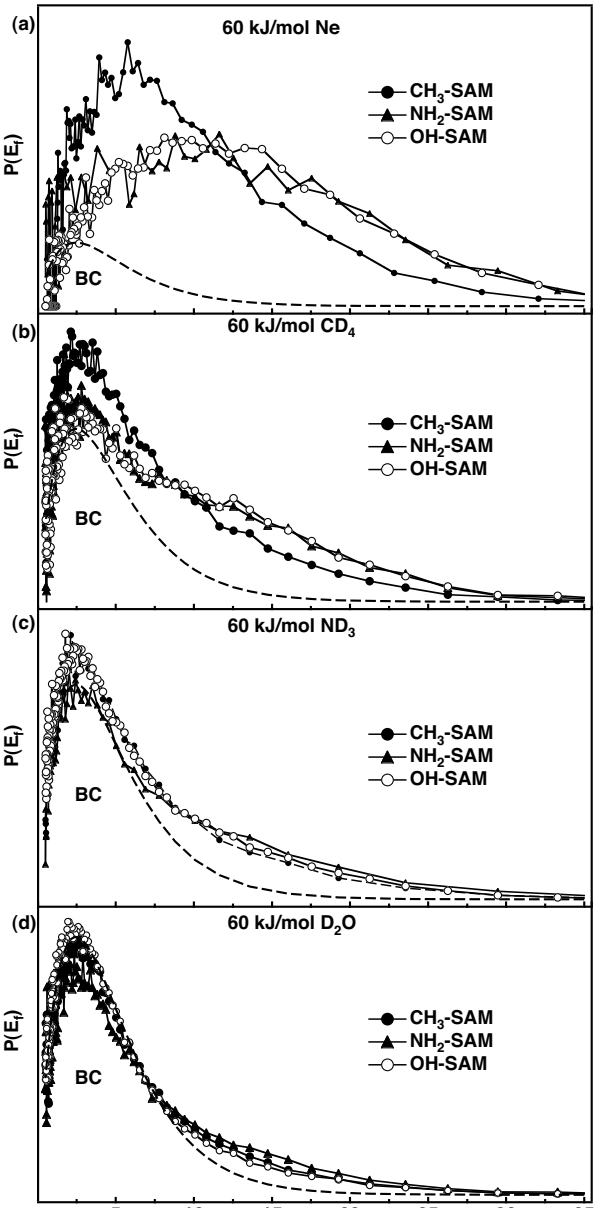

Figure 2. $P(E_f)$ distributions for (a) Ne, (b) CD_4, (c) ND_3, and (d) D_2O scattering from CH_3, NH_2, and OH-SAMs. The dashed line in each figure represents the best fit for a Boltzmann distribution to the OH-SAM data at the temperature of the surface.

pulled into the well, where they readily dissipate their remaining excess energy. Although attractive forces dominate the dynamics for the polar SAMs, the non-polar CH_3-SAM produces final energy distributions that are also composed primarily of low-energy molecules that appear thermal in nature. The relatively large BC intensity for ND_3 and D_2O scattering from the CH_3-SAM, as compared to the polar SAMs, is due to the flexible nature of the chains within this monolayer that serve as an excellent energy sink for facile dissipation of the translational energy of the impinging gases.

Our observed trends in the scattering dynamics are very similar to those for previous molecular beam experiments involving collisions on polar and non-polar liquid surfaces. Nathanson *et al.* reported that the final energy distributions for 55 kJ/mol NH_3 and D_2O scattering from liquid glycerol and squalane are both composed of large trapping-desorption components and that trapping is most likely for D_2O impinging on the polar liquid, glycerol.[1] Furthermore, their studies reveal that the opposite trend applies to the non-polar gases. Specifically, the high-energy impulsive channel is much more prominent in the final energy distributions for Ne and CH_4 scattering from the hydrogen-bonding glycerol liquid than for these gases scattering from the pure hydrocarbon liquid. Our results suggest that, for both SAMs and liquid surfaces, the interfacial hydrogen bonding network that can form between polar surface groups creates a more rigid or glassy surface and makes thermal accommodation and trapping less likely than for collisions on non-polar hydrocarbon surfaces.

IV. Summary

Molecular beam studies of the energy exchange and thermal accommodation efficiencies for Ne, CD_4, ND_3, and D_2O have been conducted to explore how polar and non-polar gases interact with hydrogen-bonding and pure hydrocarbon organic surfaces. These experiments enable direct comparisons to the dynamics of the same gases when they collide with liquids. Previous experiments that probed collisions of Ne, CH_4, NH_3, and D_2O with liquid glycerol, a hydrogen-bonding liquid, and squalane, a liquid hydrocarbon,[1] have revealed unique insight into the first steps of gas solvation into a liquid. The overall trends in the extent of energy exchange and the thermal accommodation fractions for the gas-liquid collisions are remarkably similar to the dynamics of the same gases scattering from the well ordered, densely packed self-assembled monolayers. The similarities suggest that the structure of an organic surface is not as important as the character of the interfacial functional groups in determining the overall dynamics. Furthermore, the comparison implies that SAMs may be a good model of liquid organic surfaces for exploring gas-surface collision dynamics.

V. Bibliography

[1] Saecker, M. E.; Nathanson, G. M., J. Chem. Phys. 99, 7056 (1993).
[2] Day, B. S.; Shuler, S. F.; Ducre, A.; Morris, J. R., J. Chem. Phys., 19, (15), 8084-8096 (2003).
[3] Ferguson, M. K.; Lohr, J. R.; Day, B. S.; Morris, J. R., Phys. Rev. Lett., 92, (7), 073201 (2004).
[4] Tasic', U. S.; Day, B. S.; Yan, T.; Morris, J. R.; Hase, W. L., J. Phys. Chem. B (2007).

Deceleration and trapping of neutral polar molecules

Gerard Meijer
Fritz-Haber-Institut der Max-Planck-Gesellschaft,
Faradayweg 4-6, D-14195 Berlin, Germany
e-mail: meijer @ fhi-berlin.mpg.de

Getting full control over both the internal and external degrees of freedom of molecules has been an important goal in molecular physics during the last decades. In this presentation I will detail the experimental approach that we have developed to produce samples of trapped neutral molecules. Arrays of time-varying, inhomogeneous electric fields are used to reduce in a stepwise fashion the forward velocity of molecules in a beam. With this so-called 'Stark decelerator', the equivalent of a linear accelerator for charged particles, one can transfer the high phase-space density that is present in the moving frame of a pulsed molecular beam to a reference frame at any desired velocity; molecular beams with a computer-controlled velocity and with a narrow velocity distribution, corresponding to sub-mK longitudinal temperatures, can be produced [1,2]. These decelerated beams offer new possibilities for collision studies, for instance, and enable spectroscopic studies with an improved spectral resolution; first proof-of-principle experiments have been performed [3,4]. These decelerated beams have also been used to load ND_3 molecules and OH radicals in an electrostatic trap at a density of 10^7 mol/cm^3 and at temperatures of around 50 mK [5,6]. Optical pumping of trapped neutral molecules due to blackbody radiation has been investigated [7], and trapping of molecules in vibrationally or electronically excited metastable states has been used to directly measure their radiative lifetimes [8]. Ground-state molecules have been trapped in AC electric field traps [9], decelerated molecular beams have been injected in a prototype molecular synchrotron [10], and, using micro-structured electrode arrays, a “decelerator on a chip” has been constructed and tested.

References:

[1] H.L. Bethlem, G. Berden, and G. Meijer, *Phys. Rev. Lett.* 83, (1999) 1558-1561.
[2] H.L. Bethlem and G. Meijer, *Int. Rev. Phys. Chem.* 22, (2003) 73-128.
[3] J.J. Gilijamse, S. Hoekstra, S.Y.T. van de Meerakker, G.C. Groenenboom, and G. Meijer, *Science* 313, (2006) 1617-1620.
[4] J. van Veldhoven, J. Küpper, H.L. Bethlem, B. Sartakov, A.J.A. van Roij, and G. Meijer, *Eur. Phys. J. D* 31, (2004) 337-349.
[5] H. L. Bethlem, G. Berden, F.M.H. Crompvoets, R.T. Jongma, A.J.A. van Roij and G. Meijer, *Nature* 406, (2000) 491-494.
[6] S.Y.T. van de Meerakker, P.H.M. Smeets, N. Vanhaecke, R.T. Jongma, and G. Meijer, *Phys. Rev. Lett.* 94, (2005) Artn. 023004.
[7] S. Hoekstra, J.J. Gilijamse, B. Sartakov, N. Vanhaecke, L. Scharfenberg, S.Y.T. van de Meerakker, and G. Meijer, *Phys. Rev. Lett.* 98, (2007) Artn. 133001.
[8] S.Y.T. van de Meerakker, N. Vanhaecke, M.P.J. van der Loo, G.C. Groenenboom, and G. Meijer, *Phys. Rev. Lett.* 95, (2005) Artn. 013003.
[9] J. van Veldhoven, H.L. Bethlem, and G. Meijer, *Phys. Rev. Lett.* 94, (2005) Artn. 083001.
[10] C.E. Heiner, D. Carty, G. Meijer, and H.L. Bethlem, *Nature Physics* 3, (2007) 115-118.

Production and Study of Ultra-cold Molecules Produced by Kinematic Cooling

David W. Chandler
Combustion Research Facility
Sandia National Laboratory
Livermore, CA 94551-0969
Email:chand@sandia.gov

The goal of this program is to develop new tools for the study of gas phase chemical dynamics and to use them to study the dynamics of fundamental collisional processes. The processes we have studied in the past include inter- and intra- molecular energy transfer, photodissociation dynamics and reactive scattering. The primary tool we use to study these processes has been Ion Imaging. Ion Imaging is a technique for the measurement of the velocity (speed and direction) of a laser-produced ion. As such it extends and enhances the sensitivity of Resonant Enhanced Multi-Photon Ionization (REMPI) detection of molecules and atoms. We have been using Ion Imaging to study a new method for the production of ultra-cold molecules, kinematic cooling. We continue to develop the kinematic cooling technique for the production of samples of ultra-cold molecules and their use in the study of collisional processes. We also are studying half collisions that are sensitive to the long range part of the potential energy surface by the study of photodissociation of small molecules and clusters near threshold. In the future we are extending the kinematic cooling technique to the trapping and cooling molecules in a Magneto Optical Trap (MOT) for the purpose of collisional studies.

Background and Recent Progress

The cooling of atoms to ultra-cold temperatures (microKelvin to nanoKelvin) has resulted in spectacular discoveries such as the realization and study of new states of matter that include Bose Einstein Condensates, Bardeen-Cooper-Schrieffer (BCS) gasses and degenerate Fermi gasses. The production of ultra-cold atoms has enabled ultra-high resolution spectroscopy studies leading to more precise atomic clocks, the most accurate determination of the energy of the highest bound vibrational levels in diatomic wells, along with such things as the development of gravity gradient detectors and the production of matter-wave lasers. All of these areas of research have molecular analogs that can be explored when methods for achieving molecules at ultra-cold temperatures are developed. Furthermore, the added complexity of molecules including, permanent dipoles and quadapole moments, complex rotational and vibrational structure and chemistry, offer rich areas of unexplored scientific investigation and possible new sorts of measurements (i.e. dipole moment of the electron and studies of quantum entanglement) and devices (i.e. quantum computers) in the future. All of these areas have remained unexplored due to the inability to routinely make ultra-cold samples of molecules. The cooling and trapping of molecules has proven more difficult than cooling and trapping of atoms because the electronic structure of even the simplest molecules renders laser cooling ineffectual. We have demonstrated a unique technique for formation of milli-Kelvin temperature molecules based on our own fundamental research in molecular collision dynamics.

My research focuses on the field of chemical dynamics of gas phase molecular species. Our interest is to study collisions at very low collision energies in an effort to learn about the long range potential between the atoms and molecules. At low energies the deBroglie wavelengths of the particles grow to be much larger than their hard-sphere collision

diameter and understanding the coupling between collision partners at long range is what we hope to uncover. These collisions are important for many practical reasons, for instance collisions that change the quantum state of a molecule, by a reorienting collision, can take a trapped molecule and allow it to escape a magnetic or electrostatic trap. Collisions that exchange translational energy but do not change internal quantum state of the molecules will contribute to the thermalization of a sample of molecules in a trap. Our immediate goal is to trap some of the cold molecules. We have demonstrated we are capable of producing and measuring their lifetime in a trap as a function of density and well depth of the trap. Here we report on the progress we have made toward this goal.

Our collisional cooling method does not rely on any specific physical property of either colliding species except their masses, because production of a zero velocity sample is a consequence of the experimentally selectable energy and momenta of the collision pair. Moreover, this technique can be used to prepare a single, selectable ro-vibronic quantum state for trapping. We first demonstrated this technique using inelastic collisions between NO molecules in one beam and Ar in the other, specifically $NO(^2\Pi_{1/2},j=0.5) + Ar \rightarrow NO(^2\Pi_{1/2},j'=7.5) + Ar$. Using the Ion Imaging technique for measuring the velocity distribution, we measured scattered $NO(^2\Pi_{1/2},j'=7.5)$ with a velocity distribution that is centered about zero, with an upper limit root-mean-square (rms) velocity of 15 m s^{-1}.

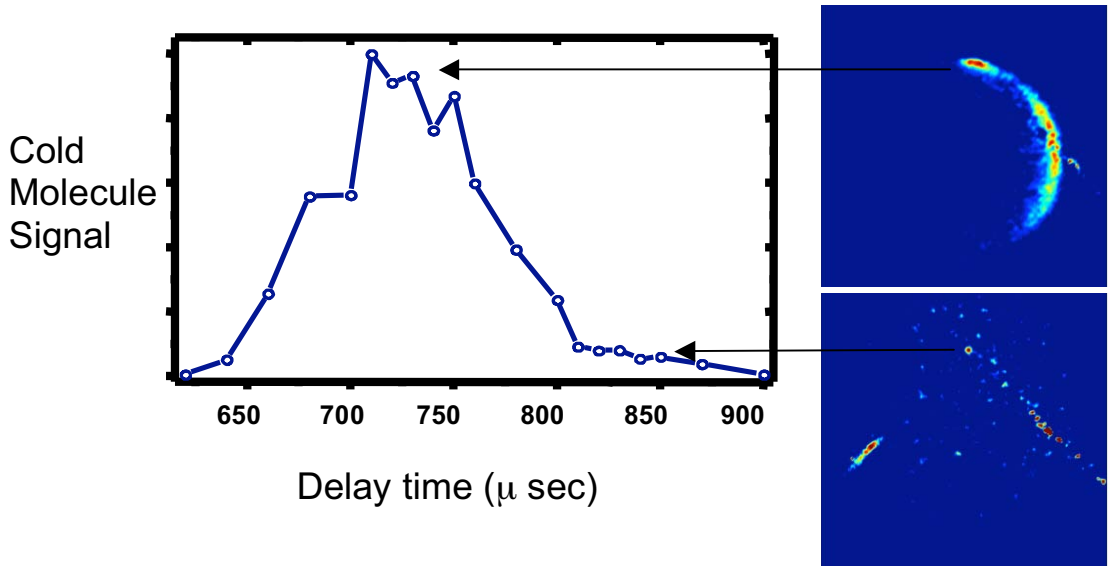

The largest hurdle to trapping molecules produced by this collisional cooling technique is that the molecule that are slowed are stopped (upper image Fig. 1) at the intersection of the two molecular beams. These slow molecules are then collided with and removed by the effusive molecular beam that follows the supersonic beam. We have worked hard to develop experimental condition such that the cold molecules are left in the wake of the atomic and molecular beams. In Figure 1 is shown a plot of the time evolution of the cold molecules as the 120 μsec long molecular beam collides with the atomic beam. We have now been able to have cold molecules live for longer than 100 microsecond after the beams have been turned off (lower image of Fig. 1). It should be now possible to trap these molecules. From measuring the "fly out" time of the ultra-cold molecules from the laser beams we estimate the mean velocity of the NO to be about 4.5 m/s corresponding to a temperature of roughly 40 milli-Kelvin.

In a separate group of experiments we are studying the near threshold dissociation of the NO-Ar complex. The NO-Ar cluster forms a T-shaped cluster with a well depth of about 88 cm^{-1}, which will dissociate when excited by light at slightly higher energy than the NO (A-X) transitions at 226 nm. The dissociation products are NO (A) and an Ar atom. In the past we[3], and others, have studied the rotational distribution obtained when this cluster is dissociated at several energies above the threshold for dissociation (44290 cm-1). In 1993 the group of Tsuji, Shibuya and Obi[4] published a paper where they state-selectively monitored the A state NO dissociation products by using resonant ionisation through the E state of NO. As the NO (A) state has a lifetime of about 80 nanoseconds it is possible to monitor the nascent distribution of NO formed in the dissociation by this resonant ionisation scheme. They reported observing broad resonances near threshold when monitoring the NO (A, J=0,1,2,3) states. A spectrum we recorded of these resonances is shown in Figure 2. These resonances were assigned to tunnelling resonances of the NO (A) state and a barrier to dissociation of approximately 25 cm^{-1} was postulated for the cluster at the NO (A) state asymptote. The problem is that if one does a simplified calculation of the tunnelling probability of an NO molecule through a 25 cm^{-1} high barrier 1 angstrom wide one finds the probability to be on the order of 10^{-14},corresponding to a lifetime of seconds, yet dissociation must take place on a nanosecond time scale for the products to be observed in the experiment. The nature of these resonances is what we wish to explore. We have measured action spectra, the recoil energy of the products, the alignment of the NO products and the time evolution of the products. In figure 2 are two images taken using resonant ionisation to select a particular state of the NO (A) product. They were taken with a 10 nanosecond time delay between the excitation laser and the probe (ionisation) laser.

Spectrum and Images of NO (A) recoil
after NO-Ar dissociation at 44316.5 cm^{-1}

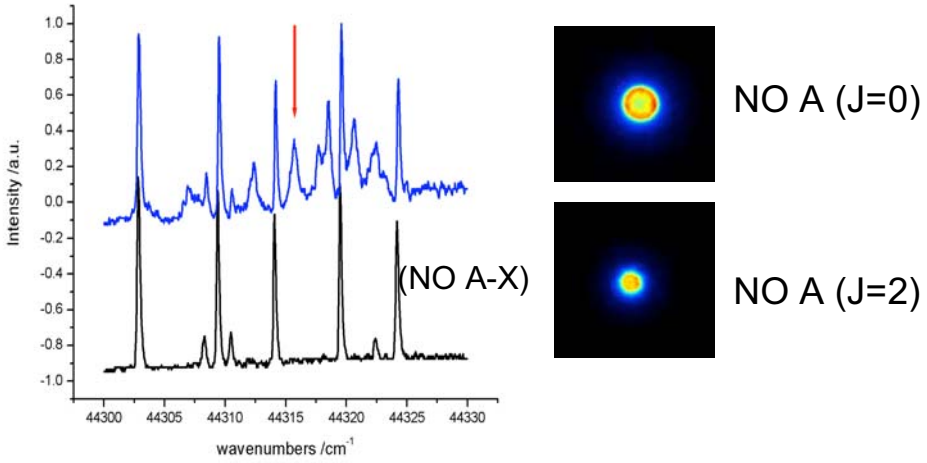

Imaging nucleophilic substitution dynamics

J. Mikosch, S. Trippel, R. Otto, C. Eichhorn, P. Hlavenka, M. Weidemüller, and R. Wester
Deptartment of Physics, University of Freiburg, Hermann-Herder-Str. 3, 79104 Freiburg, Germany

U. Lourderaj, J. X. Zhang, and W. L. Hase
Department of Chemistry and Biochemistry, Texas Tech University, Lubbock, TX 79409, USA

To study the quantum dynamics of molecular collisions and reactions, kinematically complete experiments with crossed molecular beams are an invaluable tool [1]. We extend such crossed-beam studies to slow ion-neutral collisions in order to unravel quantum scattering properties such as resonances and product branching ratios under the influence of the long-range ion-dipole interaction. One of the most important examples for this purpose is the class of nucleophilic substitution S_N2 reactions of negative ions, $X^- + RY \rightarrow RX + Y^-$ [2].

To carry out kinematically complete experiments on the reactions of slow ions with neutral targets, we have combined a crossed-beam imaging experiment with a source of low-energy ions. The reactant ions feature kinetic energies between 0.4 and 5 eV and 200 meV energy resolution (FWHM). This system allowed us to observe a transition in the charge transfer dynamics of Ar^+ with N_2 below 1 eV relative energy, represented by a switch to large-angle scattering [3]. Together with the observation of vibrationally excited

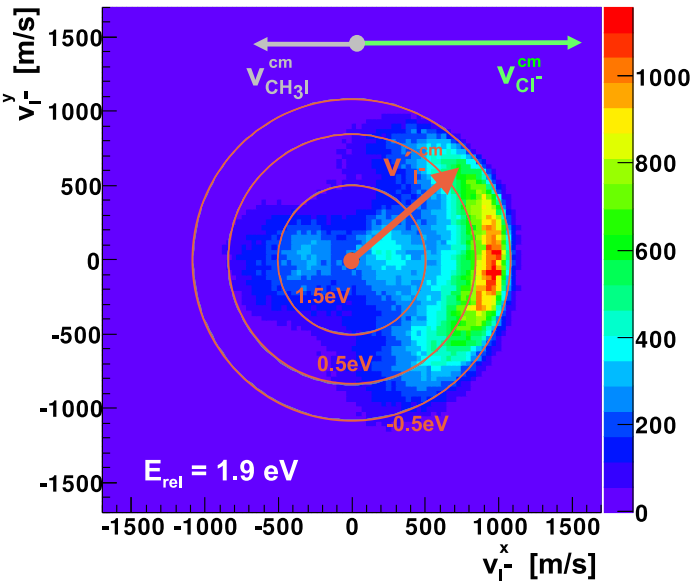

Figure 1: Contour plot of the differential cross section for $Cl^- + CH_3I$ at 1.9 eV relative collision energy

N_2^+ products, which is not expected from calculations [4], this may indicate the presence of a quantum scattering Feshbach resonance [5].

Here we report on experiments on the S_N2 reaction

$$Cl^- + CH_3I \longrightarrow ClCH_3 + I^-,$$

where we investigate the differential scattering cross section for this important class of reactions [6]. At collision energies between 1 and 5 eV we observe highly structured differential cross sections that change significantly with collision energy (see Figure). These data allow us to differentiate between several different reaction mechanisms. Above 1 eV collision energy the reaction proceeds predominantly by the classical co-linear S_N2 mechanism. At the lower collision energies of 0.4 eV, we observe a different mechanism, namely capture into a long-lived ion-dipole complex. These experimental results are compared with a statistical phase space model and with high-level direct dynamics trajectory calculations [7]. This comparison has revealed an unexpected "roundabout" mechanism, which involves a rotation of the CH_3I molecule and a different product energy partitioning [6].

In further experiments we are working towards bringing the reactant CH_3I molecule into a strong laser field to study reactions with laser-aligned molecules. In the future we will also use of the new ion-molecule crossed beam imaging system to study microsolvation effects in S_N2 reactions with anions embedded into water clusters.

[1] P. Casavecchia, Rep. Prog. Phys. 63, 355 (2000)

[2] M. L. Chabinyc, S. L. Craig, C. K. Regan, J. I. Brauman, Science 279, 1882 (1998)

[3] J. Mikosch, U. Frühling, S. Trippel, D. Schwalm, M. Weidemüller, and R. Wester, Phys. Chem. Chem. Phys. 8, 2990 (2006)

[4] R. Candori et al., J. Chem. Phys. 115, 8888 (2001)

[5] J. Mikosch, S. Trippel, R. Otto, C. Eichhorn, P. Hlavenka, M. Weidemüller, and R. Wester, J. Phys. Conf. Series, in press

[6] J. Mikosch, S. Trippel, C. Eichhorn, R. Otto, U. Lourderaj, J. X. Zhang, W. L. Hase, M. Weidemüller, and R. Wester, Science, accepted for publication

[7] U. Lourderaj, K. Song, T. L. Windus, Y. Zhuang, and W. L. Hase, J. Chem. Phys. 126, 044105 (2007)

DNA base clusters as models of prebiotic chemistry

Mattanjah S. de Vries
University of California, Santa Barbara, CA 93106, USA

From a chemical perspective one may define the origin of life as the synthesis of the first macromolecule with a replication scheme. For life, as we know it on earth, this macromolecule would have been an RNA molecule, according to prevailing current theories. Once such a replicating, or autocatalytic, macromolecule exists, evolution can be called on as the model for further development of life. One might postulate the formation of random polymers of which at some point those that could self-replicate survived. Today such synthesis is mediated by an extensive biochemical machinery, involving complex proteins and enzymes. Therefore a central question for any prebiotic scenario is how such synthesis could have taken place absent the current biological pathways. Furthermore other base pair schemes and even alternative backbones would be possible for the construction of self-replicating biopolymers. Therefore the question needs to be addressed whether there is anything in the possible prebiotic chemistry of the nucleobases that makes the outcome that we know today more likely, if not inevitable.

In order to study the fundamental properties of nucleobases without the contemporary biological environment we study them as *isolated* molecules, in the gas phase. We investigate their interactions by studying isolated clusters. We achieve this isolation by combining neutral laser desorption and jet cooling to form molecular beams of biomolecular building blocks and their clusters. We study the target molecules with a combination of double resonant laser spectroscopy and mass spectrometry, analyzed with the help of quantum chemical computations. We also investigate the possible role of water as a solvent by creating mass selected clusters with specific numbers of water molecules[1, 2].

We focus on two basic questions that govern fundamental nucleobase interactions:

(a) What are possible preferred structures that various heterocyclic compounds can form with each other? These compounds can adopt multiple tautomeric forms and a variety of hydrogen bonded and π stacked structures. Only a few very specific forms of the many possible structures make up today's critical biomolecules. The relative stabilities of these non-covalently bound structures must be investigated to asses the likelihood of different possible synthetic intermediates and products.

(b) How can excited state dynamics mitigate UV photochemical damage in nucleobase interactions? This question is motivated by the observation that most of the heterocyclic compounds that today are involved in replication are uniquely photochemically stable while other *derivatives of the same compounds* often are not. Yet more surprisingly, we have found many cases in which the biologically most relevant tautomeric form is UV stable, while other *tautomeric forms of the same compound* are not. We have even found that the Watson-Crick structure, adopted by the guanine-cytosine (GC) base pair in DNA, exhibits a self healing mechanism upon UV absorption, while other *structures of the same base pair* are vulnerable to UV radiative damage. These findings are very intriguing, because under prebiotic conditions there would have been no ozone layer in the atmosphere and thus UV photochemistry may have played a much more important role than is the case today.

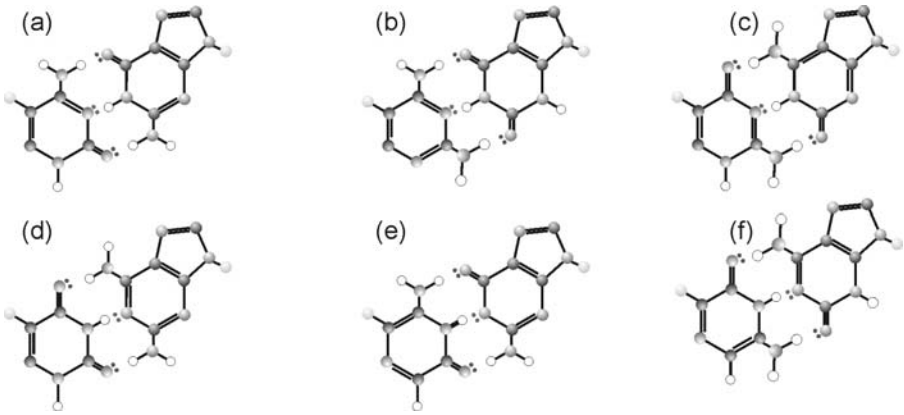

Figure 1 – 6 possible alternate base pair structures formed by an extended genetic lexicon, proposed by Yang et al. [3]. (a) GC Watson-Crick; (b) 2,4amino-perymidine-xanthine.

We focus on N-heterocyclic compounds, such as purines and pyrimidines. These compounds include, but are not limited to, the five nucleobases that make up life as we know it today, guanine (G), cytosine (C), adenine (A), thymine (T), and uracil (U). We also include variations and derivatives of these compounds, such as xanthine (X), hypoxanthine (HX) and various methyl, amino, and hydroxyl derivatives of all of these.

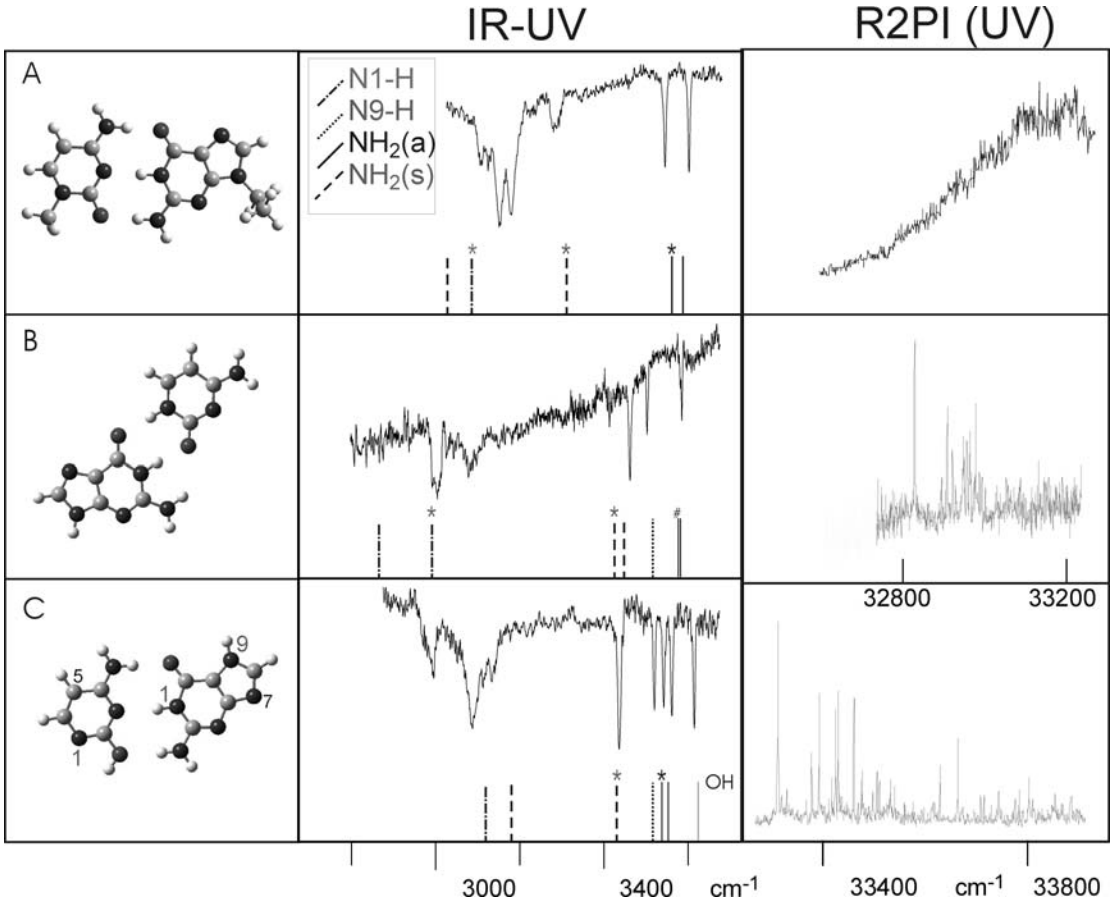

Figure 2: IR-UV double resonant and R2PI spectra of three guanine-cytosine cluster structures.

It is not at all obvious how in a richly diverse mixture of heterocyclic compounds the RNA and DNA bases would be selected to form the preferred building blocks of replicating macromolecules. Other nucleobase combinations could possibly have led to successfully replicating compounds. Figure 1 shows examples of alternate base pairs that adopt geometries identical to that of the canonical GC pair in the Watson-Crick (W-C) configuration in DNA, shown in Figure 1(a)[4]. A key question therefore for prebiotic chemistry is whether there are any chemical properties that we can identify that would make the canonical RNA and DNA bases stand out in early macromolecular synthesis, such as exceptional stabilities of specific structures.

Figure 2 shows data we obtained for three isolated GC base pair structures[5, 6]. Row A shows results for the Watson-Crick (WC) structure. Row B and C represent the second and third lowest energy structures, respectively. The second column shows the IR-UV double resonance data, compared with the *ab initio* calculations of the vibrational frequencies. The third column shows the UV excitation spectra, measured by resonant two-photon ionization (R2PI). The UV spectrum is broad for the WC structure (A) and exhibits sharp vibronic lines for the other structures.

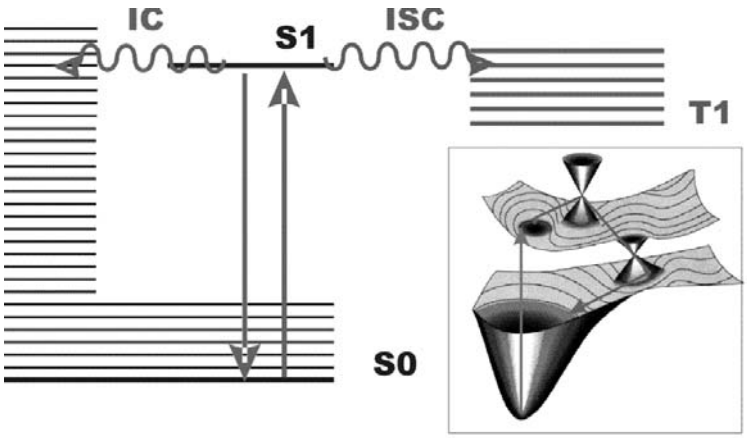

Figure 3: Jablonkski diagram, demonstrating competition between internal conversion (IC), intersystem crossing (ISC) and fluorescence. Rapid IC converts electronic excitation from UV absorption to heat in the electronic ground state (S0). Absent IC the excited electronic state (S1) or triplet state (T1) can lead to various chemical reactions. The inset shows a schematic model for rapid IC through conical intersections that couple S1 and S0, possibly via a third "doorway" state.

In the WC structure the excited state (S1) is coupled to the ground state (S0) by an intermediate state (of charge transfer character) via barrierless conical intersections[7]. For the other structures small differences in relative energies cause the existence of barriers that lead to discrete spectra and lifetimes that can be two orders of magnitude longer. The rapid internal conversion pathway indicated here for the WC structure provides it with significantly enhanced photochemical stability, absent in the other longer lived structures. This implies that structure specific excited state lifetimes may have affected the eventual chemical makeup of critical biomolecules.

.

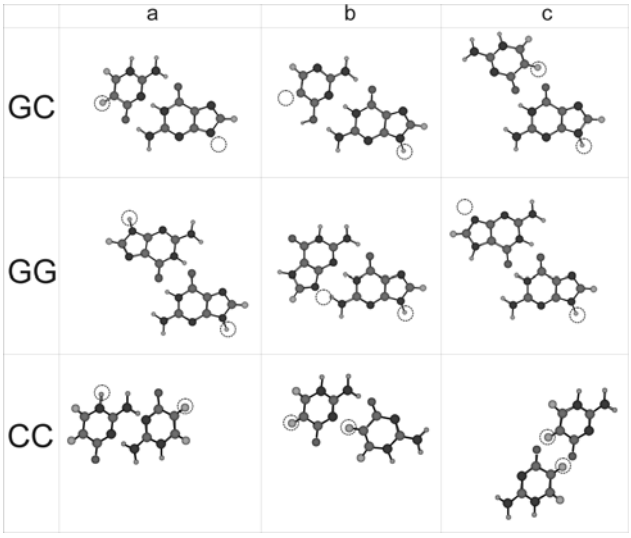

Figure 4: Low energy structures of GC, GG, and CC base pairs, according to *ab initio* calculations. The left most column, shaded in red, is the biologically relevant structure – Watson-Crick in the case of GC. Of these the GC structure has a broad UV spectrum and we have not observed the others in nanosecond R2PI experiments. The right hand two columns represent non-biological structures. We have observed all of these as sharp, structured UV spectra in R2PI experiments. Yellow circles indicate position of sugar in corresponding nucleosides.

The process of "self healing" by internal conversion, following UV absorption, shown schematically in Figure 3, appears to be quite general. All nucleobases involved in replication have short excited state lifetimes. This phenomenon is often even more subtle and specific. For example, for guanine the biologically most relevant tautomer (the 9H keto form) has a short lived excited state due to a conical intersection that does not affect other tautomers in the same way[8]. The same is true for specific isomers, such as adenine which is short lived while its non-biological structural isomer 2 aminopurine is not[9-12]. Figure 4 shows the example of base pair structures that appear to exhibit short lived excited states only in the biologically most relevant structure.

We will also report on results with alternate nucleobases and on clusters with water

1 M. S. de Vries and P. Hobza, Annual Review of Physical Chemistry **58**, 585 (2007).
2 R. Weinkauf, J. P. Schermann, M. S. de Vries, et al., European Physical Journal D **20**, 309 (2002).
3 Z. Y. Yang, D. Hutter, P. P. Sheng, et al., Nucleic Acids Research **34**, 6095 (2006).
4 S. A. Benner, C. Y. Switzer, J. D. Bain, et al., Abstracts of Papers of the American Chemical Society **203**, 67 (1992).
5 E. Nir, K. Kleinermanns, and M. S. de Vries, Nature **408**, 949 (2000).
6 A. Abo-Riziq, L. Grace, E. Nir, et al., Proceedings of the National Academy of Sciences of the United States of America **102**, 20 (2005).
7 A. L. Sobolewski, W. Domcke, and C. Hättig, PNAS **102**, 17903 (2005).
8 C. M. Marian, Journal of Physical Chemistry A **111**, 1545 (2007).
9 A. Broo, J.Phys. Chem. **A 102**, 526 (1998).
10 S. Perun, A. L. Sobolewski, and W. Domcke, Molecular Physics **104**, 1113 (2006).
11 K. A. Seefeld, C. Plutzer, D. Lowenich, et al., Physical Chemistry Chemical Physics **7**, 3021 (2005).
12 C. M. Marian, Journal of Chemical Physics **122**, 10 (2005).

Photodetachment and photodissociation mass spectrometry of DNA multiply charged ions

V. Gabelica, F. Rosu, E. De Pauw
Mass Spectrometry Laboratory, Department of Chemistry, University of Liège, Belgium

R. Antoine, T. Tabarin, M. Broyer, P. Dugourd
Laboratoire de Spectrométrie Ionique et Moléculaire, Université Lyon I et CNRS, France

We recently explored the effects of irradiating DNA polyanions stored in a quadrupole ion trap (QIT) mass spectrometer with an optical parametric oscillator (OPO) laser between 250 nm and 285 nm. We studied DNA 6-mer to 20-mer single strands, and 12-base pair double strands. In all cases, laser irradiation causes electron detachment from the multiply charged DNA anions (**Figure 1**). Electron photo-detachment efficiency directly depends on the number of guanines in the strand, and maximum efficiency is observed between 260 and 275 nm. Collisional activation of the radical anions results in extensive fragmentation, which can be used to sequence the DNA strands. It has therefore important potential applications in analytical chemistry [1].

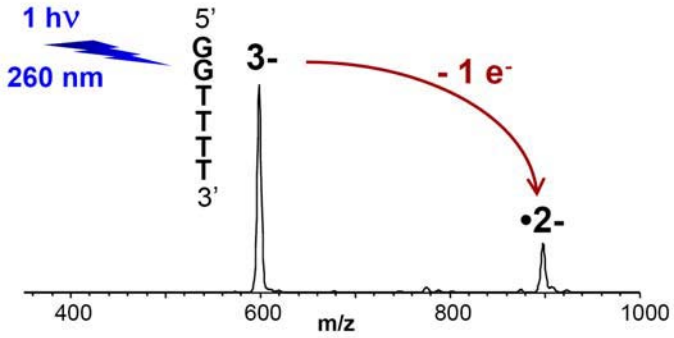

Figure 1: Example of electron photodetachment mass spectrum.

We will discuss the electron photodetachment mechanism (**Figure 2**). Electron photodetachment at 260 nm (4.77 eV) is a one-photon process. It is likely very fast, given that it is able to compete with internal conversion and/or radiative relaxation to the ground state. The DNA $[6\text{-mer}]^{3-}$ ions show a marked sequence-dependence of electron photodetachment yield [2]. Remarkably, the photodetachment yield ($dG_6 > dA_6 > dC_6 > dT_6$) is inversely correlated with the base ionization potentials (G < A < C < T). Sequences with guanine runs show increased photodetachment yield as the number of guanine increases, in line with the fact that positive holes are the most stable in guanine runs. This correlation between photodetachment yield and the stability of the base radical may be explained by tunneling of the electron through the repulsive Coulomb barrier. The calculations and the wavelength dependence suggest that the electron photodetachment is initiated at the bases and not at the phosphates. This also indicates that, although direct photodetachment could also occur, autodetachment from excited states, presumably corresponding to base excitation, is the dominant process at 260 nm.

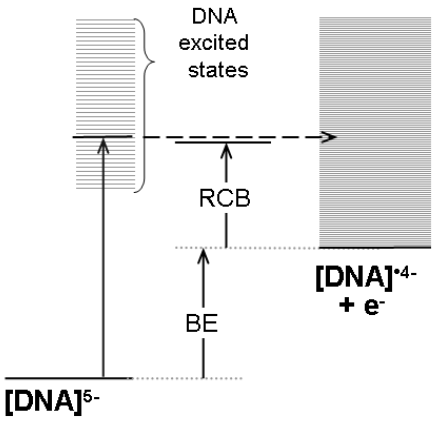

Figure 2: Photodetachment mechanism proposed for DNA excited around 260 nm. Slight changes in electron binding energy (BE) result in large changes in photodetachment efficiency because of the repulsive Coulomb barrier (RCB).

The wavelength-dependence of electron detachment yield was studied for dG_6^{3-}. Maximum electron photodetachment is observed in the wavelength range corresponding to base absorption (260-270 nm) [2]. This demonstrated the feasibility of gas-phase UV spectroscopy on large DNA anions. We recently have compared the action UV spectra of single-stranded and double-stranded DNA (**Figure 3**). Interestingly, we found that for a 12-mer duplex containing 100% of GC base pairs, action spectra are shifted in the duplex compared to the single strand. This shows that the bases' environment (possible the base stacking) plays a role in the absorption efficiency or in the photodetachment efficiency. This will be further explored in the near future.

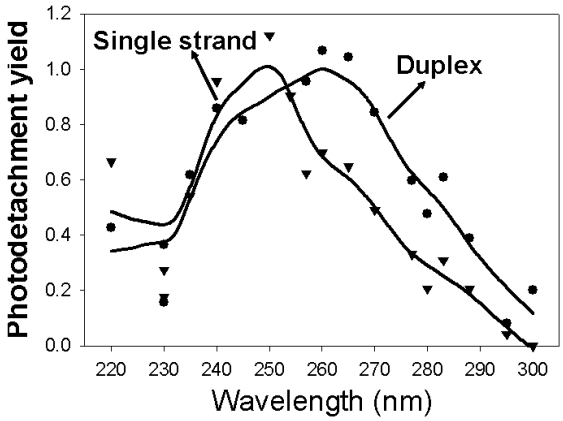

Figure 3: Action UV spectrum of single-stranded and double-stranded DNA ions: photodetachment yield as a function of the excitation wavelength for single-stranded $[dCGCGGGCCCGCG]^{3-}$ and the double-stranded $[(dCGCGGGCCCGCG)_2]^{5-}$ ions.

Finally, we also obtained preliminary results on laser irradiation of DNA coupled to other chromophores (covalently bound or noncovalently bound). Depending on the chromophore, three different behaviors are encountered [3]: (1) the photon energy can be redistributed in the molecule by internal conversion, (2) electron photodetachment was observed for a few chromophores, and (3) specific photodissociation was observed for a porphyrin chromophore (see poster presentation of F. Rosu). Interestingly, the chromophores resulting in electron detachment are all known fluorescent molecules, but the fluorophore needs to be noncovalently bound near the DNA bases for photodetachment to occur. Furthermore, photodetachment was found to be multiphotonic. The proposed mechanism (**Figure 4**) is therefore a two-step photon absorption by the ligand, followed by coupling to the DNA excited states, from which electron photodetachment can occur.

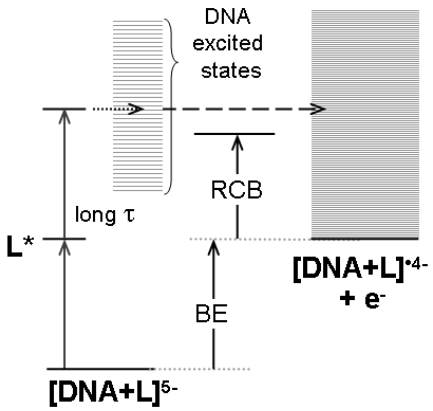

Figure 4: Photodetachment mechanism proposed for DNA complexes with noncovalently bound chromophore, excited at the chromophore absorption wavelength where DNA does not significantly absorb. (d) DNA with noncovalently bound fluorophore ligands L can absorb two photons and electron photodetachment occurs via coupling with the DNA excited states. (BE = electron binding energy; RCB = repulsive Coulomb barrier)

References:

[1] Gabelica, V.; Tabarin, T.; Antoine, R.; Rosu, F.; Compagnon, I.; Broyer, M.; De Pauw, E.; Dugourd, P. Electron Photodetachment Dissociation of DNA Polyanions in a Quadrupole Ion Trap Mass Spectrometer. *Anal. Chem.* **78**, 6564 (2006).

[2] Gabelica, V.; Rosu, F.; Tabarin, T.; Kinet, C.; Antoine, R.; Broyer, M.; De Pauw, E.; Dugourd, P. Base-Dependent Electron Photodetachment from Negatively Charged DNA Strands upon 260-nm Laser Irradiation. *J. Am. Chem. Soc.* **129,** 4706 (2007).

[3] Gabelica, V.; Rosu, F.; De Pauw, E.; Antoine, R.; Tabarin, T.; Broyer, M.; Dugourd, P. Electron Photodetachment Dissociation of DNA Anions with Covalently or Noncovalently Bound Chromophores. *J. Am. Soc. Mass Spectrom.* **18,** 1990 (2007).

Top-down Structural Analysis of Biomolecules in the Gas Phase by Electron Capture/Transfer Dissociation

Yury O. Tsybin
Biomolecular Mass Spectrometry Laboratory, Ecole Polytechnique Federale de Lausanne, 1015 Lausanne, Switzerland

Gas-phase activation/dissociation of charged macromolecules, with a focus on peptides, proteins, and DNA, due to interaction with charged and neutral small molecules, photons and electrons form a solid basis of tandem mass spectrometry – an indispensable analytical tool in modern life-science oriented research. The application area of tandem mass spectrometry is very wide – from targeted small molecule analysis (organic chemistry) to structural analysis of complex mixtures of small molecules (metabolomics, petroleomics, etc.), higher up to peptide structure elucidation (peptidomics and bottom-up proteomics) and protein primary and high order structure analysis (top-down proteomics).

A decade ago in a manuscript entitled "Electron Capture Dissociation of Multiply Charged Cations. A Nonergodic Process" for the first time the use of low energy electrons was demonstrated for peptide and protein structural analysis [1]. Since then, 445 papers cited the original ECD paper with on of the latest ones being "Is Dissociation of Peptide Radical Cations an Ergodic Process?" [2]. The number of citations indicates application-oriented power of ECD in peptide and protein structural analysis whereas titles of these two papers reveal exciting debates over the past 10 years on understanding of the process fundamentals. The question mark in the second title indicates that the electron capture dissociation (ECD) code is yet to be unveiled. Development of younger electron transfer dissociation (ETD) has been noticeably accelerated by the knowledge accumulated in ECD community. Rapid progress allows ETD to complement and extend ECD role in the upfront research activities.

In ECD/ETD, interaction of a multiply charged peptide or protein ion with an electron/anion results in cleavage of N-C_α bonds along the peptide backbone, including charge site-remote backbone cleavages. The complementary N-terminal and C-terminal ECD/ETD products may be held together by weak bonds, for instance hydrogen bonds, forming $[c+z]_{complex}$ as a radical intermediate. Although several attempts to reveal the influence of amino acid distribution and other precursor ion properties on ECD product ion formation have improved fundamental understanding of ECD, practical utility has not advanced significantly.

Here we will present recently gained experimental and fundamental insights into peptide and protein ion activation/dissociation in the gas phase due to low-energy electron capture/transfer. Particularly, we will describe analytical utility of gas-phase radical ion chemistry (hydrogen atom rearrangement between dissociation products) upon ECD/ETD [3], the role of amino acid hydrophobicity in the probability of product ion formation (product ion abundance), correlation of product ion abundance distribution with peptide secondary structure in solution and suggest our model for ECD/ETD dissociation reaction.

[1] Zubarev R.A., Kelleher N., McLafferty F.W. *JACS* **120(13)**, 3265-3266 (1998)
[2] Laskin J. *et al. JACS* **129**, 9598-9599 (2007)
[3] Tsybin Y.O. *et al. Anal. Chem.* **79**, 7596-7602 (2007)

MOLECULAR BEAM STUDIES OF ELECTRONICALLY NONADIABATIC MOLECULE-SURFACE INTERACTIONS

A. M. Wodtke[1], H. Nahler[1], J.D.White[1] , J. Larue[1], D.J. Auerbach[2] I. Rahinov, R. Cooper, Cheng Yuan[3]
[1]*Dept. of Chemistry and Biochemistry, UCSB, Santa Barbara, CA, 93106-9510, USA*
[2]*Gas Reaction Technologies Inc., 861 Ward Dr., Santa Barbara, CA, 93111, USA*
[3]*Dalian Institute of Chemical Physics, 457 Zhongshan Rd. Dalian, Liaoning 116023, P. R. China*

The so-called "Standard Model of Chemical Reactivity" was first described by Michael Polanyi and Henry Eyring in 1935[1], when they realized that the Born-Oppenheimer approximation[2] could be used to dramatically simplify the solution to the many-body Schrödinger equation. This insight led to the computational machinery that allows one to construct a potential energy surface describing all of the forces between the atoms taking place in a chemical reaction. Knowledge of the inter-atomic forces allows accurate computer simulations of chemical reactions, in principle providing every knowable characteristic of that reaction under any conceivable set of reaction conditions. Since that time, our methods for solving Schrödinger equations, especially the advent of Density Functional Theory[3], have advanced significantly. Development of ever more powerful computers has accelerated the rise in importance of theoretical chemistry. Some remarkable successes include: The quantitative agreement between experiment and theory for the prototypical H + HD → H_2 + D[4] and the advent of the successful use of theoretical advice for new industrial heterogeneous catalyst development[5].

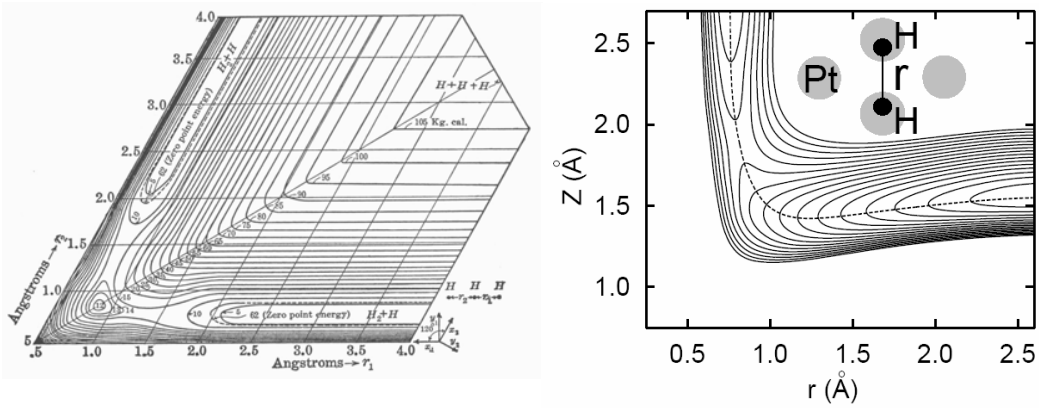

Figure 1: The first potential energy surface for a chemical reaction was devised in 1935 to explain the simplest H + H_2 → H_2 + H reaction (Left). Today, theoretical chemists are able to accurately explain reactions occurring at the surface of a bulk metal, providing a quantitatively accurate look at the inner workings of reactions important to heterogeneous catalysis (Right).

Understanding reactivity at solids, especially solids that are models for heterogeneous catalysis is an extremely exciting forefront area of modern research. Furthermore, as heterogeneous catalysis is involved in about 1/3 of the modern economy in one way or another, how we apply modern theory to this problem has become a question of profound significance. At the heart of the "Standard Model" is the Born-Oppenheimer approximation, which requires that electrons not be promoted to excited states by the motion of the heavy atoms as they react. The physical picture that justifies this assumption is the large difference in time-scales for electron motion compared to the atomic nuclear motion. While this assumption has proven highly accurate for many gas-phase reactions, it is inherently suspicious for reactions taking place at the surface of solid metals. The Heisenberg Uncertainty Principle tells us that confining electrons in space drives up their translational energy. The high speeds they obtain on small isolated molecules a few Å in size, ensures they move much more rapidly than the atomic nuclei. For metallic (or for that matter semiconductor) conduction electrons in solids that are delocalized over large distances, electron translational energies can be much smaller and the separation of time scales need not necessarily hold.

In recent years there has been a flurry of new work probing the limits of the validity of the Born-Oppenheimer approximation and therefore the "Standard Model" for reactions at metals. These include the failure of the Standard Model to accurately account for the experimentally observed N_2 vibrational excitation in the recombination of N-atoms desorbing from Ruthenium[6] the direct observations of 'chemicurrents'[7] and in another case the incidence energy dependence of O_2 dissociative adsorption on Aluminum[8].

We have performed experiments showing that hundreds of kJ/mol of vibrational energy can be transferred from a vibrationally excited molecule to electrons of a metal[9]. For example, when collisions occurring at a Cs(0.5ML)/Au(111) surface involve NO molecules with vibrational energy exceeding the surface work function, electron emission is observed. This phenomenon, dubbed "vibrationally promoted electron emission" is a convenient approach to the study of Born-Oppenheimer breakdown in molecule-surface interactions [10].

Recently, we have used molecular beams of highly vibrationally excited molecules and controlled, narrow speed distributions colliding with low work-function surfaces to characterize the molecular velocity dependence of this phenomenon. The vibrationally promoted electron emission increases as the velocity of the molecule is decreased and at the lowest velocities attainable in our instrument, we find electron emission probabilities as large as 0.2. In contrast previous reports of exoelectron emission (without vibrational excitation)exhibit a strong positive velocity dependence and probabilities of 10^{-4}-10^{-6} [11]. We observe similar behavior when we work with NO molecules in their vibrational ground state.

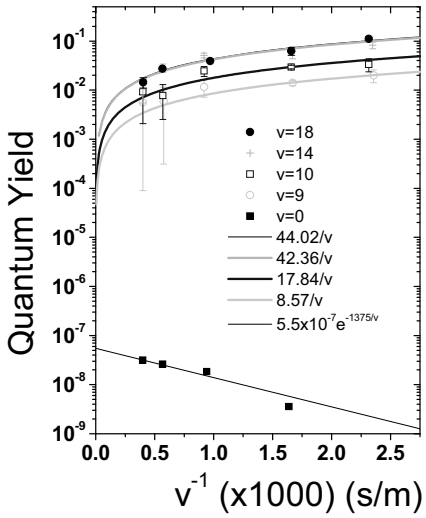

Figure 2: The velocity dependence for vibrationally promoted electron emission quantum yield. In this experiment, NO in specific vibrational states collides with a surface with a work function equal to the energy of NO(v=7.5).For the ground vibrational state, a positive velocity dependence is observed following the predicted $e^{-v0/v}$ dependence. For vibrational states whose energy exceeds the work function, an inverse velocity dependence is seen, indicating a different mechanism is at play. Furthermore absolute quantum yields are about 1 million times larger. This provides the direct evidence for the breakdown of the "Standard Model" in molecule-surface interactions. We infer from this that adsorbed atoms and molecules (that is molecules in the "zero-velocity limit") undergoing bond formation may exhibit similar catastrophic breakdown of the Born Oppenheimer approximation.

The remarkable new behavior seen here occurs for large amplitude vibration in the limit of zero velocity. This signifies that it is not the motion of the molecule toward the surface that is responsible for Born-Oppenheimer breakdown. Rather it is the high inter-atomic speeds associated with large amplitude vibrational motion similar to bond formation that excites the electrons. This has quite-thought provoking implications for surface chemistry as it suggests that the kind of Born-Oppenheimer breakdown we have seen for scattered molecules from surfaces may also be at play for molecules in the "zero-velocity limit", that is to say atoms and molecules adsorbed to metal surfaces.

But how general is such behavior? In the absence of predictive theories of electronically nonadiabatic effects, we seek 'intuitive proxies' that might guide our thinking, perhaps even provide the basis for chemical trends. The energy of the affinity level is one such proxy, which (if valid) would order the electronically nonadiabatic propensity of three common molecules as follows: NO>HCl>H_2. While electronically nonadiabatic effects for NO are now reasonable well established, and at least much of H_2 surface chemistry is explained by the standard electronically adiabatic model[12], HCl is an interesting intermediate case.

With an improved apparatus developed over the last three years, we were able to observe vibrational excitation of HCl ($v=0\rightarrow1$) in collisions with Au(111), even where vibrational excitation probabilities are lower than 10^{-6}. In this work we find results that we interpret as a transition from a low surface tempera-

ture regime where mechanical energy transfer dominates, to a regime at high surface temperature that resembles the incidence energy and surface temperature dependence behavior originally reported by Rettner and Auerbach for NO/Ag[13]. We are able to construct a model that accurately decomposes the contribution of the two energy transfer mechanisms in 24 experiments at different surface temperatures and incidence energies. Interestingly, these results suggest that a high temperature regime may exist for many systems where molecule-surface interactions are dominated by electronically nonadiabatic influences, a speculation that may have significant implications for many high temperature chemical systems.

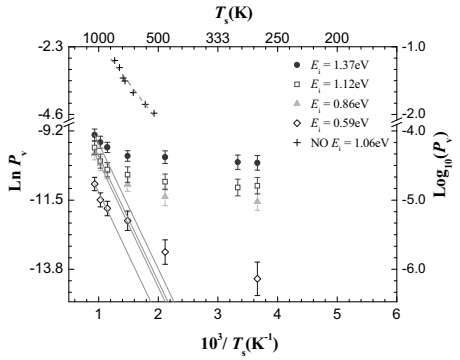

Figure 3: Surface temperature-dependence of the vibrational excitation probability of HCl (v=0→1) scattered from Au(111) for 4 incidence translational energies. Comparison to NO data is also shown (from previous work). The Arrhenius-like dependencies with the expected E_a (slope) fixed at the HCl v=0-1 energy spacing (0.36 eV) are shown as solid lines. The Arrhenius dependence expected for NO with E_a (slope) set by the vibrational spacing in NO (0.23 eV) is shown as a dashed line. These results appear to indicate a transition to an electron mediated energy transfer mechanism at high surface temperatures.

We have also begun the first studies of vibrationally excited HCl(v=2) prepared by overtone pumping. With our new instrument, we are able to excite the HCl molecules in a very small (0.1 mm or less) packet very close to the surface (within 0.5 mm). Then by performing REMPI detection of recoiling molecules at only a 15 mm distance, we may obtain high resolution TOF information, reflecting the changes in velocity that accompany the scattering events. Figure 4 shows some of the first results in this direction, after the raw TOF data (upper two panels) has been inverted to Flux vs. Translational energy (lower panel). The energy distribution shows that even for the vibrationally elastic channel, more than 60% of the incident translational energy is transferred to surface excitation. Comparison to purely mechanical systems, like Ar/Pt with a similar mass ratio, exhibits much less energy transfer. We speculate that this data may be some of the first clear evidence for strong translational excitation of electron hole pairs. For vibrational relaxation (also shown in the lower panel) the translational energy distribution is remarkably similar, suggesting that vibrational to translation energy transfer plays only a minor role here. While comparison with theory is critically needed, these observations imply that trapping probabilities might depend on electronically nonadiabatic molecule-surface interactions.

REFERENCES

[1]H. Eyring and M. Polanyi, Sonderdruck aus Z. Phys. Chem. **B4**, 12 (1930).

[2]M. Born and E. Oppenheimer, Ann. Physik **84**, 457 (1927).

[3]W. Kohn, Rev. Mod. Phys. **71** (5), 1253 (1999).

[4]D. X. Dai, C. C. Wang, S. A. Harich, X. Y. Wang, X. M. Yang, S. D. Chao, and R. T. Skodje, Science (USA) **300** (5626), 1730 (2003).

[5]C. J. H. Jacobsen, S. Dahl, A. Boisen, B. S. Clausen, H. Topsoe, A. Logadottir, and J. K. Norskov, Journal of Catalysis **205** (2), 382 (2002).

[6]L. Diekhoner, L. Hornekaer, H. Mortensen, E. Jensen, A. Baurichter, V. V. Petrunin, and A. C. Luntz, J. Chem. Phys. (USA) **117** (10), 5018 (2002); L. Diekhoner, H. Mortensen, A. Baurichter, E. Jensen, V. V. Petrunin, and A. C. Luntz, J. Chem. Phys. (USA) **115** (19), 9028 (2001).

[7]B. Gergen, H. Nienhaus, W. H. Weinberg, and E. W. McFarland, Science (USA) **294** (5551), 2521 (2001).

[8]J. Behler, B. Delley, S. Lorenz, K. Reuter, and M. Scheffler, Phys. Rev. Lett. **94** (3) (2005).

[9]A. M. Wodtke, Y. Huang, and D. J. Auerbach, J. Chem. Phys. **118** (17), 8033 (2003); M. Silva, R. Jongma, R. W. Field, and A. M. Wodtke, Ann. Rev. Phys. Chem. **52**, 811 (2001); Y. H. Huang, C. T. Rettner, D. J. Auerbach, and A. M. Wodtke, Science (USA) **290** (5489), 111 (2000); Y.

Huang, A. M. Wodtke, H. Hou, C. T. Rettner, and D. J. Auerbach, Phys. Rev. Lett. **84** (13), 2985 (2000); A. M. Wodtke, H. Yuhui, and D. J. Auerbach, Chem. Phys. Lett. **413** (4-6), 326 (2005).

[10]J. D. White, J. Chen, D. Matsiev, D. J. Auerbach, and A. M. Wodtke, J. Chem. Phys. (USA) **124** (6) (2006); J. D. White, J. Chen, D. Matsiev, D. J. Auerbach, and A. M. Wodtke, Journal of Vacuum Science & Technology A **23** (4), 1085 (2005); J. D. White, J. Chen, D. Matsiev, D. J. Auerbach, and A. M. Wodtke, Nature **433** (7025), 503 (2005).

[11]A. Bottcher, A. Morgante, T. Giessel, T. Greber, and G. Ertl, Chem. Phys. Lett. **231** (1), 119 (1994).

[12]P. Nieto, E. Pijper, D. Barredo, G. Laurent, R. A. Olsen, E. J. Baerends, G. J. Kroes, and D. Farias, Science (USA) **312** (5770), 86 (2006).

[13]C. T. Rettner, F. Fabre, J. Kimman, and D. J. Auerbach, Phys. Rev. Lett. **55** (18), 1904 (1985).

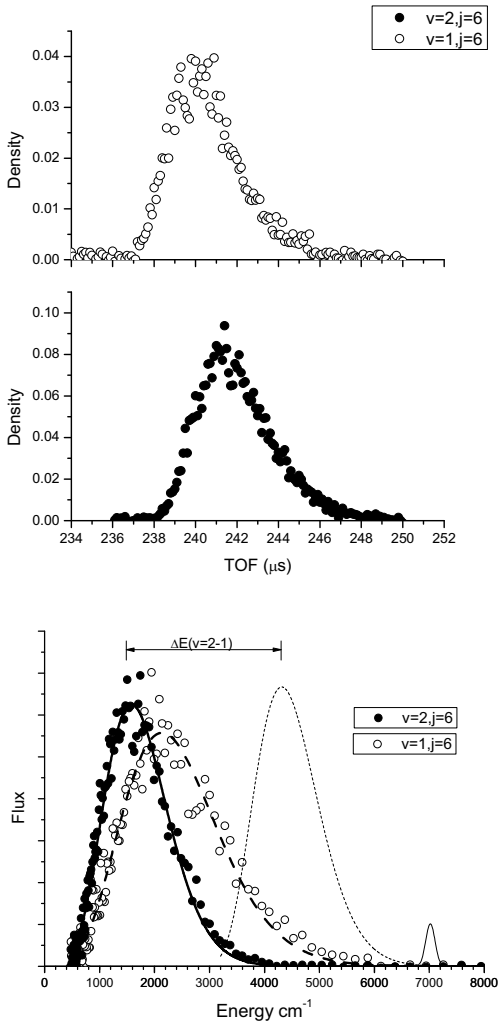

Figure 4. High resolution TOF measurements of HCl(v=2,1) resulting from the scattering of HCl(v=2) from Au(111) (upper two panels) and after direct inversion to flux vs. translational energy (lower panel). The vibrationally elastic channel (●) transfers on average 60% of the 4700 cm^{-1} of translational energy to the surface. The dotted curve shows the observed vibrationally elastic distribution shifted by the v=2-1 energy gap. The observed vibrational relaxation channel is also shown (○). There is remarkably incomplete conversion of vibrational energy to translation. The Gaussian at ~7000 cm^{-1} indicates the maximum translational energy available to the vibrational relaxation channel, neglecting thermal surface energy. The surface temperature was 298K.

Time-resolved measurements of surface diffusion induced by ultrashort laser pulses

K. Stépán, M. Lawrenz, M. Dürr, J. Güdde, U. Höfer
Fachbereich Physik und Zentrum für Materialwissenschaften, Philipps-Universität, D-35032 Marburg, Germany

Surface diffusion of adsorbates is an important elementary step for many chemical reactions at surfaces. Moreover, it plays a decisive role in/for all growth processes, in particular for the fabrication of epitaxial thin films. Normally, diffusion is a thermal activated hopping process. Microscopically, this involves the interconversion of adsorbate-substrate vibrations and frustrated translational or rotational modes. Recent experiments have shown that diffusion at metal surfaces can also be induced electronically by ultrashort laser pulses [1, 2, 3]. This does not only have potentially interesting applications for the growth of novel materials at low temperature. It has also allowed the first time-domain investigation of an atomic hopping process [2]. The experiments utilize ultrashort laser pulses which for some 100 fs create high electron temperatures (thousands of Kelvin) without substantially heating the substrate lattice. The hot electrons or holes at the metal surface couple to adsorbate levels and after multiple excitations lead to nuclear motion through a kind of electronic friction process.

The experiments performed in our group have exploited the special properties of stepped surfaces for the sensitive detection of lateral motion. In case of the system O/Pt(111) the surface is first exposed to molecular O_2. Under certain conditions the

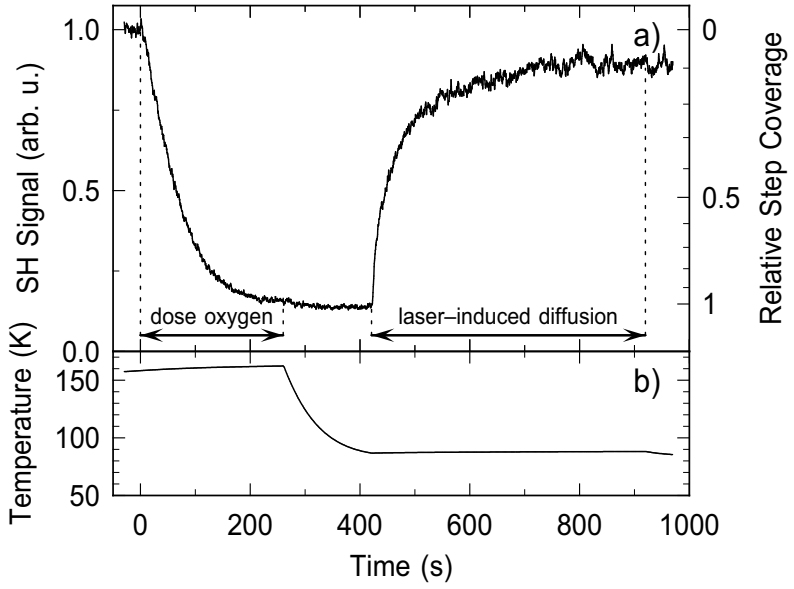

Fig. 1: SHG signal (a) and temperature (b) recorded a function of time during O_2 exposure and laser-induced diffusion of O/Pt(111). Diffusion is induced by 50-fs laser pulses with an absorbed fluence of 5.6 mJ/cm^2 at a repetition rate of 1 kHz. It leads to a recovery of the SH-signal due to the depopulation of the step edges (from Ref. [4]).

molecules dissociate only at the step edges. In this way a starting condition differing from thermal equilibrium is created. Subsequent laser-induced diffusion leads to an almost random distribution of oxygen atoms at step and terrace sites. It is possible to detect this redistribution with high sensitivity by means of optical second-harmonic generation (SHG) [4]. A regular array of steps represents a symmetry break at the surface and, for appropriately chosen polarization of the incoming and detected laser light, step sites become the main SHG sources (Fig. 1).

Information about the temporal dynamics of the energy transfer from the optical excitation to lateral motion of the adsorbate is obtained by performing two-pulse cross-correlation experiments [2]. For this purpose, the diffusion rate is measured as a function of time delay between two short pump pulses. This type of experiment is possible because the diffusion rate R depends in a strongly nonlinear way on absorbed laser fluence F ($R \propto F^{15}$). The results (Fig. 2) show that the adsorbate excitation created by the first pulses persists for about 1.5 ps, much longer than the laser pulse duration of 50 fs but shorter than typical vibrational lifetimes. This behavior is characteristic for a process driven by multiple electronic excitations.

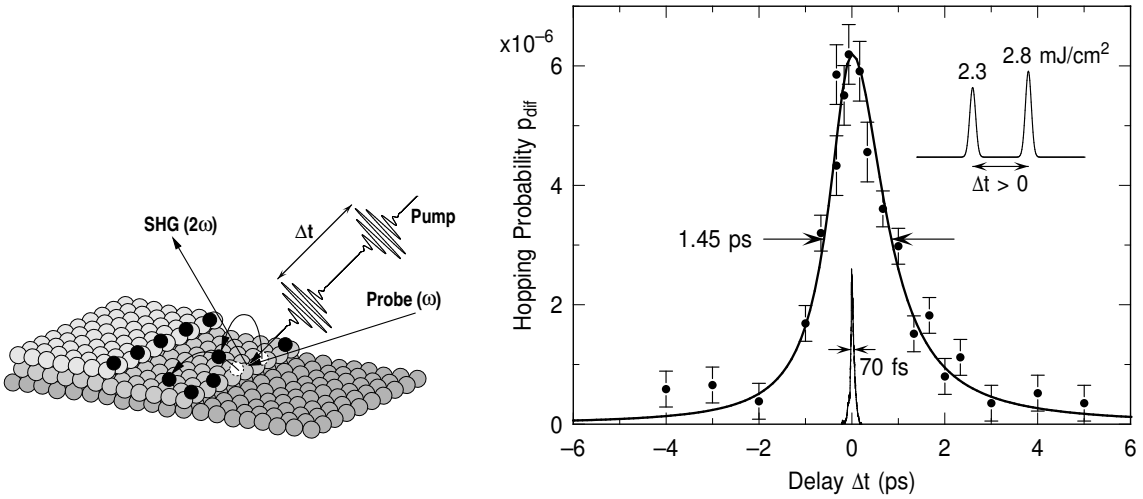

Fig. 2: Schematic view of the two-pulse correlation experiment and measured hopping probability per laser shot as a function of delay between two pump pulses (symbols). The thick solid line is a guide to the eye. The thin line shows the SHG cross correlation of the two pump pulses generated at the sample surface (from Ref. [2]).

Presently there are no full microscopic theoretical descriptions for such diffusion processes. For this reason we have employed an electronic friction model to evaluate our data [5]. In this empirical model, electronic and phononic excitations of the substrate and vibrational excitations of the adsorbate are represented by coupled heat baths. We find that a consistent description of the experimental data cannot be achieved with a constant electronic friction coefficient for the coupling between the electronic excitation of the substrate and the lateral motion of the adsorbate. Our calculations suggest that the coupling increases appreciable with the electron temperature, or in other words with the density of excited electrons. We interpret these results in terms of a two-step process. The hot substrate electrons primarily excite the O-Pt stretch vibration. Only if high vibrational

levels are populated to a sufficient extend, anharmonic coupling between these modes and frustrated translations leads to appreciable lateral adsorbate motion and thus to diffusion (Fig. 3).

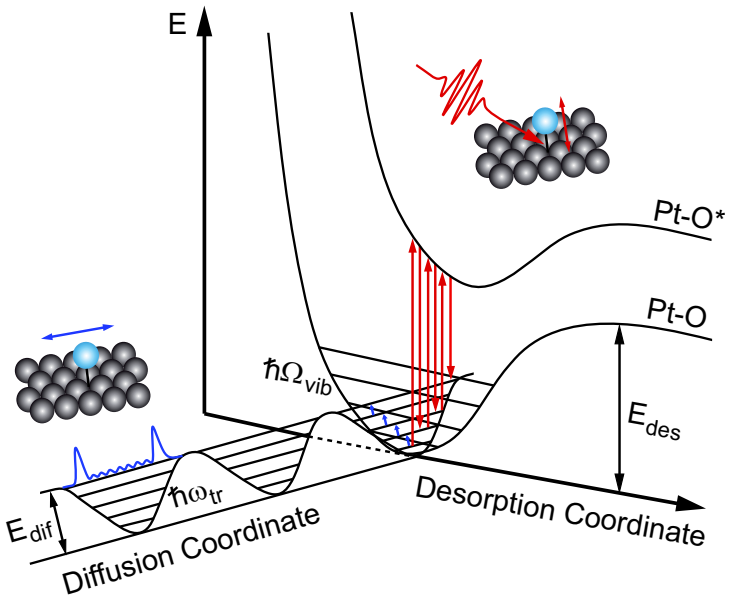

Fig. 3: Schematic potential energy scheme for an indirect excitation of diffusion by anharmonic coupling with the Pt-O vibration (from Ref. [5]).

Similar experiments have been performed for CO/Pt(111) [6]. This adsorbate has a substantially higher binding energy at the step sites than at the terrace sites. For this reason the steps serve as traps for adsorbed CO at low temperatures and SHG cannot only be used to monitor laser-induced CO-diffusion from the steps to the terraces but also from terrace to step sites. For step to terrace diffusion we find considerably narrower two-pulse correlations than for O/Pt. This is in agreement with infrared-visible pump-probe experiments which have shown very efficient coupling of hot electrons to frustrated rotational CO modes [3]. For terrace diffusion of CO with a barrier of only 0.2 eV our correlation measurements at different substrate temperatures indicate the transition from an electronically driven to a phonon driven process [6].

Current efforts of our group focus on performing two-pulse correlation experiments with scanning tunneling microscopy (STM). Experiments utilizing nanosecond laser pulses and STM have shown that in order to combine high time with atomic lateral resolution it is often not necessary to excite the system with short laser pulses while simultaneously imaging it with the STM. If there is a well defined starting situation a post-mortem analysis can provide the same quantitative information [7, 8, 9].

Supported by the Deutsche Forschungsgemeinschaft (DFG Priority Programme SPP 1093, *SPP 1093 Dynamics of Electron Transfer Processes at Interfaces*, the German-Israeli Foundation for Scientific Research and Development (GIF) and the DFG International Research Training Group 790 *Electron-electron interactions in solids*.

[1] L. Bartels, F. Wang, D. Moller, E. Knoesel, and T. F. Heinz, Science **305**, 648 (2004).

[2] K. Stépán, J. Güdde, and U. Höfer, Phys. Rev. Lett. **94**, 236103 (2005).

[3] E. H. G. Backus, A. Eichler, A. W. Kleyn, and M. Bonn, Science **310**, 1790 (2005).

[4] K. Stépán, M. Dürr, J. Güdde, and U. Höfer, Surf. Sci. **593**, 54 (2005).

[5] J. Güdde and U. Höfer, J. Phys.: Condens. Mat. **18**, S1409 (2006).

[6] M. Lawrenz, K. Stépán, J. Güdde, and U. Höfer, in preparation

[7] M. Dürr, A. Biedermann, Z. Hu, U. Höfer, and T. F. Heinz, Science **296**, 1838 (2002).

[8] C. H. Schwalb, M. Lawrenz, M. Dürr, and U. Höfer, Phys. Rev. B **75**, 085439 (2007).

[9] M. Lawrenz, *et al.*, Phys. Rev. B **75**, 125424 (2007).

Optimizing the photoreactivity of adsorbates at surfaces

Peter Saalfrank, Ivan Andrianov, Stephanie Beyvers, Tillmann Klamroth, Mathias Nest, Tijo Vazhappilly
Institut für Chemie, Universität Potsdam, D-14476 Potsdam-Golm, Germany
Rigoberto Hernandez
School of Chemistry and Biochemistry, Georgia Institute of Technology, Atlanta, GA 30332-0400, USA

Cross sections of photochemical reactions at surfaces are often very small, due to the ultrafast quenching of adsorbates after photoexcitation. To overcome this problem, the enhancement of photodesorption cross sections, for example, by shaped laser pulses or by microstructuring the surface, has been suggested [1].

Here we investigate these possibilities from a theoretical, quantum dynamical point of view. Three model systems are chosen. The first one is H:Si(100)-(2×1), where IR-laser induced desorption of H atoms by bond-selective vibrational excitation and "ladder climbing" in the ground electronic state is demonstrated [2, 3, 4]. In the simulations, both anharmonic intermode and vibration-phonon coupling were accounted for, by "reduced" (open-system density matrix theory) and "full" dynamical models (multi-dimensional wavepacket propagation).

The second system is H:Ru(0001)-(1×1), where a hybrid IR+UV/vis scheme is adopted with the goal to increase the desorption cross section of H_2 after hot electron-mediated electronic excitation caused by femtosecond laser pulses [6]. Here, the quantum dynamical approach is compared to a classical friction model. The feasibility to mode-selectively excite, by IR photons, adsorbates at metal substrates is also demonstrated for other systems [5].

Finally, the NO:Pt model system is chosen as an example for "incoherent" control of hot electron-mediated photodesorption (of NO) from thin metal films [7, 8].

It is concluded that even for relaxing adsorbates, bond-selective control of photochemical surface reactions should be possible to some extent.

[1] P. Saalfrank, Chem. Rev. **106**, 4116 (2006).

[2] I. Andrianov and P. Saalfrank, J. Chem. Phys. **124**, 034710 (2006).

[3] G.K. Paramonov, S. Beyvers, I. Andrianov, and P. Saalfrank, Phys. Rev. B **75**, 045405 (2007).

[4] G.K. Paramonov, I. Andrianov und P. Saalfrank: J. Phys. Chem. C **111**, 5432 (2007).

[5] S. Beyvers, Y. Ohtsuki, and P. Saalfrank, J. Chem. Phys. **124**, 234706 (2006).

[6] T. Vazhappilly, S. Beyvers, T. Klamroth, M. Luppi, and P. Saalfrank, Chem. Phys. **338**, 299 (2007).

[7] M. Nest and P. Saalfrank, Phys. Rev. B **69**, 235405 (2004).

[8] T. Klamroth, D. Kröner, and P. Saalfrank, Phys. Rev. B **72**, 205407 (2005).

X-ray radiation-induced damage in DNA monitored by XPS

Sylwia Ptasińska

Department of Physics and Astronomy, The Open University, Milton Keynes, United Kingdom MK7 6AA
e-mail: s.ptasinska@open.ac.uk

The DNA molecule is the most sensitive biological target within cells upon exposure to ionizing radiation. One of the most powerful methods of surface analysis is X-ray photoelectron spectroscopy (XPS) which can be used to perform quantitative elemental analysis of thin films and provides information about chemical transformations of functional groups.

In the present work the decomposition of the calf thymus DNA fibre under irradiation with soft X rays (magnesium Kα X-ray source) in ultra-high vacuum is studied by means of XPS. In this experimental approach the X-ray beam both damages and probes the sample. X-ray photoelectron spectra were measured using Kratos Model XSAM 800 with dual-anode X-ray source, a hemispherical energy analyzer and a channeltron detector.

Here compositional survey and detailed spectra reveal the C 1s, N 1s, O 1s and P 2p photoelectron lines and the O, N and C Auger lines. Each 1s peak is accompanied by a satellite peak located at higher binding energy and originated from shake-up and shake-off transition.

In addition, the survey spectra and high resolution C 1s spectra of films of all nucleobases, i.e. adenine, cytosine, guanine and thymine are recorded. These high resolution C 1s spectra exhibit a complicated structure due to contribution of C atoms occupying different molecular sites. The carbon species from the nucleobases include hydrocarbon (C-C and C-H), carbon bound to nitrogen (C-N, N-C-N), amide carbon (N-C=O) and urea carbon [N-C(=O)-N].

To monitor changes corresponding to X-ray induced damage to the DNA molecule, the spectra are taken repeatedly over 5 h. In most cases, the spectra have complicated shapes due to contribution of several species expected from nucleobases, sugar and phosphate group. However, a comparative analysis of changes in XPS line shapes and stochiometry indicates that the DNA molecule is decomposed during X-ray irradiation time.

Sodium controlled selectivity in metastable decay of gas phase oligonucleotide ions

O. Ingólfsson, and H. D Flosadottir
University of Iceland, Faculty of science, Department of Chemistry, Science Institute, Dunhaga 3, 107 Reykjavik, Iceland

M. Stano
Comenius University, Faculty of Math Phys & Informat, Dept Expt Phys, Bratislava 84248, Slovakia

Biologically relevant molecules such as DNA, protein and peptides have found increasing interest across the scientific disciplines. One clear example of the cross disciplinary interest in biological molecules is the study of radiation damage to living organism, a subject which occupies physicists and physical chemists as well as biochemists, biologists and medical researchers[1-5]. Also the need for new analytical methods and mass spectrometric techniques to shed light on the complex molecular structure and composition of biologically relevant molecules has drawn the attention of physicists and physical chemists more in this direction[6-10]. However, in particular such biomolecules as DNA, proteins and lipids are of inciting interest simply due to their exceptional properties, which understanding may very well be the key to successful molecular engineering of the future. The capabilities of molecular self-regulation, self-organization and signaling as well as the active interaction of these molecules with their surrounding environment makes them ideal models for the future engineering of molecular devices[11-16]. These groups of macro molecules all have in common that they possess acetic and/or basic functional groups and that they are capable of hydrophilic and hydrophobic inter- and intra-molecular interactions. Consequently the pH and the ion strength is imperative for the stability and functionality of these molecules in their aqueous native environment.

Here we present a study on the stability of negatively and positively charged oligonucleotides in the metastable time frame when these are formed through deprotonation or protonation in matrix assisted laser desorption/ionization (MALDI). We study systematically the influence of the degree of sodiation i.e., when the acetic protons are one by one exchanged against sodium, and we show that the sodium adduct formation is not of less significance in the gaseous phase than it is in aqueous solutions[17].

In the case of the negatively charged oligonucleotides the sodiation gradually quenches all dissociatin channels that lead to back bone cleavage in the favor of simple base loss showing clearly the role of proton transfer in the fragmentation mechanism. In the case of the positively charged oligonucleotides a similar effect is observed, however, superimposed we observed a drastic and abrupt *switching* between completely different dissociation channel as the degree of sodium increases.

The model systems used in this study are all combinations of the synthetic hexameric nucleotides 5′-d(TTXYTT)-3′, where X and Y are dC, dG or dA. The sodium free and the sodium adducts with 0-5 protons exchanged for sodium were studied for all six combinations in the negative and with up to 7 protons exchanged positive mode. For comparison we have also studied the metastable decay of all sodium adducts of the hexameric oligonucleotide dT6.

Negative Ions

Figure 1 shows a comparison of post-source decay spectra of 5′-d(TTACTT)-3′ containing 0 – 5 sodium atoms. There are three main features that become apparent in comparing the spectra and are also observed for the other hexameric oligonucleotides measured.

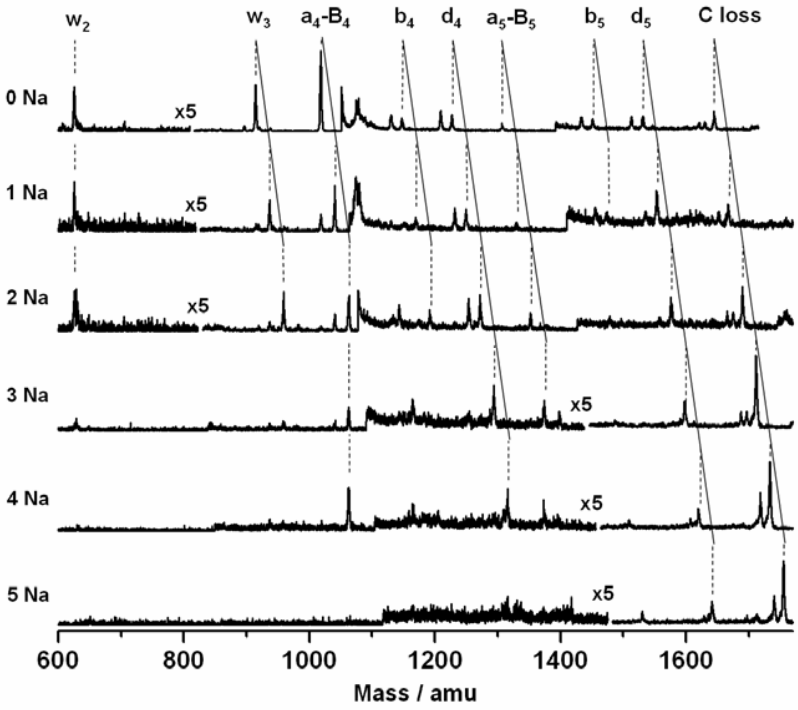

Figure 1. Comparison of the PSD-spectra of 5′-d(TTACTT)-3′ containing 0 – 5 sodium atoms.

First; the w, a – B, b and d fragmentation channels are very effectively quenched already by parent ions containing 3 sodium atoms and depending on the laser power, quantitative quenching of all fragmentation channels except the d_5 and the single base loss may be achieved with addition of four sodium atoms to the parent ion.

Second; as is most apparent for the d_4 and d_5 fragments, the water loss from these fragments is more strongly influenced by the degree of sodiation of the parent ion than is the formation of the fragment itself.

Third; it is clear from the comparison in Figure 1 that the single base loss increases with increasing degree of sodiation of the parent anion.

These observations are concordant with what would be expected for a proton transfer mechanism being responsible for the backbone cleavage, i.e., a mechanism where the acidic proton of a phosphodiester plays a crucial role in initiating the fragmentation. With increasing number of the acidic phosphodiester protons being replaced by sodium the formation of hydrogen bonded transition states involving these is blocked to increasing extend. However, it is also clear, that a proton transfer is not essential to initiate a single base loss from those ologonucleotides. Furthermore, the increase in the relative intensity of fragments from single base loss with increasing degree of sodiation shows that the backbone cleavage is preceded by the base loss.

If there is one predominating mechanism governing the metastable decay of the negatively charged oligonucleotides, this is most likely a charge controlled base loss followed by a proton initiated backbone cleavage. However, these observations may also be explained if there are two competing channels responsible for the base loss: A charge controlled mechanism that does not lead to further fragmentation and a proton transfer from an adjacent phosphodiester group to the base resulting in a neutral base loss and subsequent cleavage of the backbone. This would also cause the base loss to be independent of the degree of sodiation and further fragmentation after the base loss to halt when all acidic protons of the phosphodiester groups are exchanged against sodium[17].

Positive Ions

Figure 2 shows post-source decay spectra of the protonated 5′-d(TTCGTT)-3′ ion containing 0 – 7 sodium atoms. Similar to the deprotonated hexameric oligonucleotides, the w and the a – B fragmentation channels are also very effectively quenched in the protonated oligonucleotides with increasing degree of sodiation.

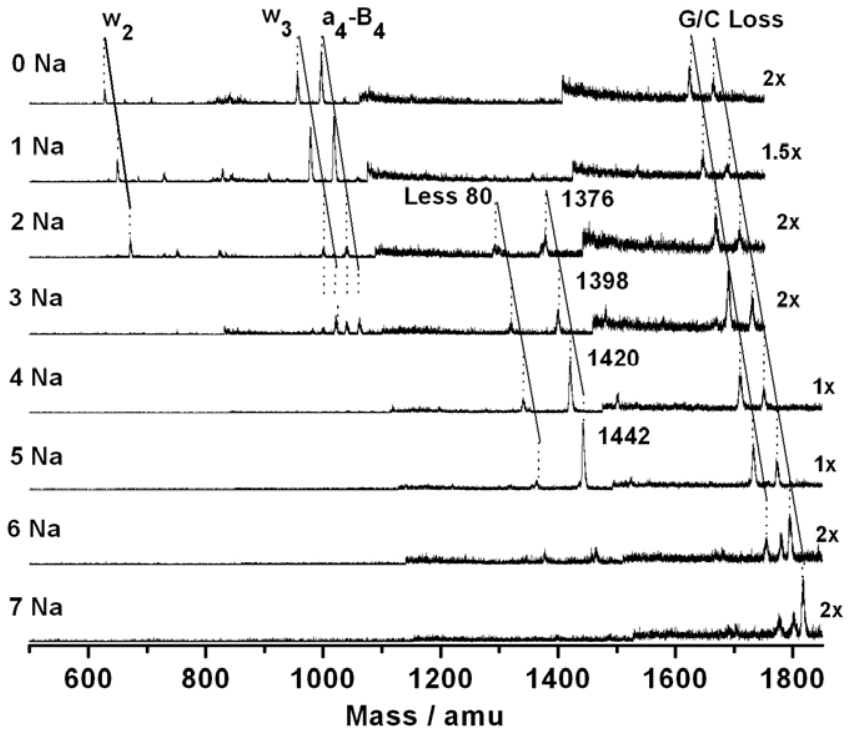

Figure 1. Comparison of the PSD-spectra of the protonated 5′-d(TTCGTT)-3′ containing 0 – 7 sodium atoms.

Though the relationship between the base loss and the backbone cleavage is not as clear as for the deprotonated speces, it is apparent that the backbone cleavage is much stronger influenced than the channel leading to the single base loss. Depending on the laser power we observe quantitative quenching of the w and the a – B fragmentation channels is by the exchange of 3-4 phosphodiester protons against sodium, showing that the backbone cleavage leading to the w and the a-B fragments is governed by a proton transfer mechanism. The base loss on the

other hand is to an much lesser extend dependent on the availability of the acetic phosphodiester protons.

However, the most remarkable observation in the case of the protonated oligonucleotides is that the exchange of 2 protons against sodium ions opens up a new dissociation channel that is completely independent of the nature of the central bases and their sequence. This channel leads to the loss of the two central bases with one sugar and one diphosphoester unit from the center of the backbone. The two terminal TT units recombine in the process presumably over a cyclic phosphate intermediate leading to the formation of either a 5′-d(TpTpdpTpT)-5′ or the corresponding 3′-d(TpTpdpTpT)-3′ sequence. The first sequence would result from a recombination of the 3′ end with the second phosphodiester group the second sequence from a recombination of the 5′ end with the fourth phosphodiester group.

This channel, which gradually increases in intensity with increasing sodiation, is then again abruptly closed when six protons are exchanged against sodium ions. This show clearly that the dissociation paths of the protonated oligomers depend even more strongly on the degree of sodiation than those of the deprotonated and that the number of sodium atoms determines with high selectivity which dissociation channels are active.

Acknowledgement
This work was supported by the European Science Foundation (ESF) program; Electron Induced Processing at the Molecular Level (EIPAM), by the Icelandic Centre for Research (RANNIS) and by the University of Iceland Research Fund.

References:

[1] Sanche L, 2002 *Mass Spectrometry Reviews* **21** 349-69.
[2] Demple B, DeMott M S, 2002 *Oncogene* **21** 8926-34.
[3] Toyokuni S, 1999 *Pathology International* **49** 91-102.
[4] Colson A O, Sevilla M D, 1995 *International Journal of Radiation Biology* **67** 627-45.
[5] Becker D, Sevilla M D, Advances in Radiation Biology, Vol 17, 1993, p. 121-80.
[6] Wittmann-Liebold B, Graack H R, Pohl T, 2006 *Proteomics* **6** 4688-703.
[7] Cheng M M C, Cuda G, Bunimovich Y L, Gaspari M, Heath J R, Hill H D, Mirkin C A, Nijdam A J, Terracciano R, Thundat T, Ferrari M, 2006 *Current Opinion in Chemical Biology* **10** 11-9.
[8] Bolbach G, 2005 *Current Pharmaceutical Design* **11** 2535-57.
[9] Marvin L F, Roberts M A, Fay L B, 2003 *Clinica Chimica Acta* **337** 11-21.
[10] Edwards G S, Austin R H, Carroll F E, Copeland M L, Couprie M E, Gabella W E, Haglund R F, Hooper B A, Hutson M S, Jansen E D, Joos K M, Kiehart D P, Lindau I, Miao J, Pratisto H S, Shen J H, Tokutake Y, van der Meer A F G, Xie A, 2003 *Review of Scientific Instruments* **74** 3207-45.
[11] Vologodskii A, 2006 *Physics of Life Reviews* **3** 119-32.
[12] Park H H, Jamison A C, Lee T R, 2007 *Nanomedicine* **2** 425-39.
[13] Liu Y, Flood A H, Bonvallett P A, Vignon S A, Northrop B H, Tseng H R, Jeppesen J O, Huang T J, Brough B, Baller M, Magonov S, Solares S D, Goddard W A, Ho C M, Stoddart J F, 2005 *Journal of the American Chemical Society* **127** 9745-59.
[14] Knoblauch M, Peters W S, 2004 *Cellular and Molecular Life Sciences* **61** 2497-509.
[15] Alberts B, 1998 *Cell* **92** 291-4.
[16] Urry D W, 1997 *Journal of Physical Chemistry B* **101** 11007-28.
[17] Stano M, Flosadottir H D, Ingolfsson O, 2006 *Rapid Communications in Mass Spectrometry* **20** 3498-502.

Electronic Spectra of Carbon Chains, Rings and their Ions

John P.Maier
Department of Chemistry, University of Basel, Klingelbergstrasse 80, CH- 4056 Basel

Our research has focused on the measurement of the electronic spectra of transient species which are presumed to be of relevance to astrophysical observations. Among these are the carbon chains and their ions. Thus we have been using and developing a number of spectroscopic methods to determine their spectra in the gas phase, including absorption via cavity ring-down and REMPI methods. The species are produced in supersonic jets coupled with discharges. With the successful laboratory detection of the electronic spectra of a number of key species, such as the bare carbon chains C_n n=4,5, comparison with astrophysical data could be made which lead to interesting implications for the future search for the species which could be responsible for the enigmatic diffuse interstellar bands. Among the recent relevant observations in the laboratory have been the electronic spectra of carbon rings, C_n n=14,18,22, the development of a method to study the electronic transitions of mass-selected ions collisionally relaxed to 20 K and held in a 22-pole rf trap, and the study of metal containing carbon chains, such as AlCCH.

Isolation of molecules in helium nanodroplets: spectroscopy and dynamics at ultra-cold temperatures

P. Claas, G. Droppelmann, M. Mudrich, F. Stienkemeier

Physikalisches Institut, Universität Freiburg, Hermann-Herder-Str. 3, D-79104 Freiburg, Germany, email: frank.stienkemeier@physik.uni-freiburg.de

Claus-Peter Schulz

Max-Born-Institut, Max-Born-Str. 2a, D-12489 Berlin, Germany

Molecules attached to superfluid helium nanodroplets have been studied for quite some time in order study the properties of matter at low temperatures and in the environment of a size limited quantum fluid. Recently, new directions of such studies in terms of short-time dynamics [1] and metal clusters [2] have been reviewed. The variety of dopants has been widely extended. We demonstrated that using kilohertz laser ablation both fragile bio-molecules as e.g. Guanine, as well as refractory metals could be efficiently doped in helium droplets [3]. In order to study the superfluid properties of the nanodroplets we took a closer look at the dynamics of alkali dimers which we probed by femtosecond pump-probe spectroscopy at the surface of the droplets [4,5]. In comparison with quantum calculations the energy dissipation of the dimer's vibrational motion interaction with the droplet has been modeled (Fig.1). The evolution of the vibrational motion in time could nicely be reproduced. In this way we obtain information on the excited internal modes of the droplet.

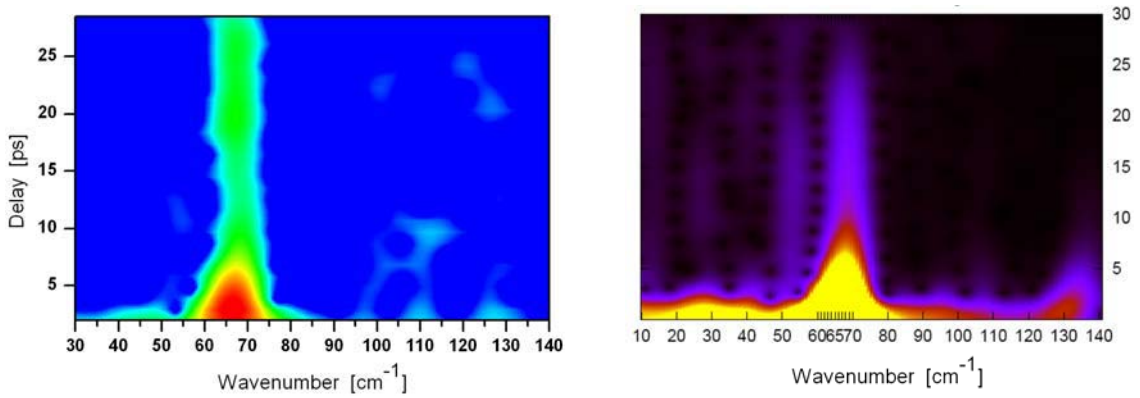

Fig.1: Comparison of the spectrogram of potassium dimers attached to helium droplets with model calculations (M. Schlesinger and W. Strunz, unpublished results). The prominent energy around 66 cm^{-1} corresponds to a vibration in the excited $A^1\Sigma_u$ state.

[1] Frank Stienkemeier, Kevin K. Lehmann, J. Phys. B. **39,** R127–R166 (2006).
[2] Tiggesbäumker J., Stienkemeier F., PCCP **9** (34), 4748-4770 (2007).
[3] M. Mudrich, B. Forkl, S. Mueller, M. Dvorak, O. Bünermann, F. Stienkemeier, Rev. Sci Instr., **78**, 103106 (2007).
[4] P. Claas, G. Droppelmann, C. P. Schulz, M. Mudrich, F. Stienkemeier, J. Phys. Chem. A. **111** (31), 7537-7541 (2007).
[5] P. Claas, G. Droppelmann, C. P. Schulz, M. Mudrich, F. Stienkemeier, J. Phys. B **39,** S1151-S1168 (2006).

Fragmentation dynamics inside helium nanodroplets: new theoretical results

N. Halberstadt
LCAR-IRSAMC, Université Toulouse 3 and CNRS, 118 route de Narbonne, 31062 Toulouse CEDEX 09, France

D. Bonhommeau
University of Minnesota, 207 Pleasant Street S.E., 230 Smith Hall, Minneapolis, MN 55455-0431, USA

M. Lewerenz
Université Paris Est, EA 2180, Laboratoire de Chimie Théorique, 5 Bd Descartes, 77454 Marne la Vallée Cedex 2, France

Helium droplets provide a unique low-temperature (0.38 K), inert, liquid environment, with superfluid properties that can be studied at the molecular level. In particular, they were initially considered as a potential refrigerant for cooling newly formed ions, with the hope that parent ions could be observed. This idea was based on the exceptionally high heat conductivity and the specific type of heat propagation in bulk (superfluid) helium II. On the other hand, bulk helium II also exhibits a vanishing viscosity for the flow through fine capillaries, which could imply that dissociation inside superfluid helium should occur exactly like in the gas phase, without any interference from the superfluid "solvent". Experimental results have shown that the "caging" effect is important, although fragmentation is usually not completely hindered [1, 2, 3, 4, 5, 6, 7]. In their photodissociation experiment on CF_3I inside helium droplets, Braun and Drabbels [8, 9, 10, 11] have concluded that binary collisions play an important role in high kinetic energy dynamics. In addition, the cooling by helium atom evaporation has been found to be highly non thermal for some ions in small droplets [12, 13]. It is therefore of great importance to understand the mechanisms that are responsible for energy dissipation inside helium droplets.

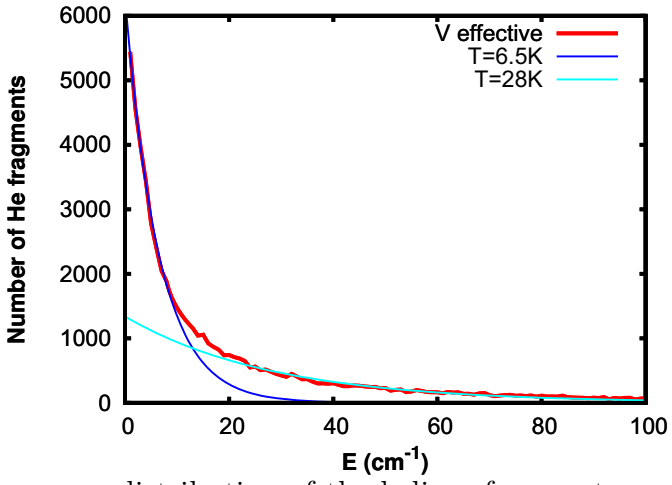

Figure 1: Kinetic energy distribution of the helium fragments. results of the simulation ("V effective") and fit by a sum of two Boltzmann distributions.

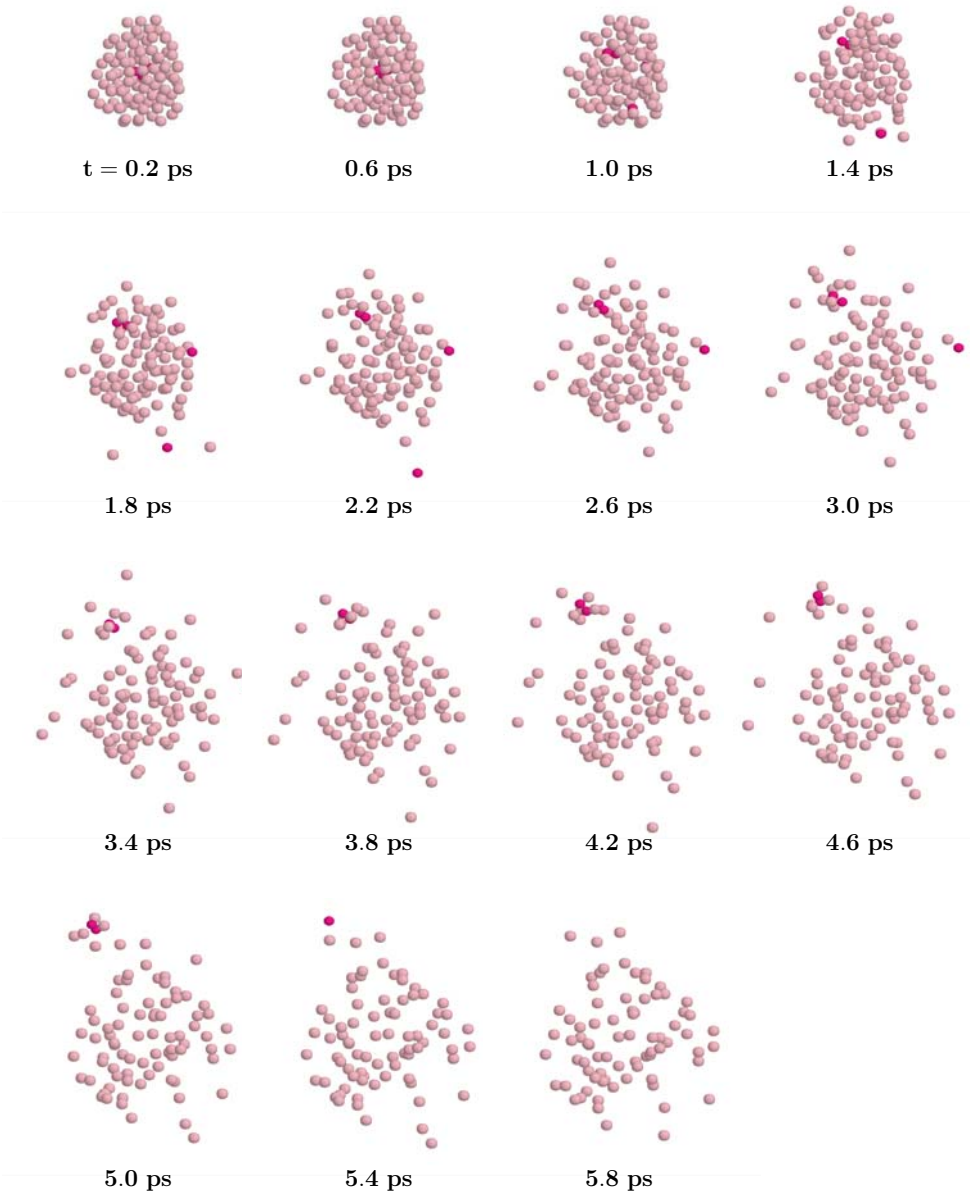

Figure 2: $He_{100}Ne_4^+$ trajectory showing ionic species ejection. Light and dark grey atoms are heliums and neons, respectively. Snapshots are taken every 0.4 ps, starting at t=0.2 ps. After dissociation of the first (t=1.4 ps) and second (t=2.2 ps) neon, the recoil energy starts ejecting Ne_2^+ (t=3.8ps) with helium attached to it.

We present simulation results on the effect of a helium nanodroplet environment on the fragmentation dynamics of embedded molecular systems. Ionized rare gas clusters are chosen as model systems because they are well known for extensively fragmenting upon ionization [14, 15, 16, 17]. In addition, their well known fragmentation patterns [18, 19, 20, 21] allow for comparisons with experiments both in the gas phase and inside helium

nanodroplets.
The helium atoms are treated explicitly, with zero-point effects taken into account through an effective helium-helium interaction potential [22, 23]. Previous attempts at describing the helium environment implicitly through a friction force [24, 25] have given good results compared to the experiment of Janda and coworkers [5]. However, the value obtained for the friction coefficient by fitting this sole parameter to the experimental fragment distribution was very large, indicating that some other processes must be playing an important role. All the nonadiabatic effects between electronic states of the ionized rare gas cluster are taken into account in the same fashion as in our previous works on rare gas cluster dissociation upon ionization in the gas phase [26, 27, 28, 29].

The results [30, 31] on $Ne_n@He_N$ (n=4–6, N=100, 300) reveal a predominance of Ne_2^+ and $He_pNe_2^+$ fragments and the absence of bare Ne^+ fragments, in agreement with available experimental data [5, 7]. Caging is important, since $He_pNe_2^+$ fragments are about 3 times as abundant as Ne_2^+ ones. For Ne_6, the sum of the Ne_2^+ species proportions (summing Ne_2^+ and $He_pNe_2^+$ fragments) is even significantly smaller than the proportion of Ne_2^+ fragments for ionization of the gas phase cluster (82% instead of 96%).

The neutral monomer fragments exhibit a rather wide kinetic energy distribution that can be fitted to the sum of two Boltzmann distributions, one with a low kinetic energy and the other with a higher kinetic energy (see Fig. 1). This indicates that cooling by helium atom dissociation is more efficient than was believed so far, as suggested by the recent experimental results of Miller and coworkers [12, 13].

Purely classical calculations are shown to strongly overestimate the amount of cage effect (cooling), clearly indicating the need to take into account zero-point effects.

Also, most of the dissociation dynamics occurs in the first 10 ps, which shows that the dynamics is fast. A more detailed analysis of the trajectories reveals that in 32% to 23% of the cases (for Ne_4 to Ne_6 dopants), the intermediate ionized species is ejected from the surrounding helium droplet. An example of such a trajectory is shown in Fig. 2

[1] M. Lewerenz, B. Schilling, and J. P. Toennies, J. Chem. Phys. **102**, 8191 (1995).

[2] B. E. Callicoatt, K. Förde, T. Ruchti, L. Jung, K. C. Janda, and N. Halberstadt, J. Chem. Phys. **108**, 9371 (1998).

[3] B. E. Callicoatt, K. Förde, L. F. Jung, T. Ruchti, and K. C. Janda, J. Chem. Phys. **109**, 10195 (1998).

[4] M. Ovchinnikov, B. L. Grigorenko, K. C. Janda, and V. A. Apkarian, J. Chem. Phys. **108**, 9351 (1998).

[5] T. Ruchti, K. Förde, B. E. Callicoatt, H. Ludwigs, and K. C. Janda, J. Chem. Phys. **109**, 10679 (1998).

[6] T. Ruchti, B. E. Callicoatt, and K. C. Janda, Phys. Chem. Chem. Phys. **2**, 4075 (2000).

[7] J. H. Kim, D. S. Peterka, C. C. Wang, and D. M. Neumark, J. Chem. Phys. **124**, 214301 (2006).

[8] A. Braun and M. Drabbels, Phys. Rev. Lett. **93**, 253401 (2004).

[9] A. Braun and M. Drabbels, J. Chem. Phys. **127**, 114303 (2007).

[10] A. Braun and M. Drabbels, J. Chem. Phys. **127**, 114304 (2007).

[11] A. Braun and M. Drabbels, J. Chem. Phys. **127**, 114305 (2007).

[12] W. K. Lewis, B. E. Applegate, J. Sztáray, B. Sztáray, T. Baer, R. J. Bemish, and R. E. Miller, J. Am. Chem. Soc. **126**, 11283 (2005).

[13] W. K. Lewis, R. J. Bemish, and R. E. Miller, J. Chem. Phys. **123**, 141103 (2005).

[14] A. J. Stace and A. K. Shukla, J. Mass Spectr. and Ion Phys. **36**, 119 (1980).

[15] K. Stephan and T. D. Märk, Chem. Phys. Lett. **90**, 51 (1982).

[16] D. R. Worsnop, S. J. Buelow, and D. R. Herschbach, J. Phys. Chem. **88**, 4506 (1984).

[17] H. Haberland, Surf. Sci. **156**, 305 (1985).

[18] U. Buck and H. Meyer, Phys. Rev. Lett. **52**, 109 (1984).

[19] U. Buck and H. Meyer, J. Chem. Phys. **84**, 4854 (1986).

[20] P. Lohbrandt, R. Galonska, H. Kim, M. Schmidt, C. Lauenstein, and U. Buck, in *Atomic and Molecular Beams: The State of the Art 2000*, R. Campargue Ed., pp 623–636, Springer, Berlin, 2000.

[21] C. Steinbach, M. Fárník, U. Buck, C. A. Brindle, and K. C. Janda, **to be published**.

[22] Georg Portwich, Diplomarbeit, Georg-August University Göttingen (Germany, 1994).

[23] P. Slavíček, P. Jungwirth, M. Lewerenz, N. H. Nahler, M. Fárník, and U. Buck, J. Phys. Chem. A **107**, 7743 (2003).

[24] D. Bonhommeau, A. Viel, and N. Halberstadt, J. Chem. Phys. **120**, 11359 (2004).

[25] D. Bonhommeau, N. Halberstadt, and A. Viel, J. Chem. Phys. **124**, 024328 (2006).

[26] D. Bonhommeau, A. Viel, and N. Halberstadt, J. Chem. Phys. **123**, 54316 (2005).

[27] D. Bonhommeau, T. Bouissou, N. Halberstadt, and A. Viel, J. Chem. Phys. **124**, 164308 (2006).

[28] D. Bonhommeau, N. Halberstadt, and A. Viel, J. Chem. Phys. **124**, 184314 (2006).

[29] D. Bonhommeau, N. Halberstadt, and U. Buck, Int. Rev. Phys. Chem. **26**, 353 (2007).

[30] D. Bonhommeau, P. T. Lake, Jr., C. L. Quiniou, M. Lewerenz, and N. Halberstadt, J. Chem. Phys. **126**, 051104 (2007).

[31] D. Bonhommeau, M. Lewerenz, and N. Halberstadt, subm. .

From Helium Clusters to Helium Droplets: Spectroscopy and Dynamics of Embedded Molecules

R. Lehnig, P. Raston, J. Michaud, J. Landry, Y. Xu, and W. Jäger
Department of Chemistry, University of Alberta, Edmonton, AB, Canada T6G 2G2

Microwave and infrared spectroscopy, in combination with molecular beam methods, has allowed us to study small to intermediate-sized doped He_N [1,2,3] and $(H_2)_N$ clusters [4,5] with atom-by-atom resolution. *N*, the number of helium atoms or hydrogen molecules, reaches up to 70 for the case of He_N – OCS. The non-classical behaviour of rotational constant *B* signals the onset of 'microscopic superfluidity' at rather small cluster sizes with *N* around 10. Oscillatory behaviour of *B* at larger cluster sizes is indicative of the *aufbau* of a helium solvation shell structure. At *N*=70, *B* has still not converged to the nanodroplet limit and the line widths are narrow and instrument limited. [6]
Microwave spectra of the corresponding rotational transitions of OCS in helium droplets (N~5000), have line widths of about 0.4 GHz, broader by about a factor of 10000 than the microwave cluster transitions. [7] Helium droplet rotational spectra of OCS with J up to 3 show fine structure, similar to what was observed in the corresponding infrared – microwave double resonance spectra. [8] We also found distinct fine structure in the *J*,*K*=1,1 microwave inversion tunneling transition of ammonia in helium droplets near 21.7 GHz (gas phase value 23.7 GHz). The spectrum consists of a broad feature, about 1.5 GHz wide, with a sharp peak of only 25 MHz width on top. The fine structures can be explained in terms of the development of sublevel structures of molecular energy levels in helium droplets.

[1] J. Tang, Y. Xu, A. R. W. McKellar, and W. Jäger, Science **297**, 2030 (2002).
[2] Y. Xu, W. Jäger, J. Tang, and A. R. W. McKellar, Phys. Rev. Lett. **91**, 163401 (2003).
[3] W. Topic, W. Jäger, N. Blinov, P.-N. Roy, M. Botti, and S. Moroni, J. Chem. Phys. **125**, 144310, (2006).
[4] J. M. Michaud and W. Jäger, HRMS Dijon 2007, Dijon, France, 03.-07. Sept. 2007, F1.
[5] J. N. Landry and W. Jäger, PRAHA 2006, Prague, Czech Republic, 29. Aug.-02. Sept. 2006, L11.
[6] A. R. W. McKellar, Y. Xu, and W. Jäger, Phys. Rev. Lett. **97**, 183401 (2006).
[7] R. Lehnig, P. Raston, and W. Jäger, manuscript in preparation.
[8] S. Grebenev, M. Havenith, F. Madeja, J. P. Toennies, A. F. Vilesov, J. Chem. Phys. **113**, 9060 (2000).
[8] R. Lehnig and W. Jäger, submitted to J. Chem. Phys.

Ionization Dynamics in Helium Droplets and Mercury Clusters

Daniel M. Neumark
Department of Chemistry
University of California
Berkeley, CA 94720
USA

Photoionization dynamics in clusters can be very different from those observed in isolated atoms and molecules. The cluster environment can mediate the ionization mechanism itself and affect the resulting photoelectron energy and angular distribution. In this talk, two such examples will be presented, covering (a) photoionization of He droplets doped with rare gas atoms using tunable synchrotron radiation and (b) time-resolved photoelectron imaging of mercury cluster anions. In the He droplet work, the droplets are excited at 21.6 eV. This excitation migrates to the rare gas atom and ionizes it via a Penning process. The resulting photoelectron image and spectrum shows direct ionization from He* in its $1s2p(^1P_1)$ and $1s2s(^1S_0)$ states, inelastically scattered electrons with energies exceeding the conduction band energy of liquid He (1.3 eV) in the largest droplets, and very slow electrons attributed to electrons that become temporarily trapped at the cluster surface.

Hg_n clusters in the 10-30 atom size regime act as semiconductors with a filled *s*-band and well-separated, empty *p*-band. In the Hgn^- anions, the excess electron resides at the bottom of the *p*-band. In recent time-resolved experiments, conducted in collaboration with Ori Cheshnovsky, we excite the $p \leftarrow s$ transition with a femtosecond laser pulse and use time-resolved photoelectron spectroscopy to follow the ensuing dynamics, specifically the lifetime of the transient excited state created by the pump pulse and the time scale for electron-hole relaxation, recombination, and ejection of the excess electron by Auger decay. For Hg_{13}^-, these processes occur on a time-scale of about 400 fs. We are currently investigating the competing roles of electron and hole relaxation in these dynamics.

Positive and negative ion formation upon free electron interaction with doped helium droplets

S. Denifl, F. Zappa, I. Mähr, O. Echt, A. Mauracher, M. Probst, T.D. Märk and P. Scheier
Institut für Ionenphysik und Angewandte Physik, Universität Innsbruck, Technikerstr. 25, A-6020 Innsbruck, Austria

The inelastic electron interaction (ionization/attachment) with doped helium droplets is studied utilizing a two sector field mass spectrometer. The dopands range from diatomic molecules such as I_2 to water, halocarbons, biomolecules and fullerenes. Positive mass spectra are recorded and are compared with results in the gas phase. Moreover, negative ion mass spectra are recorded at the electron energies where resonances appear. Both negative and positive mass spectra show that clusters are easily formed by embedding single molecules in the helium droplets. For anions appearing in the mass spectra, the ion yield is determined as a function of the electron energy. In several cases we observe a substantial stabilization of complex product ions compared to the gas phase. Solvation of both anions and cations in He is observed in several cases and investigated mass spectrometrically.

The interest in the studies of helium clusters doped with atoms or molecules [1,2] can be explained by the remarkable ability of helium droplets in picking-up atoms and molecules and the subsequent possibility to create new molecular complexes inside the droplet. Helium droplets provide thereby an extremely low temperature environment at T = 0.37 K. Embedded neutral atoms or molecules are cooled efficiently by the transfer of their internal energy to the surrounding helium matrix. Subsequently this excess energy is then released by thermal evaporation of the loosely bound helium atoms from the droplet. This can cause a substantial shrinking of the droplet as the binding energy of a helium atom in the droplet is only 0.6 meV [1]. The ultra-low temperature enables state selective experiments that are hardly possible with other techniques [3].

So far experiments with pure and mixed doped clusters of atmospherical and biological relevance have been mainly carried out by means of optical spectroscopy (see reviews in [1,2]). Also recently several electron impact ionization studies of molecules embedded in helium droplets have been reported [4-9]. In contrast electron attachment processes to (doped) helium droplets have been rarely studied (see review in [10]). Northby et al. proposed that electron capture to pure helium clusters is only possible in large droplets ($N > 0.75\times10^5$) and that electron attachment produces bubbles in the interior of the cluster [11]. Indeed the smallest pure helium cluster anion with a size of 9.3×10^4 was observed by Toennies and co-workers [12]. Moreover, electron attachment to SF_6, O_2 and H_2O embedded in He clusters was observed indirectly by the decrease of the neutral cluster yield [13]. Very recently we have published the first mass spectrometric investigation of negative ions formed via electron attachment to molecules embedded in helium clusters [14]. The molecules chosen for this first study have been the nucleobases adenine, thymine and partially methylated or deuterated thymine, respectively. Previously these biomolecules were studied intensively in the gas phase where a remarkable site selectivity of the dissociative electron attachment (DEA) was observed [15] which also remained for DEA to these molecules in helium droplets (see [14]).

Here we present as an example a detailed study of electron attachment to chloroform embedded in helium droplets. We have chosen this molecule as the first case in our systematic investigations with doped helium droplets due to its very high cross section upon dissociative

electron capture close to zero eV. We present the negative mass spectrum of chloroform recorded at the electron energy of 1.5 eV und for anions identified in the spectra we show the corresponding ion efficiency curves in the electron energy range from about 0 eV up to about 27 eV. We compare the present results with previous observations for gas phase chloroform [16]. In addition to our study of negative ions we have also recorded the positive mass spectrum at the electron energy of about 70 eV which is compared with the mass spectrum of chloroform in the gas phase.

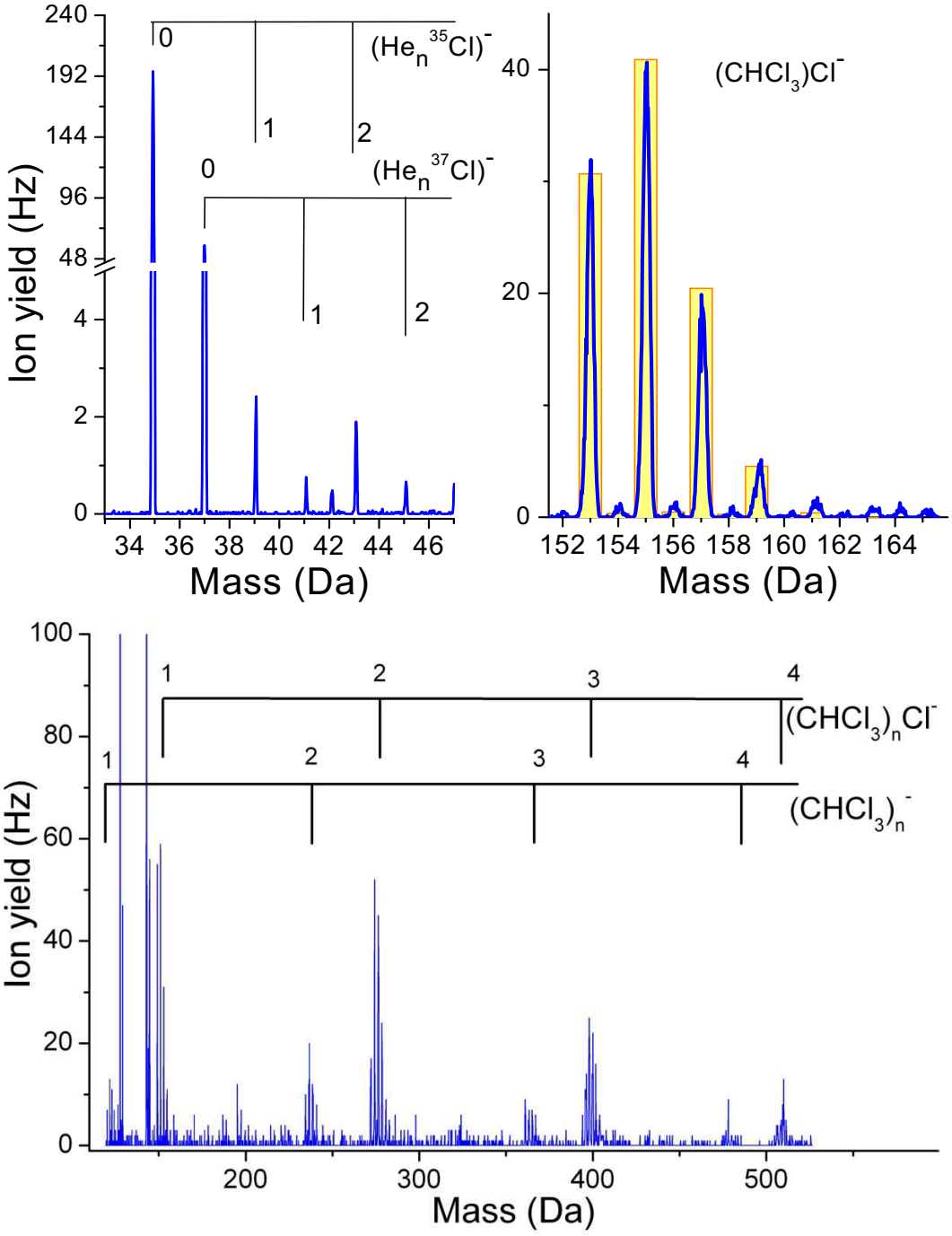

Figure 1: Negative ion mass spectrum of chloroform embedded in helium droplets in the mass range from 115 Da up to 520 Da (bottom) recorded at the electron energy of 1.5 eV. The

intense peaks at 127 Da and 146 Da can be ascribed to SF_5^-/SF_6 and SF_6^-/SF_6, respectively. The panel top left shows the mass region close to Cl^-. The panel top right shows the measured spectrum (line) for the chlorinated monomer anion compared with the calculated isotope pattern (columns).

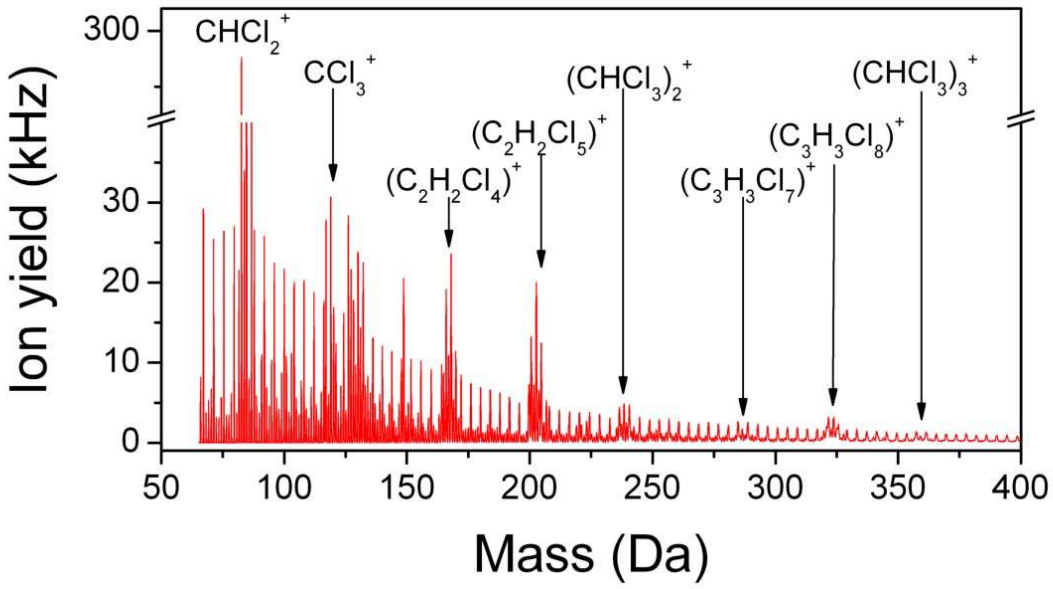

Figure 2: Positive ion mass spectrum of chloroform embedded in helium droplets in the mass range between 85 Da and 400 Da recorded at the electron energy of 70 eV.

Figure 1 shows the negative mass spectrum of chloroform embedded in helium in the mass range from about 115 Da up to 530 Da. The mass spectrum is recorded at the electron energy of 1.5 eV; close to the energy where the strongest signal of anion formation can be observed. Non-dissociated cluster anions of chloroform are only weakly present in this mass spectrum, however, more intense are the ion yields of anions formed via fragmentation of chloroform clusters upon DEA. This result is in accordance with many previous experiments with homogenous clusters (albeit not available for chloroform) showing that fragment cluster anions formed by intracluster fragmentation are more abundant than undissociated cluster anions [17]. The fragmentation pattern is clearly different to the positive ion case shown in Figure 2. The most abundant fragment anions are the chlorinated cluster anions while for positive ions singly or doubly dechlorination of the parent cluster ions are the main fragmentation processes. Also included in Figure 1 is a close up of the mass region of the Cl^- anion. This mass spectrum is not corrected for background ion signal of $^{35}Cl^-$ and $^{37}Cl^-$ resulting from electron attachment to gas phase chloroform streaming along the droplets into the ion source. The huge cross section for the gas phase reaction of DEA to chloroform close to 0eV electron energy (s-wave attachment) results in a high anion yield of Cl^- from this background contamination. At the same time the electrons require a kinetic energy of roughly 2 eV to penetrate into the droplets which immediately reduces the capture cross section by several orders of magnitude. Furthermore, autodetachment of the electron from the droplet in competition to DEA to the embedded chloroform reduces the anion yield even more. Therefore most of the ion signal appearing at mass 35 Da and 37 Da arises from DEA to isolated chloroform carried into the ion source. The background corrected energy scan shows that only very little of the signal originates at this electron energy from DEA to chloroform in

the droplet. However, emphasis should be placed on the series of peaks visible in the mass spectrum at masses above Cl^- which can be unambiguously ascribed to Cl^- dissolved in helium atoms. The abundance of these complexes is about half of the bare anion while for larger fragment anions this helium solvation effect is much weaker and the abundance is reduced to a few percent of the bare anion, e.g. see panel top right in Fig. 1, where the measured spectrum for the chlorinated monomer anion is compared with the calculated isotope pattern.

The positive mass spectrum recorded at 70 eV (Figure 2) shows that for chloroform no quenching of fragmentation occurs and instead the relative abundance of the parent ion even decreases upon ionization inside the helium droplet. In addition, for higher cluster series of chloroform less fragmentation can be observed, i.e. a softening effect is rather induced by the presence of a chloroform cluster than by the helium droplet. In the case of negative ions a substantial difference to the processes in the gas phase can be observed: large cross sections at low energies which can be ascribed to s-wave attachment process (like for Cl^-) are reduced to the same order of magnitude like core excited resonances at higher electron energies. The present results demonstrate that processes in the helium droplet environment can differ substantially from those of free electron attachment reactions in the gas phase.

Acknowledgements: This work has been supported by the FWF, Wien, Austria and the European Commission, Brussels. F.Z. gratefully acknowledges a post-doc grant from Brazilian agency CNPq.

References:

[1] J.P. Toennies and A.F. Vilesov, Angew. Chem. Int. Ed. **43**, 2622 (2004) and references cited therein
[2] F. Stienkemeier, and K.K. Lehmann, J. Phys. B: At. Mol. Opt. Phys. **39**, R127 (2006)
[4] M. Lewerenz, B. Schilling and J.P Toennies, J. Chem. Phys. **102**, 8191 (1995)
[5] T. Ruchti, K. Forde, B.E. Callicoatt, H. Ludwigs and K.C. Janda, J. Chem. Phys. **109**, 10679 (1998)
[6] F. Zappa, S. Denifl, I. Mähr, J. Lecointre, F. Rondino, O. Echt, T.D. Märk and P. Scheier, Eur. Phys. J. D **43**, 117 (2007)
[7] S. Yang, S.M. Brereton, M.D. Wheeler and A.M. Ellis, J. Phys. Chem. A **110**, 1791 (2006)
[8] S. Yang, S.M. Brereton, M.D. Wheeler and A.M. Ellis, Phys. Chem. Chem. Phys. **7**, 4082 (2005)
[9] S. Yang, S.M. Brereton, M.D. Wheeler and A.M. Ellis, Int. J. Mass Spectr. **253**, 79 (2006)
[10] J.A. Northby, J. Chem. Phys. **115**, 10065 (2001)
[11] J.A. Northby, C. Kim and T. Jiang, Physica B **197**, 426 (1994)
[12] U. Henne and J.P. Toennies, J. Chem. Phys. **108**, 9327 (1998)
[13] M. Farnik and J.P. Toennies, J. Chem. Phys. **118**, 4176 (2003)
[14] S. Denifl, F. Zappa, I. Mähr, J. Lecointre, M. Probst, T.D. Märk and P. Scheier, Phys. Rev. Lett. **97**, 043201 (2006)
[15] S. Ptasinska, S. Denifl, P. Scheier, E. Illenberger and T.D. Märk, Angew. Chem. Int. Ed. **44**, 6941 (2005)
[16] S. Denifl, A. Mauracher, P. Sulzer, A. Bacher, T. D. Märk and P. Scheier, Int. J. Mass Spectrom. **265**, 139 (2007)
[17] E. Illenberger, Chem. Rev. **92**, 1589 (1992)

Elementary aspects of chemical reactions on oxide surfaces: Case Studies for ZnO and TiO_2

Christof Wöll
Chair for Physical Chemistry I, Ruhr-University Bochum, 44780 Bochum, Germany

Presently, methanol, the third most-important chemical product of chemical industry, is produced using a $Cu/ZnO/Al_2O_3$ catalyst, with small Cu particles promoted by their interaction with the ZnO substrate as the active component. Despite this importance there has been a general lack of information about fundamental chemical processes on ZnO surfaces, in particular in the case of single crystal substrates. In contrast to surfaces of metal single crystals, the structure of adsorbate phases is typically not well known, even for simple molecules like CO the presence of ordered phases has been demonstrated only for very few cases. In addition, there is a general lack of information about the vibrational spectra of adsorbates on single-crystalline oxide substrates. This is a disturbing lack of information considering the wealth of vibrational spectroscopic data available for ZnO powders. A similar lack of information – which also makes a theoretical analysis of these adsorbate systems difficult - is present for TiO_2 single crystalline substrates.
In this talk I will briefly review recent data obtained by a variety of techniques, STM, EELS and He-atom scattering (HAS), which allow to draw a rather consistent picture of ordered phases of small adsorbates (H,CO,CO_2) on ZnO and TiO_2 substrates.
Subsequently, I will present discuss methanol formation on ZnO-substrates, where the elementary processes can be understood in considerable detail, both experimentally and also theoretically [1], and allow to put forward a model for the formation of CH_3OH from CO at O-vacancies (Bochum model, [2]).
Finally, the activation of CO_2 on a mixed-terminated ZnO(10-10)-surface [3] and the interaction of the resulting carbonate species with other coadsorbates will be discussed. The talk will close with a brief description of the situation for the rutile TiO_2(110)-substrate and an outlook for the investigation of metal atoms adsorbed on these substrates.

References

1. *The Chemistry and Physics of Zinc Oxide Surfaces*, Ch. Wöll, Prog. Surf. Sci., **82**, 55-120, (2007)
2. *Active sites on oxide surfaces: ZnO-catalyzed synthesis of methanol from CO and H_2* M. Kurtz, J. Strunk, O. Hinrichsen, M. Muhler, K. Fink, B. Meyer, Ch. Wöll Angew. Chem. Int. Ed., **44**, 2790-2794, (2005)
3. *CO_2 Activation by ZnO via Formation of an Unusual Tridentate Surface Carbonate: Results of a Combined Experimental and Theoretical Study*, Y.Wang, R.Kováčik, B.Meyer, K.Kotsis, D.Stodt, V.Staemmler, H.Qiu, F.Traeger, D.Langenberg, M.Muhler and Ch.Wöll, Angew. Chem. Int. Ed., (2007), in print

Infrared and ultraviolet spectroscopy of cold, protonated biomolecules

J. Stearns, O. Boyarkin, and T. Rizzo
Ecole Polytechnique Fédérale de Lausanne, Lausanne, Switzerland

One common approach to studying the conformational preferences of biological molecules is to transfer them into the gas phase to remove the complicating effects of the solvent. With the additional step of cooling the molecules, even relatively large systems can become amenable to high-resolution spectroscopic techniques. In particular, we are interested in spectroscopically identifying key structural features of folded proteins. The α-helix is one of the most important structures in biological molecules and has been studied previously in the gas phase only by ion mobility techniques. We use electrospray ionization to create gas-phase protonated peptides and trap them in a 22-pole ion trap maintained at 6 K. Collisions with helium in the cold trap cool the ions to 10-15 K before they are interrogated by ultraviolet and infrared lasers. We record ultraviolet spectra by photofragmentation, and use double-resonance methods to record infrared spectra of individual conformations. By comparing the infrared spectra to calculated frequencies, we can determine the conformations present.

We applied our spectroscopic tools to a series of helical peptides, which all include an aromatic amino acid as an ultraviolet chromophore. The infrared spectra of all the helices show resolved amide NH stretches, allowing assignment of each transition to a particular NH group, which in turn allows us to determine the conformations. For Ac-Phe-$(Ala)_5$-Lys-H^+, we observe two hydrogen-bonding arrangements of the peptide backbone and two orientations of the phenylalanine side chain, for a total of four conformers, all of which are helical. By contrast, the larger peptide Ac-Phe-$(Ala)_{10}$-Lys-H^+ has only two conformers, so the low-energy conformational landscape does not necessarily become more complex with increasing size.

Because of their rigid structures, helical peptides incorporating aromatic amino acids also offer the opportunity to study the interaction between the aromatic ring and the ammonium group. In protonated tryptophan, this interaction leads to an extremely short excited state lifetime, such that the ultraviolet spectrum is broad and unresolved even at low temperature. In the helical peptide Ac-Trp-$(Ala)_5$-Lys-H^+ the indole ring of the Trp residue and the charge on the Lys are separated in space, and the ammonium group is additionally capped by hydrogen bonding interactions. The result is a longer excited-state lifetime and a resolved ultraviolet spectrum. In contrast to the phenylalanine helices, Ac-Trp-$(Ala)_5$-Lys-H^+ appears as a single major conformer, suggesting that even a subtle change in the amino acid sequence can have significant consequences on conformation.

Excited-state deactivation pathways of protonated amino acids and peptides

G. Grégoire, J. P. Schermann and C. Desfrançois
Laboratoire de Physique des Lasers du CNRS, Institut Galilée, Université Paris13, 93430 Villetaneuse, France

C. Jouvet, P. Carçabal and C. Dedonder-Lardeux
Laboratoire de Photophysique Moléculaire du CNRS, Université Paris-Sud, 91405 Orsay Cedex, France

B. Lucas, M. Barat and J. A. Fayeton
Laboratoire des Collisions Atomiques et Moléculaires du CNRS, Université Paris-Sud, 91405 Orsay Cedex, France

Electrospray ionization (ESI) is a soft-ionization method that enables gas phase experiments on large biomolecules such as amino acids and peptides. UV photo-excitation studies of gas phase protonated amino acids and peptides have emerged in recent years with the combination of mass spectrometry and laser spectroscopy techniques and have revealed some of the non-radiative deactivation channels that cannot be studied directly by means of fluorescence spectroscopy.

In recent experiments, we have recorded the excited-state lifetimes of protonated aromatic amino acids ($TrpH^+$ and $TyrH^+$) by means of pump-probe photodissociation technique.[1] Besides, comparison with conventional collision induced dissociation (CID) experiments has revealed that among the ionic fragmentation channels observed, some are common to both excitation schemes while new de-activation pathways involving formation of radical species are evidenced in the UV-LID fragmentation pattern.

The excited state deactivation pathways of protonated aromatic amino acids (Tyrosine, Tryptophan and Tryptamine) have been studying by means of *ab initio* calculations using the coupled-cluster method with single and double excitation (CC2).[2] Excited state structure optimization has been performed and has revealed the very important role of an excited state dissociative along the NH stretch of the protonated amino group, the $\pi\sigma^*$ state. The coupling between the optically excited $\pi\pi^*$ state and the $\pi\sigma^*$ state induces an electron transfer from the indole ring towards the NH_3^+ group, which results in the neutralization of the amino group producing an unstable radical species, as for NH_4. Depending on the studied molecules, several deactivation pathways compete for, H^+ transfer to the aromatic chromophore, H loss and H transfer to the nearby carbonyl group. If the former will lead to internal conversion process to the electronic ground state, the two latter ones seem to imply direct dissociation in the excited state prior to energy redistribution (IVR) that leads to non-statistical type of fragmentation.

Furthermore, small peptides containing aromatic amino acids also exhibit a rich photo fragmentation pattern, with the presence or not of radical species. Interestingly, even when the aromatic residue is not directly protonated but embedded in GWG or GYG tripeptide, a rather short lifetime has been recorded that emphasizes a through-space mechanism for the electron transfer from the locally excited $\pi\pi*$ state to the $\pi\sigma*$ state located on the protonated amino group of the N-terminal glycine.[3]

References:
[1] H. Kang, C. Jouvet, C. Dedonder-Lardeux, S. Martrenchard, G. Gregoire, C. Desfrancois, J. P. Schermann, M. Barat, and J. A. Fayeton, Phys. Chem. Chem. Phys. 7, 394 (2005).
[2] G. Gregoire, C. Jouvet, C. Dedonder, and A. L. Sobolewski, J. Am. Chem. Soc. **129**, 6223 (2007).
[3] G. Gregoire, C. Dedonder-Lardeux, C. Jouvet, C. Desfrancois, and J. A. Fayeton, Phys. Chem. Chem. Phys. **9**, 78 (2007)

Gas-phase biomolecules investigated with FELIX

Jos Oomens
FOM Institute for Plasma Physics 'Rijnhuizen', Nieuwegein, The Netherlands
Nick Polfer
University of Florida, Gainesville, FL

Particularly since the invention of electrospray ionisation (ESI) by John Fenn [1], mass spectrometry (MS) has become one of the key analytical technologies in biochemistry. Compared to other tools such as nuclear magnetic resonance (NMR), x-ray crystallography (XRD) and infrared (IR) spectroscopy, the extreme sensitivity of typical MS methods allows characterization of samples in attomole quantities. However, the structural information obtained from standard MS methods is generally limited to the primary molecular structure. Nonetheless, the amount of information that can be extracted from MS^n experiments is impressive, as exemplified by MS based proteomics, where the amino acid sequence of peptides is recovered from the fragment masses that result from collision induced dissociation (CID) of the peptide [2].

To obtain higher order structural information on gas-phase biomolecules in MS research, more specialistic methods have in recent years been developped. Ion mobility, i.e. ion chromotagraphy, yields the collision cross-section of the ions, which allows one to discriminate between folded and extended structures. More detailed information on secondary structures can be obtained by IR spectroscopy, mainly on account the high sensitivity of vibrational frequencies to hydrogen (and metal) bonding interactions, which determine the main secondary structural motifs.

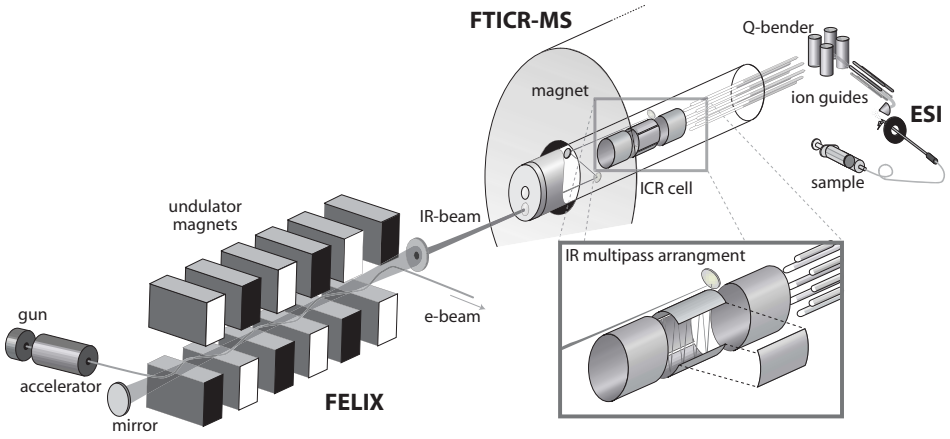

Figure 1: Schematic of the experiment showing the free electron laser FELIX and the FTICR-MS with the ESI ion source and ion inlet system.

IR spectroscopy on gas-phase ions has been notoriously difficult due to the extremely low ion densities as a consequence of space charge. Over the past decades, efficient action spectroscopy methods based mainly on photodissociation have been developped, see e.g. Ref. [3]. Our experiments, outlined in Figure 1 [4], make use of the free electron

laser FELIX, which induces multiple photon dissociation (MPD) upon resonance between the laser wavelength and an IR allowed transition in the biomolecular ion. The ions are generated by ESI and mass-selectively stored in a Fourier Transform Ion Cyclotron Mass Spectrometer (FTICR-MS). The FELIX induced dissociation products are detected by the mass spectrometer and their intensity is plotted against the IR wavelength to generate a 'surrogate' for the actual absorption spectrum. Comparison of these spectra to spectra computed using density functional theory have shown that the IRMPD spectra are surprisingly close to linear absorption spectra and hence, computations for different possible conformers allow to identify secondary structures.

In this contribution, we present some of our recent studies on biomolecules, in particular on the structure of peptide fragments resulting from CID and on the balance between zwitterionic and non-zwitterionic structures in the gas phase.

CID fragments. Fragmentation of protonated peptides by CID is the most widely used method in peptide sequencing MS, recovering the amino acid sequence of peptides and proteins. Much less is known about the actual molecular structure of the resulting fragments, mainly due to the fact that they occur only in minute quantities as charged gas-phase species in a mass spectrometer. Condensed phase structural methods that are widely used in biochemistry, such as XRD and NMR, are therefore not applicable.

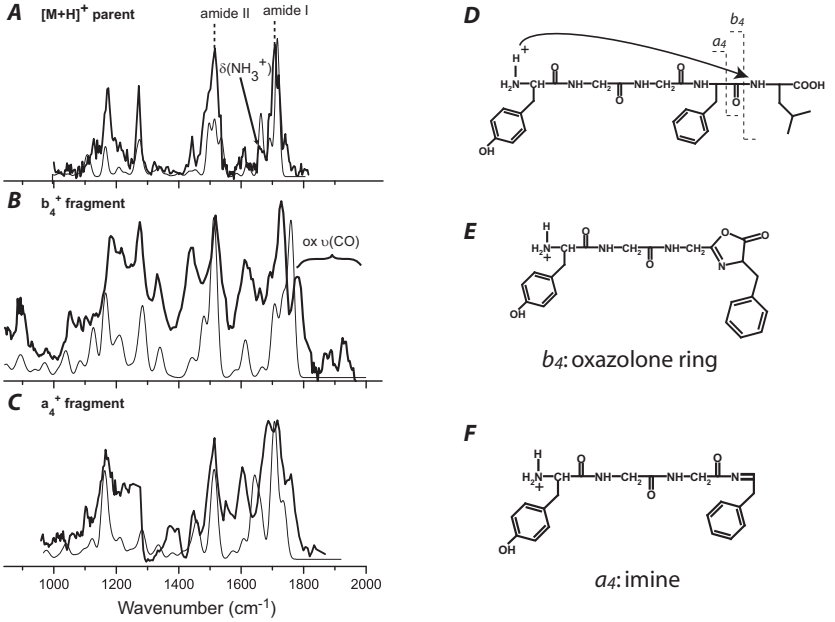

Figure 2: IRMPD spectra compared to the best theoretical spectra for the protonated parent and the two fragment ions (A-C). Linear representation of protonated Leucine-enkephalin, showing cleavages leading to the b_4 and a_4 fragments (D) and the proposed linear structures of the fragments (E-F).

Our IR spectroscopic studies have mainly focused on the pentapeptide Leu-enkephalin (Tyr-Gly-Gly-Phe-Leu) and its CID induced fragments. They reveal not only the molecular structure of the fragments, but also give information on the reaction mechanisms, which have been widely investigated using mainly theoretical and MS methods [7]. The

IR spectra of the protonated peptide and its b_4 and a_4 fragments are shown in Figure 2 (b_4 results from cleavage of the fourth amide bond; a_4 results from CO loss from b_4).

The two strongest bands in the spectrum of the protonated parent are easily recognized as the unresolved CO stretch and NH bend modes of the amide moieties in the molecule. In condensed phase IR spectroscopy, these bands are referred to as the amide I and amide II bands, respectively. The NH_3^+ deformation mode (arrow) indicates that the molecule is protonated on the N-terminus.

Historically, *b*-type fragments were believed to feature an acylium $-C{\equiv}O^+$ moiety at the C-terminus [5], although later, formation of an oxazolone ring (Figure 2) was found to be more favorable [6]. Our b_4 fragment spectrum confirms this conclusion, particularly by the appearance of several bands blue shifted with respect to the amide I band. They are assigned to CO stretching modes of the oxazalone ring, where the exact position of the band depends on the site of protonation [8]. Hence, observing the intensity of each of the oxazolone CO stretch modes as a function of time delay after the fragmentation event, gives direct experimental evidence [9] for a mobile proton [11].

The a_4 fragment spectrum clearly lacks oxazolone ring features, but instead shows bands that agree well with an imine type structure [9], i.e. containing a C=N double bond, as was indeed theoretically predicted [7]. In addition, evidence is found for cyclized fragment structures [9]; upon re-opening of such cyclic peptides, permutation of the amino acid sequence may occur, potentially undermining the interpretation of MS^n data [10].

Zwitterions in the gas phase. Although it is now well established that even the most basic amino acids do not form zwitterionic structures in the gas phase [12], the question remains how much stabilization from polar solvent molecules or counter ions is required to favor zwitterionic structures over canonical structures. We explore this fine balance in a number of studies on tryptophan (Trp) and several other amino acids.

In solution, amino acids adopt zwitterionic structures and a basic question is how many water molecules are necessary to induce conversion from the canonical form to the zwitterion. We address this question by studying the IR spectra of microsolvated Trp clusters generated in a moisturized molecular jet expansion. The transition from canonical to zwitterionic structures can be traced conveniently in the mid-IR because of the $\approx$100 cm^{-1} red-shift of the carboxylate COO^- stretch compared to the carboxylic acid C=O stretch. A gradual increase of the carboxylate stretch is observed starting at five attached water (or methanol) molecules, in excellent agreement with DFT calculations [13].

In overal ionic species such as metal cationized amino acids, a zwitterionic amino acid structure forms a salt-bridge complex, versus a charge-solvated complex for an amino acid in its canonical form. To some extent, alkali metal ions are able to induce zwitterionic amino acids: only the most basic amino acid aginine becomes zwitterionic and only for alkali metals larger than Na [14]. Even the next basic amino acid, lysine, is non-zwitterionic regardless of the alkali ion attached [15]. Doubly charged alkaline earth metals, on the other hand, were very recently found to form salt-bridge complexes readily, even with a non-basic amino acid such as Trp [16].

Given the high diagnostic value of the CO stretch modes in either carboxylic or carboxylate moieties, it is of interest to find an intrinsic value for the (asymmetric) carboxylate stretch mode. Although this vibrational band is well-known from condensed-phase IR spectra, the free, unbound stretching vibration of a carboxylate moiety has to date

not been reported. At the meeting we will show mid-IR negative ion spectra that reveal the carboxylate stretch mode in free space for a variety of systems.

Acknowledgments. We gratefully acknowledge the fruiful collaborations with R.C. Dunbar (Cleveland, OH), R.A. Jockusch (Toronto), B. Paizs (Heidelberg), and E.R. Williams (Berkeley, CA) as well as the excellent support by the FELIX staff.

[1] J.B. Fenn, M. Mann, C.K. Meng, C.M. Whitehouse, Science **246**, 64 (1989).

[2] H. Steen, M. Mann, Nat. Rev. Mol. Cell Biol. **5**, 699 (2004).

[3] C. Kapota, J. Lemaire, P. Maitre, G. Ohanessian, J. Am. Chem. Soc. **126** 1836 (2004). M.F. Bush, J.T. O'Brien, J.S. Prell, R.J. Saykally, E.R. Williams, J. Am. Chem. Soc. **129**, 1612 (2007). U.J. Lorenz, N. Solca, J. Lemaire, P. Maitre, O. Dopfer, Angew. Chemie Int. Ed. **46**, 6714 (2007). E.J. Bieske, Chem. Soc. Rev. **32**, 231 (2003). K.R. Asmis, G. Santambrogio, J. Zhou, E. Garand, J. Headrick, D. Goebbert, M.A. Johnson, D.M. Neumark, J. Chem. Phys. **126** 191105 (2007). G.E. Douberly, A.M. Ricks, B.W. Ticknor, P.v.R. Schleyer, M.A. Duncan, J. Am. Chem. Soc. DOI: 10.1021/ja0753593. J.A. Stearns, O.V. Boyarkin, T.R. Rizzo, J.Am. Chem. Soc. DOI: 10.1021/ja076507s.

[4] N.C. Polfer, J. Oomens, PCCP **9**, 3804 (2007).

[5] K. Biemann, Biomed. Environ. Mass Spectrom. **16** 99 (1988).

[6] T. Yalcin, C. Khouw, I.G. Czismadia, A.G. Harrison, J. Am. Soc. Mass Spectrom. **6**, 1165 (1995).

[7] B. Paizs, S. Suhai, Mass Spectrom. Rev. **24**, 508 (2005).

[8] N.C. Polfer, J. Oomens, S. Suhai, B. Paizs, J. Am. Chem. Soc. **127** 17154 (2005).

[9] N.C. Polfer, J. Oomens, S. Suhai, B. Paizs, J. Am. Chem. Soc. **129** 5887 (2007).

[10] A.G. Harrison, A.B. Young, C. Bleiholder, S. Suhai, B. Paizs, J. Am. Chem. Soc. **128** 10364 (2006).

[11] A.R. Dongre, J.L. Jones, A. Somogyi, V.H. Wysocki, J. Am. Chem. Soc. **118**, 8365 (1996).

[12] C.J. Chapo, J.B. Paul, R.A. Provencal, K. Roth, R.J. Saykally, J. Am. Chem. Soc. **120**, 12956 (1998).

[13] M.N. Blom, I. Compagnon, N.C. Polfer, G. von Helden, G. Meijer, S. Suhai, B. Paizs, J. Oomens, J. Phys. Chem. A **111** 7309 (2007).

[14] M.W. Forbes, M.F. Bush, N.C. Polfer, J. Oomens, R.C. Dunbar, E.R. Williams, R.A. Jockusch, J. Phys. Chem. A, accepted.

[15] M.F. Bush, M.W. Forbes, R.A. Jockusch, J. Oomens, N.C. Polfer, R.J. Saykally, E.R. Williams, J. Phys. Chem. A **111**, 7753 (2007).

[16] R.C. Dunbar, N.C. Polfer, J. Oomens, J. Am. Chem. Soc. accepted.

Hot topic papers

Experimental studies of the surface-catalysed recombination of H and D atoms at 15 K with relevance to the formation of H_2 in the interstellar medium

S.D. Price
Chemistry Department, University College London,
20 Gordon Street, London, WC1H 0AJ. UK.

Summary
This presentation will describe the results of experiments to measure the ro-vibrational energy distribution of HD molecules generated from atomic recombination on a cold (15 K) graphite surface. Such measurements are of direct relevance to understanding the energy budget in interstellar clouds, where molecular hydrogen is synthesized by atomic recombination on cold interstellar dust grains. Our results indicate considerable vibrational excitation of the nascent HD molecules. Recent theoretical work, and astronomical observations, supports this general conclusion that recombination of H atoms on surfaces relevant to the interstellar medium results in considerable internal excitation of the nascent molecular hydrogen.

1. Introduction

Di-hydrogen (H_2) is the most abundant molecule in the interstellar medium (ISM) and is the precursor for all interstellar chemistry.[1] In the ISM H_2 is found in interstellar clouds, large cold objects consisting of gas and dust. It is these interstellar clouds that collapse to form stars. There are two general classes of cloud in the ISM: diffuse and dense.[1] Diffuse clouds can be easily penetrated by UV radiation, which can dissociate any H_2. Hence, in these regions, there must be an efficient formation pathway for molecular hydrogen to account for its observed abundance.[2] The synthesis of H_2 on the surfaces of the interstellar dust grains is now believed to be the most significant pathway for H_2 formation in the ISM.[3] Studies of stellar extinction curves have shown that the dust grains in the clouds are comprised of dielectric matter such as silicates and carbonaceous materials. In denser clouds, the grains are coated with molecular ices consisting of, for example, H_2O, CO_2, CO and CH_3OH.[4] However, in diffuse clouds the grains are essentially bare and at temperatures of 10 – 15 K.
Recombination of H atoms to form H_2 releases 4.5 eV of binding energy, and it is uncertain how this energy is redistributed in the ISM. This excess energy can flow into the dust grain but also can result in the internal or translational excitation of the nascent molecule. There may be a considerable impact on interstellar chemistry, and the overall interstellar energy budget, if the nascent H_2 molecules possess significant internal excitation.
This contribution reports the results of laser spectroscopic experiments which probe the internal excitation of HD formed on a dust grain analogue at 15 K. The HD molecules are formed from separate atomic beams of H and D that impinge directly on a highly orientated pyrolitic graphite (HOPG) surface that is held at 15 K. Resonance Enhanced Multi-Photon Ionisation (REMPI) is used to detect the excited ro-vibrational levels of HD ($v''>0$, J'') formed on the surface.[5-7]
There has been both experimental and theoretical work focussing on the formation of H_2 on interstellar dust, which has been summarised recently.[6,7] For experiments involving "low-energy" hydrogen atoms, which cannot chemisorb on graphite, early bolometric work clearly

showed that heterogeneous recombination occurs on a cryo-deposit at low temperatures (4 K).[8] More recent experimental work has often used the technique of temperature programmed desorption (TPD) to study the kinetics of the recombination of low-energy H atoms on a variety of surfaces, including olivine, amorphous carbon and water ice.[9-13] For the formation of HD on graphite surfaces' TPD has been used to estimate the recombination efficiency as a function of surface temperature.[11] These experiments indicate that there is some desorption of HD from the cold surface (5 – 7 K), but the flux for this "prompt" reaction is found to be low in comparison to the number of HD molecules desorbed between 10 and 20 K during the heating process. TPD experiments have also shown that the formation of HD on amorphous carbon surfaces is efficient between 8 - 20 K[11] and, when formed on amorphous water ice, the nascent HD is translationally cold.[13] Related TPD experiments to study recombination of amorphous water ice surfaces clearly showed nascent HD molecules thermalise in the pores of the porous film.[14,15]

The chemisorption of H(D) atoms to a graphite surface is an activated process; there is a barrier to chemisorption of 0.2 eV. This barrier is due to a carbon atom puckering out of the plane of the surface to bond with the H atom. This surface reconstruction, and thus chemisorption, is only possible with a hyper-thermal beam of incident atoms. Using such a H-atom source, this reconstruction has been observed by Hornaeker *et al. via* scanning tunnelling microscopy (STM).[16] These investigations indicate that hot D atoms binding to a graphite surface form two different characteristic structures, one with the two D atoms on opposite sides of a graphite hexagon (para) and the other with the D atoms adjacent on the graphite ring (ortho). Recombination of D atoms was found to proceed through the para structure. A subsequent study[17] found that the average translational energy for nascent D_2 moving normal to the surface was approximately 1.3 eV, leaving about 60% of the desorption energy to be distributed between ro-vibrational energy or to be deposited into the surface.

Zecho *et al*. have carried out STM experiments studying the chemisorption of D atoms on graphite surfaces,[18] and at low deuterium coverages only isolated D atoms were observed on the surface. However, when the coverage was increased deuterium dimers were found to dominate. Earlier work by Zecho *et al*. has verified experimentally the 0.2 eV barrier to chemisorption when H and D atoms chemisorb onto a HOPG surface.[19]

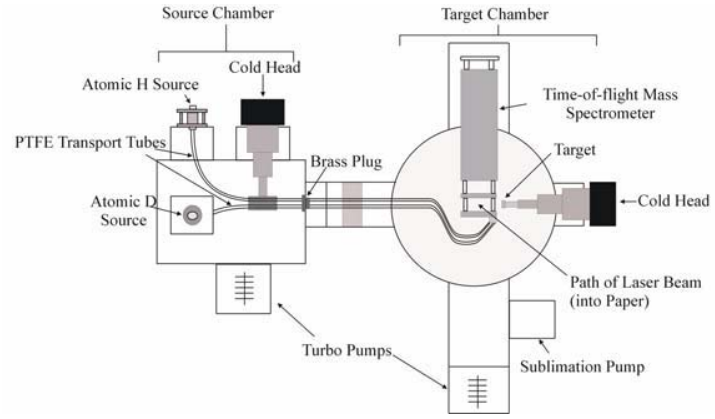

Figure 1. Schematic of the experimental apparatus

There has been a considerable amount of the theoretical work investigating the formation of H_2 on dust grain analogues. The majority of this work has concentrated on the Eley-Rideal mechanism.[20-26] Indeed, computational investigations first predicted the 0.2 eV barrier to H-atom chemisorption. More recent theoretical work has concentrated on the LH mechanism, which may be the more relevant for cold interstellar clouds.[27,28] Overall, all the theoretical

investigations have indicated that H_2 formed on dust grain analogues should possess considerable internal excitation.

As shown above, to date there is no information on the internal energy of the H_2 molecules formed on cold (15 K) prototypical interstellar surfaces. The objective of the experimental programme described in this presentation is to address this shortcoming and reveal the ro-vibronic excitation of the nascent hydrogen molecules.

2. Experimental

The UHV experimental apparatus is designed to probe the ro-vibrational excitation of nascent HD formed on an HOPG surface cryogenically cooled to 15 K (Figure X) and has been previously described in detail in the literature.[5,6] Separate thermal (300K) beams of H and D atoms, formed by the microwave dissociation of H_2 and D_2, continuously irradiate the surface. The HD formed on the surface is state selectively ionised using 2+1 REMPI *via* the E, F $^1\Sigma_g^+$ state. For example, ionisation of the $v'' = 5 - 7$ vibrational states requires wavelengths ranging from 235 – 241 nm. The resulting HD^+ signals are detected using time-of-flight mass spectrometry (TOFMS). For each vibrational state the REMPI signal is appropriately corrected for laser power variations and rotational transition strengths to yield the relative population for each J'' state detected.

It is important to note that the TOFMS measures the density of the HD molecules in a given (v'',J'') state and not the flux from the surface; the density and flux are related to each other by the molecular velocity. Thus, assuming that the nascent HD molecules do not have markedly different velocities then the fluxes of HD in the different (v'',J'') states, and hence the relative populations formed at the surface, should be well represented by the densities detected by the TOFMS.

3. Results

Our experiments clearly observe the formation of HD in v''=1-7. This contribution will present our recent results showing the first experimental ro-vibronic distribution for the formation of HD (v''>0, J'') form H and D atoms on a graphite surface at 15 K. A typical ro-vibrational distribution is shown in Figure 2 and clearly indicates that HD is predominantly formed with considerable vibrational excitation, v''= 4 appears the most densely populated vibrational state. These results will be placed in context of other experimental and theoretical work. In addition, the recent observation of interstellar infrared transitions, which have been assigned to the relaxation of nascent H_2 molecules which are ro-vibrationally excited (formation pumping), supporting our experimental observations, will also be discussed. The consequences of our measurements for interstellar chemistry will also be considered.

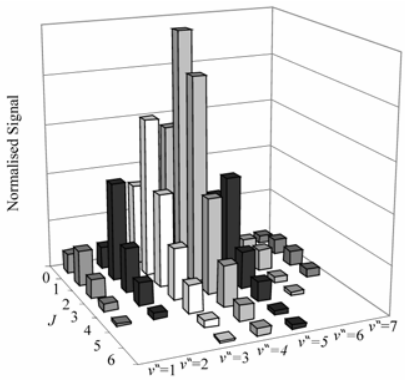

Figure 2. A ro-vibrational distribution measured for HD formed by atomic recombination on a cold graphite surface.

Acknowledgements

These experiments have been generously supported by the EPSRC and the Leverhulme Trust. The experiments form part of the UCL Centre for Cosmic Chemistry and Physics and the authors gratefully acknowledge valuable discussions with other members of the Centre. The support of the UK ASTROSURF network for allowing the authors to interact with the astronomical community is also invaluable.

References

[1] D.A. Williams and T.W. Hartquist *Acco. Chem. Res.* 32 (1999) 334
[2] R.J. Gould and E.E. Salpeter *Astrophys. J.* 138 (1963) 393
[3] D.J. Hollenbach and E.E. Salpeter *Astrophys. J.* 163 (1971) 155
[4] D.A. Williams and E. Herbst *Surf. Sci.* 500 (2002) 823
[5] J.S.A. Perry, J.M. Gingell, K.A. Newson, J. To, N. Watanabe and S.D. Price *Meas. Sci. Tech.* 13 (2002) 1414
[6] S.C. Creighan, J.S.A. Perry and S.D. Price *J.Chem.Phys.* 124 (2006) ArtNo:114701
[7] F. Islam, E.R. Latimer and S.D. Price *J.Chem.Phys.* 127 (2007) 064701
[8] T.R. Govers, L. Mattera and G. Scoles *J.Chem.Phys.* 72 (1980) 5446
[9] V. Pirronello, O. Biham, C. Liu, L.O. Shen and G. Vidali *Astrophys. J.* 483 (1997) L131
[10] O. Biham, I. Furman, N. Katz, V. Pirronello and G. Vidali *Mon. Not. Roy. Astron. Soc.* 296 (1998) 869
[11] N. Katz, I. Furman, O. Biham, V. Pirronello and G. Vidali *Astrophys. J.* 522 (1999) 305
[12] V. Pirronello, C. Liu, J.E. Roser and G. Vidali *Astronomy and Astrophysics* 344 (1999) 681
[13] J.E. Roser, S. Swords, G. Vidali, G. Manico and V. Pirronello *Astrophys. J.* 596 (2003) L55
[14] L. Hornekaer, A. Baurichter, V.V. Petrunin, D. Field and A.C. Luntz *Science* 302 (2003) 1943
[15] L. Hornekaer, A. Baurichter, V.V. Petrunin, A.C. Luntz, B.D. Kay and A. Al-Halabi *J.Chem.Phys.* 122 (2005) ArtNo:124701
[16] L. Hornekaer, Z. Sljivancanin, W. Xu, R. Otero, E. Rauls, I. Stensgaard, E. Laegsgaard, B. Hammer and F. Besenbacher *Phys. Rev. Lett.* 96 (2006) ArtNo:156104
[17] S. Baouche, G. Gamborg, V.V. Petrunin, A.C. Luntz, A. Baurichter and L. Hornekaer *J.Chem.Phys.* 125 (2006) ArtNo:084712
[18] A. Andree, M. Le Lay, T. Zecho and J. Kupper *Chem.Phys.Lett.* 425 (2006) 99
[19] T. Zecho, A. Guttler, X.W. Sha, B. Jackson and J. Kuppers *J.Chem.Phys.* 117 (2002) 8486
[20] P. Parneix and P. Brechignac *Astronomy and Astrophysics* 334 (1998) 363
[21] A.J. Farebrother, A.J.H.M. Meijer, D.C. Clary and A.J. Fisher *Chem.Phys.Lett.* 319 (2000) 303
[22] M. Rutigliano, M. Cacciatore and G.D. Billing *Chem.Phys.Lett.* 340 (2001) 13
[23] X.W. Sha and B. Jackson *Surf. Sci.* 496 (2002) 318
[24] A. Meijer, A.J. Fisher and D.C. Clary *J. Phys. Chem. A* 107 (2003) 10862
[25] S. Morisset, F. Aguillon, M. Sizun and V. Sidis *J. Phys. Chem. A* 108 (2004) 8571
[26] R. Martinazzo and G.F. Tantardini *J.Chem.Phys.* 124 (2006) ArtNo:124702
[27] S. Morisset, F. Aguillon, M. Sizun and V. Sidis *J.Chem.Phys.* 122 (2005) art. no.
[28] B. Kerkeni and D.C. Clary *Chem.Phys.Lett.* 438 (2007) 1

New methods in slowing down supersonic beams

Uzi Even
Sackler school of Chemistry, Tel Aviv University, Israel

We are developing two new methods to slow down supersonic beam. The first one is using reflection of a seeded supersonic beam from an "atomic paddle". The beam is generated by a cryogenic pulsed valve fed with a mixture of 10% Helium in Neon and cooled to 80K. The beam has a velocity of 520m/s with good uniformity (3%). After collimation the beam is reflected from a fast receding crystal surface. The crystal is mounted on a long rotating arm. If the tangential speed of the receding crystal is half of the beam velocity, that Helium atoms will come to rest at the laboratory frame.

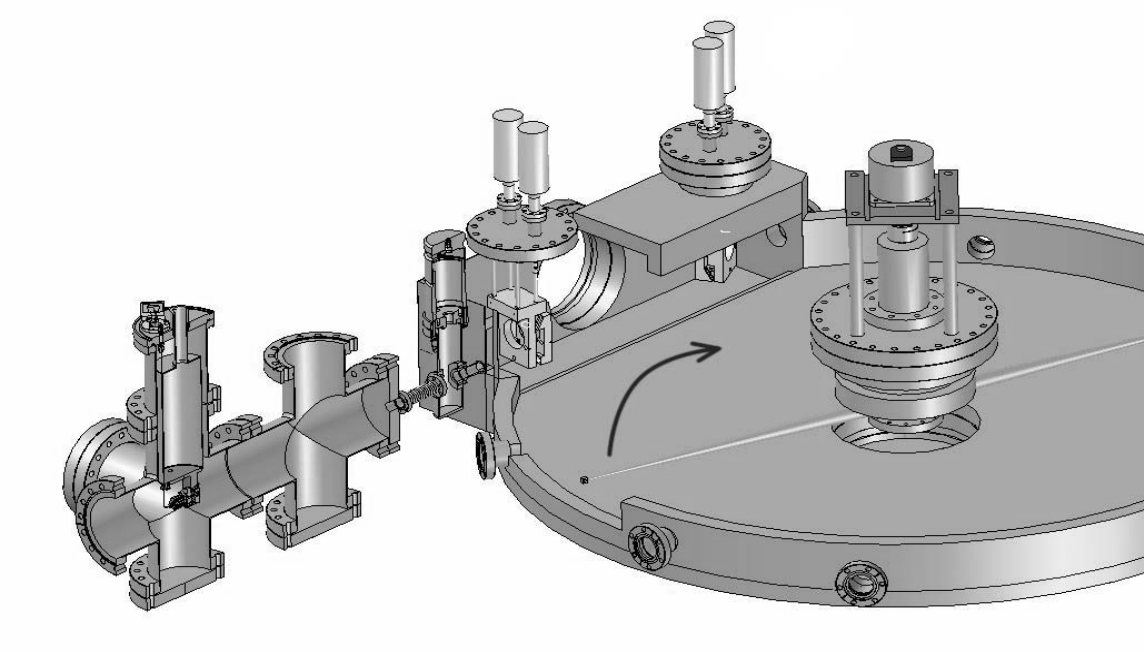

Figure 1:The cryogenic fast pulsed valve is on the left. The skimmed beam hits a silicon crystal mounted on a rotating arm and is elastically reflected to the detector chamber.

The first results (Figure 2) are promising and we managed to produce intense, directed beams of slow helium. Possible uses will open new roads in low energy collision with molecules, surface physics and quantum metrology.

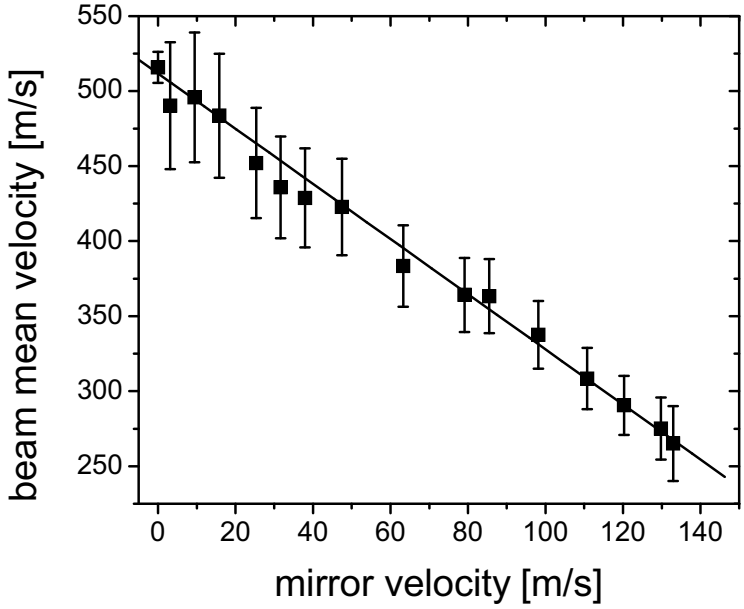

Figure 2: Reflected Helium velocity as a function of the receding mirror velocity

Another ongoing effort is producing a Zeeman slower of atoms and molecules. A series of pulsed intense magnetic fields is shown to be similar to a Stark slower for dipolar molecules. First results will be shown of slowing Ne^* with an array of 18 slowing stages.

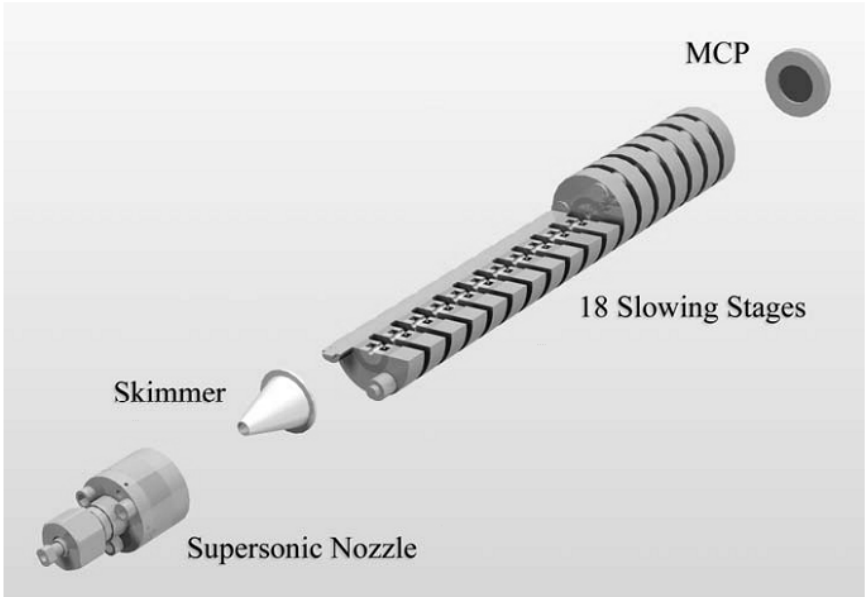

Figure 3: an array of 18 magnetic slowing stages

Dissociative Electron Attachment to Fragile Biomolecules Using Laser Induced Acoustic Desorption

Ilko Bald, Eugen Illenberger
Institut für Chemie und Biochemie, Freie Universität Berlin, Germany

Helga D. Flosadottir, Oddur Ingolfsson
Department of Chemistry, Science Institute, University of Iceland, Iceland

The interaction of low energy electrons with biomolecules is vitally important for the molecular mechanisms of radiation damage. The irradiation of a living cell leads to a cascade of ionisation events producing reactive secondary electrons with a most probable energy below 10 eV [1]. Previously it was demonstrated that electrons with kinetic energies below 12 eV are able to effectively induce single and double strand breaks in plasmid DNA [2]. The yield of DNA single strand breaks is even higher at electron energies below 1 eV [3]. The characteristic resonant features in the strand break yields indicate that dissociative electron attachment (DEA) may be the initial step of decomposition.
To elucidate the intrinsic properties of individual DNA building blocks, DEA of nucleobases [4], sugars [5] and phosphate esters [6] were studied previously in the gas phase.
However, a better understanding of electron induced processes in DNA requires the transfer of larger systems into the gas phase, which are composed of different DNA building blocks, for instance whole nucleotides. While the individual subunits of DNA (nucleobases, sugars and phosphate esters) can usually be transferred into the gas phase as intact molecules by appropriate thermal heating, this technique is no longer feasible for larger systems. Moderate heating of thymidine, e.g. (thymine coupled to 2-deoxy-D-ribose), showed that it is partly subjected to decomposition in the course of the evaporation process [7]. The standard methods matrix assisted laser desorption/ionisation (MALDI) and electrospray ionisation (ESI) are of limited use for DEA since a large number of ions are generated. However, the investigation of DEA requires neutral and intact molecules. A new experimental setup is presented here that utilises laser induced acoustic desorption (LIAD), which was successfully employed previously to desorb only neutral molecules [8].
A gentle desorption of intact molecules is demonstrated using thymidine. The ion yield curve of $[Thymine\text{-}H]^-$, which is generated by N-glycosidic bond cleavage in thymidine [7], exhibits a single maximum around 7 eV. The low-energy resonance at 1.2 eV that is observed in isolated thymine [4] is completely suppressed in thymidine.
Dissociative electron attachment to ribose-5-phosphate is studied applying laser-induced acoustic desorption. Electron attachment close to zero eV is observed resulting in the formation of $H_2PO_4^-$ and $(Ribose\text{-}H)^-$, which are created by a C-O and P-O bond cleavage, respectively. Both reactions represent a strand break in DNA or RNA at very low electron energies. DEA to ribose-5-phosphate is compared with metastable decay spectra of deprotonated ribose-5-phosphate obtained in MALDI measurements.

[1] S.M. Pimblott, J.A. LaVerne, Rad. Phys. Chem. **76**, 1244 (2007).
[2] B. Boudaiffa, P. Cloutier, D. Hunting, M.A. Huels, L. Sanche, Science **287**, 1658 (2000).
[3] F. Martin, P. D. Burrow, Z. Cai, P. Cloutier, D. Hunting, and L. Sanche, Phys. Rev. Lett. **93**, 068101 (2004).

[4] H. Abdoul-Carime, S. Gohlke, and E. Illenberger, Phys. Rev. Lett. **92**, 168103 (2004**)**.
[5] Bald, J. Kopyra and E. Illenberger, Angew. Chem. Int. Ed. 45 (2006) 4851.
[6] C. König, I. Bald, J. Kopyra and E. Illenberger, Phys. Rev. Lett. 97 (2006) 018105.
[7] S. Ptasinska, S. Denifl, P. Scheier, T. D. Märk, S. Gohlke, and E. Illenberger, Angew. Chem. Int. Ed. **45,** 1893 (2006).
[8] J. Perez, C.J. Petzold, M.A. Watkins, W.E. Vaughn, H.I. Kenttamaa, J. Amer. Soc. Mass Spectrom. 10, 1105 (1999).

Hydrogen for Energy Storage? – Probably, but not in my Car, and preferably not in yours either.

Thomas R. Govers
Aecono Consulting
59, rue de Prony, 75017 Paris, France

1. Introduction:

"*WEO 2006 reveals that the energy future we are facing today, based on projections of current trends, is dirty, insecure and expensive. But it also shows how new government policies can create an alternative energy future which is clean, clever and competitive – the challenge posed to the IEA by the G8 leaders and IEA ministers*" [1]. Such a challenge necessarily offers many opportunities, but I have the distinct impression that political and commercial lobbies are seizing these with more mediatic impact than do most scientists or university professors.

Transportation, which most readily relates to public opinion, is receiving widespread attention. Thanks to Governor Arnold Schwarzenegger "*California is investing millions of dollars to line our freeways with hydrogen fuelling stations so that low emission cars can travel up and down our wonderful state*," [2] and Governor Hillary Clinton "*Voted YES on targeting 100,000 hydrogen-powered vehicles by 2010*" [3]. As some of you (or few of you, as this is a October 10, 2007 release) may know, "*The European Union on Wednesday proposed a project worth as much as €1 billion to fund development of hydrogen-powered cars*" [4]. The - questionable, but politically highly attractive - argument is that hydrogen driven cars are environmental friendly because their exhaust contains only water vapour. The question where the hydrogen comes from is of course generally "forgotten" and proponents do not hesitate to claim that (untaxed) hydrogen as a fuel is no more expensive than gasoline, thereby also "forgetting" that public energy prices in many parts of the world consist mostly of taxes.

Hydrogen is bound to play an increasingly important role in the elaboration of sustainable energy policies. But not as a fuel for private vehicles, for which its physical and chemical properties are just not suitable. Europe's scientific community should not, I would think, remain silent when well-organised lobbies are attempting to convince the EC to waste €1 billion on a project [4] that has little innovative content and even less potential benefits.

2. Hydrogen facts rather then myths:

According to the EIA's 2007 International Energy Outlook, world energy consumption should exceed 700 Quadrillion Btu/year by the year 2030, as compared to the present value of about 500 Qbtu/year [5]. Most of the increase will take place in fast-developing countries in Asia, which will double their energy consumption over that same period. Coal will contribute the major share in meeting these new requirements, especially in China, where new energy

requirements are large and where coal is plentiful. The predicted increase in Chinese coal consumption, 47 Qbtu/year; is more than twice as large as present-day coal consumption in the US, the world's second largest coal consumer at about 23.5 Qbtu/year. It is not realistic to expect the people in developing countries to adopt consumption patterns that do not make economic sense. As there is little doubt that oil and –increasingly- coal will remain the main source of energy for several decades to come, the short- and medium term focus should be on saving energy, improving the efficiency of fossil-fuel extraction and conversion, optimising combined-power cycles, and, most urgently, developing CO_2 sequestration processes that are reliable and economically sustainable. When considering different fuel options for private and public transport, the overriding criteria should be overall energy efficiency and global CO_2 reduction rather than showcase ecology. For private transport, hydrogen-driven vehicles are about the least attractive option that one can imagine, especially if it relies on the "good old internal combustion" engine as proposed in BMW's 12 cylinder dual-fuel sedan [6].

Running an IC engine with hydrogen as a fuel is not exactly a new idea: the first IC engine, built in 1805 by Swiss inventor Isaac de Rivaz, used hydrogen as a fuel [7]. Starting in 1886, French army engineer Charles Renard developed an IC engine designed to propel a military hydrogen-filled airship, fueled by a mixture of gasoline and hydrogen. At the end of WW2, oil shortage prompted the re-discovery of gas-powered IC with bio-fuel generators to produce syngas typically containing 50% hydrogen. On-site generation of hydrogen, advertised as a potential solution for decentralised filling stations, was implemented by the French army at the battle of Fleurus, in 1794.

But running an IC engine on hydrogen results in an energy efficiency of only 10 to 15%, as compared to about 25% for a common-rail diesel, and 30% for a hybrid diesel [7]. The fuel production efficiency can reach 80% for diesel fuel, and 70% for hydrogen obtained by steam reforming of natural gas. Hydrogen liquefaction consumes at least 25% of its useful energy content. Compounding these efficiency figures, an IC engine fueled with liquid hydrogen is found to consume about 3 times more primary fossil fuel than a hybrid diesel. And it produces 3 times more CO_2. Since one can hardly imagine cleaning up our cities by dumping 3 times more pollution in someone else's back yard (or can we?), the best we can expect from this 200-year old invention is to consume 3 times too much fuel while needing to sequester 3 times more CO_2. Who needs a fuel guzzling BMW anyway?

The situation looks more realistic when considering a vehicle powered by a hydrogen fuel cell, rather than by an IC engine. Neglecting the substantially higher energy impact of distributing hydrogen rather than diesel fuel, and optimistically assuming a fuel cell efficiency of 50%, one obtains comparable overall efficiencies, about 25%, for the hydrogen car and for the hybrid diesel. Running prototype public vehicles to develop reliable, efficient and cost effective fuel cell does make sense, not only for hydrogen, but also other liquid fuels, in particular methanol [8]. But it is not necessary to line our highways with hydrogen filling stations to develop sustainable fuel cell technology.

3. Hydrogen in an E Economy:

Hydrogen will become an even less realistic option for private vehicles when electric power from nuclear plants or from renewable resources will gain in importance, the most likely

scenario to respond to Europe's energy requirements. Producing hydrogen by electrolysis to power a fuel-cell vehicle provides an overall energy efficiency of at best 23%, while a battery powered electric vehicle could yield an efficiency of 69% [9]. Electric vehicles, in particular plug-in hybrids ("PHEV's"), have the major advantage of being able to charge their batteries during night when electricity demand is low. They can also contribute to buffering discontinuous electricity sources, such as solar cells and wind turbines. Equipped with a fuel cell, they can provide electricity back-up for private homes and provide power in remote locations [10]. They will facilitate Europe's evolution towards a sustainable E Economy [9] without requiring costly investments in a new hydrogen distribution network. SEEC© cars makes much more sense than hydrogen-powered private vehicles.

Battery technology, however, certainly needs many improvements to fully meet the specific demands of electric vehicles [10], including the vital need for sustainable manufacturing and recycling practices. Several recently announced R&D projects [11] and scientific advances [12] are witness to the growing awareness that improved battery technology is key to providing energy efficient transport that significantly decreases CO_2 emission.

Several major European companies have world-class expertise in generating and distributing electric power. ITER is without doubt the most ambitious and the most challenging project one can think of when striving to radically depart from what we have been doing ever since we learned how to light a fire [13]: use or waste solar energy from the past without worrying too much about the energy resources available to the next generations. Europe cannot afford to miss this unique opportunity to be world leader in developing fusion technology, even if industrial implementation within the next decades is not at all certain. Innovation in public and private transport technology should, I would think, be coherent with the ambition to increase the share of sustainable electric power in our energy portfolio. If the EU wishes to invest an additional € 1 Billion in transport R&D, let us opt for fuel cells and batteries.

Hydrogen is used in increasing amounts in oil refining, ammonia synthesis and the production of methanol and other base chemicals, and it is mostly produced by steam-reforming of natural gas [14]. As access to oil and natural gas becomes more difficult and costly, hydrogen will increasingly be produced by gasification of coal under the form of syngas (a mixture of hydrogen and CO) which is burned in a gas turbine to drive an electricity generator [15]. Such IGCC (Integrated Gasification Combined Cycle) technology can also be fueled by asphalt, refinery waste or petroleum coke. The syngas can also be converted by Fisher-Tropsch technology to produce synthetic high-quality diesel fuel, naphtha, LPG and methanol. The methanol can be used as base chemical, it can power fuel cell vehicles, or it can be upgraded to high-octane gasoline. South Africa's SASOL perfectioned the production of synthetic fuels when the country had limited access to oil, and to-day successfully competes on the market for low-sulphur fuels when crude oil quotes at $ 70 or more. At time of writing, crude oil exceeded $ 90 a barrel. Coal-based power generation or fuel synthesis, however, generate large amounts of CO_2, and are sustainable only if the carbon dioxide is efficiently captured and sequestered. Industrial sites that integrate coal gasification, power generation and the production of syngas-derived chemicals with reliable sequestration of CO_2 will provide opportunities for buffering electric power requirements through large-scale storage of hydrogen. Such storage facilities may also serve to fuel buses and other transportation vehicles for which the low energy to volume ratio of hydrogen is not as serious a problem as

for private vehicles. In addition, safety precautions required by the characteristics of hydrogen (low ignition energy, broad flammability range, risk of destructive shock-wave detonation when confined) will be more reliably mastered in an industrial site than at a highway gas station. Preparing a possible future for hydrogen as an energy carrier, I would argue, does not require highway filling stations, but technology for large-scale sequestration of CO_2, development of industrial fuel cells and efficient electrolysers for power buffering, and large-scale, safe storage of hydrogen that preferably avoids energy-intensive liquefaction.

References:

[1] C.Mandil, quoted from: http://www.iea.org/Textbase/press/pressdetail.asp?PRESS_REL_ID=187

[2] A. Schwarzenegger quoted from:

http://www.schwarzenegger.com/en/news/uptotheminute/news_upto_cleanair2.asp?sec=news&subsec=uptotheminute

[3] http://www.issues2000.org/Senate/Hillary_Clinton_Energy_+_Oil.htm

[4] http://iht.com/articles/2007/10/10/business/cars.php

[5] Report #:DOE/EIA-0484(2007), available at: http://www.eia.doe.gov/oiaf/ieo/index.html

[6] http://www.nationalledger.com/cgi-bin/artman/exec/view.cgi?archive=4&num=8383

and http://www.businessweek.com/autos/content/sep2006/bw20060912_166232.htm

[7] http://www.iea.org/dbtw-wpd/textbase/papers/2003/opmoving.pdf

[8] See the website of the European Fuel Cell Forum: http://www.efcf.com/

[9] U. Bossel, Proc. IEEE, 94, 1826 (2006).

[10] T. Turrentine, at http://hydrogen.its.ucdavis.edu/workshops/TRB_Brief/

[11] See, e.g. GM's June 5th, 2007 press release available at:
http://www.reuters.com/article/idUSN0527492620070605

[12] K. Bullis, MIT Technology Review, Feb. 21, 2006, available at:
http://www.technologyreview.com/R&D/wtr_16384,295,p1.html

[13] M.J. Hoffert et al., Science 298, 981 (2002)

[14] A brief summary is available at: http://perso.orange.fr/govers/hydrogen.htm

[15] MIT study issued in 2007 and available online at: http://web.mit.edu/coal/

[16] See a financial analysis of SASOL's potential at:

http://seekingalpha.com/article/23025-sasol-and-the-liquid-coal-revolution

Anionic carbon chains of type $C_{2n+1}N^-$ (n = 1-4): theory and experiment

P. Botschwina

Institut für Physikalische Chemie der Georg-August-Universität Göttingen, Tammannst. 6, D-37077 Göttingen, German.

R. Kołos and M. Gronowski

Institute of Physical Chemistry, Polish Academy of Sciences, Kasprzaka 44, 01-224 Warsaw, Poland

The potential importance of negative ions in the chemistry of interstellar clouds, suggested as early as 1973 by Dalgarno and Cray [1], was subsequently revoked and analysed in some theoretical studies [2-6]. However, the unambiguous detection of the first interstellar molecular anion took rather long time. In 2006, McCarthy et al. [7] were able to record the radio spectrum of C_6H^- in the laboratory and could show that this seven-atomic anion is the carrier of the harmonic sequence of molecular lines B1377, detected a decade earlier by radio astronomy in the circumstellar envelope of the evolved carbon star IRC+10216 [8]. Very recently, two more members of the $C_{2n}H^-$ series of anions, C_4H^- and C_8H^-, could be detected in astronomical sources [9, 10], following studies of their pure rotational spectra in the laboratory [11].

Since the cyanopolyynes ($HC_{2n+1}N$), which are chemically closely related to the above anions, have been well known interstellar molecules for some decades, we may anticipate that their anions, $C_{2n+1}N^-$, may be of interest to interstellar cloud chemistry, as well. Previous quantum-chemical studies on $C_{2n+1}N^-$ ions [12-15] reported *ab initio* predictions on geometries, vertical electron detachment energies, fragmentation energies and harmonic vibrational frequencies. The mass-spectrometric investigations of laser-ablated cyano group containing solids, and of soot or graphite arcing in nitrogen atmosphere, disclosed CN^- and C_3N^- as the principal products [16], with a clear indication that species bearing an even numbers of carbon atoms are much less stable than nearest odd-numbered species; ions as large as $C_{13}N^-$ could be detected. Furthermore, Grutter et al. [17] reported on electronic absorption spectra of $C_{2n-1}N^-$ anions (n=4-7), mass-selected and isolated in neon matrices. Some infrared absorption bands could be observed for C_5N^-, C_7N^- and C_9N^-, as well.

Several attempts have been reported to above matrix isolation IR spectra of the smallest member of the $C_{2n+1}N^-$ series with n = 1, the cyanoacetylide ion (C_3N^-) [14, 15, 18]. The present poster reports experimental results obtained at Warsaw, making mainly use of IR spectroscopy in argon and krypton matrices in conjunction with the cold-window-radial-discharge (CWRD) technique [18]. Accompanying ab initio calculations were carried out with the coupled cluster variant CCSD(T) and large basis sets; the MOLPRO suite of programs [20] was used throughout. Results of the spectroscopic studies and of the calculations are given in Fig. 1 and Table 1. Predictions are also made for the less stable isomer $CCNC^-$.

Figure 1. Kr-matrix absorption spectra resulting from CWRD experiments with ^{14}N- and ^{15}N-isotopomeres of cyanoacetylene. Arrows depict isotopic shifts. Unassigned bands marked by 'X' have their Ar-matrix equivalents at 2194 and 2170 cm^{-1}, for ^{14}N- and ^{15}N-species, respectively.

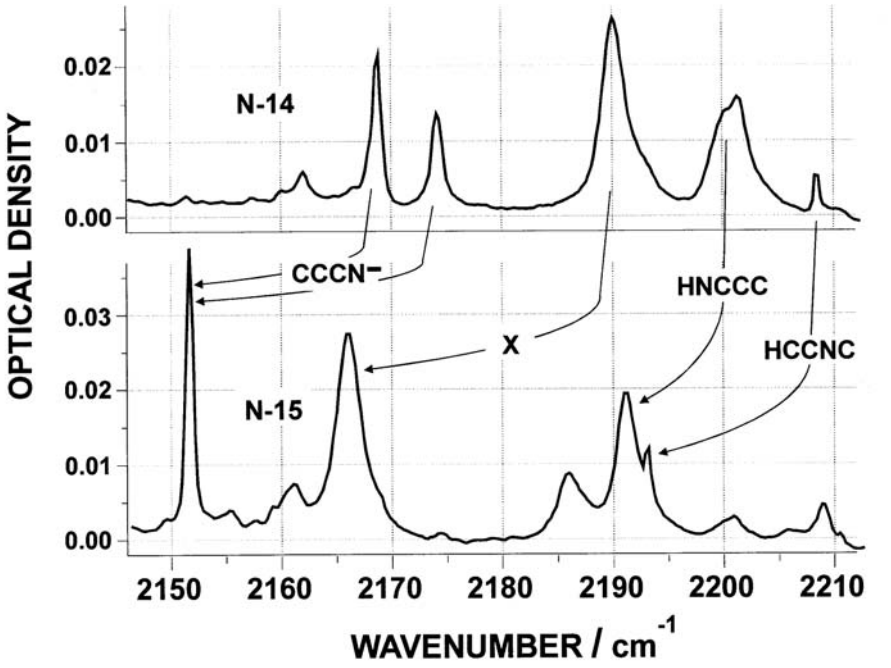

Table 1. Anharmonic wavenumbers (in cm^{-1}) and absolute IR intensities (in km mol^{-1}; in paren-theses) for stretching vibrations of C_3N^- and $CCNC^-$ isotopomers [a]

Band	C_3N^-	$C_3{}^{15}N^-$	$CCNC^-$	$CC^{15}NC^-$
ν_3	866.7 (10.0)	856.6 (10.0)	877.6 (4.5)	872.5 (4.8)
$2\nu_3$	1727.2 (1.1)	1707.1 (1.0)	1746.3 (0.4)	1736.2 (0.37)
ν_2	1940.9 (46.0)	1932.7 (33.2)	1929.0 (67.7)	1922.0 (51.0)
ν_1	2182.3 (474.6)	2164.2 (482.0)	2077.9 (100.6)	2047.7 (116.8)
$3\nu_3$	2581.2 (0.14)	2551.6 (0.13)	2604.2 (0.1)	2591.0 (0.13)
$\nu_2 + \nu_3$	2804.5 (1.0)	2786.3 (0.66)	2804.1 (0.54)	2792.3 (0.27)
$\nu_1 + \nu_3$	3046.7 (8.5)	3018.2 (8.9)	2955.7 (5.4)	2920.4 (5.5)
$4\nu_3$	3428.9 (0.005)	3389.9 (0.005)	3457.4 (0.003)	3437.1 (0.003)
$\nu_2 + 2\nu_3$	3661.9 (0.04)	3633.9 (0.02)	3670.4 (0.05)	3653.8 (0.05)
$2\nu_2$	3866.3 (3.0)	3850.7 (3.1)	3843.8 (1.4)	3831.0 (1.1)
$\nu_1 + 2\nu_3$	3904.9 (0.08)	3866.1 (0.07)	3824.2 (0.009)	3783.8 (0.005)
$\nu_1 + \nu_2$	4108.9 (0.35)	4081.4 (0.18)	3986.7 (0.18)	3946.8 (0.77)
$5\nu_3$	4270.1 (0.0002)	4221.9 (0.0002)	4294.8 (0.00004)	4274.4 (0.00004)
$2\nu_1$	4345.2 (0.008)	4310.1 (0.03)	4137.2 (4.5)	4079.0 (3.7)

[a] Results of variational calculations with an approximate stretch-only vibrational Hamiltonian [21] and three-dimensional CCSD(T)/aug-cc-pVQZ potential energy surfaces and dipole moment surfaces.

The strongest vibration (ν_1) of C_3N^- is predicted at 2182.3 cm^{-1}, with an absolute IR intensity of 475 km mol^{-1}. In the matrix spectra, absorptions (in cm^{-1}) at 2178.7/2173.0 (Ar matrix) and 2173.9/2168.5 (Kr matrix) are assigned to this band. The less intense band calculated at 1940.9 cm^{-1} has an experimental counterpart at 1935.7 cm^{-1} (Ar matrix) and 1932.0 cm^{-1} (Kr matrix).

Accurate equilibrium structures for $C_{2n+1}N^-$ anions up to n = 4, obtained from CCSD(T) calculations plus systematic corrections (see, e.g., [22]), are displayed in Fig. 2. The figure also includes the corresponding equilibrium rotational constants B_e. For C_3N^-, the zero-point vibrational contribution was calculated to be 0.606 MHz so that a ground-state rotational constant of B_0 = 4852.8 MHz is predicted for this species.

Figure 2. Recommended equilibrium bond lengths (in Å) and equilibrium rotational constants (B_e) for linear $C_{2n+1}N^\sigma$ ions.

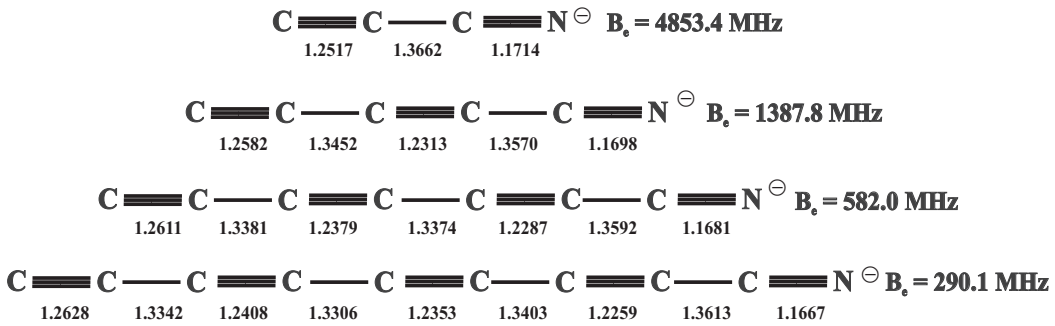

Electric dipole moments, the squares of which are proportional to the intensities of radioastronomical lines, were calculated at the recommended equilibrium structures of Fig. 2 and refer to the molecular centre of mass. CCSD(T) results are 3.101 D (C_3N^-), 5.233 D (C_5N^-), 7.545 D (C_7N^-) and 10.173 D (C_9N^-). There is thus a huge increase with increasing chain length, much stronger than calculated earlier for the $HC_{2n+1}N$ series [23].

The adiabatic electron affinity of C_3N is calculated to be 4.34 eV. The most reliable experimental value found in the literature is 4.59±0.25 eV, obtained through a study of dissociative electron attachment to HC_3N in the electron energy range 0-12 eV [24].

Further predictions for properties of the larger cyanopolyyne anions with n = 2-4, in particular vibrational wavenumbers and absolute IR intensities, are made on the poster.

References

[1] A. Dalgarno and R. A. McCray, Astrophys. J. **181**, 95 (1973).

[2] W. W. Duley and D. A. Williams, Interstellar Chemistry; Acad. Press: New York 1984; 123, pp. 59.

[3] S. Petri and E. Herbst, Astrophys. J. **491**, 210 (1997).

[4] R. Terzieva and E. Herbst, Int. J. Mass Spectrom. **201**, 135 (2000).

[5] S. J. Blanksby, A. M. McAnoy, S. Dua, and J. H. Bowie, Mon. Not. R. Astron. Soc. **328**, 89 (2001).

[6] T. J. Millar, E. Herbst, and R. P. A. Bettens, Mon. Not. R. Astron. Soc. **316**, 195 (2000).

[7] M. C. McCarthy, C. A. Gottlieb, H. C. Gupta, and P. Thaddeus, Astrophys. J. **652**, L141 (2006).
[8] K. Kawaguchi, Y. Kasai, S.-I. Ishikawa, and N. Kaifu, PASJ **47**, 853 (1995).
[9] J. Cernicharo, M. Guélin, M. Agündez, K. Kawaguchi, M. C. McCarthy, and P. Thaddeus, Astron. Astrophys. **467**, L37 (2007).
[10] S. Brünken, H. Gupta, C. A. Gottlieb, M. C. McCarthy, and P. Thaddeus, Astrophys. J. **664**, L43 (2007).
[11] H. Gupta, S. Brünken, F. Tamassia, C. A. Gottlieb, M.C. McCarthy, and P.Thaddeus, Astrophys. J. **655**, L57 (2007).
[12] C.-G. Zhan and S. Iwata, J. Chem. Phys. **104**, 9058 (1996).
[13] G. Pascoli and H. Lavendy, Chem. Phys. Lett. **312**, 333 (1999).
[14] Z. Guennoun, I. Couturier-Tamburelli, N. Piétri, and J. P. Aycard, Chem. Phys. Lett. **368**, 574 (2003).
[15] L. Khriachtchev, A. Lignell, H. Tanskanen, J. Lundell, H. Kiljunen, and M. Räsänen, J. Phys. Chem. **110**, 11876 (2006).
[16] C.-R. Wang, R.-B. Huang, Z.-Y. Liu, and L.-S. Zheng, Chem. Phys. Lett. **237**, 463 (1995).
[17] M. Grutter, M. Wyss, and J. P. Maier, J. Chem. Phys. **110**, 1492 (1999).
[18] R. Kołos, Habilitationsschrift.
[19] R. Kołos, Chem. Phys. Lett. **247**, 289 (1995).
[20] MOLPRO, a package of *ab initio* programs designed by H.-J. Werner and P. J. Knowles, version 2002.6 and later (http://www.molpro.net/).
[21] P. Botschwina, Chem. Phys. **68**, 41 (1982).
[22] P. Botschwina, Mol. Phys. **103**, 1441 (2005).
[23] P. Botschwina, Phys. Chem. Chem. Phys. **5**, 3337 (2003).
[24] K. Graupner, T. L. Merrigan, T. A. Field, T. G. A. Youngs, and P. C. Marr, New Journal of Physics **8**, 117 (1996).

CHBrIF and molecular parity violation: First high resolution rovibrational analysis of the CF-stretching mode

S. Albert[1], K.K. Albert[1], S. Bauerecker [1,2] and M. Quack[1]
[1]*Physical Chemistry, ETH Zurich, CH-8093 Zurich, Switzerland*
[2]*Institute for Technical and Physical Chemistry, TU Braunschweig, Germany*

Abstract
We report the analysis of high resolution FTIR spectra of the chiral molecule CHBrIF. The spectrum was measured with the high resolution Zurich collisional cooling setup consisting of the Bruker IFS125 HR Zurich prototype [1] and a collisional cooling cell [2]. The infrared spectrum of CHBrIF was recorded in the range 600-1300 cm^{-1} at 190 K and 295 K with a resolution of 0.001 cm^{-1}. A rovibrational analysis of the CF-stretching mode of the two isotopomers $CH^{79}BrIF$ (ν_0 = 1060.81587cm^{-1}) and $CH^{81}BrIF$ (ν_0 = 1060.77877 cm^{-1}) is presented and the relation to parity violation is discussed [3].

1. Introduction

Molecular parity violation is of great interest for fundamental aspects of molecular dynamics and symmetries [3-5] (and references cited therein). In this context there have already been quite early suggestions and unsuccessful attempts towards infrared spectroscopic study [6-8] as well as early attempts towards a quantitative theory of molecular parity violation [9]. An experiment has also been suggested to measure the very small parity violating energy difference $\Delta_{pv}E$ between enantiomers of chiral molecules [10], on the order of 100 *aeV* (corresponding to 10^{-12} cm^{-1} or 10^{-11} J mol^{-1}), depending on the molecule considered, of course.

Recent theoretical work has shown that $\Delta_{pv}E$ is typically one to two orders of magnitude larger [11-13] than anticipated on the basis of the older theories, and this substantial theoretical increase can be considered to be well established now from independent work of several groups (see reviews [3-5]). Still, the effects remain very small and the experimental detection of parity violation in chiral molecules remains one of the major challenges of high resolution molecular spectroscopy. As a first basic step towards this goal, we have started to analyse the rovibrational spectra of chiral molecules some time ago (see reviews [1-5]). For instance, some initial work concentrated on microwave, infrared diode laser and FTIR spectroscopy of CHFClBr in molecular beams [14]. While sufficient to achieve the first rovibrational analysis for chiral molecules, this technique can be estimated to be able to resolve at best relative frequency shifts $\Delta\nu/\nu \simeq 10^{-9}$ between separate enantiomers in low temperature beams at the Doppler limit [5,14]. Subsequent Doppler free spectroscopy on room temperature samples of CHFClBr resulted in an experimental limit of about $\Delta\nu/\nu \simeq 10^{-14}$ [15] whereas the theoretical prediction is about $\Delta_{pv}\nu/\nu \simeq 10^{-17}$ [16]. Similar values apply to CDFClBr [16], for which also high resolution analyses of IR spectra have been reported [17,18]. Using methods closely mirroring the work on CHFClBr [14], some recent spectroscopic work has been conducted also on CHFClI [19], for which larger values of $\Delta_{pv}\nu/\nu$ are expected. However simple scaling rules based on the early work in [11] suggest that still larger values should be obtained in molecules with two highly charged and heavy nuclear centers such as CHBrIF [20,21] (see also ref. [22] for some early history of calculations of frequency shifts). Quantitative calculations confirm this expectation for

CHBrIF with predictions for $\Delta_{pv}\nu/\nu$ on the order of 10^{-15} [23,24], which comes close to current experimental limitations [15].

Here, we present IR-spectroscopic results and a first high resolution analysis for the infrared spectrum of CHBrIF. We were able to analyse the FTIR spectra of the two isotopomers $CH^{79}BrIF$ and $CH^{81}BrIF$ in the CF-stretching region and we can discuss line coincidences with CO_2 laser lines. Moreover, we can now propose which kind of transitions (*a*- or *c*-type) should be preferably used. The challenging task consists first of resolving the highly congested FTIR spectrum of CHBrIF and second of performing the rovibrational analysis of this infrared spectrum. We were able to rotationally resolve the infrared spectrum of CHBrIF in the range 600-1300 cm^{-1} using our high resolution FTIR Bruker prototype spectrometer [18] in combination with a collisional cooling cell and we were able to conduct a line-by-line assignment.

2. Experimental

The FTIR spectrum of CHBrIF was recorded at 190 K and 295 K in the region 600-1300 cm^{-1} with an instrumental resolution of better than 0.001 cm^{-1} and a pressure of 0.2 to 0.5 mbar. For the spectra taken at 190 K a newly designed multi-reflection, collisional and enclosive cooling cell cell with a optical path length up to 15 m [2] was combined with the Zurich 2001 prototype IFS125 Bruker spectrometer. Doppler widths are a little less than 0.007 cm^{-1} at 190K, close to the instrumental bandwidth. The room temperature spectra were recorded in a White-type cell with path lengths up to 19.6 m. 150 scans were coadded and the spectrum was calibrated with OCS.

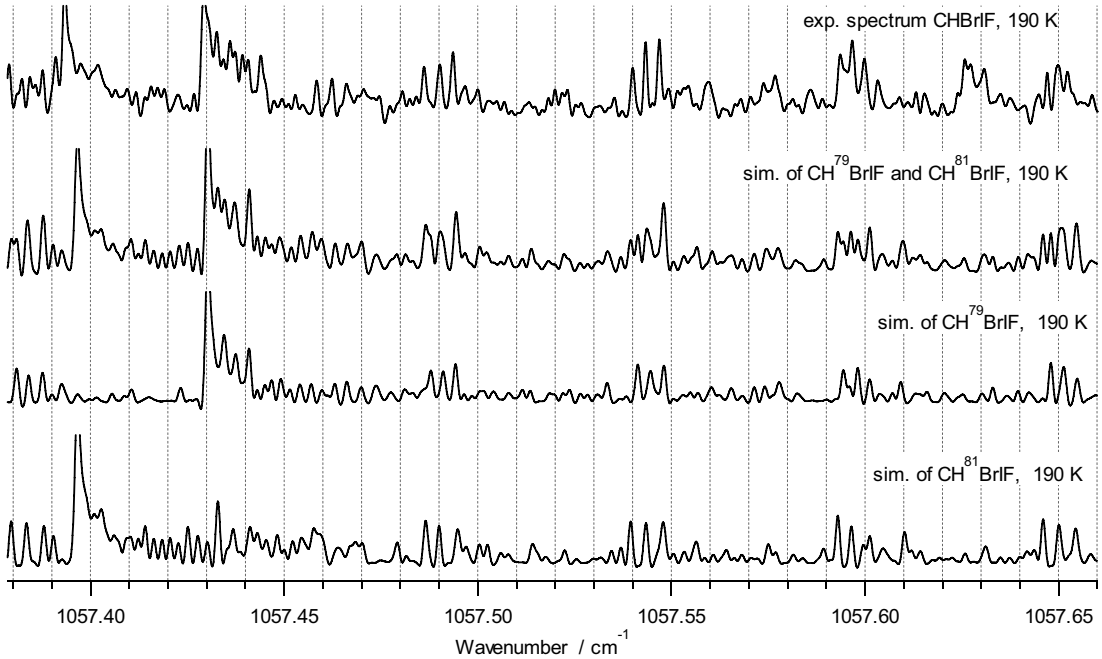

Figure 1: A comparison of a small part of the measured P and Q branch *a*-type lines of the CF-stretching band of $CH^{79}BrIF$ and $CH^{81}BrIF$ (top trace experiment, T = 190 K, path length = 15 m, Doppler limited resolution = 0.0008 cm^{-1}) with a simulation of $CH^{79}BrIF$ and $CH^{81}BrIF$ (second trace, resolution = 0.001 cm^{-1}), a simulation of $CH^{79}BrIF$ (third trace, resolution = 0.001 cm^{-1}) and a simulation of $CH^{81}BrIF$ (lower trace, resolution = 0.001 cm^{-1}).

3. Analysis and discussion

CHBrIF exists as a mixture of two major isotopomers $CH^{79}BrIF$ and $CH^{81}BrIF$. Due to the two heavy atoms the rotational structure of the bands is dense, extremely congested and complicated. Hybrid bands of *a*- and *c*-type have been observed. We have analysed the CF-stretching band in the present work. The assignment of the observed rovibrational transitions belonging to a particular subband consisting of P and R branches has been carried out efficiently with an interactive Loomis-Wood assignment program previously designed for linear molecules [25]. The *a*- and *c*-type bands were identified as P and R branches up to $J < 110$, $K_a < 23$ for *a*-type series and $J < 75$, $K_c < 47$ for *c*-type series in both isotopomers.

The rovibrational analysis was carried out with Watson's *A* reduced effective Hamiltonian in the III^r representation up to sextic centrifugal distortion constants using the WANG program described in [26]. The spectroscopic constants of each band of $CH^{79}BrIF$ and $CH^{81}BrIF$ were fitted separately according to the *A* reduction for the ground state and upper state levels with standard deviation of d_{rms} = 0.000287 cm^{-1} for $CH^{79}BrIF$ and d_{rms} = 0.000295 cm^{-1} for $CH^{81}BrIF$. There were no spectroscopic constants of the ground state nor of any excited state available for either isotopomer prior to our study. The *c*-type transitions are globally perturbed for both isotopomers as opposed to the *a*-type transitions which do not illustrate any sign of perturbation even up to $J = 110$. A comparison of the experimental spectrum and a simulation of the CF-stretching band for $CH^{79}BrIF$ and $CH^{81}BrIF$ based on the adjusted spectroscopic constants is shown in Figure 1. Part of the *a*-type P and Q branch and *c*-type P branch lines is illustrated. The agreement with the simulation is quite good considering that the simulation does not include hot bands in such a congested and complicated spectrum. As one can see the *a*-type Q branches are widely spread over the spectral range labelled by the strong bandheads in Figure 1. Surprisingly, the *a*- and *c*-type P branch lines are partially resolved. Only the asymmetric splitting of the lines is not resolved at this stage. The *a*-type P branch lines are at quite similar positions for both isotopomers $CH^{79}BrIF$ and $CH^{81}BrIF$ as opposed to the *a*-type Q branch lines which are at quite different positions for both isotopomers but are not well resolved within each isotopomer spectrum. The *c*-type lines of both isotopomers are partially resolved. However, the *c*-type lines are globally perturbed.

4. Conclusions

We have rovibrationally resolved the infrared spectrum of CHBrIF at room temperature and at 190 K using high resolution FTIR spectroscopy in combination with collisional cooling methods. We were able to analyse the spectrum in the CF-stretching regions for both isotopomers. We determined the spectroscopic constants of the ground state and the excited states of $CH^{79}BrIF$ and $CH^{81}BrIF$ for the first time. Using these ground state constants we can now analyse the submm wave spectrum of $CH^{79}BrIF$ and $CH^{81}BrIF$. The present analysis provides the basis for future experimental tests of parity violation in $CH^{79}BrIF$ and $CH^{81}BrIF$ using spectroscopy at ultra high resolution. In this context we have already derived some coincidences with CO_2 laser lines. Considering our analysis we recommend *a*-type lines instead of *c*-type lines for ultra-high resolution experiments due to the global perturbation of the *c*-type lines. While in the long run quantitative measurements of parity violation in lighter molecules are important for reasons discussed in [3-5], CHBrIF may still be very useful as an important experimental starting point because CO_2 laser- [15] and submillimeter wave spectroscopy [27] can be conducted on this molecule.

Acknowledgment
We thank Reto Ulrich and Guido Grassi for their help with the synthesis of CHBrIF. Our work is supported financially by the Schweizerischer Nationalfonds and ETH Zürich.

References:

[1] S. Albert and M. Quack. *ChemPhysChem*, **8**, 1271 (2007).
[2] S. Albert, S. Bauerecker, M. Quack, and A. Steinlin, *Mol. Phys.*, **105**, 541 (2007).
[3] M. Quack. Electroweak quantum chemistry and the dynamics of parity violation in chiral molecules. In Kevin J. Naidoo, John Brady, Martin J. Field, Jiali Gao, and Michael Hann, editors, *Modelling Molecular Structure and Reactivity in Biological Systems, Proc. 7th WATOC Congress, Cape Town January 2005*, pages 3 – 38. Royal Society of Chemistry, Cambridge, 2006,
M. Quack. *Angew. Chem. Intl. Ed. (Engl.)*, **41** 4618 (2002).
[4] M. Quack and J. Stohner, *Chimia*, **59**, 530 (2005).
[5] M. Quack, J. Stohner and M. Willeke, *Annu.. Rev. Phys. Chem.,* **59**, 2008 in press.
[6] V.S. Letokhov, *Phys. Lett. A*, **53**, 275 (1975).
[7] O.N Kompanets, A.R. Kukudzhanov, V.S. Letokhov and L.L. Gervits, *Opt. Commun*., **19**, 414 (1976).
[8] E. Arimondo, P. Glorieux and T. Oka, *Opt. Commun*., **23**, 369 (1977).
[9] R.A. Hegström, D.W. Rein, P.G.H. Sandars, *J. Chem. Phys.*, **73,** 2329 (1980).
[10] M. Quack*, Chem. Phys. Lett*. **132**, 147 (1986).
[11] A. Bakasov, T.K. Ha, and M. Quack, Proc. of the 4th Trieste Conference 1995, ed. J. Chela-Flores, F. Raulin, pp. 287-296, Kluwer Academic Publishers, Dordrecht 1996, A. Bakasov, T.K. Ha, and M. Quack, *J. Chem. Phys.*, **109,** 7263 (1998).
[12] A. Bakasov and M. Quack, *Chem. Phys. Lett.*, **303,** 547 (1999).
[13]R. Berger and M. Quack, *J. Chem. Phys* **112**, 3148 (2000).
[14] A. Bauder, A. Beil, D. Luckhaus, F. Mueller and M. Quack, *J. Chem. Phys*., **106**, 7558 (1997).
[15] C. Daussy, T. Marrel, A. Amy-Klein, C. Nguyen, C. Borde, and C. Chardonnet, *Phys. Rev. Lett*., **83**, 1554 (1999), M. Ziskind, C. Daussy, T. Marrel, and C. Chardonnet, *Eur. Phys. J. D*, **20**, 219 (2002).
[16] M. Quack and J. Stohner, *Phys. Rev. Lett*., 84, 3807 (2000), M. Quack and J. Stohner. *J. Chem. Phys.*, **119**, 11228 (2003).
[17] S. Albert and M. Quack, *Chimia*, **55**, 654 (2001).
[18] S. Albert, K. K. Albert, and M. Quack, *Trends in Optics and Photonics*, **84,** 177 (2003).
[19] P. Soulard, P. Asselin, A. Cuisset, J.R.A. Moreno, T. Huet, D. Petitprez, J. Demaison, T.B. Freedman, X. Cao, L.A. Nafie and J. Crassous, *Phys. Chem. Chem. Phys*, **8**, 79 (2006).
[20] M. Quack, report, unpublished in part, at the IUPAC meeting Berlin, August 1999 [21], and private communication in letter to C. Chardonnet, August 1999.
[21] M. Quack, Physical Chemical Foundations of Molecular Chirality and Fundamental Symmetries: From High Resolution Spectroscopy of CHFClBr to the possible Role of Parity Violating Potentials for the Evolution of Biomolecular Chirality, Proc. 37th IUPAC Congress, Berlin, August 1999, Vol.1, p96, GDCH publishing, Frankfurt 1999, ISBN-924763-81-Y.
[22] M. Quack and J. Stohner, *Chirality*, 13, 745 (2001).
[23] J.K. Laerdahl, P. Schwerdtfeger and H.M. Quiney, *Phys. Rev. Lett.*, **84**, 3811 (2000), P. Schwerdtfeger, J. K. Laerdahl, C. Chardonnet, *Phys. Rev. A* **65**(4), 042508 (2002).
[24] R. Berger and J.L. Stuber, *Mol. Phys*., **105**, 41 (2007).
[25] S. Albert, M. Winnewisser, B.P. Winnewisser, *Ber. Bunsen-Ges*., **100**, 1876 (1996).
[26] D. Luckhaus and M. Quack, *Mol. Phys*., **68**, 745 (1989).
[27] S. Albert, D.T. Petkie, R. Bettens, S.P. Belov and F.C. De Lucia, *Anal. Chem.* **70**, 719A (1998), F. Lewen, R. Gendriesch, I. Pak, D.G. Paveliev, M. Hepp, R. Schieder and G. Winnewisser, *Rev. Sci. Instrum.* **69**, 32 (1998)

State-Resolved Study of Direct and Precursor-Mediated Chemisorption of SiH_4 on Si(100)-(2x1)

R. Bisson, T. T. Dang, M. Sacchi and R. D. Beck

Laboratoire de Chimie Physique Moléculaire (LCPM),
Ecole Polytechnique Fédérale de Lausanne (EPFL),
CH-1015 Lausanne, Switzerland.

Silane (SiH_4) is commonly used to manufacture silicon-based devices either by molecular beam epitaxy (MBE) on Si(100)-2x1 and Si(111)-7x7 surfaces [1] or by chemical vapor deposition (CVD) processes on various silicon substrates [2]. A detailed understanding of silane chemisorption on Si(100)-2x1 is therefore of significant economic interest. We study this reaction at a fundamental microscopic level using our ability to prepare SiH_4 molecules in specific vibrationally excited quantum states by laser radiation. In addition to exploring the details of this technological important reaction, the controlled deposition of isotopically enriched silicon layers via isotope selective laser excitation is of interest to improve transport properties of silicon-based devices, such as thermal and electrical conductivity [3, 4], as well as to develop spintronic devices which could be used in quantum computers [5, 6].

We present here new results for the state-resolved dissociative chemisorption of SiH_4 on the Si(100)-2x1 surface. Using Surface Differential Reflectivity (SDR) technique, we probe the uptake of ground state SiH_4 on Si(100)-2x1 as function of incident kinetic energy and surface temperature, which provide clear evidence of the coexistence of two different pathways to chemisorption (Fig. 1).

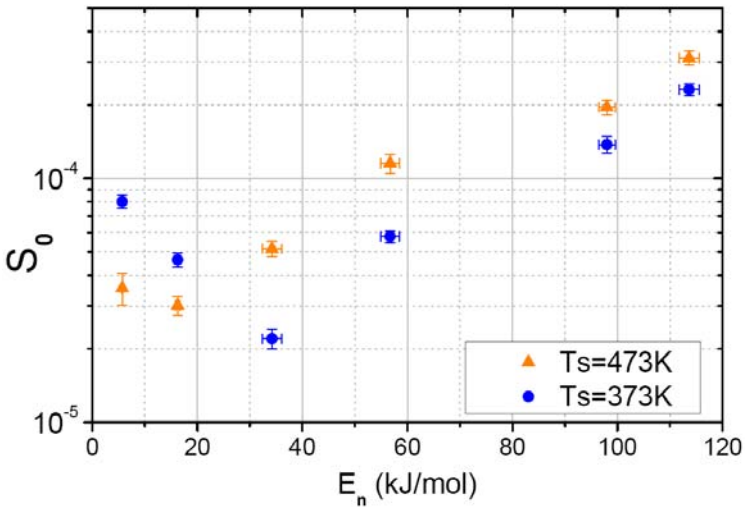

Figure 1: Reactivity of ground state SiH_4 on Si(100)-2x1 as function of normal incident kinetic energy and for a surface temperature of (▲): T_s=473 K, (●): T_s=373 K.

In the first pathway, which dominates the silane reactivity for incident kinetic energies above 30 kJ/mol, the sticking coefficient increases exponentially with the normal kinetic energy (E_n), a tell-tale sign of a ***direct activated chemisorption***. At E_n < 30 kJ/mol, the silane reactivity decreases with increasing either kinetic energy or surface temperature. Such kinetic energy and surface temperature dependence is characteristic of a ***precursor-mediated chemisorption*** mechanism, where the incident molecule is first trapped in a weakly bound physisorbed state prior to reaction or desorption. Due to the strong temperature dependence, the precursor-mediated pathway is relevant only for reactions performed at low surface temperature such as in CVD, while the direct mechanism is relevant for both CVD and MBE.

We use laser excitation of the incident silane molecule in the molecular beam to probe for the first time the effect of vibrational excitation on the chemisorption reaction via both pathways. A novel application of secondary ion mass spectrometry (SIMS) enables us to accurately quantify small amounts of chemisorption products of silane on silicon surface. Through these measurements, we demonstrate for the first time that the chemisorption of SiH_4 on Si(100)-2x1 is vibrationally activated in the direct pathway. Figure 2 shows the results of a SIMS analysis of a Si(100) sample that has been exposed twice to a molecular beam, once

with and once without laser excitation. For the laser-on deposition, about 6% of the incident SiH_4 molecules were excited to the first overtone of the local mode Si-H stretch $|1100\rangle$. For the laser-on deposition, a higher coverage of chemisorption products is detected demonstrating an increase in reactivity for the direct chemisorption pathway due to the ~4350 cm^{-1} of vibrational energy added to molecule in the form of $|1100\rangle$ vibration .

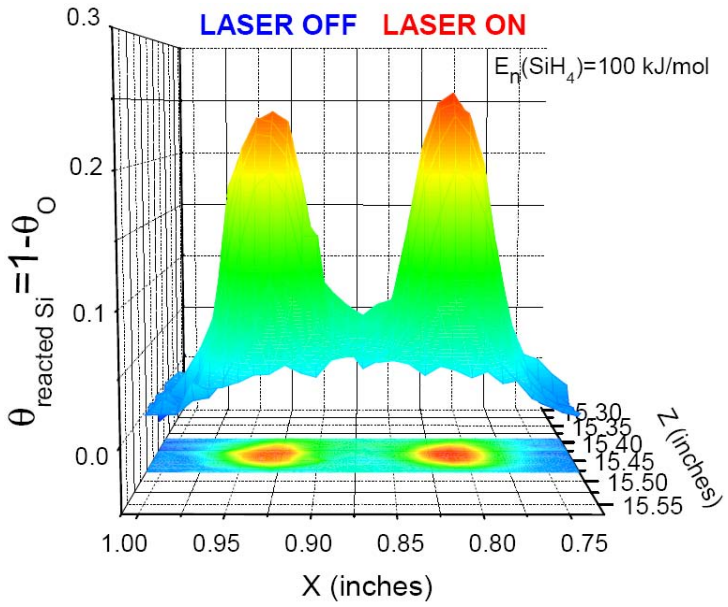

Figure 2: SIMS measurement of two molecular beam footprints from identical dose of fast SiH_4 (i.e. direct path only) on Si(100)-2x1. The footprint labeled "laser ON" results from a molecular beam irradiated by a IR laser tuned on the R(1) $|1100\rangle$ transition of SiH_4.

Furthermore, we observe different enhancement in reactivity for the two nearly isoenergetic vibrational states, $|2000\rangle$ and $|1100\rangle$, which correspond to Si-H stretch excitation of one or two Si-H bonds of the SiH_4 molecule, respectively. For E_n=54 kJ/mol, $|2000\rangle$ excited silane molecules are found to be 70% more reactive than SiH_4 excited to $|1100\rangle$ (Figure 3). The higher reactivity of the $|2000\rangle$ state compared to the $|1100\rangle$ state can be understood qualitatively in terms of the different amount of Si-H stretch amplitude in a single Si-H bond for the two states. The local mode overtone $|2000\rangle$ has one bond stretched to a larger Si-H distance than either of the two excited bonds for the $|1100\rangle$ state. The $|2000\rangle$ therefore matches more closely the transition state geometry of the dissociation reaction and should cause a larger increase in reactivity. The observed difference in the reactivity for the two nearly isoenergetic states is an evidence for mode specificity in this gas/surface reaction and shows that intramolecular vibrational redistribution (IVR) is not complete on the subpicosecond timescale of the direct chemisorption reaction. The observation of mode specificity in the reaction of silane on a semiconductor surface also

demonstrates that vibrationally mode specific chemisorption is not limited to the reaction of methane on nickel surfaces, as observed previously by us and others [7-9], but is a more general physical phenomenon.

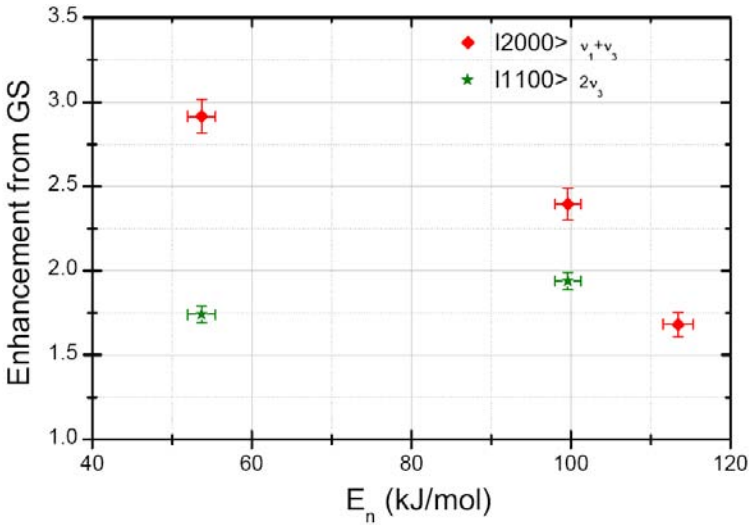

Figure 3: Reactivity enhancement compared to ground state SiH_4 for two nearly isoenergetic vibrational states as function of normal incident kinetic energy.

Finally, we observe for the first time the effect of vibrational energy on a precursor-mediated chemisorption pathway. In contrast to the effect of adding translational energy, which causes the reactivity to decrease, the reactivity of SiH_4 on Si(100)-2x1 is increased for vibrationally excited incident molecules. This result demonstrates that vibrational excitation does not prevent the trapping of SiH_4 in the weak physisorption well and that the vibrational lifetime of the physisorbed silane molecule on the Si(100)-2x1 surface is sufficently long to be useful to overcome the barrier to chemisorption.

[1] H. Rauscher, Surf. Sci. Rep. **42**, 207 (2001).

[2] S. M. Gates, Chemical Reviews **96**, 1519 (1996).

[3] W. S. Capinski *et al.*, Appl. Phys. Lett. **71**, 2109 (1997).

[4] M. Cardona, and M. L. W. Thewalt, Reviews of Modern Physics **77**, 1173 (2005).

[5] B. E. Kane, Nature **393**, 133 (1998).

[6] T. D. Ladd *et al.*, Phys. Rev. Lett. **89** (2002).

[7] R. D. Beck *et al.*, Science **302**, 98 (2003).

[8] P. Maroni *et al.*, Phys. Rev. Lett. **94**, 246104 (2005).

[9] L. B. F. Juurlink *et al.*, Phys. Rev. Lett. **94** (2005).

The endangered prehistoric paintings of Lascaux
can scientists help?

Paul-Marie Guyon

An infernal couple of bacteria and vegetal microorganisms has invaded Lacaux, the most famous prehistoric cave in the world, This cave also called "la Chapelle Sixtine de la prehistoire" was painted by Cro-Magnon artists, some 18000 years ago. The multiple microorganism that tend to cover the paintings combined with the local degradation of the calcite substrate caused by the suppression in 2000 of the microclimate control system represent a serious menace to the preservation of this unique world heritage.

Scientist of different disciplines and experts of the Lascaux caves are upset by the lack of transparent information and of global approach of this complex ecological problem. They accuse the "Monuments Historiques", administration in charge of the cave, of incoherent, and non scientific management of the caves.

What is really happening? What could possibly be done? The absolute necessity of a stable microclimate to retrieve the stability of the ecosystem will be discussed

Contributed papers

Poster session A

Formation and fate of the intermediate in the electrophilic aromatic substitution reaction of phenylium ion with benzene

Daniela Ascenzi, Pietro Franceschi, Graziano Guella, Paolo Tosi

Department of Physics, University of Trento Via Sommarive 14, I -38050 Povo, Trento, ITALY

Plasma treatment of benzene in air produces phenol and heavier O-containing species [1]. If oxygen is removed, leaving a mixture of benzene and N_2, the main molecular products after plasma treatment are biphenyl compounds [2].

The synthesis of diaryl molecules is of paramount importance in organic chemistry and a major effort is currently dedicated to understanding possible mechanisms for coupling of aromatic compounds [3]. It is mostly accomplished through a reductive symmetrical coupling of aryl halides (Ullmann reaction) or via cross-coupling reactions between aryl halides and organometallic reagents. The production of biphenyl from benzene in atmospheric pressure plasma relies on the role of the plasma, which oxidizes C_6H_6 to $C_6H_5^+$ that then acts as a powerful attacking electrophile on the neutral benzene. Thus, the plasma producing $C_6H_5^+$ plays the same role of metal catalysts in the aryl-aryl bond formation process.

We have investigated the reactivity of phenylium cations with benzene [4] by measuring both product yields as a function of benzene density, and absolute integral reactive cross sections as a function of the collision energy. The main ionic products in the reaction of $C_6H_5^+$ with C_6H_6 are detected at *m/z* 155 ($C_{12}H_{11}^+$), 154 ($C_{12}H_{10}^+$), 153 ($C_{12}H_9^+$), 129 ($C_{10}H_9^+$) and 115 ($C_9H_7^+$). Minor products have been observed as a result of charge transfer processes and H^- abstraction. At low collision energies the reactivity is dominated by the formation of a stable intermediate complex $C_{12}H_{11}^+$, having the structure of protonated biphenyl, which can be considered the Wheeland intermediate of the classic electrophilic aromatic substitution.

A significant mobility of the H atoms over both rings has been demonstrated by the statistical H/D scrambling observed in the fragmentation products by using mixed isotopic reagent pairs $C_6H_5^+$ / C_6D_6 and $C_6D_5^+$ / C_6H_6. Loss of H or H_2 from the protonated biphenyl leads to the $C_{12}H_{10}^+$ and $C_{12}H_9^+$ product ions, respectively. $C_{12}H_9^+$ is likely to be the protonated biphenylene cation. *Ab initio* calculations suggest that $C_{10}H_9^+$ is protonated naphthalene, produced via a barrierless elimination of an acetylene molecule from the intermediate complex. Therefore the reaction might be relevant for the production of condensed aromatic rings in cold environments, such as the Titan's ionosphere [5, 6], where benzene and its ions are present.

References:

[1] D. Ascenzi, P. Franceschi, G. Guella, P. Tosi *J. Phys. Chem. A*, **110**, 7841 (2006).

[2] P. Franceschi, G. Guella, G. Scarduelli, P. Tosi, G. Dilecce, S. De Benedictis, *Plasma Processes and Polymers* **4**, 548 (2007).

[3] D. Alberico, M.E. Scott, M. Lautens, *Chem. Rev.* **107**, 174 (2007).

[4] D. Ascenzi, N. Cont, G. Guella, P. Franceschi, P. Tosi *J. Phys. Chem. A*, "Giacinto Scoles Festschrift", in press (2007).

[5] Cravens TE, Robertson IP, Waite JH, Yelle RV, Kasprzak WT, Keller CN, Ledvina SA, Niemann HB, Luhmann JG, McNutt RL, Ip WH, De La Haye V, Mueller-Wodarg I, Wahlund JE, Anicich VG, Vuitton V *Geophys. Res. Lett.* **33**, L07105 (2006).

[6] V. Vuitton, R.V. Yelle, V.G. Anicich, *Astroph. J.* **647**, L175-L178 (2006).

ElectroSpray Mass Spectrometric Investigations of the Cu(II)/Cu(I) Redox Cycle in Copper-Nucleobases Complexes

Graziano Guella, Daniela Ascenzi, Davide Bassi, Eleonora Braga and Paolo Tosi

Department of Physics, University of Trento Via Sommarive 14, I -38050 Povo, Trento, ITALY

Eukaryotic and prokaryotic cells accumulate first row transition metals for various cellular functions. In particular, Cu(II) is protein bound and it is present in higher concentrations in the nucleus than in the cytosol [1]. In the nucleus, copper exists in a nuclear histone protein complex located at the base of DNA loops, where it maintains the nuclear matrix and DNA folding [2]. In presence of reducing agents, copper(II) is effective at cleaving double-stranded DNA, thus leading to transcriptional errors, mutagenesis and strand scission. Since DNA breakage often occurs near guanine residues, it has been suggested that Cu^{2+} ions bind to DNA at guanine sites, where they react with H_2O_2, a product of normal cell physiology, producing oxygen radicals which attack the DNA bases in a site-specific manner [3]. Guanine is the most sensitive nucleobase to oxidation because of its low ionization potential (8.24 eV) and its high affinity to transition metals, e.g. to the Cu(II)/Cu(I) redox system.

Although most of the phenomena involving nucleic acid bases and metal ions occur in the condensed phase, it is useful to consider gas phase ion interactions with nucleosides and isolated bases to improve our understanding of the role of metals in the biochemistry of DNA and RNA.

We have investigated the interaction of guanine, guanosine and deoxyguanosine with copper(II) ions by ESI-MS techniques to determine the metal ion affinity, the preferred coordination sites of the cation, and its redox properties.

It is worth noting that outcomes of ESI-MS experiments are not directly representative of the solution properties of the analytes, in spite of the soft character of the technique. In fact, during electrospray ionization, several processes occur [4], most noticeably charge/proton exchanges, desolvation and clusterization reactions, which may generate new species. Therefore the relative abundance of analytes as measured in the MS spectra may not reflect the initial solution stochiometry. While on the one hand this fact may represents a serious difficulty from an analytical point of view, on the other it represents a powerful tool to investigate how intermolecular interactions change in going from condensed into gas phase. A pertinent example concerns the role of the solvent in the modulation of acid/base interactions and redox processes. In this communication, relying also on Density Functional calculations, we will report on charge-reduction effects in cupric ion complexes, which result from the competition among acid-base reactions (proton transfers) and redox processes (electron transfers).

References:

[1] Bryan, S. E., Vizard, D. L., Beary, D. A., LaBiche, R. Hardy,K. J. Partitioning of zinc and copper within subnuclear nucleoprotein particles. *Nucleic Acids Res.* **9**, 5811 (1981).

[2] George, A. M., Sabovljev, S. A., Hart, L. E., Cramp, W. A., Harris, G., and Hornsey, S. DNA quaternary structure in the radiation sensitivity of human lymphocytes A proposed role of copper. *Br. J. Cancer Suppl.* **8**, 141 (1987).

[3] Lloyd, D.R., Phillips, D.H. Oxidative DNA damage mediated by copper(II), iron(II) and nickel(II) Fenton reactions: evidence for site-specific mechanisms in the formation of double-strand breaks, 8-hydroxydeoxyguanosine and putative intrastrand cross-links. *Mutat. Res.* **424,** 23 (1999); Sagripanti, J.L., Kraemer, K.H. Site-specific oxidative DNA damage at polyguanosines produced by copper plus hydrogen peroxide. *J. Biol. Chem.* **264**, 1729 (1989).

[4] Kebarle P. A brief overview of the present status of the mechanisms involved in electrospray mass spectrometry. *J Mass Spectrom.* **35**, 804 (2000); Wang HJ, Agnes GR. Evaluation of electrospray mass spectrometry as a technique for quantitative analysis of kinetically labile solution species. *Anal. Chem.* **71**, 3785 (1999).

Dynamics of intra- and intermolecular energy exchange in the collisions of two molecules with ionic bond

V.M. Azriel and L.Yu. Rusin
Institute of Energy Problems of Chemical Physics RAS,
Leninski prospect 38, Bldg.2, Moscow 119334, Russia

Dynamics of the exchange of internal energy in the system CsCl + RbJ has been investigated by quasiclassical trajectory technique for fixed initial vibrational and rotational states of the molecules. Fig. 1,a represents the distribution of final vibrational quantum numbers V_{CsCl}^{fin} of the molecules CsCl after collision for initial vibrational states of both molecules corresponding to $V_{CsCl}^{ini} = V_{RbJ}^{ini} = 15$, and equal zero initial rotational states ($J_{CsCl}^{ini} = J_{RbJ}^{ini} = 0$) at collision energy E_{rel}=0,2 eV. In this case 72,5% of all molecules keep the value of their initial vibrational quantum number, and 7,4% of the molecules have the neighbouring vibrational levels with $V_{CsCl}^{fin} = 14$ or $V_{CsCl}^{fin} = 16$. Quite different situation takes place for initial rotational excitation of the molecules corresponding to $J_{CsCl}^{ini} = J_{RbJ}^{ini} = 150$ (fig. 1,b). Here only 17% of the molecules have $V_{CsCl}^{fin} = V_{CsCl}^{ini} = 15$, for 13,5% of the molecules $V_{CsCl}^{fin} = 14$, and 52% of all collisions lead to increase of vibrational energy of the molecules of CsCl to the levels $V_{CsCl}^{fin} = 16$ and $V_{CsCl}^{fin} = 17$.

In both cases we have rather high vibrational states till $V_{CsCl}^{fin} = 30$, but the relative population of high vibrational levels with $V_{CsCl}^{fin} > 20$ decreases with the growth of initial rotational energy. The excitation of so high vibrational levels at low collision energy and $J_{CsCl}^{ini} = 0$ is possible only at effective V-V energy exchange of the partners, when the second molecule loses the significant part of her vibrational energy.

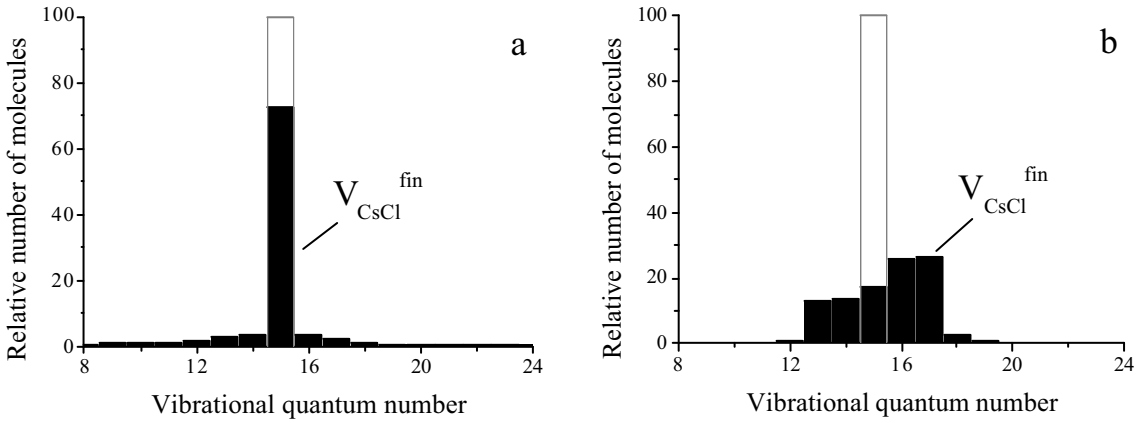

Fig. 1. Distributions of vibrational quantum numbers of the molecules CsCl after collision at E_{rel}=0,2 eV and initial internal states of the molecules with $V_{CsCl}^{ini} = V_{RbJ}^{ini} = 15$, $J_{CsCl}^{ini} = J_{RbJ}^{ini} = 0$ (a) and $V_{CsCl}^{ini} = V_{RbJ}^{ini} = 15$, $J_{CsCl}^{ini} = J_{RbJ}^{ini} = 150$ (b).

Fundamental Processes in Radiation Damage to DNA

Ilko Bald, Constanze König, Janina Kopyra [(a)], Iwona Dabkowska [(b)], and Eugen Illenberger
Institut für Chemie und Biochemie – Physikalische und Theoretische Chemie
Freie Universität Berlin
Takustrasse 3, D-14195 Berlin

In the meantime it is well recognised that in radiation damage of biological material the interaction of secondary electrons (abundantly generated along the ionisation track) with DNA and its surroundings plays an important role [1]. Within an extended research program within Europe involving also groups from overseas we have tracked this problem along a line of increasing complexity, namely from the study of single gas phase building blocks in effusive molecular beams (DNA bases [2], sugar [3], the phosphate group) over clusters in supersonic beams, and molecular films condensed on solid substrates up to short model DNA immobilised on microarrays [4].

Here we present recent results obtained from a gas phase sugar compound (1,2,3,5-tetra-*0*-acetyl-*ß*-D-ribofuranose (TAR)) [5] and a gas phase phosphate ester (dibutyl phosphate (DBP)) [6] on the response to low energy electrons (0-10 eV). TAR is a five membered ring in which both the coupling to the neighbouring phosphate groups and the coupling to the nucleobase (NB) is mimicked by acetyl groups. In DBP the butyl groups are connected to the phosphate unit by P-O-C bonds (in analogy to the neighbouring sugars in DNA), both compounds can hence be considered as appropriate model systems for the study of the behaviour of 2-deoxyribose and the phosphate group when they are coupled within the DNA network.

In both compounds we find strong resonances at low energies (< 3 eV) associated with dissociative electron attachment. The analysis of the fragment ions indicate that these reactions lead to particular bond cleavages and also the excision of the phosphate group which would both result in DNA strand breaks.

These findings indicate that in addition to the DNA bases, which act as antennas for low energy electrons (with the possibility of electron transfer to the DNA backbone resulting in strand breaks [7]), the sugar and phosphate unit play an active role in the molecular mechanism, how low energy electrons damage DNA.

Work supported by Deutsche Forschungsgemeinschaft (DFG), the Alexander von Humboldt Stiftung and the European Union.

[1] B. Boudaiffa, P. Cloutier, D. Hunting, M.A. Huels, L. Sanche, Science **287** 1658 (2000).
[2] H. A.-Carime, S. Gohlke, E. Illenberger, Phys. Rev. Lett. **92** 168103 (2004).
[3] Bald, J. Kopyra and E. Illenberger, Angew. Chem. Int. Ed. **45** 4851 (2006).
[4] T. Solomun, H. Hultschig, and E. Illenberger, Eur. Phys. J. D **35** 437 (2005).
[5] I Bald, J. Kopyra, I. Dabkowska, E. Antonsson and E. Illenberger, J. Chem. Phys. **126** 074308 (2007).
[6] C. König, I. Bald, J. Kopyra and E. Illenberger, Phys. Rev. Lett. **97** 018105 (2006).
[7] J. Simons, Acc. Chem. Res. **39** 772 (2006).

(a) permanent address: Department of Chemistry, University of Podlasie, 08-110 Siedlce, Poland
(b) permanent address: Department of Chemistry, University of Gdansk, 80-952 Gdansk, Poland

Energy dependence of Diffraction and Rotationally Inelastic Scattering of D_2 from NiAl(110)

D. Barredo, G. Laurent, P. Nieto, D. Farías
Departamento de Física de la Materia Condensada,
Universidad Autónoma de Madrid, 28049 Madrid, Spain

P. Riviere and F. Martín
Departamento de Química,
Universidad Autónoma de Madrid, 28049 Madrid, Spain

Studies of elementary collision processes of H_2 with metal surfaces can provide benchmark tests of theoretical methods that are increasingly used to aid the design of new heterogeneous catalysts [1]. Molecular beam and associative desorption experiments have been carried out to understand the main factors that govern H_2 dissociation at the surface. In addition, vibrationally inelastic and rotationally inelastic scattering experiments, complemented by theoretical research, have provided useful information on how certain features of the potential energy surface (PES) control the experimental observations [2,3].

A different point of view is provided by diffraction experiments. H_2 diffraction from metal surfaces is more complex than He diffraction, since the PES is 6-dimensional and the coupling with the dissociative adsorption channels comes into play. Thus, H_2 diffraction has been proposed some time ago as a promising (and may be unique) technique to gauge the molecule-surface PES and dynamics [4]. In addition, it can provide useful information on the dynamics of the rotational inelastic transitions of the scattered molecules, as shown by our current work.

We have measured in-plane diffraction of D_2 molecular beams scattered from a NiAl(110) surface at incident energies from 25 to 150 meV. The experiments were performed with a high-resolution time-of-flight (TOF) apparatus, which allows measurements of the rotational inelastic diffraction (RID) transitions with high accuracy. Elastic first and second-order diffraction as well as 0<->2 and 1<->3 RID peaks were observed over the whole incident energy range explored. The RID transition probabilities were extracted from the data, and compared with classical trajectory calculations performed using an ab initio determined potential energy surface. The results will be discussed at the conference.

[1] G.J. Kroes and M. F. Somers, *J. Theor. Comput. Chem.* **4,** 493 (2005).
[2] A. Gross, *Surf. Sci. Rep.* 32, 291 (1998).
[3] M. Bertino and D. Farías, *J. Phys. C* 14, 6037 (2002).
[4] D. Farías, C. Díaz, P. Rivière, H.F.Busnengo, P. Nieto, M.F. Somers, G.J.Kroes, A. Salin and F. Martín, *Phys. Rev. Lett.* **93,** 246104 (2004).

State-Resolved Reactivity of $CH_4(2\nu_3)$ on Pt(111) and Ni(111): Effects of Barrier Height and Transition State Location

R. Bisson, M. Sacchi, T. T. Dang, B. Yoder, P. Maroni, and R.D. Beck

Laboratoire de Chimie Physique Moleculaire (LCPM)
Ecole Polytechnique Fédérale de Lausanne (EPFL)
CH-1015 Lausanne, Switzerland

State-resolved reactivity measurements are fundamental to the understanding of chemical reaction dynamics for both gas phase and gas/surface reactions. The investigation of the latter reaction type has seen significant progress over the last few years due to the combination of laser excitation in molecular beams and UHV surface analysis techniques. To date, most studies concern the chemisorption of methane on the Ni(100) and Ni(111) [1-5], motivated by the fact that these surfaces are models for nickel catalysts used in steam reforming [6]. The steam reforming process, which converts natural gas into H_2 and CO, is of tremendous economical importance since it is the dominant method for large scale production of hydrogen as well as the starting point for many synthetic processes in the chemical industry. Another important and widely studied model catalytic surface is Pt(111), which has attracted interest due to its relatively simple preparation in UHV and the high selectivity of platinum catalysts for the generation of reforming products [7].

In the present study, we report state-resolved reactivity data for CH_4 on Pt(111), extending the work of Higgins *et al.* [8], and on Ni(111) over a similar range of incident kinetic energy. Comparison of the state-resolved reactivity for the ground state and $2\nu_3$ excited state of CH_4 yields information about the difference in barrier height and location for methane dissociation on the two metal surfaces [9].

Figure 1 shows a comparison of our state-resolved sticking coefficient measurements (laser-off and for $2\nu_3$) on Pt(111) and Ni(111). A couple of differences between the data sets for the two metals are readily apparent. The laser-off reactivity on Ni(111) is approximately 3 orders of magnitude lower than on Pt(111) and we detect a much stronger enhancement in reactivity upon $2\nu_3$ excitation for Ni(111).

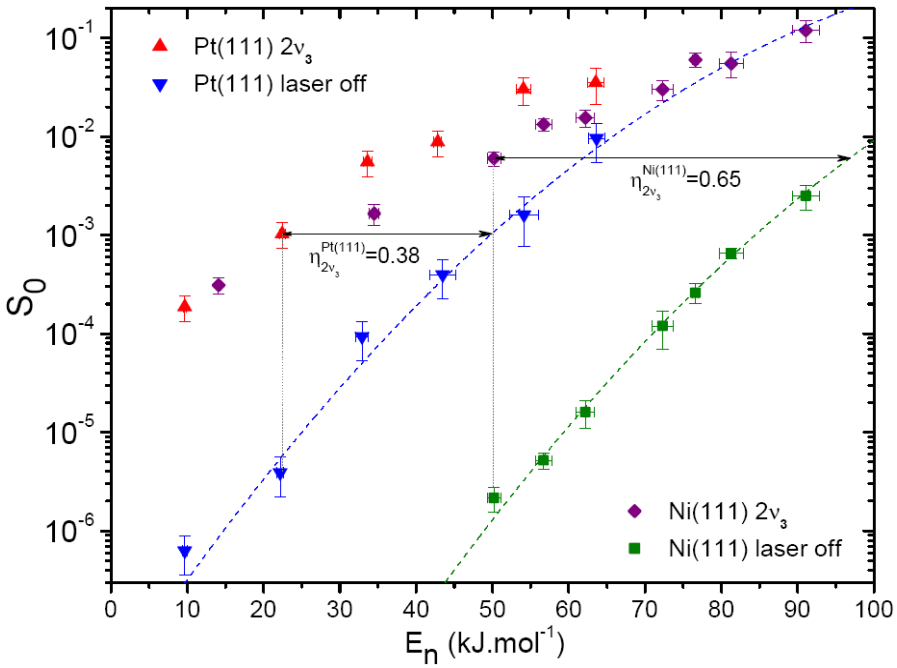

Figure 1: Comparison of the $2\nu_3$ and laser-off reactivity for Pt(111) and Ni(111). Dashed lines are "S"-shape curves, fitted to the laser-off data and used to determine the difference in average barrier height ΔE_a between Pt(111) and Ni(111). The vibrational efficacies $\eta_{2\nu_3}$ for Pt(111) and Ni(111) are calculated at the incident kinetic energies indicated by the vertical dotted lines, where similar reactivities are observed in the ground state.

The lower laser-off reactivity for Ni(111) at a given incident kinetic energy is consistent with a higher barrier for methane dissociation on Ni(111) as compared to Pt(111). Although barrier heights reported in the literature vary over a considerable range, comparative studies treating both metal surfaces at the same level of theory found a higher barrier for Ni(111) than for Pt(111) [10, 11]. We use our laser-off results for Pt(111) and Ni(111) to estimate the difference in barrier height on the two surfaces using "S"-shaped curves, initially proposed by Luntz [12], to parametrize the variation of the laser-off sticking coefficients with kinetic energy E_n:

$$S_0(E_n) = \frac{A}{2}\left[1 + \mathrm{erf}\left(\frac{E_n - E_0}{W}\right)\right] \qquad (2)$$

where E_0 is the average barrier height, W is the width of a Gaussian distribution of barrier heights and A the asymptotic value of S_0 at high E_n.

These fits yield similar values for W on both metals ($W_{CH_4 / Pt(111)} \approx W_{CH_4 / Ni(111)} \approx 31 \pm 2\,kJ/mol$), reflected in the parallel rise of the "S"-shaped curves in Figure 1. When compared to that of Pt(111), the fit for Ni(111) gives a higher average barrier height of ΔE_a = 28 ± 6 kJ/mol. Such a difference in barrier height is in good agreement with the comparative theoretical studies by Lia *et al.* [11] and Anderson *et al.* [10] which found a higher reaction barrier on Ni(111) than on Pt(111) by 31 and 21 kJ/mol, respectively.

In addition to the much lower ground state methane reactivity on Ni(111) as compared to Pt(111), we also observe a much greater reactivity increase on Ni(111) than on Pt(111) upon $2\nu_3$ excitation. While at first glance, one might consider this to be a consequence of the difference in barrier height for the two metals, we suggest that the different degree of reactivity enhancement is related to different transition state geometries on the two surfaces. Considering only a difference in barrier height, it is difficult to rationalize that at the low reaction probability of $S_0 \approx 3x10^{-6}$ where the reaction is still "starved for energy" on both surfaces, the addition of 72 kJ/mol of $2\nu_3$ vibrational energy increases the reactivity to only $1x10^{-3}$ for the lower barrier system CH_4/Pt(111) while for the higher barrier system CH_4/Ni(111) the reactivity increases all the way to $1x10^{-2}$.

This difference in the degree of vibrational activation between Ni(111) and Pt(111) is also reflected in their different vibrational efficacies $\eta_{2\nu_3}$, which compare the effect of translational and $2\nu_3$ vibrational energy on the reactivity on each surface. $\eta_{2\nu_3}$ is defined as:

$$\eta_{2\nu_3} = \frac{\Delta E_n}{\Delta E_{2\nu_3}} \qquad (3)$$

where ΔE_n is the amount of normal energy required to achieve the same increase in reactivity as observed for the addition of $\Delta E_{2\nu_3}$ = 72 kJ/mol of vibrational energy by excitation of the $2\nu_3$ state.

In Figure 1, we have indicated the $2\nu_3$ efficacies for the two surfaces, calculated at incident energies where we measure similar laser-off reactivities, on the order of $3x10^{-6}$ for both surfaces. The stronger effect of $2\nu_3$ excitation on Ni(111) is reflected by a higher efficacy

$\eta_{2\upsilon_3}^{Ni(111)} = 0.65$, nearly twice the value for Pt(111) $\eta_{2\upsilon_3}^{Pt(111)} = 0.38$. Such an increased vibrational efficacy is typically associated with a "late" barrier on a simple Polanyi type model potential energy surface[13] and corresponds to a transition state structure for which the dissociating bond is significantly stretched at the transition state. Calculated transition state geometries are consistent with this interpretation and predict the methane molecule on the top site above a surface metal atom for both Pt(111) and Ni(111), but with the reactive C-H bond more elongated on Ni(111)[10, 14-16] than on Pt(111) [10, 17]. The proposed difference in barrier location (later on Ni(111) than on Pt(111)) is also consistent with previous results reported by Luntz and Bethune [18], who reported an averaged vibrational efficiency $\beta_v = d(\ln S_0)/d(\langle E_v \rangle)$ of all thermally populated states in a hot nozzle beam to be four times higher for Ni(111) than for Pt(111).

[1] L. B. F. Juurlink *et al.*, Phys. Rev. Lett. **83**, 868 (1999).
[2] M. P. Schmid *et al.*, J. Chem. Phys. **117**, 8603 (2002).
[3] R. D. Beck *et al.*, Science **302**, 98 (2003).
[4] L. B. F. Juurlink *et al.*, Phys. Rev. Lett. **94** (2005).
[5] P. Maroni *et al.*, Phys. Rev. Lett. **94**, 246104 (2005).
[6] P. L. Spath, and M. K. Mann, National Renewable Energy Laboratory Technical Report **NREL/TP-570-27637** (2001).
[7] F. Zaera, Applied Catalysis a-General **229**, 75 (2002).
[8] J. Higgins *et al.*, J. Chem. Phys. **114**, 5277 (2001).
[9] R. Bisson *et al.*, J. Phys. Chem. A, in press (2007).
[10] A. B. Anderson, and J. J. Maloney, J. Phys. Chem. **92**, 809 (1988).
[11] M. S. Liao, C. T. Au, and C. F. Ng, Chem. Phys. Lett. **272**, 445 (1997).
[12] A. C. Luntz, J. Chem. Phys. **113**, 6901 (2000).
[13] J. C. Polanyi, Accounts of Chemical Research **5**, 161 (1972).
[14] H. Burghgraef, A. P. J. Jansen, and R. A. Vansanten, J. Chem. Phys. **101**, 11012 (1994).
[15] P. Kratzer, B. Hammer, and J. K. Norskov, J. Chem. Phys. **105**, 5595 (1996).
[16] H. Yang, and J. L. Whitten, J. Chem. Phys. **96**, 5529 (1992).
[17] G. Psofogiannakis, A. St-Amant, and M. Ternan, J. Phys. Chem. B **110**, 24593 (2006).
[18] A. C. Luntz, and D. S. Bethune, J. Chem. Phys. **90**, 1274 (1989).

Calculated spectroscopic and electric properties of the alkali metal-ammonia complexes from K^n-NH_3 to Fr^n-NH_3 (n = 0, +1)

I. S. Lim
Department of Chemistry, School of Molecular Science (BK21), Korea Advanced Institute of Science and Technology, 373-1 Guseong-dong, Yuseong-gu, Daejeon 305-701, Korea.

P. Botschwina, R. Oswald
Institut für Physikalische Chemie der Georg-August-Universität Göttingen, Tammannst. 6, D-37077 Göttingen, Germany.

V. Barone
Dipartimento di Chimica, Università Federico II, Complesso Universitario Monte S.Angelo, via Cintia, I-80126 Napoli, Italy.

H. Stoll
Institut für Theoretische Chemie, Universität Stuttgart, D-70550 Stuttgart, Germany.

P. Schwerdtfeger
Theoretical and Computational Chemistry Research Center (TCCRC), Institute of Fundamental Sciences, Massey University (Albany Campus), Private Bag 102904, North Shore MSC, Auckland, New Zealand.

The newly developed Stuttgart small-core scalar relativistic pseudopotentials for the alkali-metals are used to study spectroscopic and electric properties of the heavier alkali metal-ammonia complexes from K^n-NH_3 to Fr^n-NH_3 (n= 0, +1) at the second-order Møller-Plesset (MP2) and coupled cluster level (CCSD(T)) of theory [1]. Equilibrium geometries and dissociation energies computed at the MP2 level are in reasonable agreement with their CCSD(T) counterparts, whereas for the dipole polarizabilities MP2 is not performing well overestimating significantly electron correlation effects. The bond distances increase monotonically with increasing mass of the metal atom as relativistic effects are small in these systems. However, the dipole polarizabilities are more sensitive to such effects and we find a decrease in this property from Cs-NH_3 to Fr-NH_3. Combination of CCSD(T) harmonic frequencies and MP2 anharmonic corrections obtained from a perturbative vibrational treatment lead to fundamental frequencies in good agreement with experimental results obtained by Süzer and Andrews [2] and Loutellier et al. [3].

We also present the results of variational calculations with a three-dimensional approximate vibrational Hamiltonian (see, e.g., [4]), making use of CCSD(T) potential energy surfaces (PES) and electric dipole moment functions. A contour plot of the PES for the most strongly bound neutral complex K - NH_3 is shown in Fig. 1. Upon complex formulation, the symmetric double-minimum potential of free NH_3 undergoes significant distortion which shows up in a considerable blue-shift of the wavenumber of the umbrella bending vibration (ν_2).

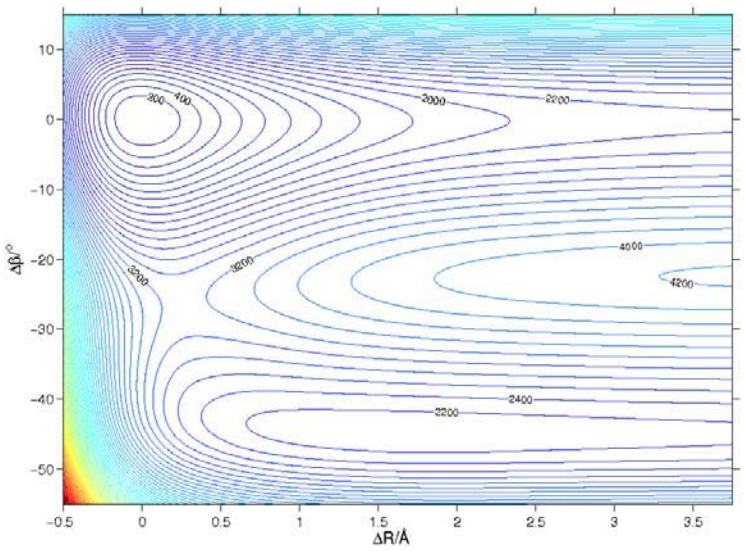

Fig. 1. Two-dimensional cut through the CCSD(T) potential energy surface of K-NH_3, with R_e(N-H) kept fixed at its value for the equilibrium structure of the complex. Contour lines in intervals of 200 cm^{-1}; $\Delta\beta$ is the difference in M-N-H angle with respect to its equilibrium value in the complex.

The variation of the electric dipole moment with the intermolecular separation R_{MN} (M = K-Fr) is shown in Fig. 2. At long range, the change in the dipole moment results mainly from induction, with the induced dipole moment being proportional to the third inverse power of the intermolecular separation. Since the static dipole polarizabilities of the Rb and Fr atoms are very similar, the curves for Rb-NH_3 and Fr-NH_3 almost coincide for R > 6 Å. The Cs atom has clearly the largest polarizability and consequently the Cs-NH_3 system exhibits the strongest long-range interaction connected with the strongest increase in the dipole moment. Pauli repulsion sets in earliest for this complex and therefore the corresponding dipole moment curve reaches its maximum at the largest R value of all systems.

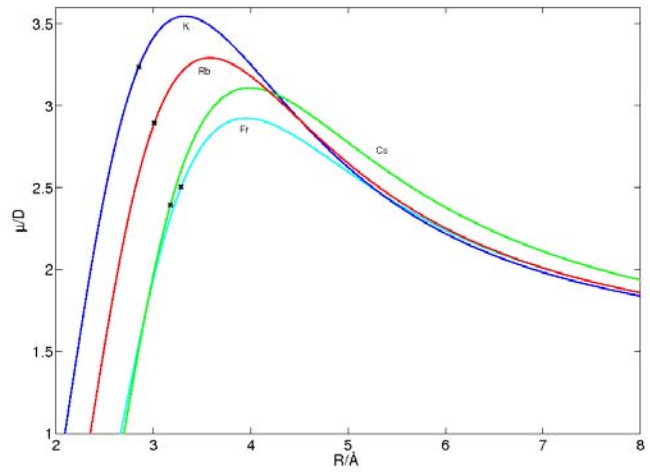

Fig. 2. Variation of the CCSD(T) electric dipole moment of alkali-ammonia complexes with the intermolecular separation R(M-N), with the geometrical parameters of the NH_3 moiety being kept fixed at the values of the equilibrium structure of the complex. The equilibrium positions (R_e) are marked by crosses.

The unusual large increase of the symmetric NH_3 stretching vibration (ν_1) occurring upon complex formation is analyzed in detail. The crucial information is provided by the variation of the electric dipole moment with the symmetric NH stretching coordinate (see Fig. 3). In order to illustrate the big importance of electron correlation, which was found earlier for Li-NH_3 [5, 6], the figure includes also curves obtained with the restricted Hartree-Fock approximation. Throughout, the CCSD(T) dipole moment curves exhibit substantially larger

slopes at the equilibrium position compared with the corresponding Hartree-Fock curves. The much stronger decrease of μ with increasing Δr_{NH} observed for the CCSD(T) results may be qualitatively explained through the increase of the importance of antibonding NH orbitals which remain unoccupied in a Hartree-Fock treatment. An increase in the occupation of such orbitals corresponds to a slight charge transfer to the site of the NH bonds within the ammonia molecule, thereby reducing the electric dipole moment.

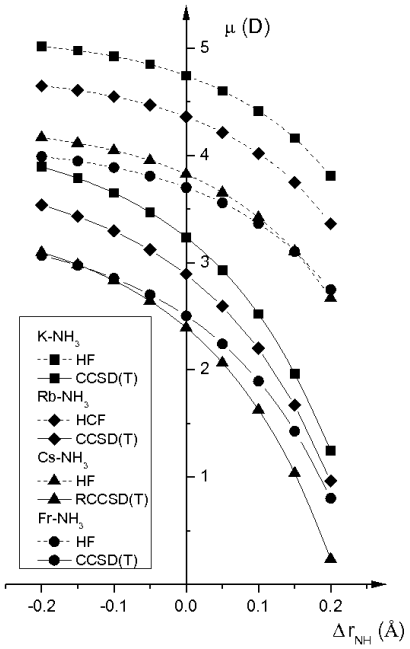

Fig. 3. Variation of the electric dipole moment with symmetric displacement of all three hydrogen atoms along the NH bond vectors, where Δr(N-H) = 0 corresponds to the equilibrium structure of the complex.

Results of the variational calculations and experimental results are summarized in the table below.

Band	K-NH_3[b]	Rb-NH_3	Cs-NH_3[b]	Fr-NH_3
ν_1	3305 (477)	3306 (452)	3304 (557)	3311 (353)
ν_2	1052 (207)	1043 (210)	1040 (208)	1025 (216)
ν_s	158 (6.6)	133 (6.8)	125 (11.4)	112(5.3)
Band	K-ND_3	Rb-ND_3	Cs-ND_3	Fr-ND_3
ν_1	2396[c] (219)	2397 (210)	2395 (263)	2400 (163)
ν_2	814[c] (108)	809 (109)	806 (104)	796 (114)
ν_s	150 (6.2)	125 (6.2)	117 (10.2)	104 (4.7)

[a] CCSD(T) results, involving single-parameter correction for the anharmonic interaction between symmetric and asymmetric NH_3 stretching vibrations (see the text).

[b] Ar matrix data are ν_1 = 3292 cm^{-1} and ν_2 = 1064 cm^{-1} for K-NH_3 (Refs. 2, 3) and ν_1 = 3287 cm^{-1} and ν_2 = 1049 cm^{-1} for Cs-NH_3 (Ref. 2).

[c] Exp. values (Ar matrix, Ref. 3) are 2393 and 822 cm^{-1}.

The intensity of the ν_1 vibration has its maximum in Cs-NH_3 at a very large value of 557 km mol^{-1} and, owing to relativistic effects, drops down to 357 km mol^{-1} for Fr-NH_3. Anharmonicity contributions for the ν_1 bands vary between 10.6 and 12.2 %, while those for the ν_2 bands are of the order of 7 %. Assuming that the intensity of the ν_2 band is the same for K-NH_3 and Cs-NH_3 isolated in an argon matrix, some comparison with the experimental values of Süzer and Andrews is possible (cf. Table I of ref. [2]) The ratio of relative intensities of the ν_1 bands of these authors A_1(Cs-NH_3) / A_1(K-NH_3) = 70/60 ≈ 1.17 agrees nicely with the present value of 557.1/477.2 ≈ 1.17. For the intensity ratio of the ν_2 versus ν_1 bands of K-NH_3, Süzer and Andrews [2] and Loutellier et al. [3] quoted a value of 0.7. Compared to the results of the present work, these authors have probably employed a different definition for the IR intensities. While the CCSD(T) value for the ratio A_1/A_2 is 2.30, the corresponding ratio Γ_1/Γ_2 amounts to 0.73, where the alternative intensity definition $\Gamma_i \approx A_i / \tilde{\nu}_i$ is employed.

References

[1] I. S. Lim, P. Botschwina, R. Oswald, V. Barone, H. Stoll, and P. Schwerdtfeger, J. Chem. Phys., in press, and references therein.

[2] S. Süzer and L. Andrews, J. Am. Chem. Soc. **109**, 300 (1986).

[3] A. Loutellier, L. Manceron, and J. P. Perchard, Chem. Phys. **146**, 179 (1990).

[4] P. Botschwina and R. Oswald, Z. Phys. Chem. **219**, 399 (2005).

[5] J. Flügge, *Ab initio Studie kleiner Molekül-Lithium-Komplexe*, Dissertation, Cuvillier Verlag, Göttingen, 1994.

[6] J. Flügge and P. Botschwina, in *Structures and Dynamics of Clusters*, Universal Academic Press, (1996); pg. 599.

Quartet alkali trimers on He nanodroplets: Laser spectroscopy and *ab initio* calculations

J. Nagl, G. Auböck, A. W. Hauser, O. Allard, C. Callegari, and W. E. Ernst
Institute of Experimental Physics, Graz University of Technology, Graz, Austria

Helium nanodroplets ($N = 10^4$) are produced by supersonic free jet expansion and provide a cold environment ($T = 0.4$ K) for dopants. Helium clusters can dissipate energy very efficiently by evaporating their own atoms (binding energy per He atom: 5 cm^{-1}). Alkali atoms are deposited on the helium surface by passing the droplet beam through one or more heated pick-up cells containing alkali vapor. Capture of multiple atoms per cluster leads to molecular formation. Due to the amount of binding energy released into the cluster, a strongly bound low-spin molecule will be expelled from the droplet beam, while a weakly bound high-spin van der Waals molecule will remain on its droplet. We have located, in the wavelength range 10500–17500 cm^{-1}, a variety of electronic spectra of the homo- and heteronuclear trimers K_3, Rb_3, K_2Rb and KRb_2 in their high-spin quartet state. Various schemes of beam depletion spectroscopy, such as two-laser excitation and mass-selective depletion are applied to separate overlapping spectral features, and to assign the individual bands (Fig. 1).

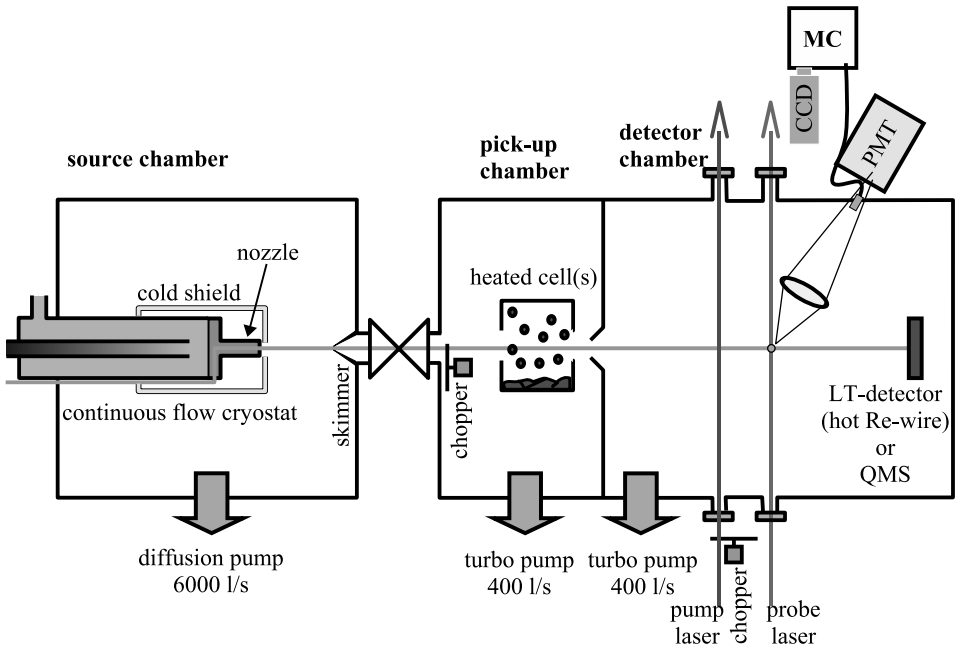

Figure 1: Experimental setup

We calculate the electronic structure of all these trimers in their ground electronic state, and in several excited states (spin doublet as well as quartet), with *ab-initio* methods. For the doublet manifold of K_3 we have completed two-dimensional scans, over (Q_s, Q_x) and (Q_x, Q_y) [1], of the ground state electronic surface (doublet spin state) at the UCCSD(T) level of theory [2], as well as scans of the first 10 electronic states over

Q_x near the equilibrium position, at the CASSCF level of theory (Fig. 2). We find the BSSE-corrected equilibrium geometry to be an isosceles triangle (C_{2v}, $2B_2$ symmetry), with bond length $b = 4.322$ Å and bond angle $\theta = 74.0°$ (corresponding to $Q_s = 4.59$ Å, $Q_x = -0.61$ Å, $Q_y = 0$) [3].

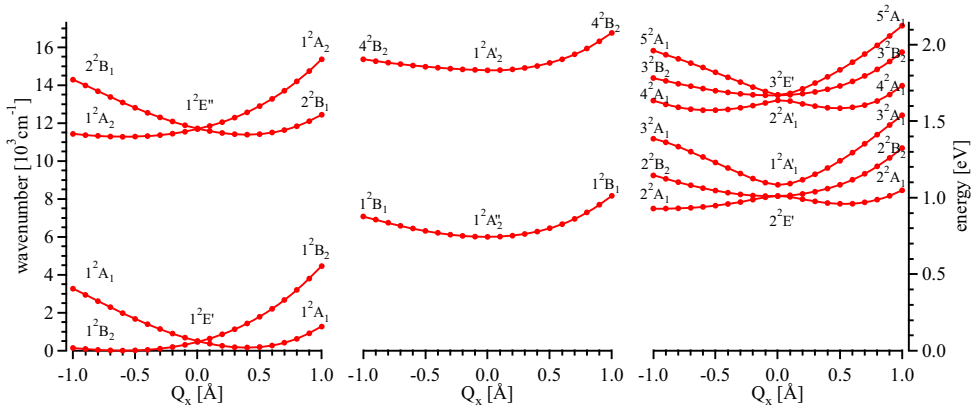

Figure 2: CASSCF potential energy curves of K_3, scanned along the Q_x normal coordinate at $Q_s = 4.59$ Å and $Q_y = 0$, grouped according to their Jahn-Teller distortion pattern.

For the quartet manifold we have calculated the lowest-energy geometry, and a scan over Q_x including the 16 lowest excited states: for the homonuclear trimers we find an equilateral equilibrium structure with bond length 5.06 Å (K_3) and 5.52 Å (Rb_3); for K_2Rb and KRb_2 the structure is an isosceles triangle with bond length 5.26 and 5.29 Å, and angle 57.61° and 62.19°, respectively.

We find several regular patterns in the level structure of these trimers, which we are in the process of explaining by means of symmetry arguments and simplified models.

[1] Q_x: breathing mode; Q_x: symmetric bending mode; Q_y: asymmetric mode.

[2] Acronyms:
UCCSD(T): Unrestricted Coupled Cluster calculations with Single, Double and non-iterative Triple excitation
CASSCF: Complete Active Space Self-Consistent Field
BSSE: Basis Set Superposition Error

[3] J. Nagl, A. W. Hauser, G. Auböck, C. Callegari, and W. E. Ernst, Optical spectroscopy of potassium-doped argon clusters. Experiments and quantum-chemistry calculations. J. Phys. Chem. A, in press.

Magnetic interactions on doped He droplets. Visible-spectroscopy investigation of electron-spin relaxation and spin-orbit effects

G. Auböck, J. Nagl, C. Callegari, and W. E. Ernst
Institute of Experimental Physics, Graz University of Technology, Graz, Austria

Helium nanodroplets ($N \approx 10^4$ atoms) are formed in a supersonic expansion, and doped by passing through a pick-up cell containing low pressure alkali gas. Alkali atoms are unique dopants as they remain on the droplet surface. Most degrees of freedom of dopant atoms and molecules are immediately cooled to the droplet internal temperature (0.37 K). The released energy leads to evaporation of helium atoms from the droplet. Due to their smaller binding energy it is the high spin alkali complexes (triplet dimers, quartet trimers) which preferentially survive the formation process.

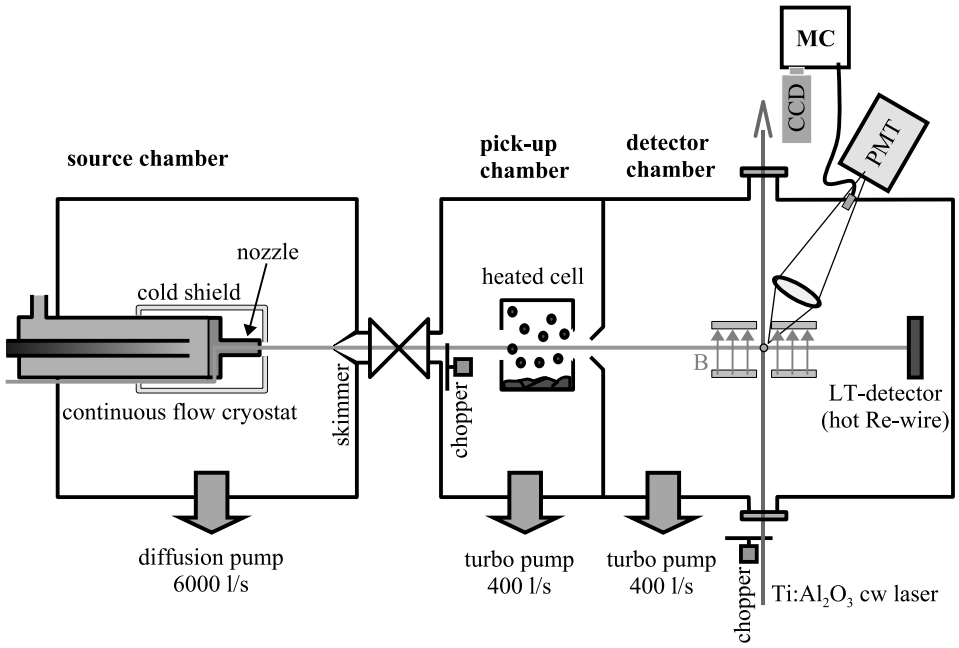

Figure 1: Experimental apparatus

ESR spectroscopy can become a versatile tool to investigate oligomers formed on He droplets, once spin lifetimes have been determined, and a detection method for spin states has been developed. In a first step, we have measured magnetic dichroism spectra of potassium atoms on He nanodroplets 1) to estimate the spin-relaxation time; 2) to demonstrate that a spin-polarized sample can be easily created and that optical detection is a viable technique for ESR in He droplets. Laser induced fluorescence was used to probe the K $4P \leftarrow 4S$ atomic transition and the $1^3\Pi_g \leftarrow 1^3\Sigma_u$ bands of K_2 and Rb_2 (Fig. 1). A magnetic field of 2.9 kG was applied and the laser beam polarization continuously varied with a Pockels cell from σ^- through π to σ^+. Magnetic circular dichroism spectroscopy probes the populations of Zeeman sublevels: No dichroism was observed for atomic potassium

on helium droplets, indicating that the sublevels have not thermalized. This sets a lower limit for the spin relaxation time of 1.9 ms [1], based on the geometry of the molecular beam apparatus. Spectra of the molecules K_2 and Rb_2 on He_N showed, however, strong dichroism, whose analysis yields a population of Zeeman sublevels at thermal equilibrium with the helium droplet. This represents the first measurement ever of the droplet surface temperature. Geometric considerations put an upper limit of $\approx 40\mu$s to the spin relaxation time in this case. Such a different behavior between atoms and molecules will have to be rationalized on the basis of their interaction with the helium environment. We also measure the optical saturation of the spectra and evaluate the different experimental routes available to prepare spin-polarized samples on cold droplets.

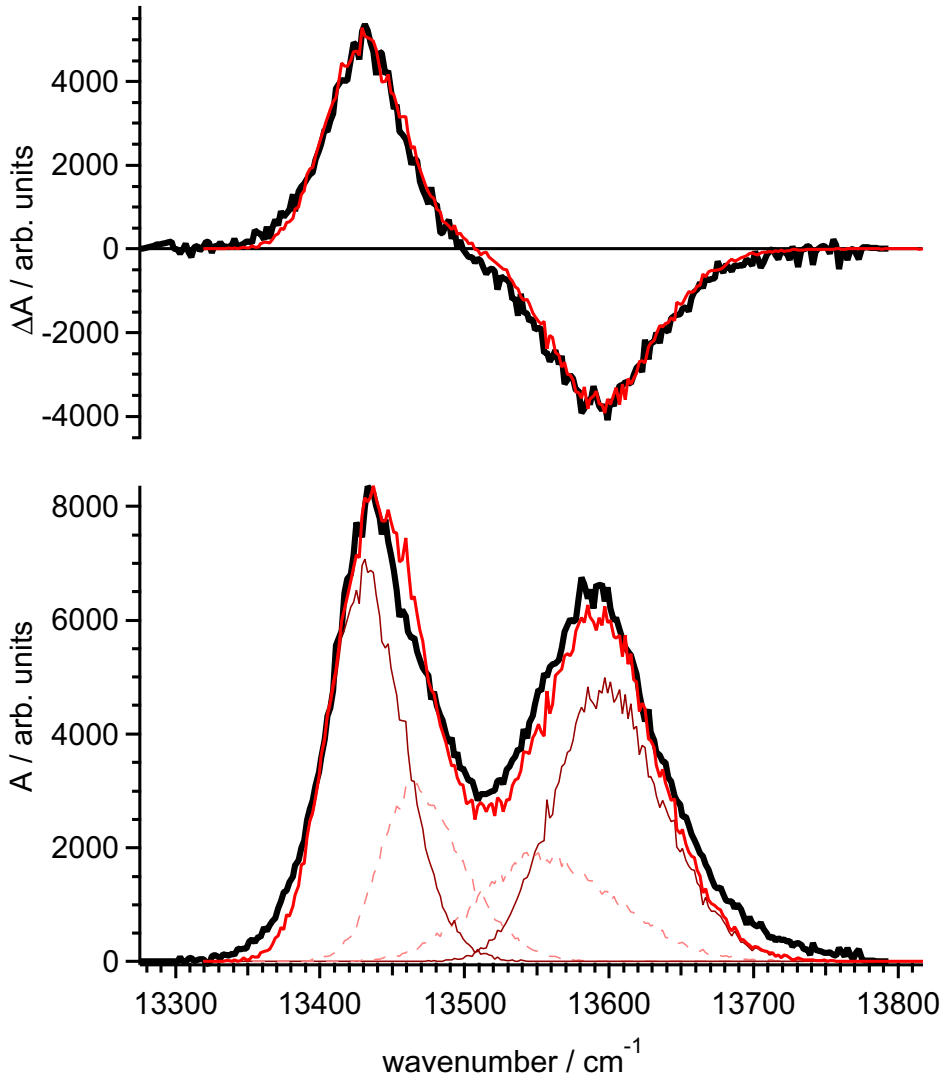

Figure 2: MCD (upper panel) and LIF (lower panel) spectra of Rb_2 on He nanodroplets. Shown are the measured fluorescence signals (thick lines) and simulated spectra (thin lines; the LIF spectrum is further subdivided into its spin-orbit multiplet components.

We discuss in detail the electronic structure of alkali dimer molecules in $^3\Pi_g$ states on the surface of a helium droplet. The perturbation due to the droplet will in general not satisfy rotational symmetry around the internuclear axis of the diatom and thus, in addition to a broadening and blue shift, will cause a splitting of electronic levels that are degenerate in the free molecules. We propose a model based on general symmetry arguments and on a small number of physically reasonable parameters [2]. The model accounts for the essential features of laser induced fluorescence (LIF) and magnetic circular dichroism (MCD) spectra of the $1^3\Pi_g$–$1^3\Sigma_u^+$ transition of Rb_2 and K_2 (Fig. 2). It may also be capable to explain unusual features of other alkali dimer spectra on He droplets (i.e. "missing" spin orbit components in $^3\Pi$ excitations of NaCs and LiCs). As mentioned above, the MCD spectra allow a determination of the populations of Zeeman sublevels in the ground state and thus a measurement of the surface temperature of the droplet. The latter agrees with the accepted temperature, 0.37 K, measured in the interior of a droplet. This is the first instance of a He droplet surface thermometer.

[1] J. Nagl, G. Auböck, C. Callegari, and W. E. Ernst Phys. Rev. Lett. **98**, 075301 (2007) http://dx.doi.org/10.1103/PhysRevLett.98.075301

[2] G. Auböck, J. Nagl, C. Callegari, and W. E. Ernst J. Phys. Chem. A **111**, 7404 (2007) http://dx.doi.org/10.1021/jp070891y

Radical-radical reaction dynamics: a combined crossed-beam and theoretical study

Jong-Ho Choi
Department of Chemistry and Center for Electro- and Photo-Responsive Molecules, Korea University, 1, Anam-dong, Seoul 136-701

We present an overview of our recent studies of the gas-phase reaction dynamics of $O(^3P)$ with a series of hydrocarbon radicals [allyl (C_3H_5), propargyl (C_3H_3), t-butyl (t-C_4H_9)] as prototypal radical-radical oxidation reactions. High-resolution laser spectroscopy in a crossed-beam configuration was applied to examine the nascent rovibrational state distributions and Doppler profiles of the reactive scattering products. The analyses of the product energy and population distributions demonstrated the existence of unusual dynamic characteristics and competition between the addition and abstraction reaction mechanisms at the molecular level. These features, which are in sharp contrast with those of the oxidation reactions of closed-shell hydrocarbon molecules, are discussed with the aid of the *ab initio* and quantum statistical calculations.

References:

[1] Jong-Ho Choi, Int. Rev. Phys. Chem. **25**, 613 (2006), and references therein.

Electron Induced Proton Transfer as a Trigger of DNA Strand Breaks

Iwona Dąbkowska,[a,b] Janusz Rak,[b] and Maciej Gutowski[b,c]

[a] *Institut für Chemie, Physikalische und Theoretische Chemie, Freie Universität Berlin, 14195 Berlin,* Germany

[b] *Department of Chemistry, University of Gdańsk, Sobieskiego 18, 80-952 Gdańsk, Poland*

[c] *Heriot-Watt Unviersity, Chemistry-School of Engineering and Physical Sciences, Edinburgh EH14 4AS, United Kingdom*

We propose a mechanism of single strand breaks in DNA induced by low-energy electrons. The proposed process advances through bound anionic states, not through metastable states with finite lifetimes and discrete energy positions with respect to the neutral target. A clear advantage of dealing with bound anionic states is that that strand break formation does not have to compete with the very fast electron autodetachment process (ca. 10^{14} s^{-1}). We used a nucleotide of thymine as a model system and we performed all calculations at the density functional level of theory with the B3LYP exchange-correlation functional. No geometry constraints have been imposed on the system and stationary points have been identified on the potential energy surface of the anion. The following steps have been identified:

1. The thymine moiety is hydrogenated at the O4 position, producing $(T+H)^{\bullet}$. The hydrogenation develops as either an excess electron attachment followed by a barrier-free proton transfer from a neighboring acid, or in consequence of the interaction of $H^{\bullet}$ with O4 of thymine.

2. $(T+H)^{\bullet}$ binds an excess electron and forms a closed shell moiety, $(T+H)^{-}$. $(T+H)^{-}$ is characterized by a significant electron vertical detachment energy of 40 kcal/mol and is adiabatically bound with respect to $(T+H)^{\bullet}$ by 14 kcal/mol. The excess charge is localized primarily on the C6 atom of $(T+H)^{-}$.

3. A proton is transferred from the C2' atom of the adjacent sugar unit to the C6 atom of $(T+H)^{-}$ with a barrier smaller than 5 kcal/mol. The second proton transfer is followed by a barrier-free sugar-phosphate C-O bond cleavage.

The rate of the C-O bond cleavage in the anion of hydrogenated nucleotide of T is estimated to be in a range 3.0×10^{10} – 1.1×10^{11} s^{-1}, which makes the proposed mechanism very probable in DNA. In the future study we will explore proton transfer to the sites of thymine other than O4. We will also explore whether an analogous strand break mechanism applies to the nucleotide of cytosine. Finally, we intend to improve our model system by replacing neutralizing protons with metallic counteractions and by including hydration effects.

One more question to be answered is what is the origin of the resonance structure in the damage quantum-yield versus incident electron energy[5] if the strand break might develop through bound anionic states? We believe that the role of resonance states is to allow for energy transfer between the impinging electron and the neutral target. The energy transfer is efficient if the energy of the impinging electron matches the position of the resonance state. We believe that the primary role of resonance states is to provide avenues for the free electron to cool down by transferring kinetic energy to the internal degrees of freedom of the target. In other words, we view anionic resonance states as doorways to bound anionic states. The latter may be involved in chemical transformations, such as DNA strand breaks, while the former are required to absorb excess electrons into the DNA environment.

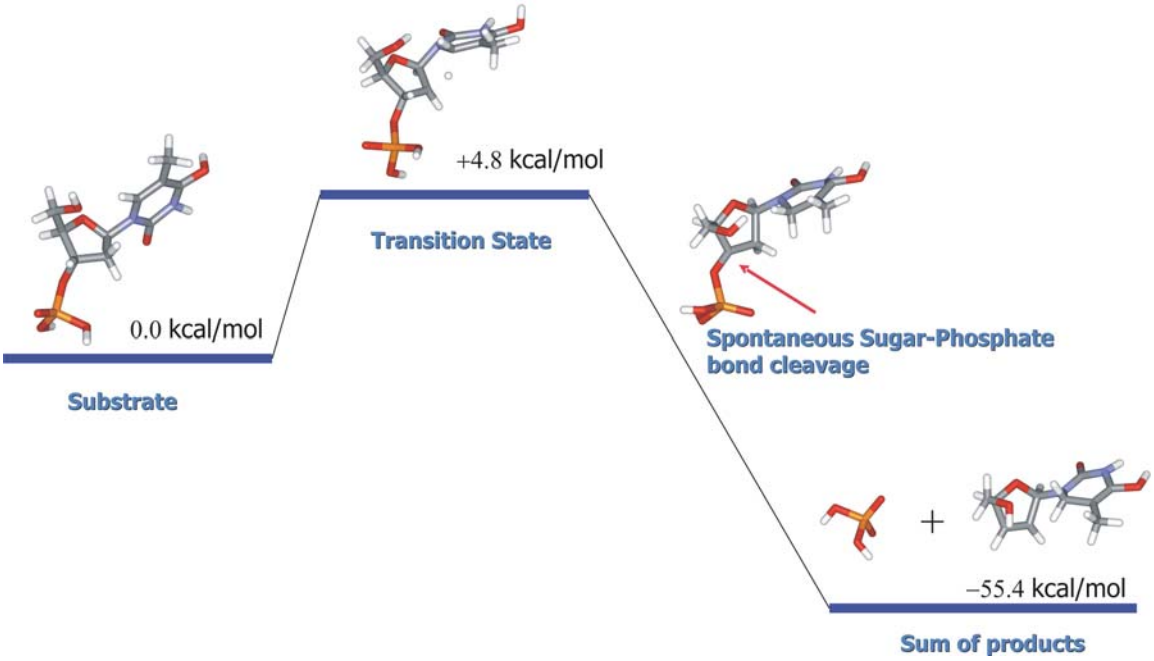

B3LYP/6-31++G** free energies for a rupture of sugar-phosphate bond in the nucleotide of thymine upon interaction with excess electrons

Site dependent dissociation of adenine: influence of functional groups upon dissociative electron attachment

S. Denifl, P. Sulzer, F. Zappa, M. Probst, T.D. Märk, P. Scheier
Institut für Ionenphysik und Angewandte Physik, Universität Innsbruck, Technikerstrasse 25, A-6020 Innsbruck, Austria

Natcha Injan and Jumras Limtrakul
Department of Chemistry and Center of Nanotechnology Kasetsart University, Bangkok 10900, Thailand

R. Abouaf, H. Dunet
Laboratoire des Collisions Atomiques et Moléculaires (UMR 8625), Bâtiment 351, Université Paris-Sud, 91405 Orsay Cedex, France

Introduction

So far an extended number of free dissociative electron attachment (DEA) studies have been performed with isolated biomolecules in the gas phase (see review in [1]). The interest in these molecules arose from the discovery that low energy electrons below 15 eV can induce substantial yields of single and double strand breaks in DNA [2]. This DNA damage was ascribed to fast decays of the transient negative resonances localized on the DNA basic constituents. Since low-energy secondary electrons are produced in exceeding amounts along the radiation track in cells DEA studies with DNA compounds are considered to be of relevance for the description of the damage by ionizing radiation in particular as DNA carries the genetic information for cell replication and protein synthesis.
So far the most extensively studied isolated DNA compounds have been the nucleobases [3-6]. For these molecules the dominant product anion is the dehydrogenated molecular anion $(M–H)^-$. For all nucleobases this reaction is mainly operative at electron energies below 3 eV leading in the cross section to several overlapping peaks. An important result was the discovery of site and bond selective hydrogen loss leading to this anion. This was intensively studied in the course of systematic investigations of DEA to partially methylated or deuterated pyrimidines (thymine and uracil), i.e. the captured electron with a well defined energy can induce the cleavage of a specific bond to one of the hydrogen atoms of the molecule depending on the initial electron energy [7-10]. As for the pyrimidines, DEA to partially modified adenine, where hydrogen atoms of the molecule are replaced by a deuterium or a methyl group, can also elucidate site and bond selectivity for this bicyclic molecule. Here we present a detailed study of the dehydrogenated molecular anion $(M–H)^-$ formed via DEA to adenine and partially deuterated or methylated derivatives of adenine [11].

Experimental setup

In the present collaborative study devices in two different laboratories (Orsay and Innsbruck) are used. Experiments on adenine are performed on the Orsay set up whereas the

measurements with all other molecules are carried out with the hemispherical monochromator instrument in Innsbruck.
The Orsay set up consists of an electron spectrometer equipped with two hemispherical energy analysers in tandem, both in the monochromator and the analyser sections [12]. The electron energy resolution ranges from 0.025 eV to 0.060 eV (FWHM, energy loss mode). Mass analysis (cations or anions) is achieved with a time of flight system using a Wiley-McLaren geometry. The incident electron beam is shut off during the extraction time of the TOF system in order to avoid perturbation of the signal. An effusive beam of molecules is generated by vaporizing commercial samples (Merck) in a double stage oven at 190°C.
The apparatus used for the measurements in Innsbruck is a crossed electron/molecule beams-instrument consisting of a neutral molecular beam source, hemispherical electron monochromator and a quadrupole mass spectrometer [3]. As a molecular beam source we use a Knudsen type oven. The partially deuterated adenine (2-D-Ad), 9-methyladenine (9-mAd), 6-dimethyladenine (6-dimAd) and purine (Pu) samples have stated purities of 97 %, >97 %, >98 % and 98 %, respectively. Typical oven temperatures used in the present experiment range from about 115 °C up to 185 °C depending on the sample. Through a capillary with the diameter of 1 mm the gaseous molecules effuse directly into the collision chamber of the hemispherical electron monochromator, where the interaction with the monochromatized electron beam occurs. Negative ions formed are extracted into a quadrupole mass spectrometer. The mass selected anions are finally detected by a channel electron multiplier.

Results and discussion

The ion yield of dehydrogenated $(M–H)^-$ of Ad is shown in the upper panel of Fig. 1 measured with an electron energy resolution of about 60 meV (Orsay setup). The ion yield shows narrow peaks at 0.72 eV, 0.84 eV and 1.07 eV (error bars for these values are ± 0.07 eV), followed by two wide bumps at about 1.4 eV and 2.2 eV. Also shown in Figure 1 is $(M–H)^-$ of adenine deuterated at the C2 position (2-D-Ad) recorded with an energy resolution of 80 meV (Innsbruck setup). The measured ion yield of $(M–H)^-$ is virtually identical for both molecules. The less resolved peak structure in case of 2-D-Ad can be attributed to the slightly worse energy resolution used for this molecule. Thus we can conclude that *dehydrogenation* of Ad does not occur at the C2 carbon atom, as this is blocked by D in the deuterated adenine, i.e., no $(M-D)^-$ can be observed at all.
According to calculations of bond dissociation energies one can assume that the narrow peaks at low energies (below about 1.07 eV) in Fig.1 should originate solely via H loss from the N9 position. This prediction can be easily verified by measurements with 9-methyladenine (9-mAd) where the N9 position is blocked with a CH_3 group. Indeed, the corresponding ion yield (see Fig. 1) only starts above 1.4 eV. This weakly observed signal is ascribed to H loss from the NH_2 group attached to the C6 position.

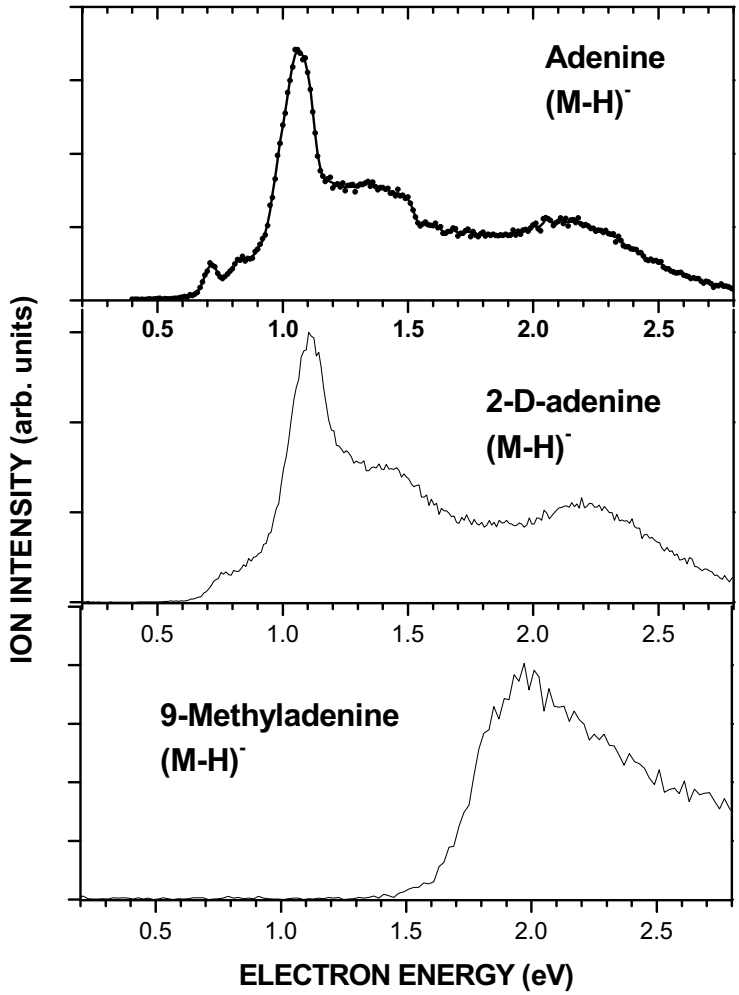

Fig. 1: Ion yield of the dehydrogenated molecular anion $(M–H)^-$ formed via DEA to adenine (top), 2-D-adenine (middle) and 9-methyladenine (bottom), respectively.

For a conclusive check we have performed an additional experiment with 6-dimethyladenine (6-dimAd) thus blocking the H positions at the amino group with CH_3. Surprisingly the corresponding ion yield of $(M\text{-}H)^-$ (not shown), does not only show a peak structure at low energies (presumably due to H loss from the 'open' N9 position), but also one at higher energies which have been attributed in the 9-mAd to loss from the amino group which should be blocked in this case. Also for purine the resonances below 1 eV are quite different. For this compound also the position of the resonance features above 1 eV is different compared to Ad.
The intriguing question is now why the C6-H, C6-NH_2, and C6-$N(CH_3)_2$ groups, that differentiate the purine derivatives from each other (Pu, Ad, and 6-dimAd, respectively) and are rather far away of the N9 group, cause these remarkably different spectra?
It is interesting to note that when going from Pu to Ad to 6-dimAd the dipole moment vector moves out of the direction of the N9-H bond and its magnitude decreases from 3.66 D to 2.19 D. This obviously will cause quite a different electrical field situation at the N9-H bond for the three molecules. More detail on this can be provided *inter alia* by looking at the electrostatic potentials (ESP) of the molecules. Whereas for Pu the only region of strongly positive ESP is around the N9-H site (and the neighboring C8-H site), in case of Ad and also for 6-dimAd besides this positive region around N9-H a second positive ESP region appears

around the NH_2 and $N(CH_3)_2$ groups. Since regions of positive ESP attract an electron, the various functional groups leading to different ESPs should therefore influence the DEA spectrum. Also the lowest virtual σ^* MOs of the neutral derivatives show distinct differences in the wave function density close to C6. It is remarkable that the lowest pair of virtual σ^* MOs for each molecule (the second one is related to the first by symmetry breaking and a changed sign of the wave function) have node surfaces intersecting the N9-H bond. This is a second indication, independent of the energy criteria, of the dissociation site.

Acknowledgements

This work has been supported by the FWF, Wien, Austria and the European Commission, Brussels.

References

[1] P. Swiderek, Angew. Chem. Int. Ed. **45,** 4056(2006).
[2] B. Boudaïffa, P. Cloutier, D. Hunting, M. A. Huels, L. Sanche, Science **287,** 1658 (2000).
[3] S. Denifl, S. Ptasinska, M. Cingel, S. Matejcik, P. Scheier, T. D. Märk, Chem. Phys. Lett. **377**, 74 (2003).
[4] G. Hanel, B. Gstir, S. Denifl, P.Scheier, M. Probst, B. Farizon, M. Farizon, E. Illenberger and T. D. Märk, Phys. Rev. Lett. **90,** 1888104 (2003).
[5] D. Huber, M. Beikircher, S. Denifl, F. Zappa, S. Matejcik, A. Bacher, V. Grill, T.D. Märk, P. Scheier, J. Chem. Phys. **125,** 084304 (2006).
[6] H. Abdoul-Carime, S. Gohlke, E. Illenberger, Phys. Rev. Lett. **92**, 168103 (2004).
[7] S. Ptasinska, S. Denifl, P. Scheier, E. Illenberger, T. D. Märk, Angew. Chem. Int. Ed. **44,** 6941–6943 (2005).
[8] P.D. Burrow, G.A. Gallup, A.M. Scheer, S. Denifl, S. Ptasinska, T. D. Märk, P. Scheier, J. Chem. Phys. **124**, 124310 (2006).
[9] S. Ptasinska, S. Denifl, V. Grill, T.D. Märk, P. Scheier, S. Gohlke, M. A. Huels, E. Illenberger, Angew. Chem. Int. Ed. **44,** 1647 (2005).
[10] S. Ptasinska, S. Denifl, V. Grill, T. D. Märk, E. Illenberger, P. Scheier, Phys. Rev. Lett. **95**, 093201 (2005).
[11] S. Denifl, P. Sulzer, D. Huber, F. Zappa, M. Probst, T.D. Märk, P. Scheier, N. Injan, J. Limtrakul, R. Abouaf, H. Dunet, Angew. Chem. Int. Ed. **46,** 5238, (2007).
[12] R. Abouaf and H. Dunet, Eur. Phys. J. D **35,** 405 (2005).

Amplification of chirality: sergeants and soldiers at surfaces

M. Parschau, R. Fasel & K.-H. Ernst

Swiss Ferdeal Laboratories for Materials Testing and Research (Empa), CH 8600 Dübendorf, Switzerland

In his most famous experiment in 1848 Pasteur manually separated left- and right-handed ammonium sodium tartrate crystals under the microscope and observed opposite optical activity of their aqueous solutions. His insight that the origin of chirality is based on molecular structure layed the foundation of modern structural organic chemistry. Moreover, there are two intriguing aspects in his experiment: i) Handedness is transferred from molecular structure into the macroscopic shape of the crystral, and ii) the two mirror-like forms of the molecules crystallized into homochiral conglomerates allowing manual separation. Up to date, the mechanisms of both processes are still poorly understood. We are not able to predict the shape of a crystal based on the molecular structure nor do we understand why mixtures of left- and right-handed molecules (racemate) separate only sometimes into homochiral conglomerates during crystallization. One of the reasons is the cooperative nature of both processes. Extremely small influences are amplified via many cooperating units into a macroscopic result. A promising approach to these complicated questions is studying two-dimensional crystallisation phenomena on well-defined substrates via STM and other surface analytical techniques.

We show that chiral doping can drive a surface lattice into homochirality. When adsorbed at surfaces, achiral molecules can become chiral because of the reduced symmetry in the molecule or the adsorbate lattice. Adsorbed on Cu(110), succinic acid and achiral (*R,S*)-tartaric acid form equal numbers of left- and right-handed domains in the absence of additional chiral influences and the surface is globally achiral. Doping with small amounts of left- or right-handed (*S,S*)- or (*R,R*)-tartaric acid, however, creates homochirality and the opposite mirror domains are not observed anymore in the LEED pattern (Fig. 1) [1,2].

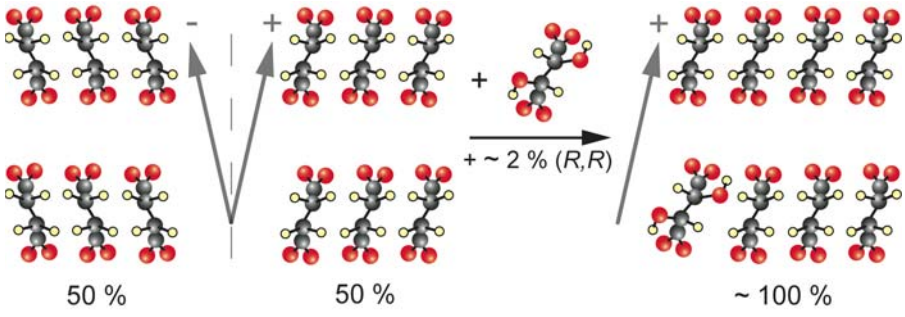

Fig. 1: Doping with small amounts of chiral tartrate molecules suppresses one mirror-like alignment of achiral succinic acid on Cu(110).

In another case, a special surface enantiomorphism is observed via STM after adsorption of the enantiomers of a helical aromatic hydrocarbon (Fig. 2) on Cu(111). Instead of crystallization into homochiral domains on the surface, racemic mirror domains are observed. That is, every single domain contains an equimolar amount of left- and right-handed molecules. Both enantiomers can be aligned in two mirror-like configurations, leading to the two mirror domains. The basic structural unit is a heterochiral pair. In this situation, however, a small excess of one chiral species is sufficient to create domains possessing single handedness throughout the entire surface layer (Fig. 3) [3]. Our findings are explained by cooperative interactions as previously described for helical polymer chains. Molecular modelling calculations (MMC) strongly support this interpretation by (i) revealing that the chiral excess favours one mirror-like alignment of the lattice and (ii) by confirming that mirror domain boundaries impose an energetically unfavourable situation.

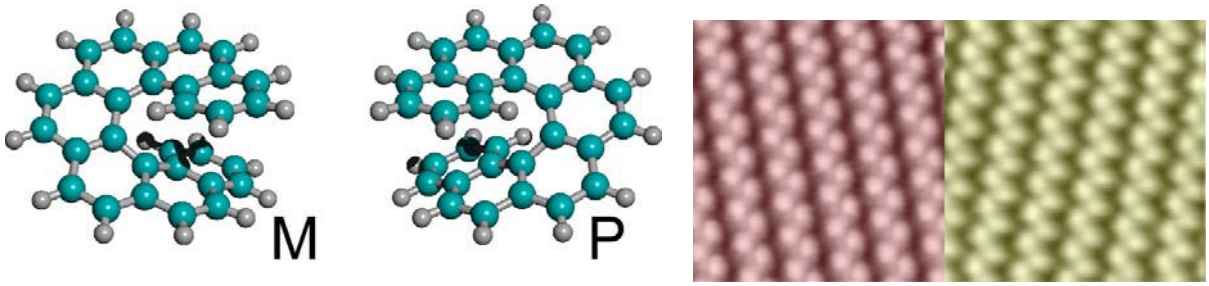

Fig. 2: An equimolar mixture of left(M)- and right(R)-handed helical aromatic molecules forms mirror-like zigzag arrangements on Cu(111).

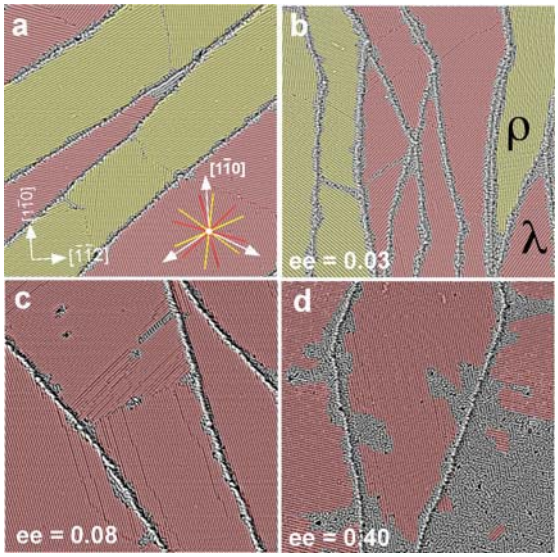

Fig. 3: Small excess of one enantiomer is sufficient to suppress the formation of one mirror domain type.

[1] M. Parschau, S. Romer, K.-H. Ernst, J Am Chem Soc 126 (2004) 15398
[2] M. Parschau, T. Kampen, K.-H. Ernst, Chem Phys Lett 407 (2005) 433
[3] R. Fasel, M. Parschau, K.-H, Ernst, Nature 439 (2006) 449

Photolysis of small biomolecules in clusters: How does a solvent influence the photochemistry

V. Profant, V. Poterya and M.Fárník
J.Heyrovský Institute of Physical Chemistry AS CR, Dolejškova 3, 18223 Prague 8, Czech Republic

P. Slavíček
Department of Physical Chemistry, Institute of Chemical Technology, Technická 5, Prague 6, Czech Republic

U. Buck
Max-Planck-Institut für Dynamik und Selbstorganisation, Bunsenstr. 10, Göttingen

Small heteroaromatic molecules, such as pyrrole (Py), imidazol or pyrazol, represent examples of the simplest units with biological relevance. They are present in many larger biological structures, e.g. hemes, chlorophylls, histidine, etc. and their UV-photochemistry has important biological consequences. Therefore their UV-absorption and photochemistry in the gas phase has been studied in great detail previously [1]. In nature, however, the photochemical processes occur in some environment, e.g. in a solvent or in a geometry dictated by a phosphate backbone of a protein molecule. Thus, as a further step towards investigation of biologically relevant processes at the molecular level, we have studied the UV-photolysis and ionization of the above molecules in various cluster environments [2,3].

The clusters provide some advantages for investigation of the photolysis processes in the condensed phase-like environment [4]: e.g. (i) the finite number of cluster constituents facilitates theoretical treatments often impossible for the infinite bulk; (ii) the evolution of the processes can be investigated as a function of the cluster size; (iii) some experimental observables which are inaccessible in the bulk can be measured in clusters, e.g., the kinetic energy of the fragments escaping from the cluster, which is what we measure in our experiment. From the fragment kinetic energy distribution (KED) we can learn the details about the photodissociation process at the molecular level.

The experiments were performed in a molecular beam apparatus for cluster studies. The clusters were produced by supersonic expansions through a conical nozzle. Different types of clusters and various cluster sizes were produced in expansions of the above molecules with either He or Ar carrier gas under different expansion conditions. The *neutral cluster size distribution* can be measured by the nondestructive deflection method [5]. The clusters can be electron impact ionized and successively mass analyzed with a quadrupole mass spectrometer. Alternatively, in the photodissociation experiments, they are UV photolyzed and the fragments

are photoionized and analyzed by a time-of-flight spectrometer. The spectrometer is operated in the low-field regime to measure the fragment kinetic energy. For the dissociation of molecules and photoionization of the H fragments a UV-laser pulse is used with wavelength 243 nm (2+1 REMPI of H atom). The molecules can be also photolyzed at 193 nm with another synchronized laser pulse. The interpretation of the experimental results was assisted by accompanied theoretical calculations at the CCSD(T) level.

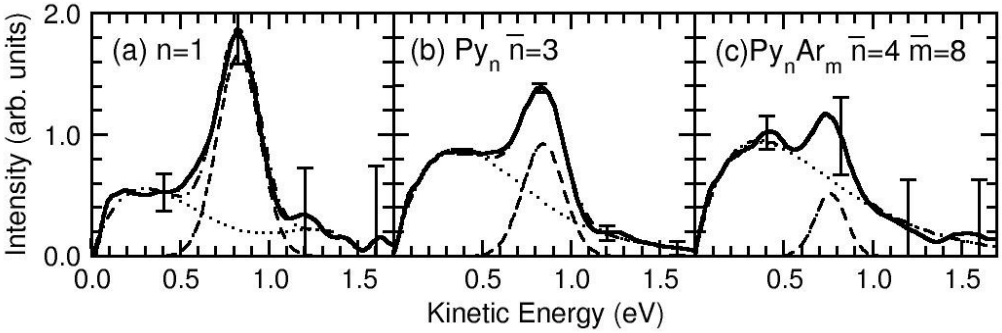

Fig. 1: H-fragment kinetic energy distributions after photolysis of (a) single Py molecule, (b) Py_n clusters of the mean size n=3, and (c) Py_nAr_m clusters with n=4 and m=8.

Figure 1 shows the H-fragment KEDs after the pyrrole photolysis for a pyrrole molecule (a) and for the various clusters (b) and (c). All the spectra exhibit the bimodal character observed previously in the photodissociation of pyrrole molecules, with a narrower peak of *fast* photofragments and a broader lower intensity distribution of the *slow* ones. However, the fast fragment contribution, which is the major channel for the molecule, decreases in intensity relative to the slow component with the increasing cluster size.

Figure 2 provides a qualitative explanation for the observed trends in the KED in terms of the potential energy surfaces (PES) based on the theoretical calculations. The molecule is promoted by the 243 nm photon to an excited state of a $\pi\sigma^*$ character. Then it evolves along the N-H coordinate resulting in a prompt N-H bond fission leading to the fast H-fragments. An internal conversion to the ground state via the conical intersection can lead to the slow fragments. Another ring-bending coordinate leading to the dissociation has to be considered too. It plays a crucial role by connecting the $\pi\sigma^*$ state with another excited $\pi\pi^*$ state and other fragmentation channels. Upon the excitation with 193 nm the $\pi\pi^*$ state can be populated, which enhances the generation of the slow H-fragments.

At the bottom panel of figure 2, the calculated influence of a structureless Ar-atom solvent on the potential is shown. The excited $\pi\sigma^*$ state is shifted in energy by the electronic interaction with the solvent and the conical intersection with the ground state disappears. This, in principle, leads to the closure of the dissociation channel leading to the fast H-fragments with the Py solvation. Further details of the solvated Py-molecule photochemistry will be discussed in our contribution.

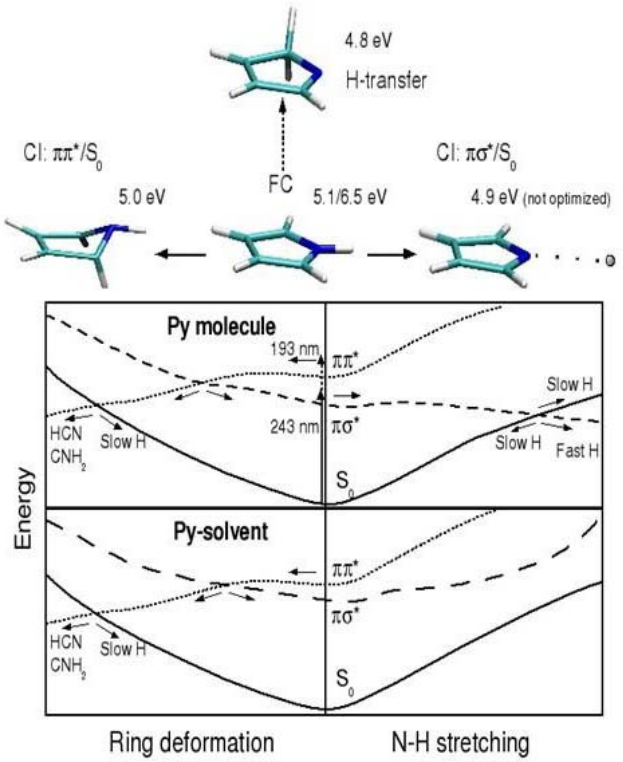

Fig. 2: Calculated potential for the ground and excited states of Py molecule (top) and the Py molecule solvated by an Ar atom (bottom).

Further, the photolysis of imidazol and pyrazol molecules in the clusters will be presented too. The principle difference to the pyrrole molecules, which are bound together in the clusters by the N-H···π bonds, the other molecules generate the hydrogen N-H···N bonds.

Acknowledgement: The present work has been supported by the special program "Nanotechnology for society" of the Czech Academy of Sciences KAN400400461, and by the Grant Agency of the Czech Republic 203/06/1290. V. Profant acknowledges the university grant 8113-10/257852.

[1] M.N.R. Ashfold, B. Cronin, A.L. Devin, R.N. Dixon, M.G.D. Nix, Science **312**, 1637 (2006).

[2] V. Poterya, V. Profant, M. Fárník, P. Slavíček, U. Buck, J. Chem. Phys. **127**, 064307 (2007).

[3] V. Profant, V. Poterya, M. Fárník, P. Slavíček, U. Buck, J. Phys. Chem. A **111**, 0751561 (2007).

[4] U. Buck, J. Chem. Phys. A **106**, 10049 (2002).

[5] U. Buck, H. Meyer, Phys. Rev. Lett. **52** (1984) 109.

Laser Induced Fluorescence detection of excited electronic states of the calcium dimer on argon and helium clusters around 380 nm

M.A. Gaveau, C. Pothier, P.R. Fournier and J.M. Mestdagh
Laboratoire Francis Perrin, CNRS URA 2453, DSM/DRECAM/SPAM, CEA Saclay, 91191 Gif-sur-Yvette Cedex, FRANCE

G. Durand, M.-C Heitz, T. Bouissou and F. Spiegelman
Laboratoire de Physique et Chimie Quantique, CNRS UMR 5626, IRSAMC, Université Paul Sabatier, 118 Route de Narbonne, F31062 Toulouse cedex,

The CICR technique ("Cluster Isolated Chemical Reactions") has been developed in our laboratory in order to investigate at a microscopic level the influence of a reaction medium on reaction dynamics [1-3]. Indeed, this method allows to deposit various reactants on large van der Waals clusters in a very controlled way, so that it is possible to determine the number of reactants involved in the reaction process, and therefore obtain its stoichiometry. This method makes also possible to study spectroscopy and dynamics of atoms, molecules and complexes that has been deposited or formed and stabilized on clusters. We have in particular worked on alkaline earth atoms like Ba [4] or Ca [5], and also calcium dimers [6] deposited on large argon and neon clusters: Laser induced fluorescence of Ca_2 was observed in the green (530-550nm) and in the red region (600-680 nm) as well as in the vicinity of the calcium resonance line (400-430 nm). More recently we have modified our Campargue-type molecular beam source [7] in a helium cluster beam source in order to extend the CICR technique to helium clusters [8]. Helium clusters are used in reaction dynamics by many groups ([9,10]) and laser induced fluorescence of calcium on helium clusters in the vicinity of the Ca(^{1}P $\leftarrow ^1$S) gave an evidence of its location at the cluster surface [11] as it is the case on argon and neon clusters [5]. The present works presents the results of laser induced fluorescence of the calcium dimer on argon and helium clusters around 380 nm.

The Ca_2 molecules are formed and stabilized on clusters after they have trapped 2 Ca atoms by collisions, when the cluster beam passes through a heated cell containing a low pressure of calcium vapour. The cluster beam is extracted by a 1 mm skimmer from a continuous free expansion with the following stagnation conditions: for Ar T_0 = 290 K, P_0 = 20 bars, D* = 0.2 mm; for He T_0 = 10 K, P_0 = 7.5 bars, D* = 5 μm. The average size of argon clusters is 2000. For helium clusters, it can be estimated to a few thousands [10]. After the Ca pick-up cell, the cluster beam crosses the observation region that is illuminated by the light of a cw titane-sapphire laser doubled by an extra cavity doubler. The induced fluorescence from this zone is collected, dispersed by a scanning grating monochromator and detected by a cooled photomultiplier. The photon counting technique is used for detection.

The experimental measurement consists in recording the fluorescence in the vicinity of the Ca(^{1}P $\leftarrow ^1$S) resonance line as a function of the wavelength of the excitation laser. In the helium experiment, the fluorescence appears exclusively as that of free calcium, i.e. the Ca (^{1}P $\leftarrow ^1$S) line at 23652 cm^{-1}. In the argon experiment, the fluorescence appears as this line plus a band on its red side centred near 429 nm, that can be assigned to solvated Ca(^{1}P) emission [5]. When monitoring the fluorescence intensity as a function of the average number of calcium atoms per cluster, it follows a second order Poisson law indicating that the

fluorescence comes from clusters carrying two calcium atoms. Hence, it can be assigned to the photodissociation of the calcium dimer: $Ca_2 + h\nu \rightarrow Ca_2^* \rightarrow Ca(4s^2\ ^1S) + Ca\ (4s4p\ ^1P)$. Figure 1 shows the excitation spectra of the Ca(^{1}P) fluorescence when Ca_2 is carried by helium (solid line) and argon clusters (dashed line). Both spectra are normalized to the same intensity to be compared easily. Both excitation spectra present a fairly large band with a small side band blue shifted by 550 cm^{-1}. The main band peaks at 26400 cm^{-1} on argon clusters and has a FWHM of 330 cm^{-1}. On helium clusters, it is blue shifted by 120 cm^{-1} peaking at 26520 cm^{-1} and the band is 10 % narrower (FWHM = 300 cm^{-1}). To our knowledge this is the first example reporting an absorption band of Ca_2 in this spectral region.

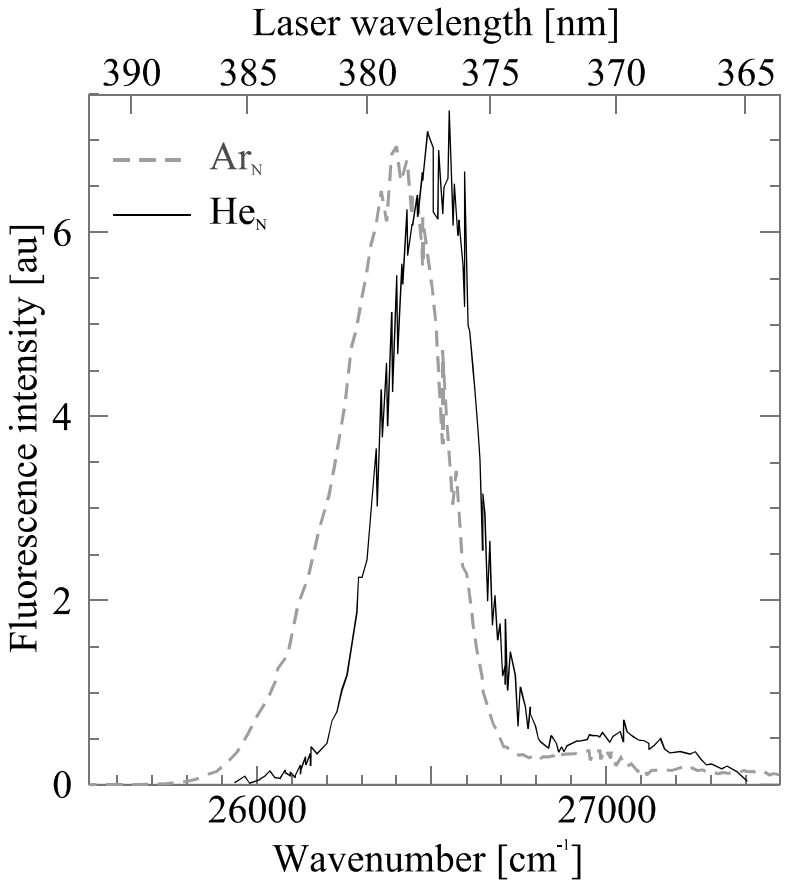

Figure.1: Excitation spectra of the Ca ($4s^2\ ^1S \leftarrow 4s4p\ ^1P$) fluorescence for Ca_2 carried on helium (solid line) and argon clusters (dashed line). The two spectra are normalized with respect to their intensity

Potential energy curves of Ca_2 have been calculated as a function of the Ca-Ca distance. Figure 2 presents three potential curves describing states of $^1\Pi_u$ symmetry, correlating to the $Ca(4s4p\ ^1P) + Ca(4s2\ ^1S)$, $Ca(4s4p\ ^3P) + Ca(4s4p\ ^3P)$ and $Ca(4s4p\ ^3P) + Ca(4s3d\ ^3D)$ asymptotes respectively. The vertical dashed line shows the Ca-Ca equilibrium distance in the ground state and represents the Franck-Condon region for the excitation of ground state Ca_2. The crossing of this line with the two potential curves at the top of Figure 2 is consistent with the experimental observation, the two maxima of the prediction being red shifted respectively by 560 and 250 cm^{-1} with respect to the experimental ones. Interestingly, the small side band

of the excitation spectrum corresponds to the excitation of a doubly electronically excited state of Ca_2.

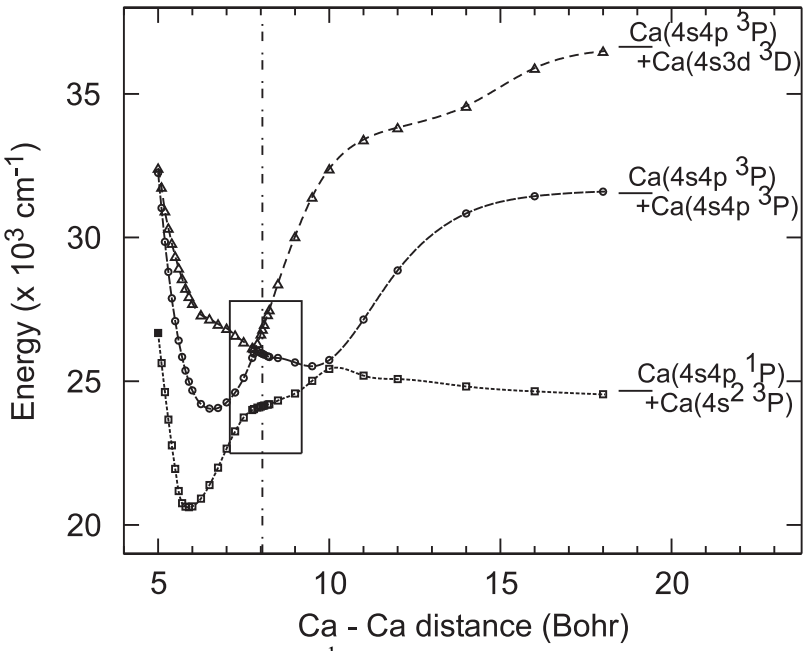

Figure 2: Calculated potential curves of $^1\Pi_u$ symmetry correlating to the asymptotes labelled in the Figure. The zero energy is taken at the bottom of the ground state well of Ca_2. This sets the $Ca(4s^2\ ^1S)$ + $Ca(4s^2\ ^1S)$ asymptote at 1016 cm^{-1}. The small horizontal lines show the experimental energy of the three asymptotes. The vertical dot-dashed line shows the calculated equilibrium distance of ground state Ca_2.

[1] C. Gée, M. A. Gaveau, O. Sublemontier, J. M. Mestdagh and J. P. Visticot, J. Chem. Phys. **107**, 4194 (1997).

[2] J. M. Mestdagh, M. A. Gaveau, C. Gée, O. Sublemontier and J. P. Visticot, Int. Rev. Phys. Chem. **16**, 215 (1997).

[3] M. A. Gaveau, C. Gée, J. P. Visticot and J. M. Mestdagh, Comments At. Mol. Phys. **34**, 241 (1999).

[4] B. Schilling, M. A. Gaveau, O. Sublemontier, J. M. Mestdagh, J. P. Visticot, X. Biquard and J. Berlande, J. Chem. Phys. **101**, 5772 (1994).

[5] M. A. Gaveau, M. Briant, P. R. Fournier, J. M. Mestdagh, J. P. Visticot, F. Calvo, S. Baudrand and F. Spiegelman, Eur. Phys. J. D **21**, 153 (2002).

[6] M. A. Gaveau, M. Briant, P. R. Fournier, J. M. Mestdagh and J. P. Visticot, J. Chem. Phys. **116**, 955 (2002).

[7] R. Campargue, J. Phys. Chem. **88**, 4466 (1984).

[8] M. A. Gaveau and P. R. Fournier, in *Proceedings of the XXVth International Symposium on Rarefied Gas Dynamics*, edited by M. S. Ivanov and A. K. Rebrov (Siberian Branch of the Russian Academy of Sciences, St Petersbourg (Russia)), 1288 (2007).

[9] J. P. Toennies and A. F. Vilesov, Angew. Chem.-Int. Ed. **43**, 2622 (2004).

[10] F. Stienkemeier and K. K. Lehmann, J. Phys. B **39**, R127 (2006).

[11] F. Stienkemeier, F. Meier and H. O. Lutz, J. Chem. Phys. **107**, 10816 (1997).

On the evolution from a molecular Rydberg gas to a cold plasma in jet-cooled NO

J. P. Morrison, C. J. Rennick, and E. R. Grant
Department of Chemistry, University of British Columbia, Vancouver, BC V6T 1Z1 Canada

J. S. Keller
Department of Chemistry, Kenyon College, Gambier, Ohio 43022 USA

The fundamental physics of ionized gases lie at the heart of a number of energetic phenomena, from the formation of stars to the plasma processing of nanomaterials. Most plasmas are hot, and this thermal kinetic energy dominates in a binary-collision, gas-like fluid dynamics. However, under extreme conditions, many-body charged-particle interactions can exceed thermal energies, giving rise to liquid- or solid-like spatial correlations. The degree of correlation depends simply on the kinetic energy of the ions compared with their Coulomb repulsion, which varies with plasma density, and one can define an index, Γ, by,

$$\Gamma = \frac{q^2}{4\pi\varepsilon_0 akT},$$

where q is the charge, and a, the Wigner-Seitz radius, is related to the particle density, ρ, by,

$$\frac{4}{3}\pi a^3 = \frac{1}{\rho}.$$

Familiar plasmas are dense ($\rho > 10^{14}$ cm^{-3}) but hot ($T > 10,000$ K), which yields $\Gamma << 1$. Strongly correlated plasmas are thought to exist at the center of heavy stars and under the conditions necessary for inertial confinement fusion.[1]

Recently, new techniques for cooling distributions of atoms to ultracold temperatures have made it possible to approach the conditions of strong coupling in highly rarified systems in the laboratory. So-called ultracold plasmas integrate atomic and mesoscopic domains, and thereby open the many-body multiscale heart of the problem to fundamental experimental study.

For example, ultracold Rydberg gases, in which particles interact by means of multipole forces, can be seen as a rarified amorphous insulator. With the promotion of constituent atoms to an orbital state for which the average radius approaches a, such systems evolve to form a correlated ultracold plasma. This evolution can be viewed as a phase change, analogous to a Mott-type insulator-metal transition.[2]

Ultracold plasmas thus offer a unique framework within which to investigate the elementary properties of condensed matter dynamics, including the elementary bases of resistance and superconductivity. Furthermore, by exciting and interrogating entangled states in such mesoscale systems, one can also explore quantum information processing strategies including such quantum logic operations as conditional phase gates.

Experiments on atomic Rydberg gases and ultracold plasmas, establishing this promise, have grown naturally from work on the production of cold atoms and atomic condensates. Now, newer methods have emerged that enable the production of ultracold ground state molecules.[3] However, despite the well-established practical importance of conventional molecular plasmas and the promise of ultracold molecular Coulomb systems for the study of electrodynamics on a nanometer length scale, the domain of molecular Rydberg gases and ultracold plasmas has yet to be explored.

In experiments on jet-cooled NO, we have found evidence for evolution from a molecular Rydberg gas to a cold plasma. This transition occurs for ensembles of molecules prepared in Rydberg states converging to the vibrational ground state of NO^+ with total energy as much as 60 cm^{-1} below the ionization threshold.

Figure 1 diagrams the apparatus. A pulsed free jet of NO seeded in He passes through a skimmer to enter a longitudinal system of perpendicular grids capped by a microchannel plate detector. In a field-free region between the first two grids, double-resonant transitions through the A $^2\Sigma^+$ state populate single nf Rydberg states converging to X $^2\Sigma^+$ NO^+ $v = 0, N^+ = 2$.

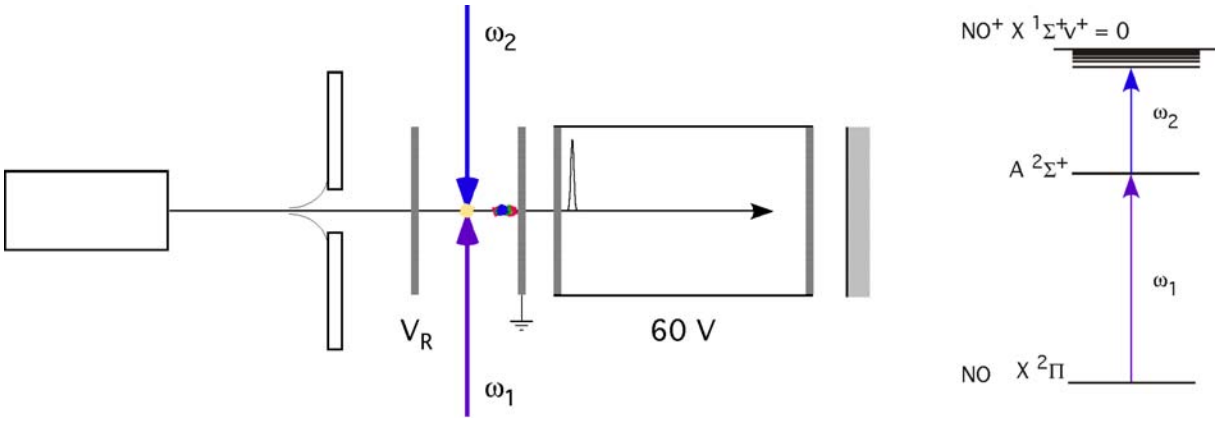

Figure 1. Schematic diagram of a differentially pumped pulsed molecular beam electron spectrometer. A pulsed jet of NO seeded at 10 percent in He passes through a skimmer and a repeller grid to enter a field-free laser interaction region. There, double-resonant excitation transfers a substantial fraction of the molecules within a small volume element to a selected high Rydberg state. As this population travels with the average longitudinal velocity of the molecular beam, the dispersion in this velocity component ($T_{||}$) causes the volume element of excited molecules to elongate.

Figure 2 shows a representative oscilloscope trace of the electron signal we observe when we prepare the $52f(2)$ state under conditions of high excited state density, in a supersonic expansion of low temperature (high Mach number). Note the prompt, field-free production of electrons, even though this Rydberg state falls nearly 70 cm^{-1} below the lowest ionization threshold of NO. Approximately 8.5 microseconds later, a large electron signal appears when the photoexcited population, traveling at the laboratory velocity of the molecular beam, passes through the extractor grid.

Under isolated conditions, states in the nf Rydberg series of NO are unstable with respect to predissociation, and decay with n-dependent lifetimes in the range of hundreds

of nanoseconds. Yet, nearly ten microseconds after production, we detect a correlated distribution of ions and electrons 1 cm downstream from the point of production. By applying a pulsed field after excitation by ω_2, we can confirm that this plasma-like distribution forms on a sub-microsecond timescale, as signaled in Figure 2 by the prompt emission of electrons. A field ionization pulse applied during this initial interval suppresses the formation of the plasma. The same voltage pulse applied microseconds later yields detectable electrons, but little diminishment of the long-lived signal.

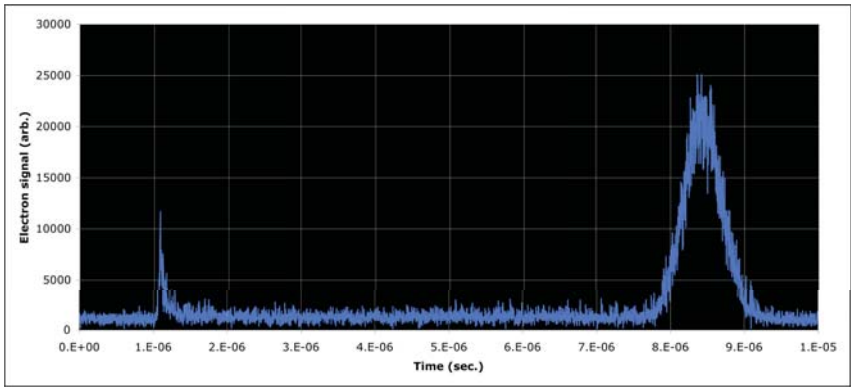

Figure 2. Oscilloscope trace showing the arrival time of electrons produced following two-color production of NO molecules in the $52f(2)$ Rydberg state built on NO^+ $^1\Sigma^+$ $v^+ = 0$. On this offset time scale, the early peak corresponds to prompt electrons produced shortly after second-photon excitation. A weak 200 mV cm^{-1} field applied between the repeller and extractor sharpens this signal. The late signal corresponds with the arrival of the photoexcited volume at the extractor grid, beyond which it passes through a field gradient of 60 V cm^{-1}.

In Figure 3, we assemble a contour plot of this late signal as a function of time and ω_2 frequency. For second photon energies near the ionization threshold, we find that the Rydberg gas collapses at its point of origin to form ions and electrons that reach the detection plane as a cloud moving with the longitudinal velocity of the 1 K seeded supersonic molecular beam.

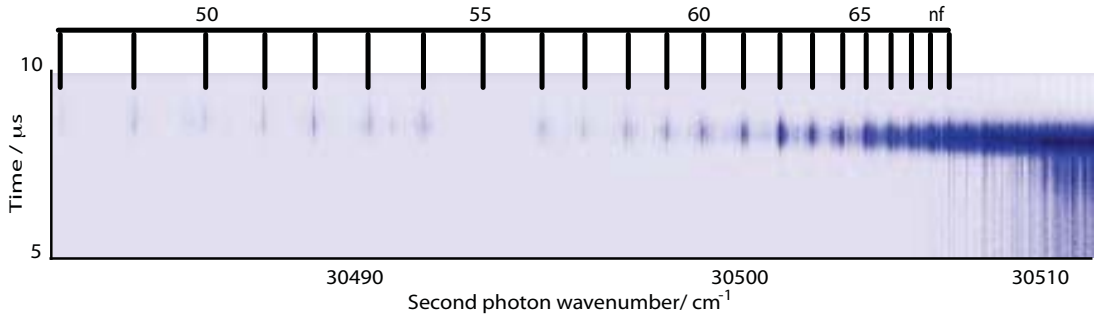

Figure 3. A contour map showing the time of flight of excited ensembles of NO Rydberg states formed below threshold by double resonance at high density and low translational temperature in a skimmed supersonic molecular beam. Note the time-of-flight retardation for lower principal quantum numbers.

The plasma forms less readily for lower principal numbers, and appears only for the molecules that arrive later at the plane of the detector. Simulations suggest that this tail of the elongating photoselected ellipsoid contains the coldest portion of the local thermal distribution. We believe that fractionation in the jet isolates cold NO molecules that undergo long-range Rydberg-Rydberg coupling like Rydberg atoms in magneto-optical traps.[4]

This work was supported by the Natural Sciences and Engineering Research Council of Canada (NSERC).

[1] T. C. Killian, Science **316**, 705 (2007); T.C. Killian, T. Pattard, T. Pohl and J.M. Rost Physics Reports 449, 77 (2007).

[2] T. Pattard, T. Pohl and J.M. Rost, Nuclear Instruments and Methods in Physics Research Section B **233**, 132 (2005).

[3] H. L. Bethlem and G. Meijer, Int. Rev. Phys. Chem. **22**, 73 (2003).

[4] T. Amthor, M. Reetz-Lamour, S. Westermann, J. Denskat, and M. Weidemller, Phys. Rev. Lett. **98**, 023004 (2007).

Scattering of very slow (3-10 eV) hydrocarbon ions CD_3^+, CD_4^+, and CD_5^+ from room-temperature carbon (HOPG) surfaces

Andriy Pysanenko, Jan Žabka, Zdenek Herman

V. Čermák Laboratory, J. Heyrovský Institute of Physical Chemistry,v.v.i., Academy of Sciences of the Czech Republic, Dolejškova 3, 182 23 Prague 8, Czech Republic

Scattering of simple hydrocarbon ions CD_3^+, CD_4^+, and CD_5^+ from room-temperature carbon (HOPG) surfaces was investigated at low incident energies of 3 – 10 eV. Mass spectra, angular and translational energy distributions of product ions were determined. From these data information on processes at surfaces, survival probability factors of incident ions, scattering diagrams and effective mass of the surface involved in the collisions were determined. Incident ions CD_5^+ and CD_3^+ showed only non-dissociative (CD_3^+) or non-dissociative and dissociative (CD_5^+) scattering; the radical cation CD_4^+ exhibited both inelastic and dissociative processes and chemical reactions of H-atom transfer and C_2-hydrocarbon formation in reactions with hydrocarbons on the room-temperature carbon surface.

The absolute survival probability, S_A, is defined as a percent ratio of the total current of product ions to the current of incident ions striking the surface The absolute survival probability was at 10 eV about 12 % for CD_5^+, 0.3-04 % for CD_3^+ and CD_4^+, and decreased towards zero at lower incident energies (Fig. 1).

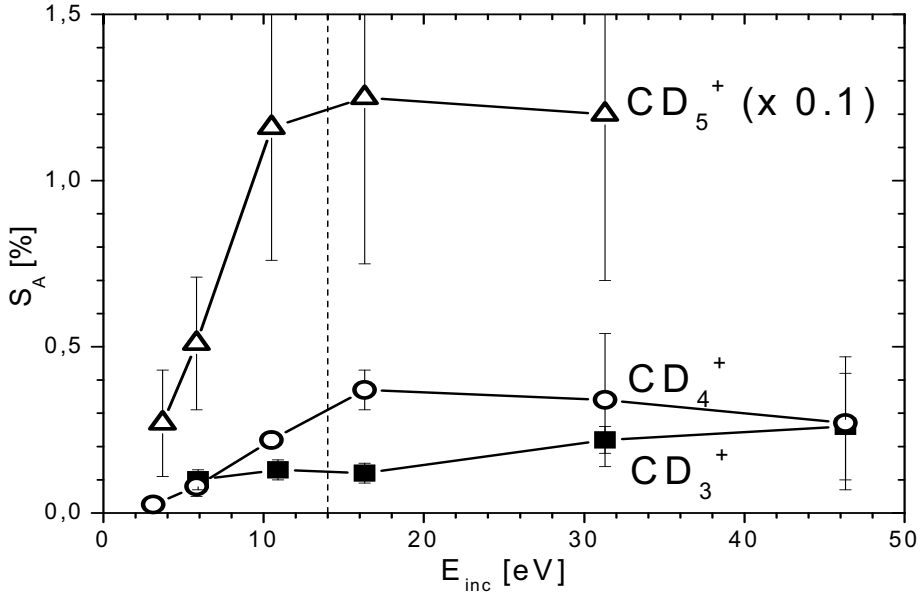

Fig .1: Absolute survival probability, S_A (%), for ions CD_5^+, CD_4^+, and CD_3^+.

The new data for energies below 10 eV fit well data for incident energies 15 – 45 eV obtained earlier [1].

From the angular and translational energy distributions of the product ions (see Fig. 2 and 3 for CD_5^+ scattering), velocity scattering diagrams were constructed (Fig. 3).

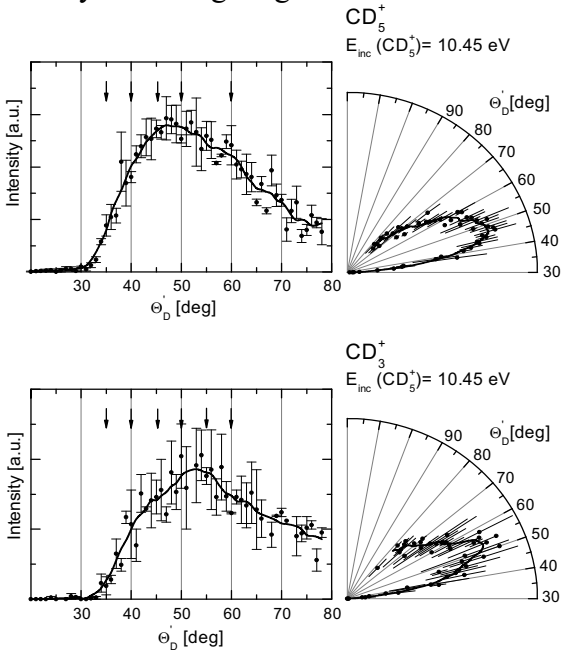

Fig. 2: Angular distributions of CD_5^+ (upper part) and its fragment CD_3^+ (lower part) from collisions of 10. 45 eV projectile ions CD_5^+ with carbon (HOPG) surfaces

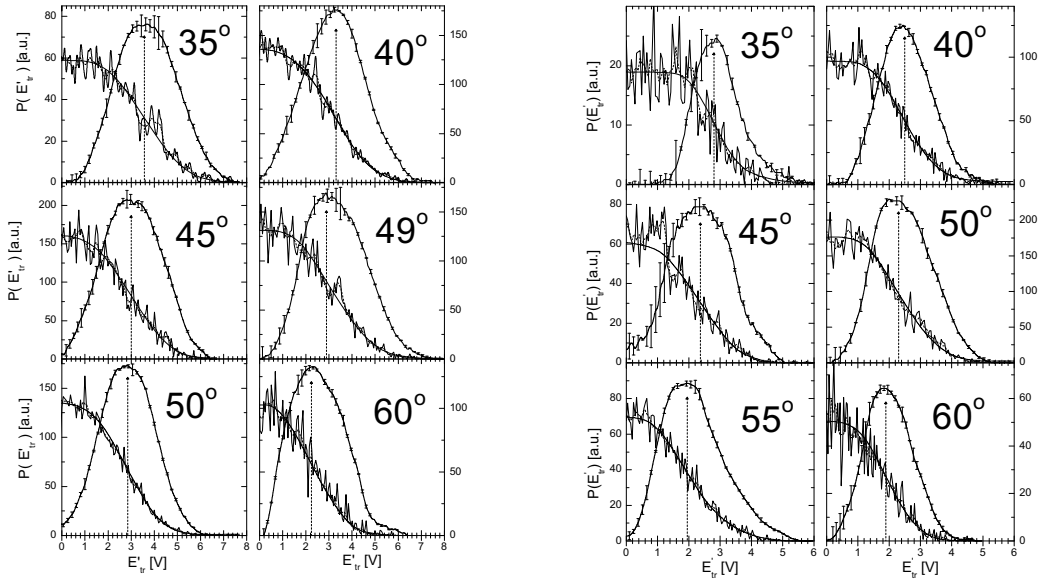

Fig. 3: Translational energy distributions of product ions CD_5^+ (left) and CD_3^+ (right) from collisions of 10.45 eV projectile ions with carbon (HOPG) surfaces.

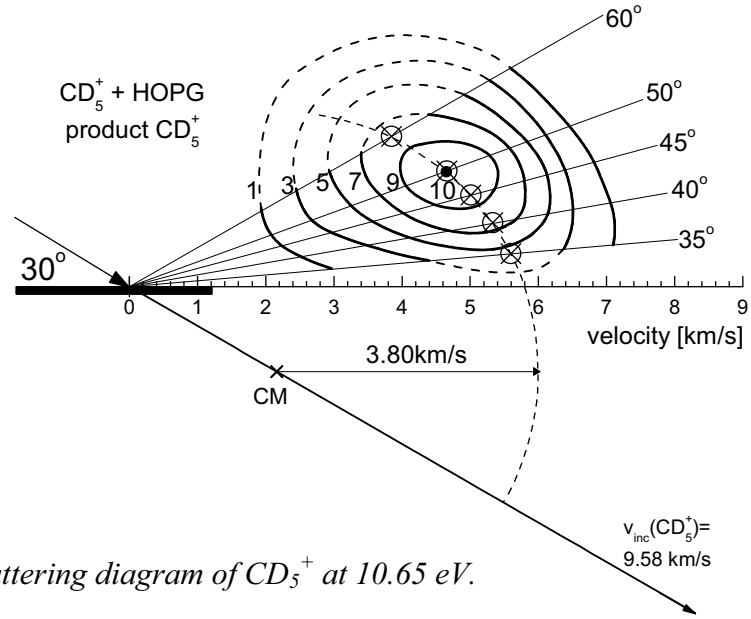

Fig. 3: Velocity scattering diagram of CD_5^+ at 10.65 eV.

The peaks of the velocity distributions fitted on a circle with its center on the relative velocity of the system incident ion – surface. From its position, the effective surface mass involved in the collisional process, $m(S)$, could be estimated. The estimated value of $m(S)_{eff}$ was about 29 m.u. for CD_3^+ collisions, 15-21 m.u. for inelastic and fragmenting collisions of CD_4^+, and 62 m.u. for CD_5^+ collisions, corresponding to the mass of one or several CH_3-terminal units of surface hydrocarbons. For the chemical reaction of H-atom transfer in CD_4^+ collisions (Fig. 4), the effective mass $m(S)_{eff}$ was about 48 m.u. suggesting a more complicated surface process than a simple direct H-atom pick-up.

*Acknowledgment*s. Partial support of this research by the Association EURATOM.IPP.CR, and by the I.A.E.A., Vienna, under the contract No. 13488 is gratefully acknowledged. We wish to thank to Fabio Zappa (University of Innsbruck, Association EURATOM-ÖAW) for his help in early stages of this work.

References

[1] J. Roithová, J. Žabka, Z. Dolejšek, Z. Herman, J. Phys. Chem. B, 106 (2002) 8293.

Ca atoms attached to ^{4}He nanodroplets

A. Hernando, M. Barranco, R. Mayol and M. Pi
Departament ECM, Facultat de Física, and IN^{2}UB, Universitat de Barcelona. Diagonal 647, 08028 Barcelona, Spain

M. Krośnicki
Institute of Theoretical Physics and Astrophysics, University of Gdansk. ul Wita Stwosza 57, PL80 Gdansk, Poland

Optical investigations of atomic impurities in superfluid helium nanodroplets have drawn considerable attention in recent years[1, 2]. In particular, the shifts of the electronic transition lines with respect to the gas-phase (atomic shifts) are a very useful observable to determine the location of the foreign atom attached to the drop. Alkaline earth atoms appear to play a unique role in this context. While, e.g., all alkali atoms reside in a "dimple" on the surface of the cluster, and more attractive impurities like all noble gas atoms reside in the bulk of drops made of either isotope[3], the absorption spectra of heavy alkaline earth atoms attached to ^{4}He drops clearly support an outside location of Ca, Sr, and Ba[4, 5], whereas for the lighter Mg atom the experimental evidence is that it resides in the bulk of the ^{4}He droplets[6].

Within density functional theory, we have obtained the structure of ^{4}He droplets doped with neutral calcium atoms. We have used the Orsay-Trento (OT) density functional[7], together with the Ca-He adiabatic potential $X^1\Sigma$ of Ref. [8], and explicitly taken into account the quantum vibration of the Ca atom.

Figure 1 shows the energy of a Ca atom attached to a drop, defined as $S_N(\mathrm{Ca}) = E(\mathrm{Ca@}^4\mathrm{He}_N) - E(^4\mathrm{He}_N)$, for several cluster sizes. On the figure are also shown the results obtained by treating calcium as an external field[9]. It can be seen that for large drops the energy of the calcium atom is about 10 K less negative due to its zero point motion.

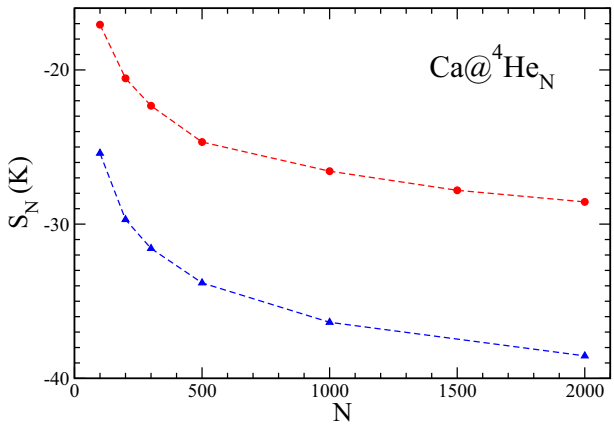

Figure 1: Energy (K) of a calcium atom as a function of the number of ^{4}He atoms in the droplet (dots). Results obtained treating calcium as an external field are also shown (triangles)[9]. The lines have been drawn to guide the eye.

We have found that the Ca atom resides in deep dimple at the surface of the drop, in agreement with the available experimental data[4] and previous DFT calculations[9]. The dimple depth ξ, defined as the difference between the position of the dividing surface at $\rho = \rho_0/2$, where $\rho_0 = 0.0218$ Å^{-3} is the bulk liquid density, with and without impurity, is ∼6.4 Å for the Ca@^{4}He$_{2000}$ drop. Due to the zero point motion the dimple depth is about 0.8 Å smaller than when the zero point motion is not included[9]. This change in the depth is large enough to produce observable effects in the calculated absorption spectrum. We have found that the total energy of the equilibrium -dimple- configuration of Ca@^{4}He$_{1000}$ is ~ -5467.4 K, only 12.4 K smaller than when Ca is forced to be at the center of the drop.

We have studied the drop structure as a function of the position of the Ca atom with respect of the center of mass of the helium moiety. The interplay between the density oscillations arising from the helium intrinsic structure[3, 7, 10] and the density oscillations produced by the impurity in its neighborhood plays a role in the determination of the equilibrium state, and hence in the solvation properties of alkaline earth atoms. We show in Fig. 2 the density of the helium moiety of Ca@^{4}He$_{2000}$, where the interference pattern can be clearly seen.

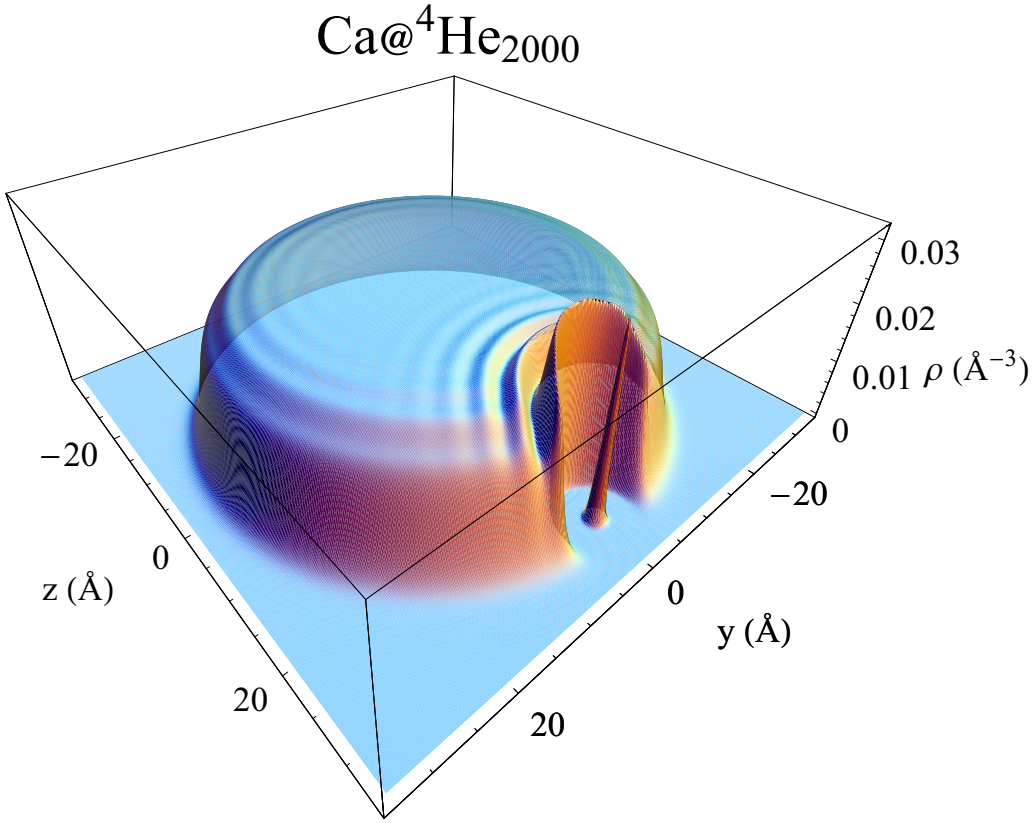

Figure 2: Helium density of the Ca@^{4}He$_{2000}$ drop on the $x = 0$ plane. The probability density of the calcium atom is also shown, rescaled multiplying it by a ρ_0 factor for the sake of clarity.

These results have been used, in conjunction with newly determined *ab-initio* $^1\Sigma$ and $^1\Pi$ Ca-He pair potentials, to address the $4s4p\ ^1P_1 \leftarrow 4s^2\ ^1S_0$ transition of the attached Ca atom. The peak energy for the Ca@^{4}He$_{2000}$ drop is 79 cm^{-1}, a 10% larger than the experimental value of 72 cm^{-1} for very large clusters[4], which indicates a fairly good agreement between theory and experiment.

Figure 3 shows the total absorption spectrum of Ca attached to ^{4}He$_N$ droplets for several N values. For the smallest clusters, the main peak is due to the contribution of the Π states while the contribution of the Σ states is seen as a blue shifted shoulder. As the size of the cluster increases, the components become broader and cannot be distinguished. Since we have neglected the fluctuations of the dimple -shape fluctuations[11]- and their coupling to the dopant dipole oscillations, as well as inhomogeneous broadening resulting from droplet size distributions, laser line width and similar effects, the model is expected to underestimate the experimental line width, which is three times larger than the theoretical value.

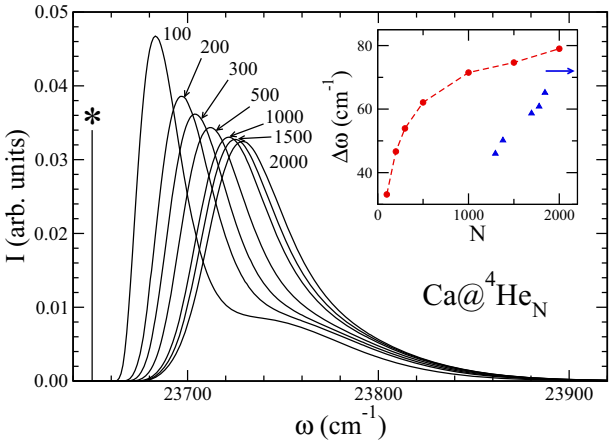

Figure 3: Total absorption spectrum of Ca attached to ^{4}He$_N$ droplets in the vicinity of the $4s4p\ ^1P_1 \leftarrow 4s^2\ ^1S_0$ transition, for the indicated N values. The starred vertical line represents the gas-phase transition. The inset shows the calculated shifts relative to the gas-phase transition (dots), defined as the energy of the maximum of the absorption line minus the energy of the gas-phase transition. The experimental values are also shown (triangles). The arrow indicates the asymptotic experimental value[4].

Since ^{4}He is superfluid, it is quite natural to wonder about the appearance and detection of quantized vortices in droplets[3, 12]. The structure of vortices attached to the calcium atom has been addressed, as well as its effect on the calcium absorption spectrum. At variance with previous theoretical predictions[13], the presence of the vortex line produces just a deeper surface dimple, rather than drawing the impurity into the center of the droplet. Fig. 4 shows the calculated spectra for the Ca@^{4}He$_{1000}$ droplet with and without vortex. Unfortunately, the experimental absorption line is so broad and asymmetric that the extra shift caused by the vortex is not enough to displace the line to a region where it could be distinguishable on top of the vortex-free absorption line.

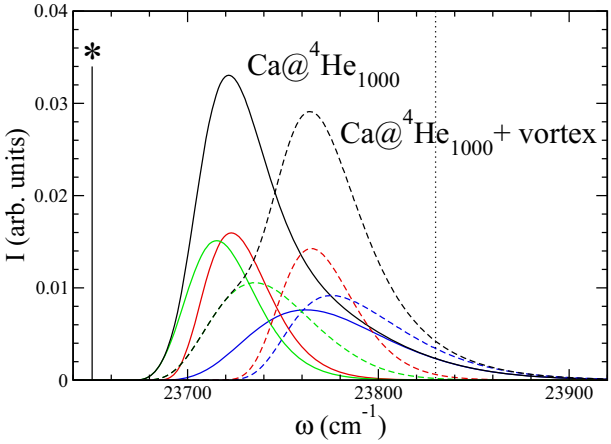

Figure 4: Ca absorption spectrum for the $N = 1000$ droplet with (dashed lines) and without a vortex line along its symmetry axis (solid lines). The absorption line has been decomposed into its three components. The starred vertical line represents the gas-phase transition, and the dotted vertical line represents the experimental value for bulk liquid ^{4}He[14].

[1] F. Stienkemeier and A.F. Vilesov, J. Chem. Phys. **115**, 10119 (2001).

[2] F. Stienkemeier and K.K. Lehmann, J. Phys. B **39**, R127 (2006).

[3] M. Barranco, R. Guardiola, S. Hernández, R. Mayol, and M. Pi, J. Low Temp. Phys. **142**, 1 (2006).

[4] F. Stienkemeier, F. Meier, and H.O. Lutz, J. Chem. Phys. **107**, 10816 (1997).

[5] F. Stienkemeier, F. Meier, and H.O. Lutz, Eur. Phys. J. D **9**, 313 (1999).

[6] J. Reho, U. Merker, M.R. Radcliff, K.K. Lehmann, and G. Scoles, J. Chem. Phys. **112**, 8409 (2000).

[7] F. Dalfovo, A. Lastri, L. Pricaupenko, S. Stringari, and J. Treiner, Phys. Rev. B **52**, 1193 (1995).

[8] C.C. Lovallo and M. Klobukowski, J. Chem. Phys. **120**, 246 (2004).

[9] A. Hernando, R. Mayol, M. Pi, M. Barranco, F. Ancilotto, O. Bünermann, and F. Stienkemeier, J. Phys. Chem. A **111**, 7303 (2007).

[10] S.A. Chin and E. Krotscheck, Phys. Rev. B **45**, 852 (1992).

[11] P.B. Lerner, M.B. Chadwick, and I.M. Sokolov, J. Low Temp. Phys. **90**, 319 (1993).

[12] K.K. Lehmann and R. Schmied, Phys. Rev. B **68**, 224520 (2003).

[13] F. Ancilotto, M. Barranco, and M. Pi, Phys. Rev. Lett. **91**, 105302 (2003).

[14] Y. Moriwaki and N. Morita, Eur. Phys. J. D **33**, 323 (2005).

Vibrational Spectra and *Ab initio* Calculations for the Study of Intramolecular Vibrational Energy Redistribution in the CH-chromophore in CHD_2I

V. Horká, M. Quack, and M. Willeke
Laboratorium für Physikalische Chemie, ETH Zürich, CH-8093, Zürich, Switzerland

Abstract

We report results on the intramolecular vibrational energy redistribution (IVR) in the CH-chromophore of CHD_2I as obtained from experimental spectra covering the range from 500 to 12000 cm^{-1} and also from *ab initio* calculations.

1 Introduction

Intramolecular vibrational energy redistribution (IVR) on the femto- to picosecond time scale is a central primary process in unimolecular chemical reaction dynamics. There are two main approaches towards its understanding. One is the analysis of the highly resolved vibrational spectra of polyatomic molecules (see [1, 2] and references cited therein), sometimes combined with *ab initio* calculations. Another approach consists in time resolved femtosecond (fs) pump-probe experiments, which we have recently carried out for a series of alkyliodides [3] including CHD_2I. For the latter molecule we present here the vibrational analysis of its overtone spectra. We have also carried out *ab initio* calculations constructing potential energy and electric dipole moment hypersurfaces in normal coordinates up to 3 dimensions. These surfaces are employed for accurate 3D vibrational variational calculations [4] for the 3 anharmonically coupled modes. The overtone absorption spectra are calculated for the CH-chromophore, which clearly dominates the entire spectrum and are analyzed in detail with respect to their anharmonic resonance dynamics. Time dependent population dynamics [2, 4] demonstrate, that close resonance couplings lead to IVR on a sub-ps time scale. As a first step in a direction of a complete understanding of the IVR dynamics in CHD_2I the isolated CH-chromophore was investigated. By increasing the dimensionality of investigated subspace step by step we should finally be able to compare the results of this approach with the corresponding results from femtosecond pump-probe experiments ([3] and ongoing work).

2 Experimental

We employed a high-resolution Fourier transform infrared spectrometer (BOMEM, DA002) equipped with a White type multi reflection cell with a path length of 35 m [1]. The infrared absorption spectra of CHD_2I have been recorded from 500 to 12000 cm^{-1} (with resolutions of 0.10 or 0.15 cm^{-1}), and a pressure ranging from 190 to 225 mbar.

3 *Ab initio* and vibrational variational calculations

The potential energy and electric dipole moment hypersurfaces were calculated on a grid based on 2500 explicitly calculated *ab initio* single point (MP2/aug-cc-pVTZ for H and C, MP2/SDB-cc-pVTZ [6, 7] for I (with the corresponding effective core potential)), by successive one dimensional spline interpolations along the three normal coordinates (see [8, 9]) covering an energy range up to 40000 cm^{-1}. The vibrational Hamiltonian is

diagonalized in a discrete variable representation DVR [8]. Scaled and unscaled harmonic frequencies are used in the vibrational calculations. The scaled harmonic frequencies are chosen in such a way that the corresponding calculated and experimental fundamentals agree.

3.1 Effective Hamiltonian for analysis the CH-chromophore overtone spectra

The CH-chromophore spectra were analyzed in terms of a 3D effective Hamiltonian [8] including Fermi resonance couplings between the CH-stretching ν_1 (A') and two CH-bending modes ν_3 (A') and ν_8 (A"). Only the pure CH-stretching overtones carry intensity in a zero order picture. The effective tridiagonal three-dimensional Hamiltonian (H_{eff}) is assumed to be block-diagonal in the polyad quantum number N, $N = v_1 + \frac{1}{2}(v_3 + v_8)$. The fundamental wavenumbers and the anharmonicities x_{11}, x_{33}, x_{88} are defined in the usual way [1]. The chromophore states within a polyad are coupled by a Fermi resonance between CH-stretching and CH-bending modes with the corresponding coupling constant k_{133} and k_{188} characterizing the anharmonic interaction. For molecules with C_s symmetry like CHD_2I, k_{138} is zero. The Darling-Dennison resonance $\gamma = k_{3388}$ was taken into account.

4 Results and conclusion

4.1 The CH-chromophore absorption spectrum and results of effective Hamiltonian analysis

In the overtone spectrum of CHD_2I 24 vibrational band centers were assigned, aided by the eigenvalue spectra obtained from the variational calculations. The assignment is also corroborated by a fit of the experimental data to the effective Hamiltonian which yields "reasonable" preliminary parameters and satisfactory RMS deviations (see table 1). In table 1 two types of data from the "scaled" calculation are included (first and second column). One is a fit of 85 calculated band centers up to polyad N=4 and the other data set comes from a fit to 142 calculated band centers up to N=6. It is obvious that the constants are changing just slightly with the increasing number of transitions included and the effective spectroscopic parameters can therefore be used for the prediction of higher polyads. In the last column of table 1 we list constants from a fit of the experimental vibrational band positions. The RMS deviation is only weakly dependent on γ showing a very flat minimum, and therefore γ=10 cm^{-1} was fixed in the fit. This is the value for the calculated absorption spectrum. The CH-stretching and CH-bending modes are strongly coupled via Fermi resonances with k_{133}=85±10 cm^{-1} and k_{188}=45±5 cm^{-1} (estimated error of 10 %). The Fermi resonance parameters k_{133} and k_{188} are fixed at the given values, which are chosen in such a way that the intensity pattern of the spectrum, resulting from the fit, is in good agreement with the calculated and measured spectra. The agreement of absolute intensities and transition wavenumbers between the "scaled" calculations and H_{eff} using experimental band centers is very good. The values for the RMS deviation of the calculated and experimental transition wavenumbers are d_{rms}= 8.1 cm^{-1} for the "scaled" data up to N=6 and d_{rms}= 5.2 cm^{-1} for the experimental fit using the effective Hamiltonian, which indicates a satisfactory agreement between experiment and theory. The spectroscopic constants are quite similar with previous analyses of

the CH-chromophore in various molecules. This indicates that the model of the isolated CH-chromophore is also transferable to similar types of molecules.

Table 1: Various fits with the effective model H_{eff} employing the calculated vibrational eigenvalues from the "scaled" calculation (see above) and the experimental data. All parameters are given in cm^{-1} and standard deviations are given in parentheses in units of the last digit.

Parameters (cm^{-1})	Variational calculations-SCALED *fit up to N=4*	*fit up to N=6*	EXPERIMENT *fit up to N=4*
$\tilde{\nu}_1$	3081.0 (14)	3072.5 (21)	3090.6 (37)
$\tilde{\nu}_3$	1173.2 (7)	1173.2 (12)	1194.9 (59)
$\tilde{\nu}_8$	1287.2 (7)	1296.2 (10)	1290.8 (43)
x_{11}	-54.4 (4)	-53.7 (4)	-61.9 (11)
x_{33}	-1.6 (1)	-1.3 (2)	-16.6 (2)
x_{88}	-2.8 (1)	-4.5 (1)	-4.3 (1)
x_{13}	-33.2 (3)	-33.9 (4)	26.1 (2)
x_{18}	-31.2 (3)	-32.2 (4)	-25.1 (4)
x_{38}	-0.7 (2)	-1.9 (2)	-0.6 (2)
k_{133}	90.0 ± 10	90.0 ± 10	85.0 ± 10
k_{188}	65.0 ± 6	65.0 ± 6	45.0 ± 5
γ	10.8 (8)	13.9 (7)	10
n_{data}	85	142	24
d_{rms}	2.9	8.1	5.2

4.2 Time dependent dynamics

The time dependent wave function $\Psi(t)$ and therefore the time evolution of the populated states of the isolated CH-chromophore can be calculated via the effective or the *ab initio* Hamiltonian [2]. The results from the effective Hamiltonian using the spectra calculated *ab initio* are in good agreement with experimental data, thus our *ab initio* model provides a realistic picture of the dominant anharmonic coupling present in CHD_2I and therefore the time dependent dynamics was performed using the effective Hamiltonian and the time evolution operator $\hat{U}(t, t_0)$ for the calculation of the time dependent wave function $\Psi(t, t_0)$. The population $p_k(t)$ of state k is given by

$$p_k(t) = |b_k(t)|^2$$

where $b_k(t)$ is the element of the time dependent vector b, which is calculated by employing time evolution matrix $\hat{U}$ [1]. The population dynamics was calculated for $|v_1{=}4, v_3{=}0, v_8{=}0>$ as initial state ($p_{|4,0,0>}(t)$), with 4 quanta of pure CH-stretching excitation and the results are shown in figure 1. This figure contains the results calculated with H_{eff} obtained from the fit of the experimental data and those calculated from the fit of the eigenvalues of the "scaled" *ab initio* calculation. The time evolution for both provides very similar results. It is obvious that $p_{|4,0,0>}(t)$ rapidly decays within about 100 fs. The states $p_{|3,0,2>}(t)$ and $p_{|3,2,0>}(t)$, gain population up to 20 % during this period. This provides

insight into how vibrational energy can flow between the CH-stretching and the CH-bending modes. The depopulation of $p_{|4,0,0>}(t)$ is not complete due to the off resonance shift of the coupled states. Our H_{eff} gives a correct description of the IVR process for short times.

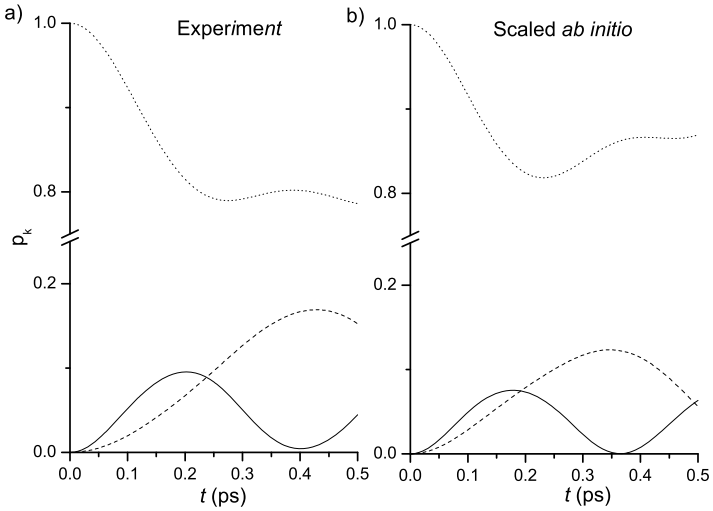

Figure 1: Population dynamics $p_k(t)$ on the ordinate: $|v_1=4, v_3=0, v_8=0>$ as initial state ($p_{|400>}(t)$ dotted line, $p_{|320>}(t)$ solid line, and $p_{|302>}(t)$ dashed line). a) Results calculated by H_{eff} obtained from the fit of the experimental eigenvalue spectra. b) Results calculated by H_{eff} obtained from the fit of the eigenvalues of the "scaled" *ab initio* calculation.

References

[1] M. Quack, Annu. Rev. Phys. Chem., **41**, 839 (1990); M. Quack, Chimia, **57(4)**, 147 (2003).

[2] J. Pochert, M. Quack, J. Stohner, and M. Willeke, J. Chem Phys., **113(7)**, 2719 (2000).

[3] V. Krylov, E. Miloglyadov, M. Quack, and G. Seyfang, Proceeding of the XV Symposium on Atomic and Surface Physics and Related topics, 229 (2006); V. Krylov, M. Nikitchenko, M. Quack, and G. Seyfang, SPIE, **5337**, 178 (2004); V. Krylov, A. Kushnarenko, E. Miloglyadov, M. Quack, and G. Seyfang, SPIE, **6460**, 64601D1 (2007).

[4] M. Quack, and M. Willeke, J. Chem. Phys., **110(24)**, 11958 (1999).

[5] D. Luckhaus, and M. Quack, Chem. Phys. Lett., **190(6)**, 581(1992).

[6] J.M.L. Martin, and A. Sundermann, J. Chem. Phys., **114(8)**, 3408 (2001).

[7] A. Bergner, M. Dolg, W. Kuchle, H. Stoll, H. Preuss, Mol. Phys., **80(6)**, 1431 (1993).

[8] A. Beil, D. Luckhaus, R. Marquardt, and M. Quack, Faraday Discuss., **99**, 49 (1994).

[9] D. Luckhaus, J. Chem. Phys., **106(20)**, 8409 (1997).

Manipulation of Films of Nanoparticles

S. Jaksch, F. Zappa and P. Scheier
Institut für Ionenphysik und Angewandte Physik, Universität Innsbruck, Technikerstrasse 25, A-6020 Innsbruck, Austria

Abstract

Films of silicon nanoparticles are formed by a magnetron sputtering source and deposition onto highly oriented pyrolytic graphite (HOPG). The effect of different parameters such as the distance between magnetron and graphite surface, pressure, discharge current, deposition time and bias-voltage of the HOPG is analyzed with a variable temperature scanning tunneling microscope (VT-STM). Well defined manipulation in the nanometer regime of the films with the STM tip is demonstrated and electronic properties of the films are probed by local scanning tunneling spectroscopy (STS).

Experimental

Silicon nanoparticles are formed by magnetron sputtering of a pure polycrystalline silicon target and deposited onto freshly cleaved HOPG. The sample preparation chamber is directly connected to the VT-STM which enables a fast transfer into the ultra high vacuum of the analyzing part of the instrument. Thereby the contamination (oxidation) of the silicon nanoparticles is reduced to a minimum.

With the STM we are investigating the structure of the sputtered silicon nanoparticles with STM images and their electronic properties with STS. The presently utilized STM enables to investigate the silicon nanoparticles in a temperature range from 25K to approximately 1300K.

Results and discussion

The growth of very homogeneous silicon nanoparticle films is observed and studied. We investigate the behavior of the films, formed with different sputtering parameters. For the present study we analyze the dependence on the distance / geometry, pressure, current, time and also bias-voltage of the HOPG. The distance / geometry has the strongest influence on the sputtering behavior. It was only possible to grow films of nanoparticles in a distance regime of approximately 8cm from the sample. It is interesting to note that the influence of walls and edges of the vacuum vessel can be neglected up to this distance.

Changes in the pressure of Ar used for sputtering affects the amount of deposited silicon nanoparticles. In addition, the sticking coefficient of the nanoparticles on the HOPG gets worse with higher pressure. For very low pressure (4×10^{-3}mbar) we obtain fractal structures and decoration of defects in the HOPG substrate (see Fig. 1, left). Moreover, the overall roughness of the film increases with higher pressure.

Fig. 1 (Right) shows the initial process of film formation where a few nanoparticles are attached to each other and form isolated hillocks on the graphite surface. On the upper left corner a step in the HOPG surface is densely covered with silicon. The low roughness of this structure indicates fusion of nanoparticles into a nanorod (nanowire) [1]. Defects like steps in the HOPG are not only decorated in the first layer of nanoparticles but also in the higher layers (Fig. 4 (Right)).

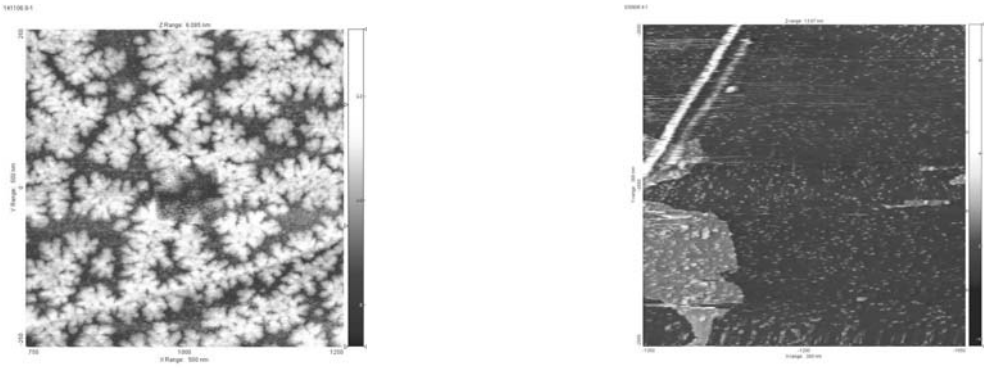

500 nm 300 nm

Fig. 1: Left: Fractal structure and decoration of defects (500 nm); Right: Formation of silicon nanoparticle islands

Modifications like vaporization, fusion and removal of nanoparticles with the STM tip on the nanometer scale are also possible. These techniques enable a novel kind of nanolithography and we are able to form different profiles and patterns in the silicon film. Fig. 2 shows a profile pattern formed by different tunneling currents. The right diagram shows a sectional scan for the white line in the image on the left.

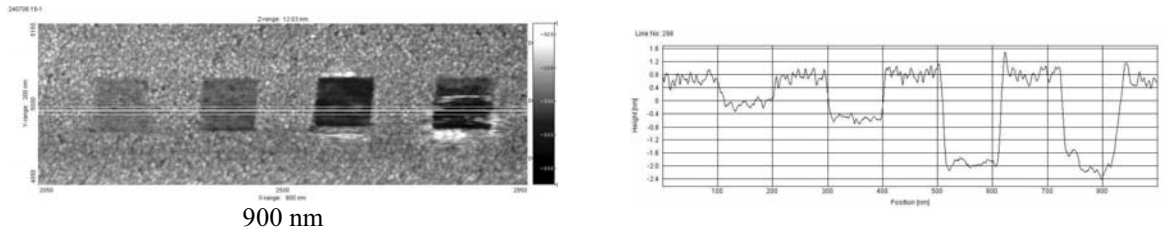

900 nm

Fig 2: Greyscale series (vaporizing) by different tunneling currents

At increased bias-voltage, applied between the tip and the silicon nanoparticle film, we are able to fuse some silicon nanoparticles into larger objects. Fig. 3 (Left) shows this behavior for 100nm × 100nm squares scanned with different gap-voltages. Also the electronic density of states is changed and probed with complementary scanning tunneling spectroscopy measurements. Fig. 3 (Right) shows the sectional scan along the white line in the left image.

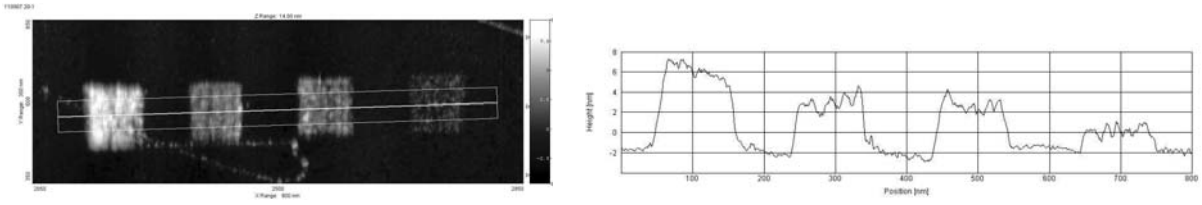

900 nm

Fig 3: Greyscale series (fusing) by different gap-voltages

By lowering the gap-voltage it's possible to remove silicon nanoparticles. Fig 4 shows a square of 50nm × 50nm that was scanned with 0.5V (for the silicon we use normally 2.7V) so the tip dipped into the film and wiped away the clusters.

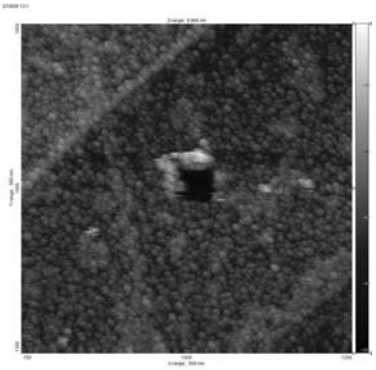

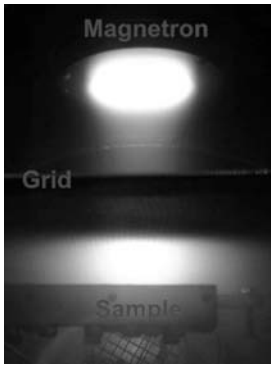

Fig. 4: Left: Removal of silicon clusters; Right: Sputtering with a positively biased sample

A change in the experimental setup allows to have a grounded grid in front of the sample and to bias the sample. Biasing the sample with a negative voltage results in very low coverage of the HOPG. Sputtering with a positive bias-voltage results in a better nanoparticle film. The film is much more stable against vaporization and can be achieved with up to 10 nA instead of 500 pA for the grounded sample. Furthermore, fusion becomes much easier (see Fig. 3). By applying the positive bias to the sample an additional lightning of the plasma appears between the grid and the sample (Fig. 4 Right).

Conclusions

We investigate in detail the growth and the properties of films of silicon nanoparticles formed by magnetron sputtering and deposition on freshly cleaved HOPG. The methods utilized are STM and STS at room temperature but with the option to perform these studies also in a wide temperature regime from 25K to 1300K. Also a better setup for biasing the sample without disturbing the plasma is currently developed. It is planned to determine the conditions for a film that has optimum properties for subsequent nanolithography as described above. A high resolution relief-like image will be imprinted on such a film. The stability of the films and the nanolithography is going to be studied at elevated temperatures in the STM.

Work is supported by the Integrated Infrastructure Initiative ITS-LEIF.

References

[1] B. Marsen, K. Sattler, Phys. Rev. B **60**, 11593-11600 (1999)

Accurate Pair Potentials for the Ground-State and Excited Metastable Helium Atoms

Bogumil Jeziorski

Faculty of Chemistry, University of Warsaw, Pasteura 1, 02-093 Warsaw, Poland

Using state-of-the-art electronic structure techniques, including an accurate treatment of the relativistic, QED, and diagonal Born-Oppenheimer corrections, we computed pair potentials for the interaction of ground-state singlet and metastable triplet helium atoms. To reduce the basis set errors to a minimum we employed specially designed explicitly correlated basis sets and as well as configuration interaction expansions with high-angular-momentum orbitals. Theoretically motivated extrapolation techniques enabled an estimation of error bars, which amount to about 0.03% relative uncertainty at the minimum of the potential well and much better at the long range and in the repulsive parts of the potential. These errors bars are about an order of magnitude tighter than those corresponding to the best previous potentials. The computed interaction energies were used to fit physically motivated analytic functions both for the potentials and for their error bars. The fits use the best available van der Waals coefficients, including the $C_{11} - C_{16}$ constants computed by us for the first time, and has also the correct analytic behavior at short range.

We found that the ground-state potential exhibits the well depth of 11.001±0.004 Kelvin and the equilibrium distance of 5.608±0.012 bohr. The only bound state resulting from the interaction of ground-state helium 4 atoms has the dissociation energy of 1.73±0.04 milliKelvin, and the average interatomic separation $\langle R \rangle$ = 45.6±0.5 Å, in agreement with experimental estimates.

The potential for the interaction of metastable triplet atoms was used to predict the S-wave scattering length a_s of spin-polarized helium 4 atoms, determined recently in the BEC experiments. The experiments led by Alain Aspect (Orsay) and Claude

Cohen-Tannoudji (Paris) gave the values of 20 nm and 16 nm, respectively, with uncertainties as large as 50% . A more recent experiment from the Aspect's group led to a value between 10.3 and 13.7 nm. Initial theoretical calculations were confirming these large values.

Theoretical value of a_s predicted by us, equal to 7.51±0.20 nm, lies well outside the error bars of all experimental determinations based on the properties of Bose-Einstein condensate. We also predicted that the highest, v=14 vibrational level is bound by D_{14}=91.6±6.7 MHz, much stronger than previous best theoretical estimate of 15.2 MHz. Both a_s and D_{14} were obtained using the atomic masses in solving the radial Schrödinger equation for the interatomic distance dependence of the wave function. Using nuclear masses would led to values differing by 0.14 nm and 4.2 MHz, respectively. Shortly after our value of a_s had been obtained Kim et al. (Paris group) measured the light induced frequency shifts in photoassociative spectra of metastable helium atoms and inferred the value of 7.2±0.6 nm, in full agreement with our prediction. In a subsequent development, Moal et al. (Paris group) carried out a two-photon photoassociation experiment and determined very accurately the dissociation energy of the v=14 state. Their result D_{14}=91.35±0.06 MHz was used to obtain a new experimental value of a_s equal to 7.512±0.005 nm agreeing perfectly with our prediction but exhibiting much smaller uncertainty.

Very recently we significantly tightened our theoretical error bars by further improving the nonrelativistic clamped-nuclei calculations and including higher relativistic and QED effects. The improved value of a_s equal to 7.56±0.03 nm is now in a slight disagreement with the most recent experimental determination. The possible origin of this disagreement will be discussed. It will also be shown that the very accurately measured value of the energy of the v=14 state provides a very stringent test for the relativistic theory of interatomic interactions, provided that the role of the (nonrelativistic) nonadiabatic effects is clarified.

Photofragment slice imaging studies of pyrrole and the Xe…pyrrole cluster

L. Rubio-Lago, D. Zaouris, Y. Sakellariou, D. Sofikitis and T. N. Kitsopoulos
Institute of Electronic Structure and Laser, Foundation for Research and Technology-Hellas and Department of Chemistry University of Crete, 71110 Heraklion, Crete, Greece
F. Wang and X. Yang
State Key Laboratory for Molecular Reaction Dynamics, Dalian, 116023, Liaoning, People's Republic of China
B. Cronin, A.L. Devine, G.A. King, M.G.D. Nix and M.N.R. Ashfold
School of Chemistry, University of Bristol, Bristol, UK BS8 1TS
S. S. Xantheas
Chemical & Materials Sciences Division, Pacific Northwest National Laboratory, 902 Battelle Boulevard, P.O. Box 999, MS K1-83, Richland, WA 99352, USA

The photolysis of pyrrole has been studied in a molecular beam at wavelengths 250 nm, 240 nm and 193.3 nm, using 2 different carrier gases, He and Xe. A broad bimodal distribution of H atom fragment velocities has been observed at all wavelengths. Near threshold at both 240 and 250 nm, sharp features have been observed in the fast part of the H-atom distribution. Under appropriate molecular beam conditions, these sharp features and the photolysis of pyrrole at both 240 and 250 nm disappear when using Xe as opposed to He as the carrier gas. We attribute this phenomenon to cluster formation between Xe and pyrrole, and this assumption is supported by observation of resonance enhanced multiphoton ionization spectra for the (Xe…pyrrole) cluster followed by photofragmentation of the nascent cation cluster. Ab initio calculations are performed to support the experimental data.

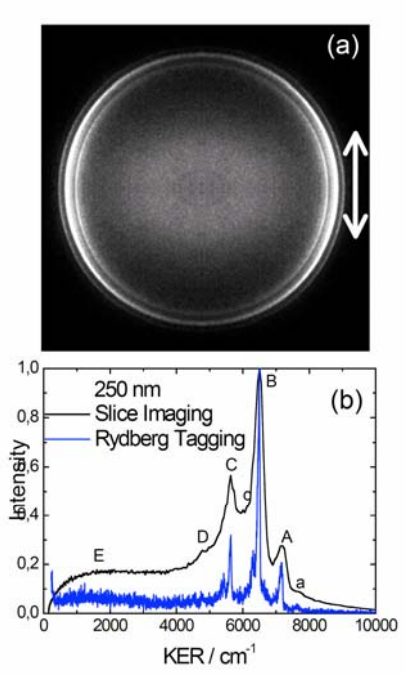

PFI-ZEKE photoelectron spectroscopy and potential curves of the six lowest ionic states of the ArKr mixed dimer

Evgueni Kleimenov, Lorena Piticco, Frédéric Merkt
Laboratorium für Physikalische Chemie, ETH Zürich, 8093 Zurich, Switzerland

Rare-gas dimers are model systems for studying atom-atom interactions [1] and represent a starting point to describe the properties of larger rare-gas clusters [2, 3].

The pulsed-field-ionization zero-kinetic-energy (PFI-ZEKE) photoelectron spectrum of the ArKr mixed rare-gas dimer has been recorded between 108000 and 120000 cm^{-1} (1 eV = 8065.544 cm^{-1}). This spectroscopic technique in combination with a narrow-bandwidth laser source allows the determination of the energy levels of an ion with respect to these of its parent neutral molecule with an accuracy of better than 1 cm^{-1}.

The ground state of the dimer is almost repulsive ($D_e \approx 116$ cm^{-1} [4]), but in several excited and ionic states the dimer is strongly bound [5, 6, 7]. The Rydberg and ionic states have been accessed by $1+1'$ resonance two-photon excitation via an intermediate state located below the $Ar(^1S_0) + Kr(5p[1/2]_0)$ dissociation limit.

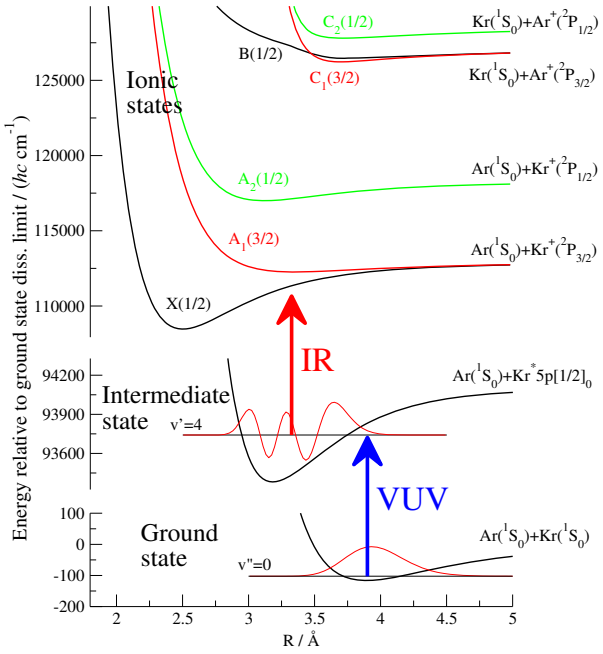

Figure 1: Potential energy curves of the states of ArKr and $ArKr^+$ relevant for the present study and photoexcitation scheme.

Lines corresponding to transitions to many vibrational levels of the X(1/2), $A_1(3/2)$ and $A_2(1/2)$ states were observed in the wavenumber region 108000-113000 cm^{-1}. Using the positions of vibrational levels of the X(1/2), $A_1(3/2)$ and $A_2(1/2)$ states and transition

energies measured in [8, 9, 6] the positions of the vibrational levels of the B(1/2), $C_1(3/2)$ and $C_2(1/2)$ could be predicted. Rotational constants for X(1/2) and $C_2(1/2)$ states were reported in [6]. Potential curves of all six ionic states in the region of the potential wells (2-5 Å) have been derived using a global potential model including long-range, spin-orbit and charge-exchange interactions.

References

[1] R. A. Aziz, W. J. Meath, A. R. Allnatt. *Chem. Phys.*, **78**, 295–309 (1983)

[2] W. R. Wadt. *Appl. Phys. Lett.*, **38**, 1030–1032 (1981)

[3] R. Kalus, I. Paidarová, D. Hrivňák, P. Paška, F. X. Gadéa. *Chem. Phys.*, **294**, 141–153 (2003)

[4] K. T. Tang, J. P. Toennies. *J. Chem. Phys.*, **118**, 4976–4983 (2003)

[5] Y. Tanaka, K. Yoshino, D. E. Freeman. *J. Chem. Phys.*, **59**, 5160–5183 (1973)

[6] F. Holland, K. P. Huber, A. R. Hoy, R. H. Lipson. *Journal of Molecular Spectroscopy*, **145**, 164–179 (1991)

[7] Y. Morioka, T. Tanaka, H. Yoshii, T. Hayaishi. *J. Chem. Phys.*, **109**, 1324–1328 (1998)

[8] M. Tsuji, M. Tanaka, Y. Nishimura. *Chemical Physics Letters*, **266**, 246–252 (1997)

[9] M. Tsuji, M. Tanaka, Y. Nishimura. *Chemical Physics Letters*, **256**, 623–628 (1996)

Intramolecular vibrational energy redistribution in CH_2XCCH (X = Cl, Br, I) measured by femtosecond pump-probe experiments

Alexander Kushnarenko, Eduard Miloglyadov, Martin Quack, and Georg Seyfang
Physical Chemistry, ETH–Zürich, CH–8093 Zürich, Switzerland

Abstract

The redistribution of vibrational energy after overtone excitation was investigated for three different propargyl-halides in femtosecond pump-probe experiments by time delayed UV-absorption spectroscopy using a hollow waveguide. Two different time scales for the intramolecular vibrational energy redistribution (IVR) were found after excitation of the first overtone of the acetylenic CH-stretching vibration on the one hand and the CH-stretching vibrations within the CH_2X-group on the other hand. For CH_2BrCCH and CH_2ClCCH a much longer relaxation time for the excitation of the acetylenic CH-stretching vibration is found compared to the one for the excitation of the CH_2-group, in agreement with previous findings of IVR in acetylenic and alkylic CH-chromophores.

1.Introduction

Intramolecular vibrational energy redistribution (IVR) is essential for unimolecular reactions [1, 2, 3]. Mode selective chemistry may be expected if the time scale for IVR is comparable to or slower than the time scale for the unimolecular reaction. IVR after near-IR overtone excitation has been investigated successfully by two significantly different methods: (1.) A molecular Hamiltonian H_{mol} for the intramolecular couplings is derived from high resolution IR-spectra and the time dependent dynamics of the initially excited vibrational levels can be obtained [3, 4, 5]. (2.) Intramolecular relaxation times can also be determined in femtosecond pump-probe experiments, where the population of the initial level, excited by the strong near-IR pump pulse, is followed by a time delayed weak probe pulse [6, 7, 8, 9]. The sensitivity of time delayed UV-absorption spectroscopy can be improved if the pump-probe experiments are made in a hollow waveguide [10].
From the analysis of high resolution overtone spectra of propyne (CH_3CCH) and trifluoropropyne (CF_3CCH) it was found that the CH-stretching vibration of the CCH-group is only weakly coupled to the low frequency vibrational modes [11, 12, 13, 14] and an IVR relaxation time $\tau = 120$ ps has been found for the first overtone of the CH-stretching vibration in CF_3CCH [15]. In our femtosecond pump-probe experiments we have investigated the transfer of vibrational energy from the initially excited CH-stretching vibration ($v_{CH} = 2$) to the CX-stretching vibration in CH_2ClCCH, CH_2BrCCH and CH_2ICCH, taking advantage of the fact that the excitation of the CX-stretching vibration results in a shift of the UV-absorption spectrum to longer wavelengths.

2.Experimental [9, 10]

Two identical optical parametric generators (OPG) (TOPAS, Light Conversion) are pumped by a femtosecond Ti:Sapphire laser (Clark CPA-1000) resulting in a pulse duration of 120 - 150 fs. The first overtone of the CH-stretching vibration is excited by the idler or signal wave of one OPG, whereas the fourth harmonic of the output from the second OPG around 420 nm is mixed with the residual light of the pump laser to obtain a wavelength around 275 nm to probe the spectral changes in the UV-spectrum of the excited molecules. To measure the time evolution, the UV-pulse is sent through a variable delay line. For the pump radiation a pulse energy of 30 - 40 μJ and a spectral width of 120 cm^{-1} is obtained. The laser beams are focused with lenses of f = 150 mm (near-IR) and f = 200 mm (UV) respectively to the entrance opening of a hollow waveguide of inner diameter d = 250 μm and a length of l = 500 mm. The waveguide is mounted into a glass cell with fused silica windows and the two beams are overlapped on a beam splitter in front of the cell. The focal lengths of the focusing lenses are chosen to match the beam diameter w of the free laser beams to the inner diameter of the waveguide. For ideal coupling conditions (w = 0.32d) more than 95% of the pulse energy of the free laser beam is coupled to the fundamental HE_{11}-mode of the waveguide [10]. To measure the change of the UV-absorption due to the near-IR excitation, the near-IR beam is modulated by an optical chopper. The relative pulse energy of the UV-beam is measured for every laser pulse before and behind the sample cell on two photodiodes D1 and D2. The difference of the ratio of the measured detector voltages U_{D2}/U_{D1} for pump laser-on minus pump laser-off is calculated after transfer of the data to the computer to obtain the time dependent UV-absorption signal.

Molecule	Excited vibr.	$\tilde{\nu}_{Pump}/cm^{-1}$	$\tilde{\nu}_{Probe}/cm^{-1}$	τ_1/ps	τ_2/ps	τ_3/ps
CH_2ClCCH	CH_2Cl-	5830	42'000	≤ 1.5	16 ± 2	-
	-CCH	6560	42'000	-	-	70 ± 9
CH_2BrCCH	CH_2Br-	5880	36'780	2.7 ± 1.0	21 ± 2	-
	-CCH	6560	35'700	-	-	102 ± 11
CH_2ICCH	CH_2I-	5880	29'400	≤ 1.0	16 ± 5	-
	-CCH	6560	29'400	6 ± 2	35 ± 9	-

Table 1: Measured relaxation times for the investigated propargyl halides

3.Results and Discussion

The first overtone of the two CH-stretching vibrations of the CH_2X-group for the propargyl halides consists of three partly overlapping bands between 5750 - 6050 cm^{-1} (see insert on figure 1). Well separated from those bands is the overtone of the acetylenic CH-stretching vibration around 6550 cm^{-1}. The combination band between the two types of CH-chromophores, expected around 6200 cm^{-1}, is weaker by nearly one order of magnitude and is not considered in our experiments. As the line width of our pump laser is around 120 cm^{-1} the different bands of the CH_2X-group cannot be excited separately.

Depending on the molecule under investigation the energy of the probe photons varies from 29'400 cm^{-1} for the propargyliodide to 42'000 cm^{-1} for the chloride.
Two examples for measured decay curves are shown on figures 1 and 2. One decay curve for the excitation of the CH_2-group in CH_2BrCCH and another one for the acetylenic group in CH_2ClCCH. The measured decay curves for the different CH-chromphores and different molecules are summarized in table 1.
Our results show clearly that the different relaxation behavior of the methylenic CH-group and the acetylenic CH-group, obtained from the analysis of the overtone spectra of CH_3CCH and CF_3CCH, is confirmed for CH_2BrCCH and CH_2ClCCH in our femtosecond pump-probe experiments. For the excitation of the first overtone of the CH_2X-group two different relaxation times could be identified. On fast component around $\tau_1 = 2.5$ ps or faster and another process with a relaxation time around $\tau_2 = 20$ ps (Fig. 1). For the excitation of the acetylenic CH-stretching vibration only a much longer relaxation time $\tau_3 = 70$ - 100 ps could be identified (Fig 2). Our preliminary experiments on CH_2ICCH do not show this expected difference in the relaxation behavior of the two excited CH-chromophores. For the excitation of the CH_2X-group a similar relaxation process is obtained as for the other two compounds. However, a quite fast relaxation process with $\tau_1 = 6$ ps is found for the acetylenic CH-stretching vibration in CH_2ICCH, in addition to a slower process with a relaxation time $\tau_2 \simeq 35$ ps. We think that this fast process could be due to an accidental resonance, as the overtone $2\nu_1$ is found around 6561 cm^{-1} and the combination vibration $2\nu_{11} + \nu_7$ (CI-stretch) is expected at 6572 cm^{-1} [16]. An analysis of the overtone spectra is planned in order to unravel the couplings.
Acknowledgment:Our work is supported financially by the ETH Zürich and the Schweizerischer Nationalfonds. We thank Andreas Schneider and Eduard Peyer for very important technical support.

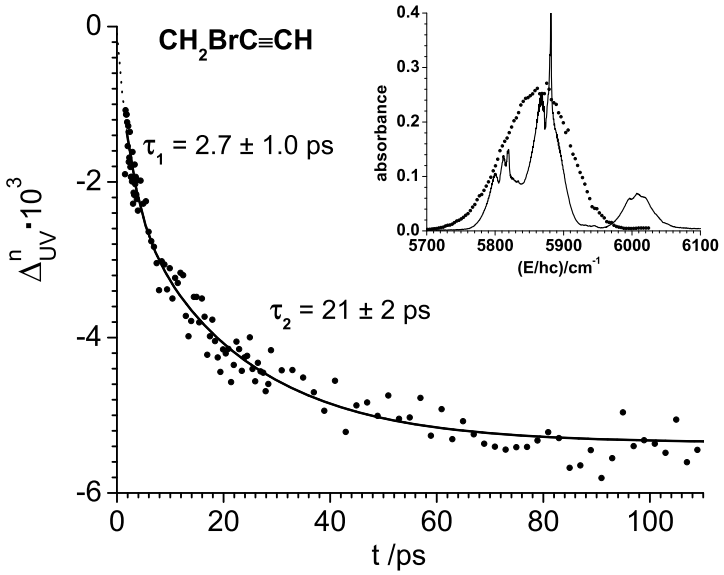

Figure 1: Measured decay curve for the excitation of the CH_2-chromophore in CH_2BrCCH. Two relaxation times τ_1 and τ_2 are obtained from a fit to the experimental data. The insert shows the IR-absorption spectra together with spectral intensity distribution of the pump pulse.

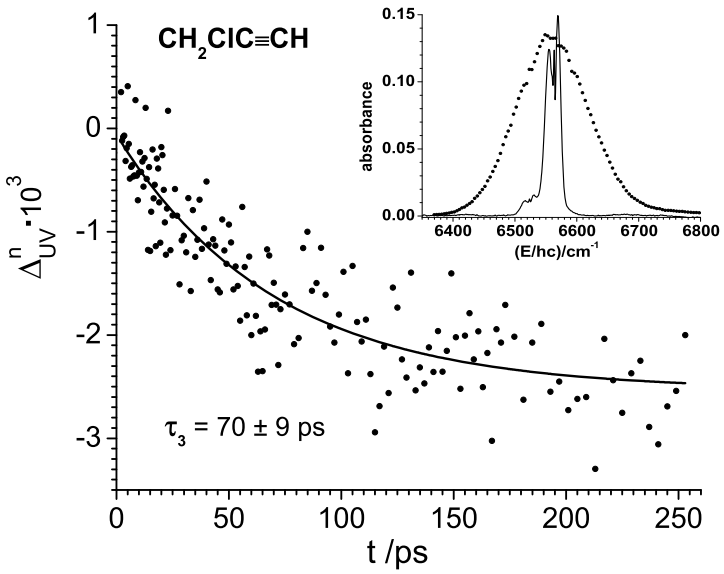

Figure 2: Measured decay curve for the excitation of the CCH-chromophore in CH_2ClCCH. One relaxation time τ_3 is obtained from a fit to the experimental data. The insert shows the IR-absorption spectra together with spectral intensity distribution of the pump pulse.

[1] M. Quack, and J.Troe, Theoretical Chemistry: Advances and Perspectives, **6B**, 199 (1981)

[2] M.Quack, Il Nuovo Cimento, **63B**, 358 (1981)

[3] M.Quack 'Molecular femtosecond quantum dynamics between less than yoctoseconds and more than days: Experiment and theory', in 'Femtosecond Chemistry' (Chap. 27), Manz, J. and Woeste, L., editors, Verlag Chemie (Weinheim), 781 (1995)

[4] M.Quack, Annu. Rev. Phys. Chem. **41**, 839 (1990)

[5] J.Pochert, M.Quack, J.Stohner, and M.Willeke, J. Chem. Phys., **113**, 2719 (2000)

[6] D.Bingemann, M.P.Gorman, A.M.King, and F.F.Crim, J. Chem. Phys. **107**, 661 (1997)

[7] A.Charvat, J.Assmann, B.Abel, D.Schwarzer, K.Henning, K.Luther, and J.Troe, Phys. Chem. Chem. Phys. **3**, 2230 (2001)

[8] T.Ebata, M.Kayano, S.Sato, and N.Mikami, J. Phys. Chem A **105**, 8623 (2001)

[9] V.Krylov, M.Nikitchenko, M.Quack, and G.Seyfang, Proc. SPIE **5337**, 178 (2004)

[10] V.Krylov, A.Kushnarenko, E.Miloglyadov, M.Quack, and G.Seyfang, Proc. SPIE **6460**, 64601D (2007)

[11] R.Dübal and M. Quack, Chem. Phys. Lett. **90**, 370 (1982)

[12] K.von Puttkamer, R.Dübal, and M.Quack, Farard. Disc. Chem. Soc. **75**, 197 (1983)

[13] M.Quack and J.Stohner, J. Phys. Chem. **97**, 12574 (1993)

[14] J.E.Gambogi, J.H.Timmermanns, K.K.Lehman, G.Scoles, J. Chem. Phys. **99**, 9314 (1993)

[15] K.O.Douglass, B.C.Dian, G.G.Brown, J.E.Johns, P.M.Nair, and B.H.Pate, J. Chem. Phys. **121**, 6845 (2004)

[16] J.C.Evans and R.A.Nyquist, Spectrochim. Acta **19**, 1153 (1963)

Studies of Hydrogen Formation on Interstellar Dust Grains Analogues

Elspeth Latimer and Stephen D Price
Chemistry Department, University College London,
20 Gordon Street, London, WC1H OAJ, UK

Much of the matter in the Universe exists in the form of stars and planets, however, the region between the stars is far from empty. This area is known as the Interstellar Medium (ISM) and it contains vast areas of gas and dust grains, called interstellar clouds.[1] These clouds vary in size, content and density but can placed into three different categories: diffuse clouds, HII regions (where atomic hydrogen exists in a mainly ionised state) and dark clouds.[2] Dark clouds are perhaps the most interesting because nearly all the hydrogen present in these regions is in the form of H_2. Cosmic rays result in the ionisation of the H_2, which initiates all of the chemistry in the ISM. There is, however, one major problem: how is the H_2 formed? The conditions of low temperature and pressure prevent the either the H + H gas phase or 3-body reactions from occurring, so there must be another reaction pathway to account for the high abundance of molecular hydrogen. It is now believed that the formation of H_2 in the ISM takes place on the surface of dust grains.

Investigations indicate that the dust grains present in the ISM are comprised of dielectric matter such as silicates and carbonaceous materials.[1,3-5] There are two main reaction pathways that are generally considered for the heterogeneous production of H_2 on the grain surfaces. These are the Eley-Rideal (ER) mechanism and the Langmuir-Hinshelwood (LH) mechanism. In the ER process an adsorbed H atom reacts with an atom from the gas phase, after which the newly formed molecule may desorb from the surface. In contrast the LH mechanism involves two adsorbed and thermalised H atoms which react on the surface and are desorbed as a molecule.

The experiment, presented in this poster, is designed to probe the ro-vibrational excitation of HD formed on an interstellar dust grain analogue.[6-8] H and D atoms impinge directly onto a Highly Orientated Pyrolytic Graphite (HOPG) surface. The HOPG is mounted on a closed-cycle helium cryostat so that it can be cooled to 15 K, a temperature comparable to the temperatures of the grains in the ISM. The HD molecules which recombinatively desorbed from the surface are detected by state-selective ionisation using laser induced (2+1) Resonance Enhanced Multiphoton

Ionisation (REMPI) via the E, F $^1\Sigma_g^+$ electronic state. The HD^+ ions produced by the REMPI process are detected using a time-of-flight mass spectrometer (TOFMS). Prior to recording a spectrum, the HOPG surface is heated to remove any adsorbates and then allowed to cool to 15 K. When this process is complete, the laser is scanned over the ro-vibrational line of interest. For each vibrational state the REMPI signal is normalised for laser power fluctuations and rotational transition strengths to yield the relative populations for each J'' state detected. These rotational populations are then analysed using Boltzmann plots.

Nascent HD formed on our HOPG surface at 15 K has been detected in the ro-vibrationally excited states $v'' = 3 – 7$.[7] Each of these ro-vibrational levels gave a clear signal, where the REMPI events caused a detectable rise in the ion count. Boltzmann analysis give the average rotational temperature, these values are shown in Table 1 below.

Ground state, X $^1\Sigma_g^+$ v'', J'' states detected	**Resonant state, E,F $X^1\Sigma_g^+$ v' ($J' = J''$)**	**Rotational Temperature /K**
$v'' = 1$, $J'' = 0 – 4$	0	246 ± 24
$v'' = 2$, $J'' = 0 – 4$	0	282 ± 31
$v'' = 3$, $J'' = 0 – 6$	1	330 ± 26
$v'' = 4$, $J'' = 0 – 6$	1	368 ± 22
$v'' = 5$, $J'' = 0 – 6$	1	338 ± 20
$v'' = 6$, $J'' = 0 – 4$	2	267 ± 55
$v'' = 7$, $J'' = 0 – 3$	3	337 ± 102

Table 1. Average rotational temperatures for all the ro-vibrational states detected following the reaction of H and D atoms on a cold HOPG surface.

Previous work from our group included the detection of HD in the vibrational states $v'' = 1$ and 2 formed on cold graphite.[6] This earlier work has been combined with our more recent results to produce a full ro-vibronic distribution for $v'' = 1 – 7$. Two different scaling methods were employed to place the rotational distributions for each vibrational level on a common scale. One methodology simply using the original data

scaled with the relevant Franck-Condon factors. A second approach involved deriving scaling factors from a series of rapid consecutive scans over one particular J'' state from each vibrational level for $v'' = 3 - 7$. Both scaling methodologies indicate that $v'' = 4$ is the most populated vibrational state for HD formed on the surface. and there is a sharp decrease in population from $v'' = 4$ to $v'' = 5$.

References

[1] D. A. Williams and E. Herbst, Surf. Sci. **500**, 823 (2002).
[2] D. A. Williams and T. W. Hartquist, Accounts Chem. Res. **32** (4), 334 (1999).
[3] W. Duley and D. A. Williams, *Interstellar Chemistry*. (Academic, London, 1984).
[4] J. E. Dyson and D. A. Williams, *The Physics of the Interstellar Medium*, 2nd ed. (Institute of Physics, Bristol, 1997).
[5] S. Tine, D. A. Williams, D. C. Clary, A. J. Farebrother, A. J. Fisher, A. Meijer, J. M. C. Rawlings, and C. J. Davis, Astrophys. Space Sci. **288** (3), 377 (2003).
[6] S. C. Creighan, J. S. A. Perry, and S. D. Price, J. Chem. Phys. **124** (11) (2006).
[7] F. Islam, E. R. Latimer, and S. D. Price, J. Chem. Phys. **127**, 064701 (2007).
[8] J. S. A. Perry, J. M. Gingell, K. A. Newson, J. To, N. Watanabe, and S. D. Price, Meas. Sci. Technol. **13** (9), 1414 (2002).

Tailoring the reactivity at the gas/solid interface

Guillaume Laurent, Paula Rivière, Fernando Martín
Departamento de Química, Facultad de Ciencias C-9, Universidad Autónoma de Madrid, 28049 Madrid, Spain

H. Fabio Busnengo
Instituto de Fisíca Rosario, Consejo Nacional de Investigaciones Científicas y Técnicas (CONICET), and Facultad de Ciencias Exactas, Ingeniería y Agrimensura, Universidad Nacional de Rosario, Avenida Pellegrini 250, 2000 Rosario, Argentina

The study of adsorption and scattering of H_2 by metal surfaces is important to understand the microscopic mechanisms behind many catalytic reactions. In recent years, full dimensional dynamical calculations based on potential energy surfaces (PES's) obtained from first principles calculations have provided unprecedented insight into those mechanisms for the case of both pure metal surfaces [1,2] and alloys surfaces [3]. An exiting challenge will be now to attempt to control the reactivity (adsorption and scattering probability) of the surface by modifying his electronic and/or geometric structure. A promising way to complete this goal could be found in the use of pseudomorphic surfaces [4]. In this work, we propose to compute the six-dimensional (6D) potential energy surface for the H_2 molecule interacting with both 1ML Cu/Ru(0001) and 1 ML Pd/Ru(0001) surfaces. Based on the DFT/GGA calculated potential energies, an analytical 6D PES has been determined using the corrugation reducing procedure [5]. First results of the PES properties and sticking coefficient as a function of the incident energy will be presented at the conference.

References :

[1] D. Farías, C. Díaz, P. Rivière, H. F. Busnengo, P. Nieto, M. F. Somers, G. J. Kroes, A. Salin and F. Martín, Phys. Rev. Lett. **93**, 246104 (2004)
[2] P. Nieto, E. Pijper, D. Barredo, G. Laurent, R. A. Olsen, E. J. Baerends, G. J. Kroes and D. Farías, Science **312**, 86 (2006)
[3] P. Rivière, M. F. Somers, G. J. Kroes and F. Martín, Phys. Rev. B **73**, 205417 (2006)
[4] M. Lischkaa, C. Moscha and A. Groß, Electrochimica Acta **52**, 6, 2219-2228 (2007)
[5] H. F. Busnengo, A. Salin and W. Dong, J. Chem. Phys. **112**, 7641 (2000)

Theoretical Investigation for the Interaction of Adenine Adducts with Thymine: II. Solvent Effect

Prabhat K. Sahu, Yu-Wei Huang, Chang –Wang Kuo and Shyi –Long Lee*
Department of Chemistry and Biochemistry,
National Chung Cheng University, Chia –Yi, 621 TAIWAN

Abstract:

The existence of DNA adducts bring the danger of carcinogenesis because of mispairing with normal DNA bases. 1,N^6-ethenoadenine adducts (εA) and 1,N^6-ethanoadenine adducts (EA) have been considered as DNA adducts to study the interaction with thymine, as DNA base. Several different stable conformers for each type of adenine adduct with thymine, have been considered with regards to their interactions. The differences in its geometrical structure, energetic properties and hydrogen bonding strengths have been compared with Watson-Crick adenine-thymine base pair (A-T).[1] Solvation free energies (ΔG_{solv}) calculations for these different stable conformers have been achieved by using COSMO model (C-PCM) at B3LYP/6-31+G*, so as to predict the association energies for the adenine adducts with thymine. The energetic computed in solvent phase has also been compared with those reported earlier in gas phase. The aim of this research is to provide fundamental understanding of adenine adduct and thymine interaction at molecular level and to aid in future experimental studies towards finding the possible cause of DNA damage.

---

*Corresponding Author
E-mail: chesll@ccu.edu.tw

References:

1.Prabhat K. Sahu, Chang –Wang Kuo, and Shyi –Long Lee*, ***J. Phys. Chem. B 111 (2007) 2991***

Magnesium doped helium clusters: Is the solvation problem solved?

M. Elhiyani and M. Lewerenz
Laboratoire de Chimie Théorique, Université Paris Est (Marne la Vallée)
77454 Marne la Vallée Cedex 2, France

We present extensive quantum Monte Carlo results for the solvation of magnesium and calcium atoms in helium clusters with up to 190 atoms based on newly computed accurate ab initio pair potentials. Magnesium is found to be solvated preferably in a near surface location but to exhibit a rather diffuse radial distribution. This finding disagrees with earlier Monte Carlo [1] and DFT calculations [2] and spectroscopic experiments [3] but supports a recent experiment based on appearance potentials and ionisation mechanisms [4].

Alkaline earth metal clusters exhibit a rich size dependent electronic structure ranging from van der Waals type binding of the dimers through molecular electronic levels in small clusters and metallic binding in large clusters. Growing magnesium clusters inside liquid helium clusters for spectroscopic studies solves several issues related to the high reactivity of magnesium [5, 6, 7] but brings along new interesting questions. Atomic transitions remain observable with significant intensity in multiple atom implantation experiments and indicate probably incomplete coagulation inside the helium cluster in spite of a Mg-Mg interaction which should render atomic solvation unlikely. The results presented here are part of a longer project aiming at the theoretical treatment of this aggregation process by a combination of state of the art ab initio potentials and an effective potential method to describe the liquid helium environment [8, 9].

While theory and experiments agree that alkali metal atoms remain on the surface of helium clusters the delicate balance between the M-He (M=Mg, Ca, Sr, Ba) and the He-He interaction leaves more room for ambiguities. The spectral shifts of M@He_n have been interpreted as indicative of solvation for Mg, and of deep dimple situations for Ca, Sr, and Ba [3, 10]. This interpretation had been confirmed by DFT calculations [2] and exploratory quantum Monte Carlo calculations [1]. As a first step in our aggregation dynamics project we chose to study atomic implantation with the best available pair potentials and accurate quantum simulation. We recomputed the Mg-He potential with very large basis sets augmented with diffuse and bond functions with the coupled cluster method with explicit inclusion of triples (CCSDT). Our pair potential largely confirms the incremental procedure of Hinde [11] and gives a very slightly deeper well. In spite of this deeper well our diffusion quantum Monte Carlo calculations with up to 190 helium atoms invariably converge to a ground state structure with a probability distribution of Mg reaching a peak in a deep dimple below the surface. This state is reached in a reproducible manner in calculations starting out with Mg on the surface and in the center of the helium cluster. The radial distribution of magnesium was computed by the method of descendant weighting and does show a tail reaching all the way to the center of the cluster for most cluster sizes. This reflects a near indifference of the ground state energy with respect to the magnesium position which might explain the difference with

respect to earlier theoretical results. Density functional theory [2] might not be accurate enough, in particular at small cluster sizes, to resolve such a delicate balance and the previous quantum Monte Carlo data appear to show some instabilities [1] and used a less accurate method for the calculation of the distribution functions. Our Monte Carlo method correctly reproduces the bound state of all Mg@He$_n$ all the way down to $n = 1$ with perfect agreement with a variational calculation in the latter case.

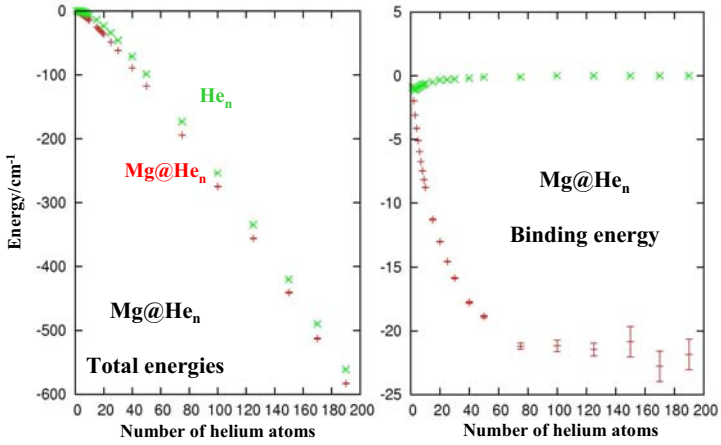

Figure 1: Total energy of helium and magnesium doped helium clusters from diffusion Monte Carlo calculations with our CCSDT Mg-He potential (left) and size dependent binding energy of magnesium to helium clusters indicating saturation at our largest cluster sizes (right).

Our present results for the binding energy of Mg@He$_n$ appear to saturate near 23 cm^{-1}, see Fig. 1, but the noticeable statistical error bars for our largest cluster sizes leave some room for a further increase at even larger sizes. Contour graphs of the helium density computed by descendant weighting in a cylinder coordinate system are shown in Fig. 2. The z-axis of the coordinate system is defined as the axis passing through the Mg atom and the center of mass of the helium atoms. Helium atom positions are binned according to their z-coordinate and their distance r from this axis with weights representing the contribution of a given atom configuration to $|\Psi_0|^2$. For both sizes shown (50 and 100 helium atoms) a zone of low helium density is visible on the positive z-axis corresponding to the position occupied on average by the magnesium atom. The onset of a weak helium density peak near the magnesium atom is also visible. The core density of helium clusters in this size range is already very close to the bulk helium value of 0.022 Å^{-3}

The recent electron impact experiments [4] have provided strong arguments in favor of a deep dimple location of magnesium and agree with our theoretical results. The incomplete magnesium aggregation observed in the pickup experiments would be very

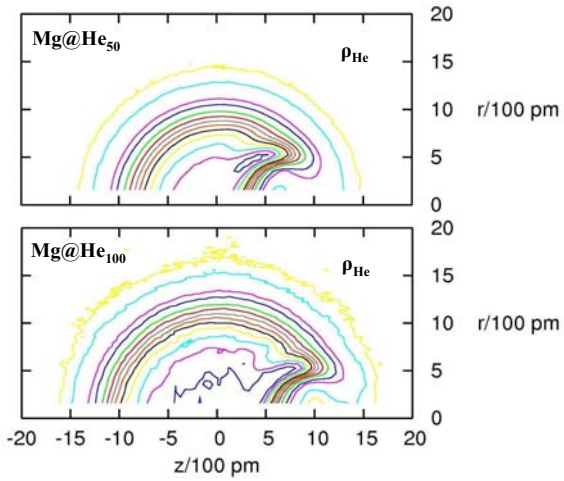

Figure 2: Helium density contours plots derived from diffusion Monte Carlo calculations with descendant weighting for $Mg@He_{50}$ (top) and $Mg@He_{100}$ (bottom), each exhibiting a deep dimple occupied by Mg.

mysterious if all implanted magnesium atoms sank immediately to the center of the helium cluster. A near surface location of Mg atoms, however, would bring in the necessity of random encounters following diffusion in the surface layer of the helium cluster and might allow survival of a certain fraction of magnesium atoms for sufficiently long times to be observed.

References

[1] M. Mella, G. Calderoni, and F. Cargnoni, *J. Chem. Phys.* **123**, 054328 (2005).

[2] A. Hernando, R. Mayol, M. Pi, M. Barranco, F. Ancilotto, O. Bünermann, and F. Stienkemeier, *J. Phys. Chem. A* **111**, 7303 (2007).

[3] J. Reho, U. Merker, M. R. Radcliff, K. K. Lehmann, and G. Scoles, *J. Chem. Phys.* **112**, 8409 (2000).

[4] Y. Ren and V. V. Kresin, *Phys. Rev. A* **76**, 043204 (2007).

[5] T. Diederich, T. Döppner, J. Braune, J. Tiggesbäumker, and K.-H. Meiwes-Broer, *Phys. Rev. Lett.* **86**, 4807 (2001).

[6] T. Döppner, T. Diederich, J. Tiggesbäumker, and K.-H. Meiwes-Broer, *Eur. Phys. J. D* **16**, 13 (2001).

[7] T. Diederich, T. Döppner, T. Fennel, J. Tiggesbäumker, and K.-H. Meiwes-Broer, *Phys. Rev. A* **72**, 023203 (2005).

[8] P. Slavíček, P. Jungwirth, M. Lewerenz, N. H. Nahler, M. Fárník, and U. Buck, *J. Phys. Chem. A* **107**, 7743 (2003).

[9] D. Bonhommeau, P. T. Lake, Jr., C. le Quiniou, M. Lewerenz, and N. Halberstadt, *J. Chem. Phys.* **126**, 051104 (2007).

[10] F. Stienkemeier, F. Meier, and H. O. Lutz, *J. Chem. Phys.* **107**, 10816 (1997).

[11] R. J. Hinde, *J. Phys. B: At. Mol. Opt. Phys.* **36**, 3119 (2003).

Widely-tunable Fourier-transform-limited terahertz pulses generated via optical frequency difference

J. Liu, H. Schmutz, and F. Merkt
Laboratorium für Physikalische Chemie, ETH Zürich, CH-8093 Zürich, Switzerland

Fourier-transform-limited terahertz (THz) pulses ($\Delta\nu < 20$MHz, peak power up to $10\,\mu$W) have been generated using (i) low-temperature-grown (LTG) GaAs spiral photomixers[1] (ν up to 3THz), and (ii) crystals of the highly nonlinear organic salt 4-*N*,*N*-dimethylamino-4'-*N*'-methyl stilbazolium tosylate (DAST[2], ν up to 30THz). In both experiments two narrow-bandwidth ($\Delta\nu < 1$MHz) Ti:Sa laser beams ($\lambda \sim 800$nm) with a well-controlled frequency difference were amplified in the same Nd:YAG pumped Ti:Sa crystal and used as optical sources to pump the THz emitters. The main limitation is the thermal damage threshold for (i) and the phase mismatching condition for (ii). Other types of photomixers and crystals can be used to increase the maximum THz pulse energy. This widely-tunable narrow-bandwidth THz source is suited to various spectroscopic applications, especially to the studies of clusters when combined with mass-selective laser photoionization.

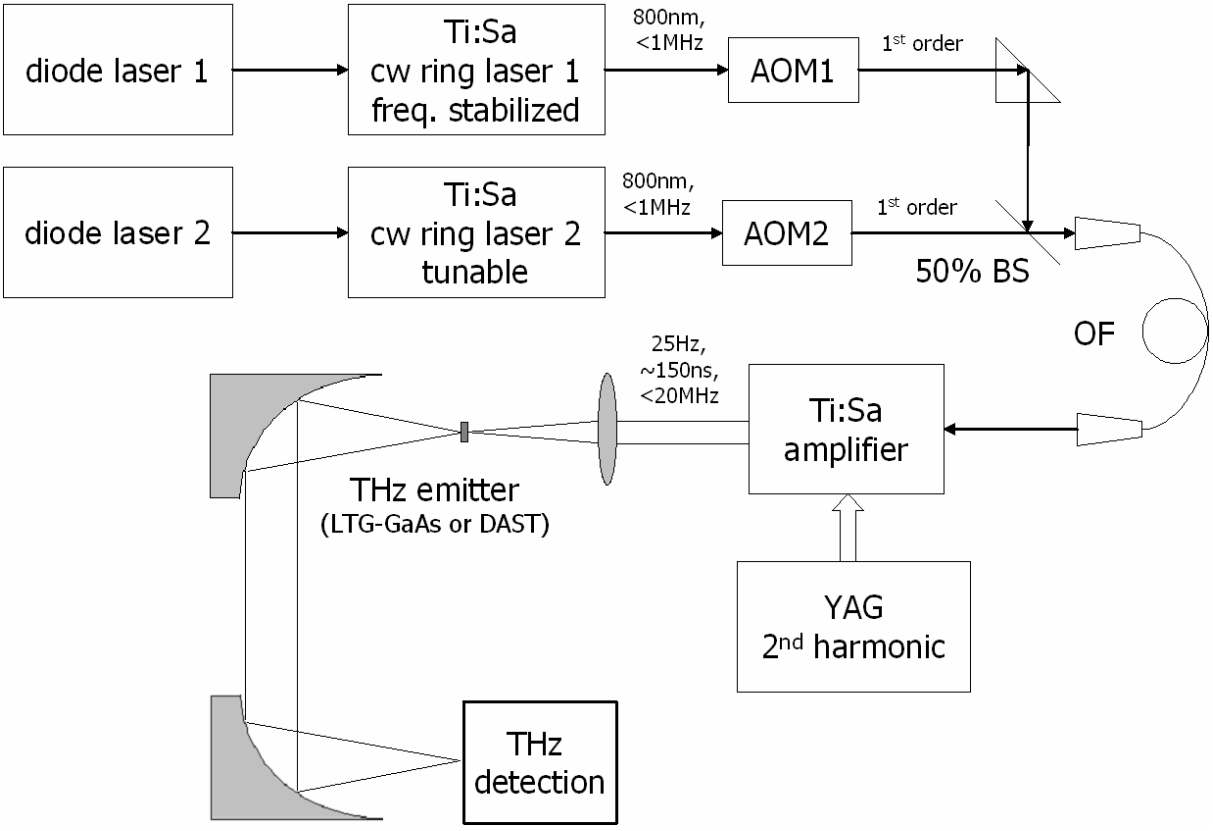

Fig. 1. Experimental setup of the THz generation experiment. AOM: acoustic-optic modulator, BS: beam splitter, OF: optical fiber.

[1] E. Peytavit *et. al.*, Appl. Phys. Lett. **81**, 1174 (2002)
[2] A. Schneider *et al.*, J. Opt. Soc. Am. B **23,** 1822 (2006)

Rydberg States of Na-doped helium nanodroplets

E. Loginov and M. Drabbels
Laboratoire de chimie physique moléculaire, Ecole Polytechique Fédérale de Lausanne, Lausanne, Switzerland

The dynamics of excited states of Na atoms deposited on the surface of helium nanodroplets has been investigated with velocity map ion imaging, photoelectron spectroscopy, time-of-flight mass-spectroscopy and mass-analyzed threshold ionization. For the first time the excitation spectra of Na-doped helium nanodroplets corresponding to Rydberg states of Na atoms have been measured from the lowest excited 3p state upto the ionization threshold, see Fig.1. All lines in the excitation spectra are shifted and broadened with respect to atomic lines. The observation of transitions to ns- and nd-states shows that the atomic selection rules are broken due to the non-spherical symmetry of "Na-helium nanodroplet" complexes.

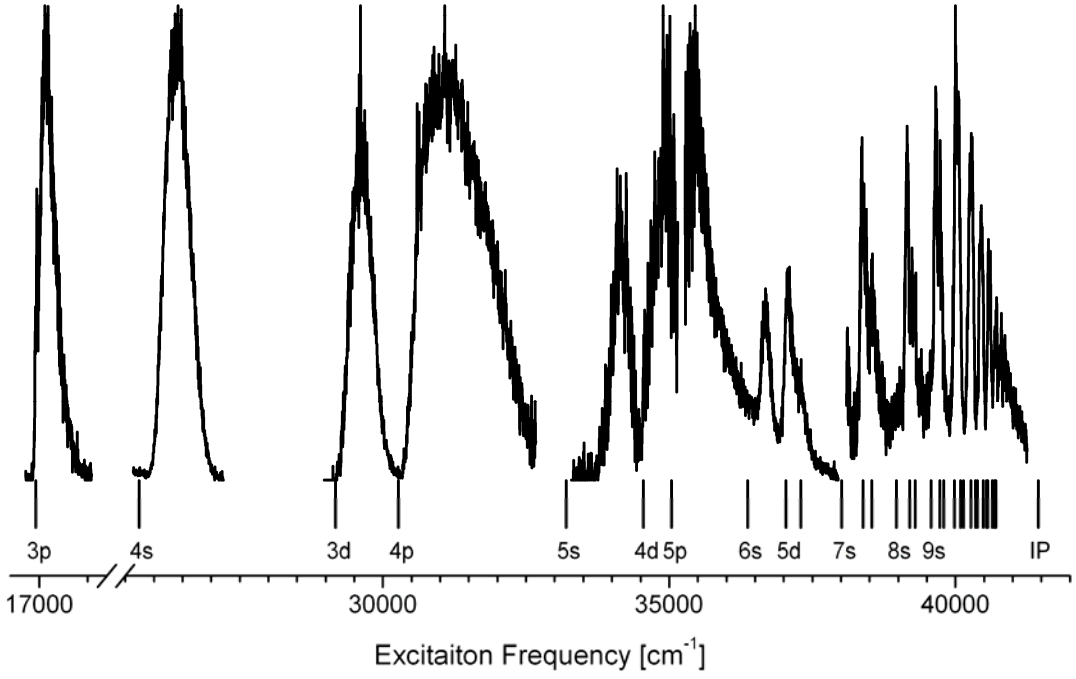

Figure 1 One-photon excitation spectrum of Na atoms on the surface of helium nanodroplets with <r> = 41 Å recorded by monitoring bare sodium atoms desorbed after the excitation step. The intensities are all normalized to unity.

Bare Na* atoms as well as Na^*He_n (n = 1-6) exciplexes, desorbed from the surface of helium nanoclusters, were detected upon excitation. The photoelectron spectroscopy of products revealed the desorption of Na* not only in the initially excited states but also in lower lying states indicating that relaxation plays an important role. The recorded velocity distributions show interesting characteristics: for the lowest states the mean kinetic energy of Na* increases linearly with excitation energy, while the angular anisotropy parameter rises monotonically with excitation frequency. The velocity distributions of Na^*He_n exciplexes do

not manifest such remarkable properties. The tentative explanation of the observed features is based on the approximation that the “Na*-helium nanodroplet“ potentials can be described by the sum of Na*-He pair potentials over the helium atoms constituting the nanodroplet. The shapes and the shifts of the transtitions to low excited states of Na obtained within this model are in a good agreement with experimental observations. The relaxation of highly excited fragments to lower states can be explained by curve crossings of the overall “Na*-helium nanodroplet” potentials. The velocity distributions of desorbed Na* can be qualitatively interpreted by the overall interaction potentials of sodium with helium nanodroplet. In contrast, the Na*He exciplex formation on the surface of nanodroplets appears to be mainly governed by the Na*-He pair potentials.

Contributed papers

Poster session B

Water Clusters Impact on Silicon Surface

U. Even and K. Luria
School of Chemistry, Raymond and Beverly Sackler Faculty of Exact Sciences
Tel Aviv University 69978 Tel Aviv, Israel

We study the impact of mass selected, protonated water clusters of well defined energy (ΔE~2eV, fig. 1), with a silicon surface. We could identify the energy region where only charge neutralization takes place and energy region where charge fragments appear. The quantum yield for charged fragmentation was measured and proved to depend strongly on the parent mass.

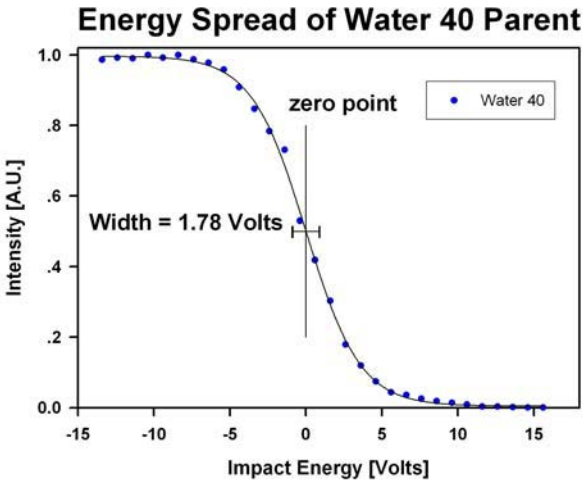

fig. 1: zero point was set to the energy at which the intenity is half max. Energy width is 1.78 Volts.

A Time of Flight, constant momentum mass spectrometer (CM-MS) with high energy resolution (0.2%) was developed for this experiment. It combines enough mass resolution (for clusters of up to 100 units) and energy resolution for our experiment. It is composed of three stages of constant and uniform fields created by resistive tubes and pulsed for duration shorter than the flight time.

We examined the impact of mass selected protonated water cluster with Silicon surface at various collision energies. Charged fragments from the parent cluster were detected as a function of the (well defined) impact energy. The charged fragments appear only above certain impact energy [3,4] (fig. 3); their yield grows to a maximum and than decline. The mass of the fragments are much smaller than that of the parent impacting cluster pointing to shattering [1,2]. Total fragmentation yield was found to be strongly dependent of the parent size. The results show that chemistry under extreme conditions can be studied for the brief interval (100 fs) during the collision.

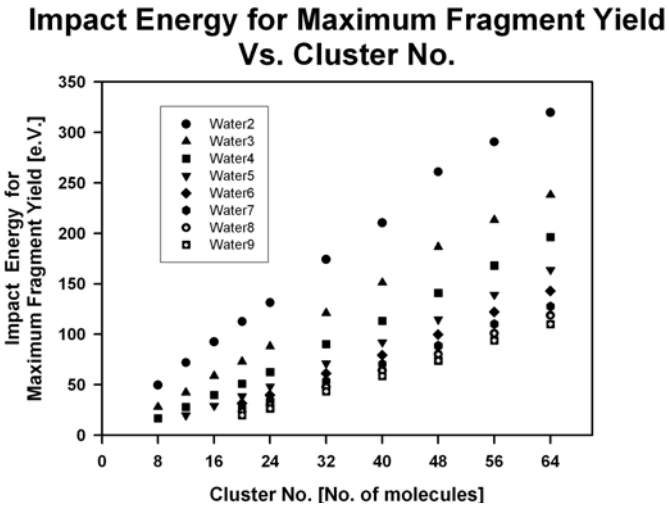

fig. 2: linear relation between impact energy needed for a certain fragment and the cluster size.

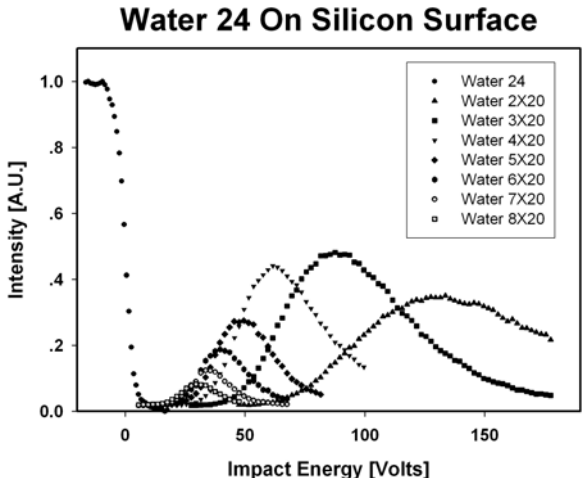

fig. 3: fragments appear above a certain energy

[1] W. Christen, U. Even, Eur. Phys. J. D **24** 283 (2003).
[2] U. Even**,** T. Kondow, R. D. Levine, T. Raz, Com. Mod. Phys. 1D, **14** (1999).
[3] A. Gross, R. D. Levine, Molecular Physics, **105** (4) 419 (2007).
[4] A. Gross, R. D. Levine, Jurnal of Chemical Physics, **125** 144516 (2006).

State Resolved Spectroscopy of Very High Vibrational Levels of Water

Maxim Grechko, Pavlo Maksyutenko, Thomas R. Rizzo, Oleg V. Boyarkin

Ecole Polytechnique Fédérale de Lausanne
LCPM, ISIC, EPFL, Station-6, Lausanne, CH-1015, Switzerland

Water is an important atmospheric molecule. It is involved in different photochemical processes and is responsible for the main fraction of solar radiation absorption. Modelling of these processes requires knowledge of rotational-vibrational energy levels of water in the electronic ground state with high precision and up to its dissociation limit. We use double and triple resonance laser spectroscopic schemes to access very high vibrational states of water molecules from single rotational-vibrational states. We also demonstrate the potential of collisionally-assisted double resonance spectroscopy to increase the number of detected states in a single scan. Here we report on results that provide accurate positions of some rovibrational levels below and just above the dissociation limit.

Dynamics in the hydrogen bonded systems $(HF)_2$ and HF·DF studied by means of cw-CRD spectroscopy

Carine Manca and Martin Quack
Laboratorium für Physikalische Chemie, ETH Zürich, CH-8093 Zürich, Switzerland

Abstract

We have improved our setup for cw-laser cavity ring-down spectroscopy of pulsed supersonic jet samples. We report high resolution spectroscopy of the dimer $(HF)_2$ and its isotopomer HF·DF in the region of the (HF)-stretching overtone near 7710 cm^{-1} corresponding to two quanta of excitation of the "free" HF.

1.Introduction

The HF dimer is among the simplest hydrogen bonded molecules. It has been frequently used as prototype system to understand hydrogen bond dynamics. In particular, much experimental work has been devoted to the characterization of the HF-stretching fundamental and overtone spectra of $(HF)_2$ and its isotopomers. High resolution spectroscopy is a powerful tool [1] for the study of dynamical properties in $(HF)_2$ like the hydrogen bond switching (1) and the vibrational predissociation (2) of the dimer (see for example references [2-13]):

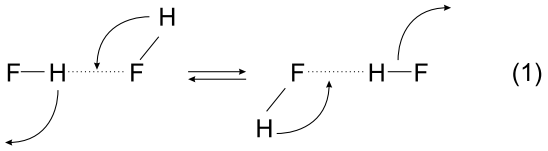

The mode selectivity of these processes has been highlighted repeatedly [3, 4, 6, 8, 9, 12, 13]. Experiments using jet cooling seem necessary since they allow a cold, collision-free environment, reducing the Doppler width and therefore allowing to reach the Lorentzian profile with the best available accuracy. This technique combined with continuous-wave cavity ring-down spectroscopy (cw-CRDS) which offers a very high sensitivity and high resolution represents an obvious interesting coupling. It has been successfully developed in our group [14, 15, 16] and was used to measure and analyze the N=2 triad of the HF dimer involving excitations with two quanta of HF stretching [13].
In this paper, we report the first and preliminary slit jet-CRDS measurements on the $N = 2$ triad of HF·DF isotopomer which we briefly compare with those recorded in our group using high resolution FTIR and diode laser supersonic jet absorption spectroscopy [12].

2.Experimental

The pulsed slit jet cw-CRDS setup has been described previously [14, 15, 16]. Briefly, a tunable external cavity InGaAsP laser diode (Radians Innova) emits a beam of a few mW between 7465 and 8025 cm^{-1} in single-frequency mode. It is coupled into the ring-down cavity to the TEM_{00} cavity mode. The cavity consists of two concave mirrors (Newport) of high reflectivity ($R \geq 99,97\%$) separated by 32.5 cm. The transmitted decaying light intensity after the cavity is detected by a fast InGaAs photodiode (NewFocus, 125 MHz). The cavity is mounted in a vacuum chamber pumped by an oil diffusion pump backed by a roots and a mechanical pumps. The residual vacuum in the cavity is few 10^{-7} mbar. A 33 mm $\times$ 100 μm slit of a pulsed solenoid valve is aligned along the spatial axis of the cavity. The laser probes the expansion 5 mm downstream from the nozzle. The stainless steel home-built pulsed valve produces gas pulses of about 1.3 ms duration with a backing pressure of 400 mbar and a nozzle repetition rate of 5 to 10 Hz; Under such conditions the pressure in the cavity during a measurement is maintained below 10^{-3} mbar.
The HF·DF dimer was obtained by thermal decomposition of KDF_2, synthesized from KHF_2 and D_2O by recrystallization [17]. A probe infrared spectrum of the gas phase obtained after the thermal decomposition indicates that we get a DF:HF ratio of $\sim$1:1. Our gas mixture for the jet expansion is composed of 4% of the obtained DF:HF, 9% of N_2O (which favors the dimer formation), Ar being the carrier gas.

3.Results and discussion

The $N = 2$ triad of $(HF)_2$ consists of the 2_1 level, approximately two quanta of excitation in the H-bonded HF, the 2_2 level, approximately two quanta in the non-bonded HF unit, and the 2_3 level, with one quantum each in the bonded and free HF, in order of increasing energy. Since the first measurements of the N=2 triad of $(HF)_2$ in our group using cw-CRDS [13], the experimental setup has been rebuilt. A considerable effort has been devoted to optimizing the pulsed valve and therefore the supersonic beam expansion conditions. The N_j=2_2 subband of the HF dimer has been remeasured to check the efficiency of the setup and get an estimation of the beam optimization. Figure 1 shows the experimental spectrum and the simulation for 26 rotational lines of the N_j =2_2 subband. Our results agree with previous work [8, 9, 12, 13].
Under our jet expansion conditions, a Voigt profile, i. e., a convolution between a Gaussian and a Lorentzian profile, is well suited to reproduce the profile of the rotational lines [13]. The contribution to the line width due to collisions, spontaneous emission and intramolecular vibrational redistribution are negligible; the Gaussian and Lorentzian contributions from the Voigt fit are due to a reduced Doppler effect and predissociation lifetime of the HF dimer, respectively. The determination of the two components has revealed to be a delicate matter since they are highly correlated and we used here the same procedure as described in reference [13]. The lines of the simulation in Fig. 1 are obtained with a Gaussian width of 0.005 cm^{-1} (150 MHz), which corresponds to a translational temperature of 32.8(1) K. The translational temperature obtained with this setup from previous measurements was 44.8(43)K which supports our optimization of the beam ex-

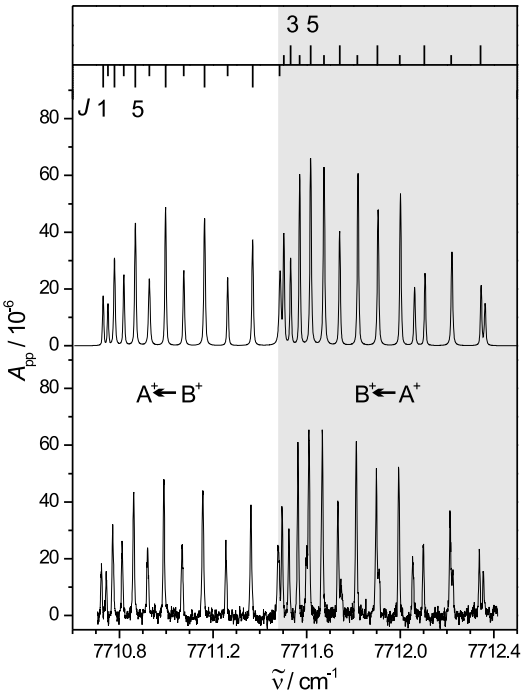

Figure 1: Q-branch region of the $K_a = 1 \leftarrow 0$ transition of the $N_j = 2_2$ of $(HF)_2$. Lower part: experimental CRD spectrum. Upper part: Simulation with a rotational temperature of 28.3 K. The J value of the 26 lines used for the fit is indicated. For previous results, see ref. [7, 9, 12, 13]

pansion conditions. Getting a smaller Gaussian contribution to the global width may help to determine long predissociation lifetimes in future measurements. Here we obtained a mean Lorentzian width which leads to a mean predissociation lifetime of 1.47(26) ns in agreement with previous results [9, 13]. From the line intensity distribution, we get a rotational temperature of 28.3(29) K, similar to previous results (25.9(4)K) [13].
The measurements for the HF·DF isotopomer are expected to be more difficult because of the lower absolute concentration of the species due to the formation of four different dimers($(HF)_2$, $(DF)_2$, HF·DF, and DF·HF). Figure 2 shows our first measurements of the relevant subband of the HF·DF dimer using the pulsed jet-CRDS setup. The signal to noise ratio is significantly improved in the present work. Our preliminary results do not indicate a clear evidence of the presence of $(HF)_2$. Further measurements will help us to optimize the conditions for the HF·DF dimer formation and the overlap between the jet and the diode laser. The position of the measured lines is in agreement with the measurements already performed in our group [12] and their assignment is indicated in Fig. 2 according to reference [12]. The line intensities seem to indicate a lower rotational temperature with our setup than in ref [12]. Further measurements will also allow us to estimate the predissociation lifetime for this isotopomer and get a better understanding in the dynamics of the HF dimer. Also a new data acquisition system which we are building at the present time might help us to increase the signal to noise ratio and detect even

weaker absorptions like combinations with low frequency modes.

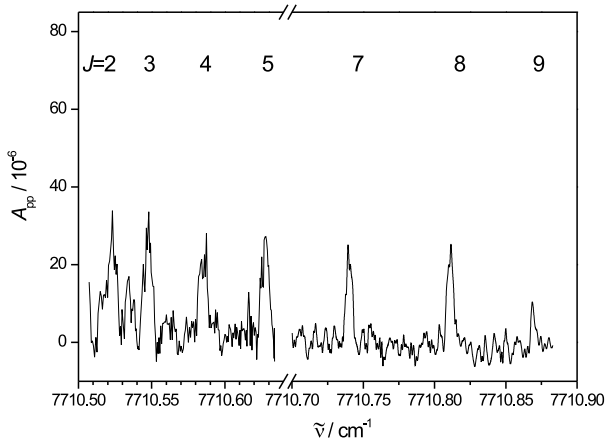

Figure 2: Q-branch region of the $K_a = 1 \leftarrow 0$ transition of the $N_j = 2_3$ of HF·DF from the cw-CRD slit-jet experiment. The assignment follows [12].

[1] M. Quack, Chimia **57**, 147 (2003).

[2] A. S. Pine, W. J. Lafferty, J. Chem. Phys. **78**, 2154 (1983).

[3] A. S. Pine, W. J. Lafferty, B. J. Howard, J. Chem. Phys. **81**, 2939 (1984).

[4] K. von Puttkamer, M. Quack, Chimia **39**, 358 (1985); Mol. Phys. **62**, 1047 (1987).

[5] A. S. Pine, B. J. Howard, J. Chem. Phys. **84**, 590 (1986).

[6] A. S. Pine, G. T. Fraser, J. Chem. Phys. **89**, 6636 (1988).

[7] K. von Puttkamer, M. Quack, M. A. Suhm, Infrared Phys. **29**, 535 (1989).

[8] K. von Puttkamer, M. Quack, Chem. Phys. **139**, 31 (1989).

[9] M. A. Suhm, J. T. Farrell, A. McIlroy, D. J. Nesbitt, J. Chem. Phys. **97**, 5341 (1992).

[10] H. C. Chang,W. Klemperer, J. Chem. Phys. **100**, 1 (1994).

[11] H. C. Chang, W. Klemperer, Faraday Discuss. **97**, 95 (1994).

[12] Y. He, H. B. Müller, M. Quack, M. A. Suhm, Z. Phys. Chem. in press **221**, (2007).

[13] M. Hippler, L. Oeltjen, M. Quack, J. Phys. Chem. A in press **111** (2007) .

[14] Y. He, M. Hippler, M. Quack, Chem. Phys. Lett. **289**, 527 (1998).

[15] M. Hippler, M. Quack, Chem. Phys. Lett. **314**, 273 (1999).

[16] M. Hippler, M. Quack, J. Chem. Phys. **116**, 6045 (2002).

[17] J. S. Kittelberger, D. F. Hornig, J. Chem. Phys. **46**, 3099 (1967).

Towards molecule interference with biomolecules and biomolecular clusters

Markus Marksteiner, Philipp Haslinger, Hendrik Ulbricht and Markus Arndt

Faculty of Physics, University of Vienna, Boltzmanngasse 5, A – 1090 Wien, Austria

We describe new methods for manipulating biomolecules with the main goal of using them in matter wave interference experiments. While earlier successful interference studies with fullerenes and fullerene derivates exploited a thermal source [1], we now built a new source to produce a beam of cold neutral biomolecules which has been tested for amino acids, amino acid clusters and polypeptides [2]. The source is driven by laser desorption followed by cooling in a mixing channel and supersonic expansion. The detection of the neutral molecules is done via single photon ionization using a VUV excimer laser (157nm).

The new source allows us for the first time to study neutral beams of large gas borne free tryptophan complexes composed of up to 30 amino acids and masses up to 6000 amu, when a metal atom like calcium, strontium, barium or copper is participating in the desorption process.

We propose to exploit the combination of matter wave interference and Stark deflectometry to measure and characterize the internal properties of the molecules through their electric susceptibility [3].

[1] B. Brezger et al., Phys. Rev. Lett. **88**, 100404 (2002)
Gerlich et al., Nature Physics, Vol. 3 Number 10, 711 (2007)
[2] Marksteiner et al., Acta Phys. Hun. B, 26/1-2, 87 (2006)
[3] Deachapunya et al., J. Chem. Phys. **126**, 164304 (2007)
Berninger et al., arXiv 0708.1936 (2007)

A new analytical representation of the potential energy surface for the adsorption process CO → CO/Cu(100)

Roberto Marquardt*
Laboratoire de Chimie Quantique - Institut de Chimie UMR 7177 CNRS/ULP
Université Louis Pasteur - F-67000 Strasbourg - *roberto.marquardt@chimie.u-strasbg.fr

Abstract

Global potential energy surfaces (PES) for molecular adsorption processes on bulk surfaces are rare, both because it is difficult to obtain accurate quantum chemical energy data in all regions of configuration space, and because analytical representations that would allow to interpolate quantum chemically calculated points are difficult to be formulated. This paper aims at filling this gap by the presentation of a new analytical, six-dimensional PES for rigid substrate structures. Results developed on the prototype system CO/Cu(100), but formally extensible to other non-dissociative and dissociative chemisorption phenomena, include a presentation of useful analytical expressions for the description of adsorption interaction terms, the comparison with a former, semi-empirical analytical representation for this prototype system, and the discussion of stationary geometries.

1. Introduction

The study of molecular adsorption processes on bulk surfaces is important both technologically and fundamentally, which is certified, nonetheless, by the award of the 2007 Nobel Prize in Chemistry to G. Ertl. While major advances have been acquired experimentally in the last decade, theoretical work progresses more slowly, although the working principles have been established for quite some time. Main difficulties reside in the accuracy of feasible quantum chemical calculations, which is related to the size and the complexity of the physical system.

Among one of the best theoretically studied systems is CO chemisorbed on a copper surface, and we cite here a few references [1–3], this list being necessarily incomplete (see also [4]). A key feature in the theoretical description of the adsorption process

$$\mathrm{CO(g)} \overset{\mathrm{Cu(100)}}{\rightarrow} \mathrm{CO(ads)/Cu(100)} \qquad (1)$$

is the potential energy surface (PES) for the nuclear motion. A semi-empirically derived PES for this process [2], which we abbreviate THG-PES in this work, has been much used in the past, among other studies for molecular dynamics simulation of the sticking probabilities of CO on copper surfaces [3, 5].

More recently, electronic structure data for the investigation of the diffusion process of adsorbed CO molecules on the copper substrate were published [6]. This data cover partially the configuration space of the adsorbed species. The present paper reports on a new, global analytical PES for process 1 that was adjusted to electronic structure data

from [6]. The analytical representation is a robust and flexible, currently six-dimensional function, but additional degrees of freedom for the motion of substrate atoms can be included straightforwardly.

2. Analytical forms

In this section we shall focus on a general adsorption process of a diatomic molecule AB on a (metal) substrate M:

$$\mathrm{AB} + \mathrm{M} \rightarrow \mathrm{AB}_{\mathrm{ads}}\mathrm{M}. \qquad (2)$$

To represent analytically the PES of such a process, we consider using the coordinates x, y and z, from Figure 1, to describe quite generally the position of the center-of-mass of molecule AB. The coordinates ϑ and φ describe its rotational orientation, while r is its interatomic distance. The substrate is represented by a grid model defined by a certain number of layers, a certain number of atoms per layer and the distance $R_{\mathrm{M-M}}$ between the atoms. The total number of atoms in the grid is given by typically $N_{\mathrm{grid}} \approx 600$, in our calculations.

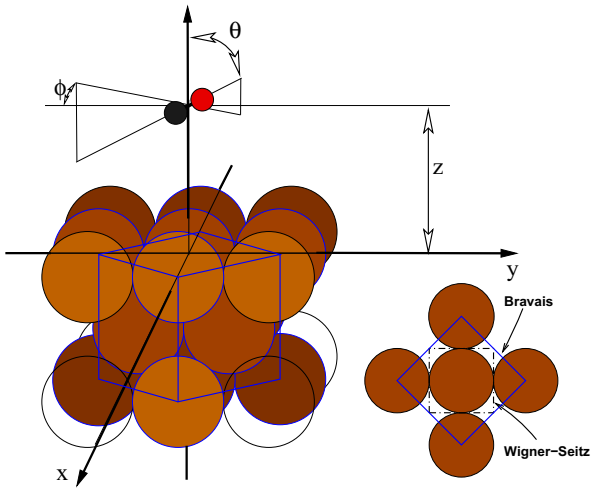

Figure 1: Substrate model used in this study.

We build up the analytical representation as a sum of two terms: $V = V_{\mathrm{ext}} + V_{\mathrm{int}}$. The external potential is a strongly varying function of the translational and rotational coordinates, which may be called external coordinates. The internal potential is defined as a Morse type potential, thus a strongly varying function of the internal coordinate r, but it will is also a smoothly varying function of the external coordinates. Such smooth variations will be implemented with appropriate switching functions: parameters of the internal potential will be switched, essentially as a function of the adsorption coordinate z (see Figure 1), from their values at the adsorption site limit at $z = z_{\mathrm{ads}}$, where z_{ads} is the value of the z coordinate at the bottom of the adsorption well, to the desorption limit ($z = \infty$). In addition, we found it very important to allow all adjustable parameters to be also smoothly varying functions of the location along the substrate surface. Depending the x and y coordinates of the adsorbed molecule's center-of-mass, any adjustable parameter will therefore "switch" values between the "top" (t), "bridge" (b) and "hollow" (h) site position.

The external potential is given as a sum of two- and three-body interaction potentials between the adsorbing AB molecule and individual atoms M from the crystal substrate:

$$V_{\mathrm{ext}} = V_0 + \sum_{n=1}^{N_{\mathrm{grid}}} \{V_{\mathrm{AM}}(r_{\mathrm{AM}}(n)) + V_{\mathrm{BM}}(r_{\mathrm{BM}}(n)) + V_{\mathrm{ABM}}(r_{\mathrm{ABM}}(n), c_{\mathrm{ABM}}(n))\} \qquad (3)$$

where values in parentheses are position variables: $r_{\mathrm{AM}}(n)$ and $r_{\mathrm{BM}}(n)$ are the distances of atoms A and B, respectively, from the n-th substrate atom, M_n. If $\boldsymbol{r}_{\mathrm{ABM}}(n)$ is the

vector leading from the position of atom M_n to that of the center of mass of the diatomic molecule AB, $r_{\mathrm{ABM}}(n)$ is its length, and $c_{\mathrm{ABM}}(n)$ is the cosine of the angle formed by this vector and the vector $\boldsymbol{r}_{\mathrm{AB}}$ leading from the position of atom A to that of atom B. The general form of the two-body potential V_{XM} between a substrate atom M and atom X (X = A or B) is given by the expression of a modified Morse potential [7].

While dispersion is neglected at the level of individual atomic units, it is taken into account explicitely, in the present work, at the molecular level via the three-body interaction terms:

$$V_{\mathrm{ABM}}(r,c) \;=\; D_{\mathrm{ABM}}\,[\exp\left(-\left(\frac{R_{\mathrm{ABM}}}{r}\right)^{6}\sum_{\ell=0}^{N_{\mathrm{leg}}} W_\ell\,P_\ell(c)\,\left(\frac{R_{\mathrm{ABM}}}{r}\right)^{\ell}\right)-1]. \qquad (4)$$

In Eq. (4), P_ℓ are Legendre polynomials, D_{ABM}, R_{ABM} and W_ℓ are parameters. In the present study, the highest Legendre polynomial order considered is $N_{\mathrm{leg}} = 6$, although there is no upper limit for this number, in principle. The sum in Eq. (4) starts at $\ell = 0$, and, for convenience, parameter W_0 is set to have the value 1.

3. Results

Figure 2 shows a one dimensional $V(z)$ profile of the present analytical representation (solid line) of the PES for the process of Eq. (1) and perpendicularly approaching CO molecules, in the sequence Cu-C-O. In the following, we shall compare such potential profiles with sections of the THG-PES (long dashed lines), and with sections of the PES obtained from an adjustment of the representation from [2] (short dashed lines) to the energy points calculated essentially as described in [6] (∘).

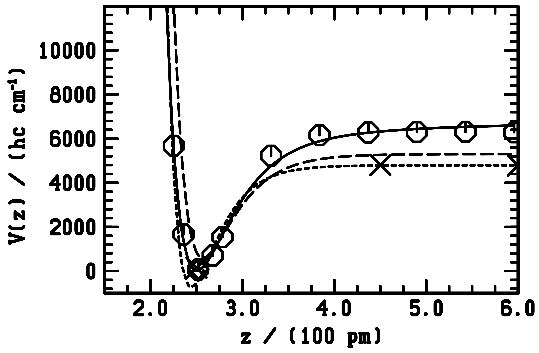

Figure 2: $V(z)$ profile at $x = y = 0$ pm, $r = 115$ pm and $\vartheta = \varphi = 0°$; see text for explanation.

The desorption energy on the electronic PES from the present work corresponds to 6272 cm^{-1} . The value obtained from the THG-PES is close to 5350 cm^{-1} . In [4] we estimated a value of roughly 6200 cm^{-1} for the desorption energy on the electronic PES from experimental data extrapolated from [8,9] at zero coverage of the substrate.

Figure 3 shows a one dimensional $V(x)$ profile of the present analytical representation along the <110> direction of the substrate. We first see that the present PES representation (solid line) describes well the *ab initio* data (◇ and ∘ marks). The THG-potentials have, both the original (long dashed lines) and the adjusted form (short dashed lines), a similar qualitative behaviour, but fail to describe the *ab initio* data. The value of the original THG-potential at the "top" site ($x = 0$ pm) is visibly higher than zero because of the contribution from the diatomic potential. The adjusted THG-potential gives too low an energy, at the "top" site.

The points marked with $\times$ in Figure 3 are results from cluster type calculations [4]. While the data follow quite reasonably the form of the potential for small values of x, and are even comparable to energies at $x = R_{\mathrm{M-M}}/2$, one sees that, latest at this point, the evolution is wrong: the "bridge" site is not a saddle point, following these data. This result underlines that cluster type calculations fail in giving the correct potential for the lateral motion. Geometries at the "bridge" saddle points are $x = 127.8$ pm, $z = 220.3$ pm and $r = 116.3$ pm (for perpendicular Cu-C-O arrangement), and the (relaxed) diffusion barrier is roughly 0.1 eV.

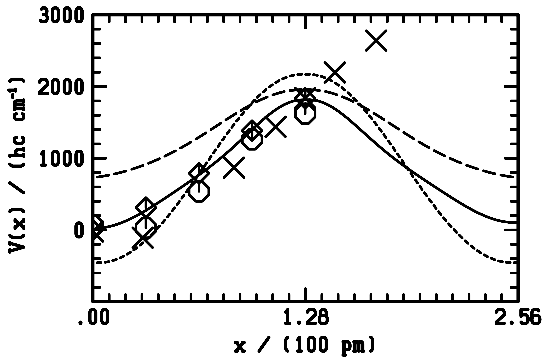

Figure 3: $V(z)$ profile at $r = 115$ pm, $y = 0$ pm, $z \approx 250$ pm, and $\vartheta = \varphi = 0°$; $\times$ indicate results from cluster type calculations as described in [4]; see also Figure 2.

4. Conclusions

A new analytical representation of the PES for the adsorption process of Eq. (1) is proposed. This representation allows, because of its flexibility, for a more accurate description of electronic structure data in those regions where they are available and, because of its robustness, it allows for physically meaningful extrapolation to regions where electronic structure calculations are more difficult to be obtained. The widely used THG surface probably underestimates the desorption energy as well as the height of the lateral diffusion barrier. More details of this work are in preparation [10].

Acknowledgement

The author thanks Prof. E. J. Baerends and Dr. R. Olsen for making accessible the raw data from [6] and for additional help and calculations for our common project.

References

[1] G. te Velde and E. J. Baerends, Chem. Phys., **117**, 399–406 (1993).
[2] J. C. Tully, M. Gomez, and M. Head-Gordon, J. Vac. Sci. Technol. A, **11**, 1914–1920 (1993).
[3] J. T. Kindt and J. C. Tully, Surface Science, **477**, 149–162 (2001).
[4] S. Hervé and R. Marquardt, Mol. Phys., **103**, 1075–1082 (2005).
[5] C. Cattarius and H.-D. Meyer, J. Chem. Phys., **121**, 9283–9296 (2004).
[6] P. Fouquet, R. A. Olsen, and E. J. Baerends, J. Chem. Phys., **119**, 509–514 (2003).
[7] F. Cuvelier, S. Hervé, R. Marquardt, and K. Sagui, CHIMIA, **58**, 296–305 (2004).
[8] J. C. Tracy, J. Chem. Phys., **56**, 2748–2754 (1972).
[9] C. M. Truong, J. A. Rodriguez, and D. W. Goodman, Surface Science Letters, **271**, L385–L391 (1992).
[10] F. Cuvelier, R. Marquardt, E. J. Baerends, and R. Olsen. To be published.

Kinetic decay measurements on MCAs using a new FT-ICR cell operating in a temperature regime T=100-500 K.

Maria Massaouti[1], Marco Neumaier[1], Oliver Hampe[1] and Manfred M. Kappes[1, 2]
[1]*Institut fürNanotechnologie, ForschungszentrumKarlsruhe, D-76021 Karlsruhe, Germany*
[2]*Institut für Physikalische Chemie, Universität Karlsruhe, D-76128 Karlsruhe, Germany*

Pavel A. Ryumin and Evgenij N. Nikolaev
Institute for Energy Problems of Chemical Physics, Russian Academy of Sciences, Moscow, Russia

Isolated multiply charged anions (MCAs) not only represent an important class of biological ions (such as proteins, oligonucleotides, peptides) which are commonly observed in gas-phase during mass spectroscopic analysis, but in the last years, they have become an emerging field of their own, due to their novel potential surfaces (repulsive Coulomb barriers-RCBs) and the interesting phenomena they display upon decay via electron detachment and/or ionic fragmentation.

A considerable interest of several groups has been devoted to investigate the temperature dependence of the decay rates and the decay activation energies of trapped multiply charged ions by performing kinetic decay measurements at room and high temperatures (T=293-500K). Among some of the interesting results, that came up from these measurements, is that blackbody radiation induced processes play a significant role on the temperature dependent decay even when the process is not an over the barrier mechanism[1] (i.e electron loss through tunnelling). In order to investigate in a more profound way the metastability of MCAs against electron loss and also to be able to extract accurate information about the activation energies of weakly bound large complexes that dissociate rapidly at room temperature, the need to perform similar kinetic measurements in low trap temperatures has come up just recently.

In this work, we present temperature dependent kinetic decay measurements that have been performed in a newly constructed Infinity ICR cell, which can be operated within the temperature range 100-500K. All the experiments are performed under UHV (i.e. collision free) conditions, so any recordable decay of the corresponding MCA is associated only with the absorption or emission of blackbody radiation. As a follow up of previous experiments[1,2], we study the decay mechanism of the small dianion $PtCl_4^{2-}$ as function of its internal energy (temperature). The particular interest in this dianion is that it exhibits negative electron affinity which is an important prerequisite for metastable MCAs to decay through tunnelling emission and it decays spontaneously only via electron detachment. These observations, in combination with the fact that it is the smallest experimentally observed dianion so far, makes it a model system for understanding, in a more profound way, the electron autodetachment decay mechanism of MCAs. The first recorded measurements on $PtCl_4^{2-}$, in a low temperature regime T<293K, using the new cell, show that the trapped dianions reach the temperature of the cell via blackbody radiation and that the tunnelling emission decay rates of the ions reduce as the temperature of the cell is reduced.

Similar kinetic measurements will be presented for the oligonucleotide dA_5^{4-} (a single-stranded oligonucleotide consisting of five adenosine units, joined by four phosphate groups). The main goal is to investigate if in the high temperature regime T>293K, this multiply

charged oligonucleotide decays via BIRD processes or through electron loss. These experiments aim to shed more light in the differences between the two decay pathways of MCAs (ionic fragmentation v.s. electron loss), since even though dA_5^{4-} has a negative fourth electron affinity[3], there is strong indication (through IR-multiphoton dissociation studies performed in our group[4]) that vibrational excitation in the ground electronic state leads exclusively to ionic fragmentation.

[1] M. N. Blom, O. Hampe, S. Gilb, P. Weis, M. M. Kappes, J. Chem. Phys., **115**, 3690 (2001)
[2] P. Weis, O. Hampe, S. Gilb, M. M. Kappes, Chem. Phys. Lett., **321**, 426 (2000)
[3] J. M. Weber, I. N. Ioffe, K. M. Berndt, D. Löffler, J. Friedrich, O. T. Ehrler, A. S. Danell, J. H. Parks, M. M. Kappes, J. Am. Chem. Soc., **126**, 8585 (2004)
[4] M. Neumaier, I. N. Ioffe, J. Lemaire, P. Maître, G. Niedner-Schatteburg, M. M. Kappes, and O. Hampe, in prep. (2007)

Identification of Explosives

A. Mauracher, P. Sulzer, S. Denifl, F. Zappa, M. Probst, T.D. Märk, P. Scheier
Institut für Ionenphysik und Angewandte Physik, Universität Innsbruck, Technikerstraße 25
6020 Innsbruck, Austria

Introduction

Nitroorganic compounds are molecules with a significant potential for industrial use, particularly as explosives or propellant. The interaction of electrons with these molecules, in particular electron attachment, plays an important role in understanding the reactivity of these compounds. Among the nitro compounds, explosives such as trinitrotoluene form a group of chemicals of considerable interest for environmental and analytical chemistry [1]. Moreover the detection of explosives is a topic of increasing interest [2].
Nitro compounds contain one or more nitro (NO_2) functional groups; thus they possess very pronounced electron-acceptor properties due to the low energy of the lowest unoccupied (π^*) orbital of the NO_2 group. Therefore, the interaction between low-energy electrons with nitro derivates was a subject of many studies [3,4,5,6]. Havey et al. [7] demonstrated by measuring the NO_2^- resonance energies for 25 different nitro aromatic compounds including several isomeric species that it is possible to distinguish structural isomers of nitro compounds.

Experimental setup

The apparatus used for the measurements is a crossed electron/molecule beams-instrument consisting of a neutral molecular beam source, hemispherical electron monochromator and a quadrupole mass spectrometer [8]. As a molecular beam source we use a Knudsen type oven. Through a capillary with the diameter of 1 mm the gaseous molecules effuse directly into the collision chamber of the hemispherical electron monochromator, where the interaction with the monochromatized electron beam occurs. Negative ions formed are extracted into a quadrupole mass spectrometer. The mass selected anions are finally detected by a channel electron multiplier.

Results and discussion

In our experiments with explosives, we observed for all explosives measured so far the two opposite reactions

$$A + e^- \rightarrow (A\text{-}NO_2)^- + NO_2 \quad (1)$$

and

$$A + e^- \rightarrow (A\text{-}NO_2) + NO_2^-, \quad (2)$$

respectively.
Here we present the differences in the resonance energies for the reaction 2 (formation of NO_2^-), for two explosives, namely trinitrotoluene (TNT) and pentaerythritol tetranitrate (PETN), figure 1. In this graph a clear difference in the ratio of the 0 eV peak to the

resonances at higher electron energies can be seen. Additionally the high-energy part of the anion efficiency curve for PETN is normalized to the curve of TNT at the resonance close to 6 eV, for better comparison.

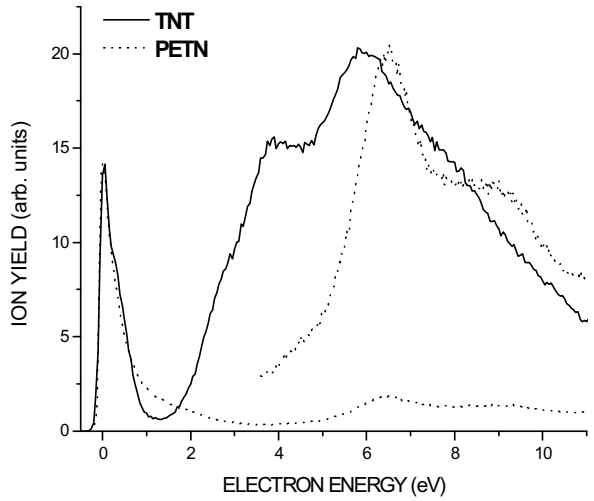

Furthermore, the same reaction process, i.e., NO_2^- formation is compared for TNT and musk xylene and musk ketone. The latter two molecules have a similar structure as TNT, but they exhibit no explosives character. Both ingredients are commonly used in perfumes. Finally we demonstrate that dissociative electron attachment is a powerful tool to distinguish between isomeric forms of various nitroaromatic compounds, such as dinitrobenzene and nitrotoluene (DNB) [9,10].

Acknowledgements

This work has been supported by the FWF, Wien, Austria, the European Commission, Brussels and the Dstl Detection Department (British Ministry of Defense).

References

[1] J. Yinon, and S. Zitrin, In *Modern Methods and Applications in Analysis of Explosives*; Wiley: New York, 1996.
[2] J. Yinon, Anal. Chem. **75**, 99A-105A (2003)
[3] W. Sailer, A. Pelc, S. Matejcik, E. Illenberger, P. Scheier and T.D. Märk, J. Chem. Phys. **117**, 7989-7994 (2002)
[4] A. Pelc, W. Sailer, S. Matejcik, P. Scheier and T.D. Märk, J. Chem. Phys. **119**, 7887-7892 (2003).
[5] A. Modellil and M. Venuti, Int. J. Mass Spectrom. **205,** l 7-16 (2001)
[6] J.A. Laramee, C.A. Kocher and M.L. Deinzer Anal. Chem. **64**, 2316-2322 (1992)

[7] C.D. Havey, M. Eberhart, T. Jones, K.J. Voorhees, L.A. Laramee, R.B. Codey and D.P. Clougherty, J. Phys. Chem. A **110**, 4413-4418 (2006)
[8] S. Denifl, S. Ptasinska, M. Cingel, S. Matejcik, P. Scheier and T. D. Märk, Chem. Phys. Lett. **377**, 74 (2003).
[9] P. Sulzer, A. Mauracher, S. Denifl, M. Probst, T.D. Märk, P. Scheier and E. Illenberger, Int. J. Mass Spectrom. **266**, 138–148 (2007)
[10] P. Sulzer, A. Mauracher, S. Denifl, F. Zappa, S. Ptasinska, M. Beikircher, A. Bacher, N. Wendt, A. Aleem, F. Rondino, S. Matejcik, M. Probst, T. D. Märk, P. Scheier, Anal. Chem. **79**, 6585-6591 (2007)

Fundamental and first overtone spectra of the CH-stretching vibration of $^{12}C_6HD_5$ and of $^{13}C^{12}C_5HD_5$ measured by the ISOS method

Eduard Miloglyadov, Martin Quack and Georg Seyfang
Physical Chemstry, ETH-Zurich,CH-8093 Zurich/Switzerland

Abstract

We report the spectrum and the vibrational analysis of the fundamental and first overtone of the CH-stretching vibration of rotationally cooled pentadeuterated benzene $^{12}C_6HD_5$ and several isotope-isomers of $^{13}C^{12}C_5HD_5$ measured by isotope selective overtone spectroscopy (ISOS). Using the results from ab initio calculations and earlier vibrational assignments, based on symmetry considerations and rules for isotopic substitution [1-3], the spectral positions of some of the combination bands in the measured spectral ranges have been identified. ^{13}C substituted C_6HD_5 has 4 different isotope-isomers, defined by the position of the ^{13}C atom relatively to the CH-bond. Ab initio calculations and experimental results show that only the isomer with the ^{13}CH-chromophore shows a significant frequency shift of about 22.1 cm^{-1} for the overtone of the CH-stretching vibration, relatively to the other isomers.

1. Introduction

Because of its high symmetry and special electronic structure benzene has been studied for many years, experimentally and theoretically [1-4]. The analysis of high resolution overtone spectra can provide insight into the intramolecular vibrational energy redistribution (IVR) in benzene and its deuterated species [4-11]. The analysis of the IR-spectra and the determination of vibrational couplings can be considered as complementary to time resolved methods which provide a direct observation of the IVR processes [12, 13]. The present investigation is based on earlier ISOS experiments [14] where the shift of the first overtone of the CH-stretching vibration in $^{13}CC_5H_6$ relative to C_6H_6 was investigated. To reduce the number of strongly coupled states and to simplify the spectrum we have chosen the pentadeuterated benzene C_6HD_5. It has a lower C_{2v}-symmetry as compared to the D_{6h}-symmetry for C_6H_6 and only one "localized" CH-stretching vibration. Measurements of ^{13}C-isotope shifts are also useful for the determination of an accurate force-field for benzene. It is also interesting to study the effect of the changes in mass and in part reduced symmetry in $^{13}C^{12}C_5HD_5$ on IVR, as the shift of vibrational states in $^{13}C^{12}C_5HD_5$ relative to the ones in $^{12}C_6HD_5$ will affect Fermi and other anharmonic resonances. We present the spectra of the fundamental and first overtone of the CH-stretching vibration of rotationally cooled C_6HD_5 and the isotope-isomers of $^{13}C^{12}C_5HD_5$, measured by the method of isotope selective overtone spectroscopy (ISOS).

2. Experimental setup [14]

To measure the NIR spectra we used infrared excitation combined with detection by the REMPI method with the advantage of isotope selectivity provided by a time-of-flight mass-spectrometer (TOF, Kaesdorf, Munich). The mass resolution of the ion spectra allowed us to separate isotope substituted ions from the main ion species. The third harmonic of an injection seeded, pulsed Nd:YAG laser (Spectra-Physics PRO 270-10, 10Hz repetition rate, 7 ns pulse length) pumps a dye laser (Lambda Physics SCANMATE OPPO) combined with a two step

optical parametric amplifier (OPA). The first OPA stage was used for the excitation of the first overtone of the CH-stretching vibration around 6000 cm^{-1}, the second OPA was used for the excitation of the fundamental of the CH-stretching vibrations around 3000 cm^{-1} with a laser linewidth of about 0.15 cm^{-1} in both spectral regions. The ionization of the benzene molecules was accomplished with UV light pulses from a frequency doubled dye laser (Lumonics Hyperdye-500), pumped by the third harmonic of the same Nd:YAG laser. The UV laser linewidth was about 0.4-0.7 cm^{-1}. Both laser beams (IR and UV) were focused by f = 30 cm lenses and overlapped in the vacuum chamber of the TOF mass-spectrometer from opposite directions in the center of a skimmed molecular beam, perpendicular to its direction of propagation. The rotational temperature of the benzene molecules in the molecular beam was estimated from the rotational band envelope to be about 3-5 K. After vibrational excitation the molecules are ionized in a two photon absorption process by the UV light, through a vibronic level in the S_1 electronic state of the molecule as an intermediate level. The ions of the different isotopomers are separated in the TOF and detected by a multichannel plate (MCP). The absorbance of the molecules during the scanning of the NIR (IR) wavelength is monitored by the change of the ion yield of the REMPI process. The NIR (IR) spectra were calibrated by methane absorption lines, measured in a photoacoustic cell in parallel.

3. Results and Discussion

The molecular beam spectrum of the CH-stretching fundamental for C_6HD_5 is presented in fig. 1. The width of the fundamental band is narrowed from 20 cm^{-1} at room temperature to ~2.4 cm^{-1} in the molecular beam with a rotational temperature of T ≅ 3 K. From the cold spectra the center of the CH stretching band is determined at 3061.6 ± 0.2 cm^{-1}. The spectra do not show additional intense peaks. To see the weak absorption lines we extended the intensity scale by a factor of 60 as shown in fig.1. At least 9 weak bands are observed in the range from 2850 to 3200cm^{-1}. For the assignment of the bands symmetry rules for intramolecular coupling would suggest to consider only combination bands with A_1-symmetry. We estimated 21 different vibrational frequencies with A_1-symmetry in the measured range around 3000 cm^{-1} including only excitation with 2 quanta. But for weak absorption bands all symmetries have to be considered. The total number of "two quanta" states of A_1- B_1- B_2- symmetry is about 60. According to [2, 3], the peak at 2953.1cm^{-1} can be assigned to $\nu_{13b}+\nu_{16a}$ (2950 cm^{-1}, Herzberg notation) with B_1-symmetry (B_1) because of the B-type structure of the band shape of the room temperature spectrum. The weaker band at 2963.3cm^{-1} fits well with the estimated position of $\nu_{13b}+\nu_{16b}$ (2968cm^{-1}, A_1). The combination band $\nu_{12b} + \nu_{18b}$ (2873 cm^{-1}, A_1) is a good candidate for a band centered at 2867.5 cm^{-1} having the same symmetry according to the low resolution absorption spectrum taken at room temperature. Nevertheless the combinations $\nu_5+\nu_{18a}$ (2863 cm^{-1}, A_1) and $\nu_{12b}+\nu_{18a}$ (2863 cm^{-1}, B_1) and $\nu_5+\nu_{18b}$ (2873 cm^{-1}, B_1) have to be taken in consideration too. The absorption band at 3141.5 cm^{-1} fits well with the positions of $2\nu_{16b}$ (3152 cm^{-1}, A_1), as well as the combination $\nu_{12a}+\nu_{14b}$ expected at 3141 cm^{-1}(B_1). For the bands around 3100 cm^{-1} we have to consider the 4 closest two quanta combinations: $\nu_{10}+\nu_{12b}$ (3107cm^{-1}, A_1), $\nu_{12b}+\nu_{14a}$ (3102cm^{-1}, B_1), $\nu_5+\nu_{14a}$ (3102cm^{-1}, A_1), $\nu_{14b}+\nu_{15a}$ (3107cm^{-1}, B_1).

The spectrum of the first overtone of the CH-stretching vibration for C_6HD_5 is presented in fig.2. The main band responsible for the first overtone of the CH-stretching vibration is centered at 5975 cm^{-1} and has a width of about 35cm^{-1} at room temperature. At a rotational temperature T ≅ 3 K it is split into two peaks: one at 5973±0.2 cm^{-1} with a width of about 6 cm^{-1} and one at 5982.9±0.2 cm^{-1} with an intensity of about 60% of the intensity of the main peak. Together with the band at 6049 cm^{-1} (about 50% of intensity of the main peak) these three bands form a triad resulting presumably from strongly coupled states. The weak band at 5847.5 cm^{-1} in the room temperature spectra is resolved into three bands at 5841, 5850.3 and 5859.1 cm^{-1} in the molecular beam spectrum. There are also a number of additional weak bands in the spectrum.

To find possible candidates for the assignment we might consider the "3 quantum combinations bands" with an excitation energy in the measured spectral range from 5750 to 6100 cm^{-1}. There are 11 such states of A_1-symmetry with one quantum of CH-stretching in the range of the measurement. The main candidates for the assignment are $\nu_1+2\nu_{16b}$ (5946cm^{-1}) for one of the bands (5841, 5850.3 and 5859.1 cm^{-1}), $\nu_1+\nu_{13b}+\nu_{16b}$ (5968cm^{-1}) and $\nu_1+\nu_{13a}+\nu_{16a}$ (6024 cm^{-1}) for the bands at 5982.9 cm^{-1} and 6049 cm^{-1} respectively.

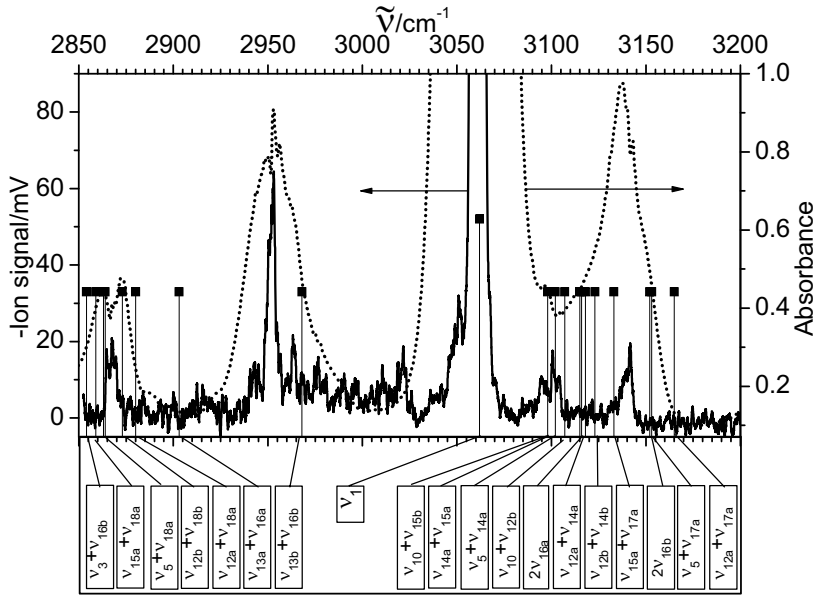

Fig.1 Molecular beam spectra of the fundamental CH-stretching vibration of C_6HD_5 with enhanced scale (—). The FTIR spectrum of C_6HD_5 measured with instrumental resolution 0.25 cm^{-1} (……) (p = 10kPa, L = 20cm^{-1} scale to the right). The stick spectrum shows the positions of the combination bands of A_1-symmetry, neglecting anharmonic corrections.

There are 4 distinguishable isotope-isomers of C_6HD_5 with one ^{13}C atom and all of them have to be present in the spectrum of the natural mixture. The only isomer that is expected to have a noticeable CH-stretching shift with respect to the others is the one with the ^{13}CH chromophore and the rough overall spectrum without resonances would consist of two bands with an expected intensity ratio of approximately 1:5. The relative isotopic shift of all ^{13}C substituted isomers of pentadeuterated benzene can be estimated using quantum chemical calculations. The harmonic frequencies for C_6HD_5 and all its isotope-isomers with one ^{13}C were calculated with ab initio methods with full optimization at the MP2/aug-cc-pVTZ basis set using Møller-Plesset perturbation theory [15]. The calculations show that only one harmonic frequency is shifted significantly: the frequency of the isomer with the ^{13}CH chromophore. It has an isotope shift of about –10.2 cm^{-1} relatively to the other isomers for the fundamental vibration and a frequency shift of around -20 cm^{-1} may be expected for the first overtone, neglecting the influence of vibrational couplings. The overtone spectrum of C_6HD_5

substituted with one ^{13}C atom (fig. 2) is presented together with the spectrum of $^{12}C_6HD_5$. If we assume that the intensity of the transitions is given by the relative abundance of the isomers we can identify the two relevant peaks in the spectra: the main peak at 5970.5 cm^{-1} and one at 5948.2 cm^{-1}(**), separated by 22.3 cm^{-1}. The third peak at 5960.2 cm^{-1}(*) may correspond to the strongly shifted coupled state which is found for C_6D_5H at 5982.9 cm^{-1}.

Acknowledgment

Our work was financially supported by the Schweizerischer Nationalfonds. We thank Michael Hippler, Lubosh Horny and Andreas Schneider for help and discussion.

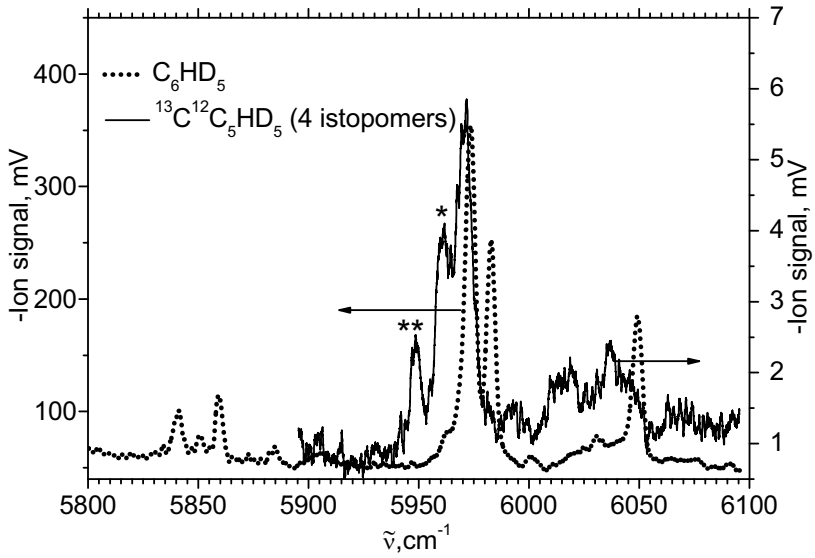

Figure 2. Molecular beam spectra of the first overtone of the CH-stretching vibration for $^{12}C_6HD_5$ (·····) and $^{13}C^{12}C_5HD_5$(—). The spectrum of the ^{13}C-isotopomers is scaled by a factor 60. The expected wavenumber shift of 22.3 cm^{-1}(**) for the isomer with the ^{13}CH-chromophore with respect to the other ^{13}C-isotope-isomers is indicated. The peak shifted by 10.3 cm^{-1}(*) is assumed to result from a not yet identified resonant level.

[1] E.B. Wilson, Phys. Rev. **45**, 706(1934); **46**, 146(1934)
[2] S. Brodersen, A.Langseth, Mat. Fys. Scr. Dan. Vid. Selsk. **1** (1959)
[3] S. N. Thakur, L. Goodman, A. G. Ozkabar, J. Phys. Chem. **84**, 6642 (1986)
[4] K.V. Reddy, D. F. Heller, M. J. Berry, J. Chem. Phys. **76**, 2814 (1982)
[5] M.Quack. Molecular femtosecond quantum dynamics between less than yoctoseconds and more than days: experiment and theory. Chapter 27 in 'Femtosecond Chemistry', J. Manz and L. Woeste editors, Verlag Chemie (Weinheim), p. 781 (1995)
[6] R.H. Page, Y.R. Shen, and Y.T. Lee, J. Chem Phys. **88**, 5362 (1988)
[7] A. Callegari, H. K. Srivastava, U. Merker, K. K. Lehmann, G. Scoles, M. J. Davis, J. Chem. Phys. **106**, 432 (1997)
[8] S. Shi, W.H. Miller, Teor. Chim. Acta **68**, 1 (1985)
[9] Y.F. Zhang, S.J. Klippenstein, R.A. Marcus, J. Chem. Phys. **94**, 7319 (1991)
[10] E.L. Sibert III, W.P. Reinhardt, J.T. Hynes, J. Chem. Phys. **81**, 1115 (1984)
[11] S. Rashev, M. Stamova, S. Djambova, J. Chem. Phys. **108**, 4797 (1998)
[12] V.N. Krylov, M. V. Nikitshenko, M. Quack, G. Seyfang, SPIE Proc. **5337**, 178 (2004)
[13] V. Krylov, A. Kushnarenko, E. Miloglyadov, M. Quack, and G. Seyfang, SPIE Proc. **6460,** 64601D-1 (2007)
[14] M. Hippler, R. Pfab, M. Quack, J. Phys. Chem. A **107**, 10743 (2003)
[15] L. Horny, E. Miloglyadov, M.Quack, G. Seyfang in preparation.

Photoionisation of compound clusters formed in helium nanodroplets

S. Müller, G. Droppelmann, M. Mudrich, F. Stienkemeier

Physikalisches Institut, Universität Freiburg, Hermann-Herder-Str. 3, D-79104 Freiburg, Germany, email: mudrich@physik.uni-freiburg.de

Helium nanodroplets offer the opportunity to explore chemical reactivity at very low temperatures [1]. In particular, helium droplets are the ideal medium for studying the ultracold chemistry of metal clusters [2]. In this contribution we present a systematic study of the stability of compound clusters formed in helium nanodroplets out of alkali metal clusters and water, ammonia and iodine clusters. High-resolution mass spectra are recorded using both femtosecond photoionisation (PI) as well as electron impact ionization. Characteristic stability patterns are identified and the role of the helium droplet environment on the product distributions is discussed. As an example, the full mass spectrum of photoionized cesium-water product clusters is depicted in Fig. 1a. Fig. 1b shows a detailed view of the various combinations of Cs_5 and O, OH, H_2O molecules. By recording multi-photon PI spectra at fixed A_N cluster masses (A stands for an alkali atom) we can distinguish between reactive processes of the neutral clusters at 0.4 K and ionic reactions occurring after ionisation of the alkali cluster component. Moreover, information about the amount of fragmentation into smaller cluster fragments is obtained from PI spectra. These studies pave the way to time-resolved reaction dynamics at very low temperatures.

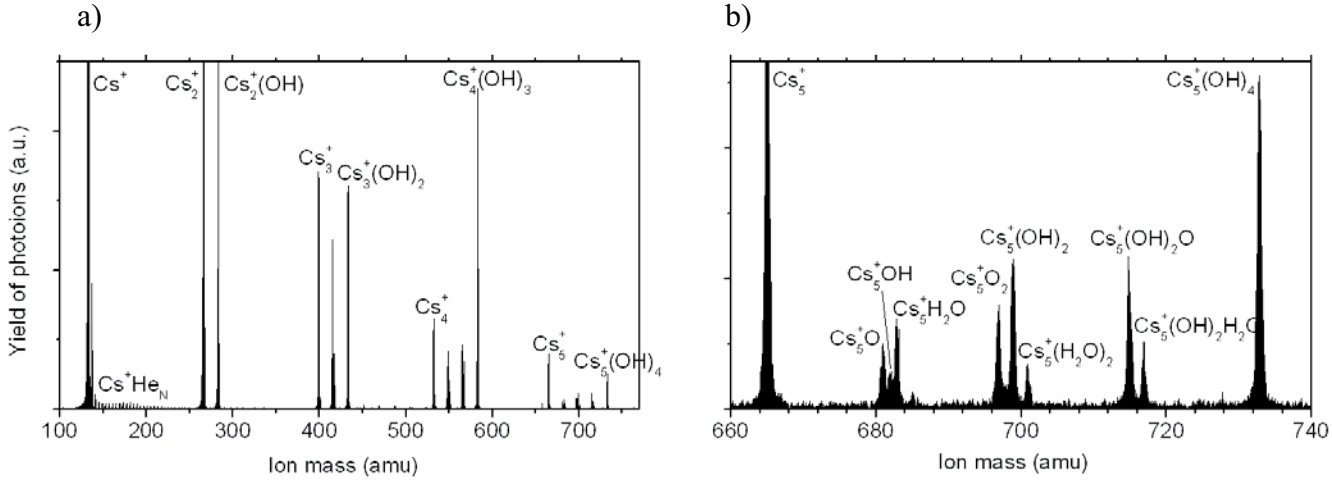

Fig.1: a) Mass spectrum of photoionized cesium-water compound clusters formed in helium nanodroplets; b) Detailed view of the mass range close to the mass of Cs_5.

[1] J.P. Toennies and A. T. Vilesov, Angewandte Chemie **43**, 2622 (2004)
[2] Tiggesbäumker J., Stienkemeier F., PCCP **9** (34), 4748-4770 (2007).

Gas phase synthesis of organo-rare gas compounds via ion-molecule reactions

Jana Roithová, Detlef Schröder
Institute of Organic Chemistry and Biochemistry, Academy of Sciences of the Czech Republic, Flemingovo nám. 2, 16610 Praha 6, Czech Republic

Daniela Ascenzi, Paolo Tosi
Department of Physics, University of Trento, Via Sommarive 14- 38050 Povo, Trento, Italy

Ever since their discovery in 1962 [1], rare-gas compounds constitute a challenging area of research. In addition to their fundamental relevance for understanding the concepts of bonding, rare-gas compounds show several interesting properties for a variety of applications (e.g. in laser and plasma processes, chemical etching etc.).

From only few examples in the beginning, meanwhile hundreds of rare-gas compounds have been synthesized [2], making use of strong oxidizing agents (*e.g.* F_2). For this reason, most rare-gas compounds known so far have bonds to the most electronegative elements (F, O and derivatives thereof). For the heavier rare gases xenon and krypton, however, also compounds with a variety of other elements are known, including those with covalent bonds to C atoms, e.g. $C_6F_5Xe^+$ salts [3], $KrCH_3^+$ ions observed in mass-spectrometric experiments [4] and HKrCN synthesized in low-temperature matrices [5].

A particularly interesting class of compounds of recent synthesis are organo-noble gas molecules prepared from acetylene, diacetylene and benzene such as HXeCCH [6-8], HXeCC [7], HXeCCXeH [7], HKrCCH [9], $HXeC_4H$ [10], $HKrC_4H$ [10] and $HXeC_6H_5$ [11]. HXeCCH was first predicted computationally by Lundell along with other large organic molecules such as Xe insertion compounds of benzene and phenol [12], and quite recently Sheng and Gerber proposed various carbon chain oligomers containing rare gas atoms [13, 14].

In the past we have discovered several new ion-molecule reactions which lead to the formation of hitherto unknown rare-gas compound such as the argon-nitride cation ArN^+ starting from the two symmetric charge-state reactants $Ar^+ + N_2$ and $N_2^+ + Ar$ [15]. We have also shown that the reaction of Ar^{2+} dications with N_2 and O_2 molecules can be used to generate the argon-nitride dication ArN^{2+} [16] and the argon-oxide ions ArO^+ and ArO^{2+} [17] respectively. Of particular interest was the production of argon-carbide dications ArC^{2+} either in the endothermic reaction of argon with CO^{2+} [18] and in the reaction of Ar^{2+} dications with CO [19].

In this communication we present results on the synthesis of new carbon-containing rare gas ions via bimolecular reactions of rare gas atoms with mass selected organic dications in a tandem mass spectrometer equipped with radiofrequency octopole for guiding and trapping of ionic products. Theoretical calculations of stability and structures of the organo-rare gas cations fully support the experimental findings.

References:

[1] N. Bartlett, *Proc. Chem. Soc.* , London **218** (1962).
[2] For an excellent review of rare-gas compounds, see: Grochala, W. *Chem. Soc. Rev.* **36**, 1632 (2007).
[3] D. Naumann, W. Tyrra, *J. Chem. Soc., Chem. Commun.* **47** (1989); H. J. Frohn, S. Jakobs *J. Chem. Soc., Chem. Commun.* **625** (1989).
[4] J. K. Hovey, T. B. McMahon, *J. Phys. Chem.* **91**, 4560 (1987).
[5] J. Lundell, L. Khriachtchev, M. Pettersson, M. Räsänen, *Fiz. Nizk. Temp*. **26,** 923 (2000); *Low Temp. Phys.* **26,** 680 (2000).
[6] H. Tanskanen, L. Khriachtchev, J. Lundell, M. Räsänen, *J. Chem. Phys.* **125** 074501 (2006).
[7] L. Khriachtchev, H. Tanskanen, J. Lundell, M. Pettersson, H. Kiljunen, M. Räsänen *J. Am. Chem. Soc.* **125** 4696 (2003).
[8] V.I. Feldman, F.F. Sukhov, A.Y. Orlov, I.V. Tyulpina *J. Am. Chem. Soc.* **125** 4698 (2003).
[9] L. Khriachtchev, H. Tanskanen, A. Cohen, R.B. Gerber, J. Lundell, M. Pettersson, H. Kiljunen, M. Räsänen *J. Am. Chem. Soc.* **125** 6876 (2003).
[10] H. Tanskanen, L. Khriachtchev, J. Lundell, H. Kiljunen, M. Räsänen *J. Am. Chem. Soc.* **125** 16361 (2003).
[11] V.I. Feldman, F.F. Sukhov, E.A. Logacheva, A.Y. Orlov, I.V. Tyulpina, D.A. Tyurin *Chem. Phys. Lett.* **437** 207 (2007).
[12] J. Lundell, A. Cohen, R.B. Gerber *J. Phys. Chem. A* **106** 11950 (2002).
[13] L. Sheng, R.B. Gerber *J. Chem. Phys.* **124** 231103 (2006); **125** 201101; **126** 021108 (2007)
[14] L. Sheng, A. Cohen, R.B. Gerber *J. Am. Chem. Soc.* **128** 7156 (2006).
[15] P. Tosi, R. Correale, WY. Lu, D.Bassi *J. Chem. Phys.* **110** 4276 (1999).
[16] P. Tosi, R. Correale, WY. Lu, S. Falcinelli, D. Bassi *Phys. Rev. Lett.* **82** 450 (1999).
[17] D. Ascenzi, P. Franceschi, P. Tosi, D. Bassi, M. Kaczorowska, JN. Harvey *J. Chem. Phys.* **118** 2159 (2003).
[18] WY. Lu, P. Tosi, D. Bassi *J. Chem. Phys.* **112** 4648 (2000).
[19] P. Tosi, WY. Lu, R. Correale, D. Bassi *Chem. Phys. Lett.* **310** 18 (1999).

Global Analysis of $^{13}CH_4$ Lines in the 0–3200 cm^{-1} Region

H. M. Niederer[1], S. Albert[1], S. Bauerecker[1,2], V. Boudon[3], J. P. Champion[3] and M. Quack[1]

[1]*Laboratorium für Physikalische Chemie, ETH Zürich, CH-8093 Zürich, Switzerland*

[2]*Institut für Physikalische und Theoretische Chemie, Technische Universität Braunschweig, D-38106 Braunschweig, Germany*

[3]*Institut Carnot de Bourgogne, Université de Bourgogne, F-21078 Dijon, France*

Abstract

We report new data on the infrared spectrum of $^{13}CH_4$ in the range 0–3200 cm^{-1} at very high resolution as well as a preliminary analysis.

1 Introduction

There has been renewed interest in the spectroscopy of methane and its isotopomers because of new developments in high resolution spectroscopy. We may mention as examples the studies of intramolecular vibrational redistribution [1, 2] or nuclear spin symmetry conservation in supersonic jet expansions [3, 4]. Also pulsed supersonic jet spectrometry using a newly developed high resolution cw-laser cavity ring down spectrometer has been recently applied to methane overtone spectroscopy [4, 5]. Furthermore, methane, a relatively abundant constituent of planetary atmospheres, has recently been observed in detail on one of the Cassini/Huygens' space mission primary targets — Titan [6]. Saturn's largest moon shows several strong CH_4 absorption regions. Even though $^{13}CH_4$ is much less abundant it is well observed on Titan and other planetary and interstellar objects. The ratio $^{13}C/^{12}C$ is important since it sheds light on the formation process of methane and consequently allows conclusions about its origin. Recent work on constructing accurate potential hypersurfaces for polyatomic molecules using the methane molecule as an important prototype [7–9] gave new motivation for reinvestigating the spectrum of methane. The aims of the present work situate themselves in the realm of these new developments. As a part of our ongoing project to investigate the low temperature spectra of methane we have recorded new infrared spectra of methane and its isotopomers. $^{12}CH_4$ [10], $^{12}CH_3D$ [11], $^{12}CH_2D_2$ [12], $^{12}CHD_3$ [11], $^{13}CH_4$ [13] and $^{12}CD_4$ [14].

2 Experimental Details

The measurements have been carried out using the Zürich prototype Bruker 125 spectrometer (ZP 2001) [15] combined with an enclosive cooling cell [16, 17], which provides a very powerful FTIR system. Complex infrared spectra can be simplified by cooling the sample gas. Hot bands appear attenuated and complex polyad patterns may be more easily analyzed. The widths of the rotation-vibration bands decrease approximately proportionally with temperature. In addition, the Doppler width of a single spectral line of the molecules roughly narrows with the square root of the temperature cf. Figure 1.

3 Results and Discussion

Like all XY_4 tetrahedral molecules, methane has four normal modes of vibration. They can be labeled by irreducible representations of the T_d point group, according to the symmetry of the associated normal coordinates. We have thus: $\nu_1(A_1)$, $\nu_3(F_2)$ (stretching modes), $\nu_2(E)$ and $\nu_4(F_2)$ (bending modes). $\nu_1(A_1)$ is a non-degenerate oscillator, while $\nu_2(E)$ is doubly degenerate and $\nu_3(F_2)$ and $\nu_4(F_2)$ are triply degenerate. The fundamental frequencies exhibit a simple approximate relation: $\nu_1(A_1) \simeq \nu_3(F_2) \simeq 2\nu_2(E) \simeq 2\nu_4(F_2)$. This leads to a well-defined polyad structure with each polyad P_n defined by the integer $n = 2\,(v_1 + v_3) + v_2 + v_4$. Then each set of (v_1, v_2, v_3, v_4), where the $v_i = 0, 1, 2, \ldots$ ($i = 1$ to 4) are the vibrational quantum numbers, defines a *vibrational level* that belongs to a unique polyad P_n. Figure 1 shows schematically the first five polyads of $^{13}CH_4$.

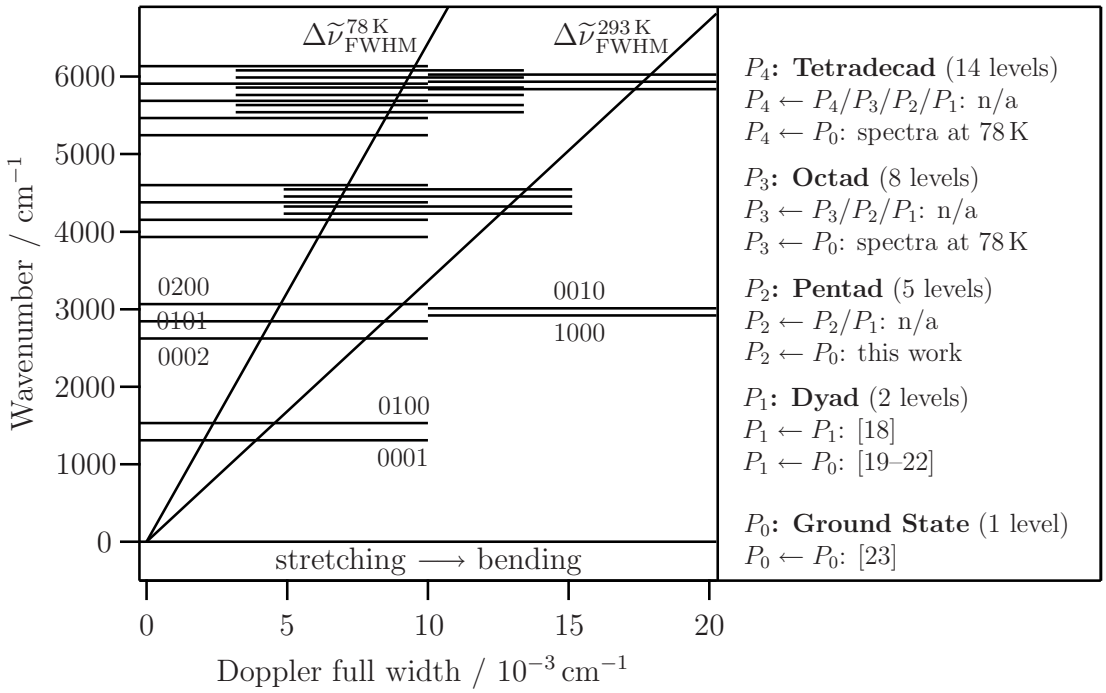

Figure 1: *The polyad scheme of $^{13}CH_4$. The vibrational levels on the left are positioned according to their stretching and bending character. Wavenumbers of the fundamental levels 1000, 0100, 0001, 0100 are due to this work. We also indicate by straight line diagonals $\Delta\widetilde{\nu}^{T}_{FWHM}$ the Doppler full widths at half maximum in the 0-6500 cm^{-1} region at 78 K and 293 K. On the right, references of the data used for this work and the current availability of experimental data are summarized. Experimental data of the hot bands and polyad internal transitions are either not available (n/a) or only so to limited extent.*

The complex interacting system has been analyzed using an effective Hamiltonian theory [24], implemented in the the STDS software package [25]. Using all the available data cited in Figure 1, a total of 4126 calibrated experimental line positions (2091 newly assigned) were included in the non-linear least-squares fit, minimizing the standard deviation. In

this work we eventually reproduced the line positions with a global standard deviation of $\sigma = 0.635$. Hence the average absolute differences of experimental and calculated wavenumbers are about half the experimental uncertainty i.e. we are able to reproduce the experimental line positions very accurately with a global rms deviation of $d_{\mathrm{rms}} = 0.000465\,\mathrm{cm}^{-1}$. Compared to the preliminary analysis of the Pentad of $^{13}CH_4$ by Jouvard *et al* [19] we gain about a factor of 2 in accuracy. Further work will include more weak line positions in the intense regions of the dyad and pentad system by using the present results to extract such weak lines from the experimental spectra, and then re-inject them into the fit. It should also be possible to investigate hot bands. The results represent a significant improvement compared to previous studies. The Hamiltonian parameters should be sufficiently reliable to allow a serious analysis of the next polyad, namely the octad. They would also certainly be very useful to improve the knowledge of methane's potential energy hypersurfaces. It would also be interesting to check how these new results affect recent planetary investigations in the pentad region. We also plan to analyze in some detail the intensities or integrated absorption cross sections. Such information will be useful in relation to electric dipole moment hypersurfaces [7–9]. Intensities are also of obvious importance for astrophysical applications and in particular for the understanding of planetary spectra.

Acknowledgements

Sincere thanks are given to the Université de Bourgogne for co-financing study visits. Our work is supported financially by ETH Zürich and the Swiss National Science Foundation.

[1] M. Lewerenz and M. Quack, *J. Chem. Phys.*, **88**, 5408 (1988).

[2] M. Quack, *Ann. Rev. Phys. Chem.*, **41**, 839 (1990).

[3] A. Amrein, M. Quack and U. Schmitt, *J. Phys. Chem.*, **192**, 5455 (1988).

[4] M. Hippler and M. Quack, *J. Chem. Phys.*, **116**, 6045 (2002).

[5] M. Quack, *Chimia*, **57**, 147 (2003).

[6] A. Coustenis, A. Negrao, A. Salama, B. Schulz, E. Lellouch, P. Rannou, P. Drossart, T. Encrenaz, B. Schmitt, V. Boudon, and A. Nikitin, *ICARUS*, **180**, 176 (2006).

[7] R. Marquardt and M. Quack, *J. Phys. Chem. A*, **108**, 3166 (2004).

[8] R. Marquardt and M. Quack, *J. Chem. Phys.*, **109**, 10628 (1998).

[9] H. Hollenstein, R. Marquardt, M. Quack, and M. A. Suhm, *J. Chem. Phys.*, **101**, 3588 (1994).

[10] A. Nikitin, V. Boudon, J. P. Champion, S. Albert, S. Bauerecker, M. Quack and L. R. Brown, 61st International Symposium on Molecular Spectroscopy, Columbus, Ohio, USA, June 19-23, Talk RC11 (2006).

[11] E. S. Bekthereva, O. N. Ulenikov, E. A.Sinitsin, S. Albert, S. Bauerecker, H. Hollenstein and M. Quack,20th Colloquium on High-Resolution Spectroscopy, Dijon, France,posterJ30/p127 (2007).

[12] E. S. Bekthereva, O. N. Ulenikov, S. Albert, S. Bauerecker, H. Hollenstein and M. Quack, 20th Colloquium on High-Resolution Spectroscopy, Dijon, France, poster L7/p126 (2007).

[13] H. M. Niederer, S. Albert, S. Bauerecker, V. Boudon, J. P. Champion and M. Quack, *Chimia*, **61**, 516 (2007).

[14] O. Ouardi, S. Albert, H. M. Niederer, M. Quack and V. Boudon, 20th Colloquium on High-Resolution Spectroscopy, Dijon, France, poster M1/p108 (2007).

[15] S. Albert, K. K. Albert and M. Quack, *Trends in Optics and Photonics*, **84**, 177 (2003).

[16] S. Albert, S. Bauerecker, M. Quack and A. Steinlin, *Mol. Phys.*, **105**, 541 (2007).

[17] S. Bauerecker, M. Taraschewski, C. Weitkamp and H. K. Cammenga, *Rev. Sci. Instrum.*, **72**, 3946 (2001).

[18] M. Oldani, A. Bauder, J. C. Hilico, M. Loete, and J. P. Champion *Europhys. Lett.*, **4**, 29 (1987).

[19] J. M. Jouvard, B. Lavorel, J. P. Champion and L. R. Brown, *J. Mol. Spectrosc.*, **150**, 201 (1991).

[20] L. R. Brown, J. S. Margolis, R. H. Norton, and B. D. Stedry. *Appl. Spectrosc.*, **37**, 287 (1983).

[21] J. C. Hilico, M. Loëte, and L. R. Brown, *J. Mol. Spectrosc.*, **111**, 119 (1985).

[22] J. P. Champion, J. C. Hilico, and C. Wenger, *J. Mol. Spectrosc.*, **133**, 256 (1989).

[23] R. Widmer, M. Oldani, and A. Bauder, *J. Mol. Spectrosc.*, **116**, 259 (1986).

[24] J. P. Champion, M. Loëte and G. Pierre in *Spectroscopy of the Earth's Atmosphere and Interstellar Medium,* edited by K. N. Rao and A. Weber, Academic Press, San Diego (1992).

[25] C. Wenger and J. P. Champion, *J. Quant. Spectrosc. Radiat. Transfer*, **59**, 471 (1998).

C-H bond activation at the surface of isolated transition metal clusters

S. Jaberg, B. Pfeffer, G. Niedner-Schatteburg*

Fachbereich Chemie, Technische Universität Kaiserslautern, Germany

We chose to investigate the C-H bond activation of small organic molecules by size selected transition metal clusters at the level of elementary processes and under single collision conditions. As part of an ongoing search we currently focus in the elucidation of Cobalt and Tantalum clusters. Cluster ions of either charge states originate from a standard pulsed laser vaporization source, and they are made to react within the ion trap of a Fourier Transform Ion Cyclotron Resonance (FT-ICR) mass spectrometer.

In general, most of the investigated clusters are found to be highly reactive towards the chosen substrates (ethane, acetonitrile, benzene, toluene, ortho-, meta-, para-xylene, mesitylene) with weak dependencies of the reaction rate on the sizes of the clusters and on their charges. Some general trends, and some particular exceptions prevail, however. For example, only the particular Cobalt cluster anion, Co_{19}^-, refrains to activate acetonitrile, CH_3CN, at all. In this case, intact adsorption takes place instead. Together with the results from previous investigations this is taken as a strong indication for an icosahedral geometry of the cluster. All other cluster sizes (both cations and anions) unconditionally activate and dehydrogenate the acetonitrile substrate. Up to five consecutive reaction steps are observed and fitted to pseudo first order kinetics. The observed products reveal a strong propensity for pairwise dehydrogenation, that is for H_2 elimination. The influence of cluster charge is strong in Tantalum – a reactivity threshold (with CH_3CN) for anions observed – and weak in Cobalt – a mere trend in the size independent total reactivity prevailing.

With benzene, Tantalum clusters react very much like those of Niobium and of Vanadium. Total dehydrogenation takes place in general. A few "exceptional" cluster sizes (here: Ta_{12}^+) allow for the intact adsorption of the aromatic substrate, presumably in a half sandwich like η^6 coordination geometry. While such exceptions are outermost puzzling and resist a direct interpretation, we take them as a challenge for the future.

Reactions of alkylated benzenes provide means to refine our understanding of C-H bond activation. In the vast majority of all investigated cases - which are more than 150 combinations of cluster size, cluster charge, and isomeric substrate - neither Tantalum cluster cations nor the anions reveal isomer specific reactivity when reacting with ortho-, meta- or para-xylene. In as much as two (!) cases ($Ta_{17,18}^+ + p\text{-}C_8H_{10}$) it was found that the reaction rate significantly changes with respect to the other xylene isomers.

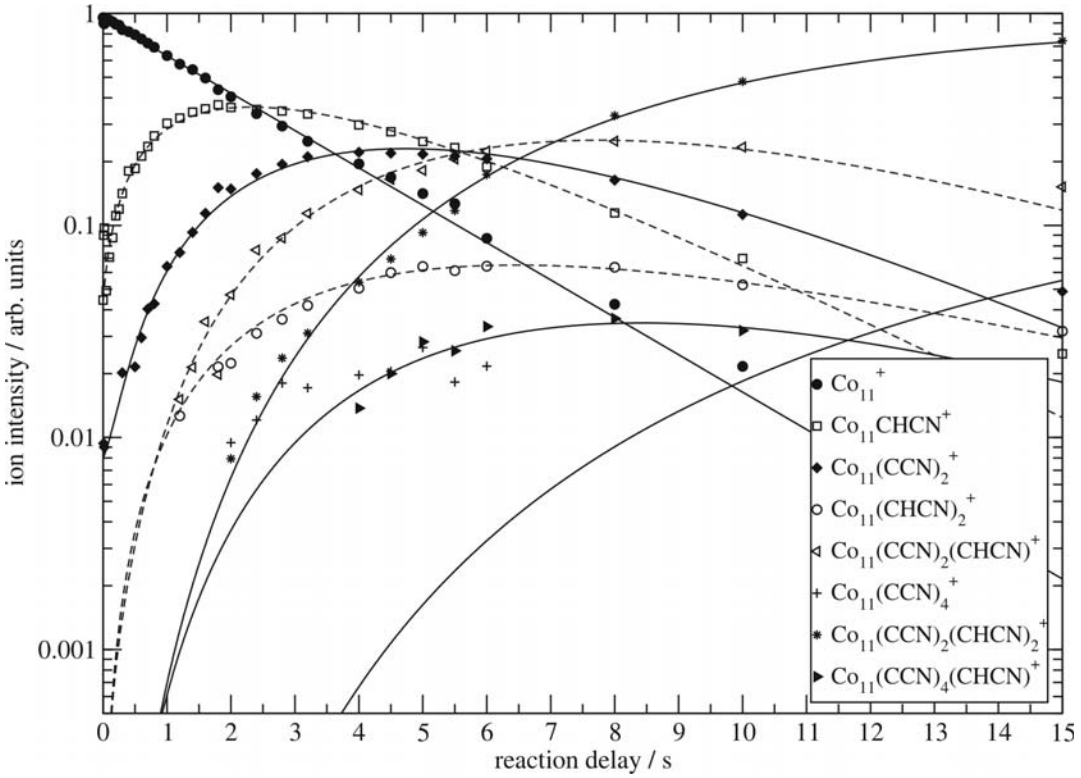

Kinetic data (symbols) for the reaction of Co_{11}^+ with acetonitrile, CH_3CN. Fits (corresponding curves) assume pseudo first order kinetics and stepwise reactions under single collision conditions. The indicated labels provide the sum formulas of the observed ionic products. The step-by-step reaction chain alternatingly comprises of the partial and of the total dehydrogenation of the reacting substrate, with a single (minor) parallel reaction (upright triangles in parallel to diamonds) prevailing. Our interpretation is based on the assumption of H_2 elimination from the cluster substrate complex.

1,3,5-Trimethylbenzene (mesitylene) is readily activated by Tantalum clusters and strongly dehydrogenated, often in total. Only through the small anionic clusters ($n \leq 6$), or by Ta_{13}^-, a second, minor reaction channel opens: One or two carbon atoms seemingly "evaporate" off the cluster substrate complexes. Making use of the particular strength of the FT-ICR-MS investigations – which is the unambiguous identification of products at high mass resolution - we meticulously balanced the hydrogen budget of these reaction channels and came to conclude that either one or two methane molecules have formed and left. The interpretation of this process in terms of consecutive C-H and C-C activation events is underway [1].

Aiming at an enhanced understanding of our current findings in reactivity it is obvious that complementary (spectroscopic) information is needed. We are outermost glad to announce that very first proof of principle experiments succeeded to photo induce the C-H activation of an adsorbed substrate molecule on the surface of a size selected cluster[2]. A corresponding proof of principle is still ahead of us in another, novel setup, the new GAMBIT experiment at BESSY. It is designed to determine spin and orbit contributions to the magnetic moments of isolated transition metal clusters.

[1] S. Jaberg, B. Pfeffer, G. Niedner-Schatteburg, manuscript in preparation
[2] L. Barzen, P. Maitre, G. Niedner-Schatteburg, to be published

Photoionization of alkyl- and alkenyl-peroxy radicals: A general rule for the stability of their cations

D. L. Osborn, G. Meloni, T. M. Selby, and C. A. Taatjes
Combustion Research Facility, Sandia National Laboratories, PO Box 969, Livermore, CA 94551, USA

F. Goulay and S. R. Leone
Chemical Sciences Division, E. O. Lawrence Berkeley National Laboratory, Berkeley, CA 94720, USA; Department of Chemistry and Physics, University of California, Berkeley, CA, 94720, USA

Organic peroxy radicals (e.g., CH_3CH_2OO) are key reaction intermediates in low-temperature oxidation and photooxidation of hydrocarbons in the atmosphere and in combustion. Despite their importance, they have seldom been detected by the very general method of positive-ion mass spectrometry. Using a newly-developed instrument that combines tunable vacuum ultraviolet (VUV) synchrotron radiation with multiple-mass, time-resolved mass spectrometry, we have observed the photoionization of many peroxy radicals.

The peroxy radicals are produced from the reaction of an alkyl (e.g., C_2H_5) or alkenyl (e.g., C_2H_3) radical with molecular oxygen. The kinetics of product formation is used to confirm the origins and assignments of the ionized species. The photoionization efficiency vs. VUV photon energy allows different isomers of a given mass-to-charge ratio to be distinguished. Using this technique, we have made the first measurement of the ionization energy of any peroxy radical: CH_3OO (I.E. = 10.33 ± 0.05 eV).

In general we find that alkyl peroxy cations have triplet ground states that are dissociative (with the exception of CH_3OO^+), whereas 1-alkenyl peroxy cations have singlet ground states that are bound and can be observed as intact parent cations.

The reason for this difference will be discussed, and lies in the nature of the molecular orbitals of the neutral peroxy radical from which an electron is removed. In the alkyl peroxy radicals, hyperconjugation reduces the stability of the alkyl peroxy cations, making the cation ground state weakly bound or unbound with respect to the ground state alkyl cation + O_2. In 1-alkenyl peroxy radicals, where the OO moiety is attached to an sp^2-hybridized carbon, such hyperconjugation effects do not occur, leading to peroxy cations with stable, singlet ground states.

We show that time-resolved mass spectrometry can successfully monitor concentrations of C_2H_5OO and larger peroxy radicals by observation of their dissociative ionization fragments.

Dissociative electron attachment to gas-phase serine. Theoretical study of fragmentation reactions.

P.Papp, J. Kočišek, Š. Matejčík, P. Mach, J. Urban
Department of Experimental Physics,Faculty of Mathematics, Physics and Informatics, Comenius University, Mlynská dolina, Bratislava, Slovakia

Y.V.Vasil'ev
Department of Chemistry, Oregon State University, Corvallis, Oregon, USA

e-mail: papp@neon.dpp.fmph.uniba.sk

Gas phase resonant electron capture (REC) by L-serine was studied at the Corvallis and Bratislava laboratories, using experimental set-ups described elsewhere [1, 2]. In both laboratories, nearly monoenergetic electron beams are generated by trochoidal electron monochromators (TEM) and negative ions that are formed by resonance capture of low energy electrons are analyzed by either a custom-made reflectron orthogonal time-of-flight mass spectrometer (Corvallis) or by a quadrupole mass filter (Bratislava). In both experiments, the compound was introduced into the ionization chamber and heated to around 420 K to vaporize it into the collision region.

Low-energy resonance reactions between free electrons and serine-molecule resulted in more than 15 different fragmentation channels. Similar to other amino acids studied so far [3, 4], $(M-H)^-$ negative ions (m/z 104) were dominant in the REC spectrum of L-serine. In general, REC by serine occurs in three different energy ranges, around 1, 5 and 8 eV that correspond to different formation mechanisms of the resonances. However these reactions leading to ionic products with more than 15 different m/Z and also the possible structures of these products are from experimental research unknown.

We combine our experimental research with the theoretical methods of quantum chemistry, which allow us to predict the structures and energies of the possible products and so the fragmentation reaction schemes and energies. First we start with DFT method (B3LYP [5, 6] functional together with 6-311++G(2df,2pd) one particle basis set), optimizing the geometries of the calculated compounds. The optimal ground state structures of all fragments are then used as inputs for the complex energy computational method G3MP2 [7]. Multiple ab initio calculations are performed within this method including an empirical correction in the final step. As the consequence more reliable results are obtained as on B3LYP level comparing to experiment.

Previous ab initio studies of neutral serine molecule in gas phase resulted in localization of 51 conformers [8], but only a few of them are energetically close. We re-optimized some of these structures (Fig.1) on B3LYP/6-311++G(2df,2pd) and G3MP2 levels of theory. Inclusion of zero point vibrational energy shows that the most stable conformer is formed via weak interaction of the carboxylic hydrogen with the nitrogen of the amino group ($COO-H^{\cdots}N-H_2$), the conformer drawn on Fig.1 in the middle. Other conformers are characterized with weak interaction of the hydrogen from amino group with the carboxylic oxygen ($HN-H^{\cdots}O=COH$), drawn on left and right hand side on Fig.1.

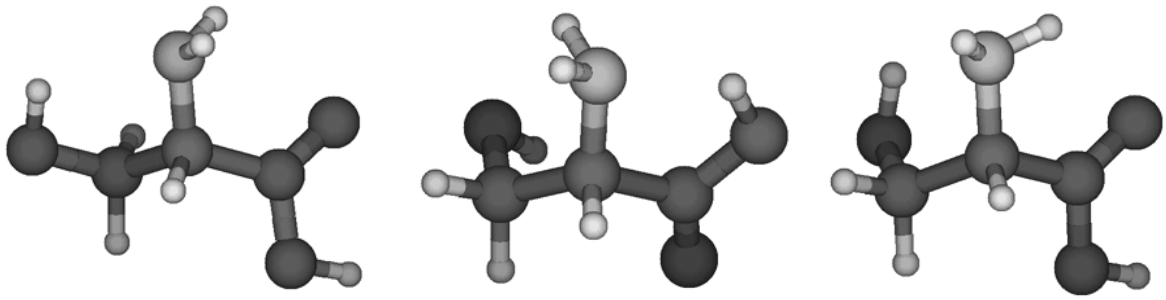

Fig.1: Three energetically lowest conformers of neutral serine amino-acid [7] that were used for modeling the fragmentation reactions to negative ions.

The most abundant species form the spectrum refer to hydrogen cleavage from the carboxylic group, having close reaction energies calculated for all the three conformers in Fig.1. Other dissociations are also taken into account (from the side chain OH goup, α-carbon, from amino group), but leading to higher reaction energies as the previous process. In the case of hydrogen dissociation from the amino group a detachment of one weak interacting hydrogen from the carboxylic group (for conformer in the middle on Fig.1) or from the side chain hydroxylic group (for the other conformers on Fig.1) occurs. These hydrogen shift effects show that the energetically lowest ion is formed first dissociating a hydrogen from the amino gorup followed by hydrogen shift form the carboxylic group to the nitrogen and not via direct hydrogen cleavage from the carboxylic group as one could expect. Unfortunately the process of dissociation of the hydrogen from the amino group cannot be described using these three conformers, another conformers with the lack of weak interaction between the nitrogen and extra hydrogen has to be considered.

Negative ions like $(M-H)^-$, $C_3H_4O_2^-$ or $(M-NH_2)^-$ (m/z 89) are predominantly formed in the lowest energy range, whereas $C_2H_4NO_2^-$ (m/z 74), $C_2H_3NO_2^-$ (m/z 73), $C_2H_4NO^-$ (m/z 58) and $C_2H_2NO^-$ (m/z 56) are exclusively registered at higher energies. $(M-OH)^-$ negative ions (m/z 88) were observed with weak intensities also at near to zero eV; there is no satisfactory explanation for this observation at the moment. The comparison of two independent measurements conducted on two instruments with different geometries helped in the interpretation of the negative ion-forming pathways of serine.

This work was partially supported by VEGA 1/3040/06 and COST CM0601 ECCL.

[1] M. Stano, Š. Matejčík, J. D. Skalný, T. D. Mirk, J. Phys. B: At. Mol. Opt. Phys. **36**, 261 (2003).
[2] V.G. Voinov, Y.V. Vasil'ev, J. Morré, D.F. Barofsky, M.L. Deinzer, M. Gonin, T.F. Egan, K. Fuhrer, Anal. Chem. **75**, 3001 (2003).
[3] Y.V. Vasil'ev, B.J. Figard, V.G. Voinov, D.F. Barofsky, M.L. Deinzer, J. Am. Chem. Soc. **128**, 5506-5515 (2006).
[4] P. Papp, J. Urban, Š. Matejčík, M. Stano, O. Ingolfsson, J. Chem. Phys. **125**, 204301(1-8) (2006).
[5] C. T. Lee, W. T. Yang, and R. G. Parr, Phys. Rev. B **37**, 785 (1988).
[6] A. D. Becke, Phys. Rev. A **38**, 3098 (1988).
[7] L. A. Curtiss, K. Raghavachari, P. C. Redfern, V. Rassolov, and J. A. Pople, J. Chem. Phys. **109**, 7764 (1998).
[8] S. Gronert, R. A. J. O'Hair, J. Am. Chem. Soc. **117**, 2071 (1995).

Dissociative electron attachment to gas-phase leucine and isoleucine. Theoretical study of fragmentation reactions.

P.Papp, Š. Matejčík, P. Mach, J. Urban
Department of Experimental Physics,Faculty of Mathematics, Physics and Informatics, Comenius University, Mlynská dolina, Bratislava, Slovakia

P. Shchukin
Institute of physics of molecules and crystals Ufa research center of the RAS, Ufa, Russia

e-mail: papp@neon.dpp.fmph.uniba.sk

Amino acids are the main "building blocks" for synthesis of tissular proteins, enzymes, peptidic hormones and other bioactive compounds. The fundamental studies of amino acids is an important task. The dissociative electron attachment to gas-phase leucine and isoleucine has been studied both experimentally and theoretically.

The experiment was carried out using crossed beams apparatus equipped with quadruple mass-spectrometer and trochoidal electron monochromator (Comenius university, Bratislava). The maximal energy resolution of this apparatus is 50 meV. However, many of fragment ions of leucine and isoleucine have low dissociative cross section and that is why we made measurements with resolution 250 meV. Both samples were evaporating to the reaction area from a heated effusive molecular beam source at the temperature of approximately 440 K.

In general, the dissociative electron attachment spectra of leucine and isoleucine have many common features with previously studied aliphatic amino acids (glycine, alanine and valine). We detected at least eleven anionic fragment channels with the following m/Z values: 130, 115, 114, 113, 112, 84, 82, 74, 45, 26, 17. Three resonant energy regions occurred during measurements at about 1.5, 5.5 and 8 eV. The first resonance due to one particle shape resonance with extra electron placed on lowest unoccupied π^* orbital and other ones probably associated with core excited resonances. As for the other amino acids [1] the most abundant species in mass-spectrum are $(M-H)^-$ ions, which are formed at 1.2 eV via cleavage OH bond. The intensities of other ions are two orders lower. In low energy resonance we also registered 115 m/z and 114 m/z ions, the other ions are mostly formed in two high-energy resonances and exhibit wide resonant peaks. Some of the m/Z ration channels show different probabilities of the same reactions comparing the relative signals obtained from leucine and isoleucine fragments.

However these reactions leading to ionic products with different m/Z and also the possible structures of these products are from experimental research unknown. Therefore we combine our experimental research with the theoretical methods of quantum chemistry. These methods allow us to predict the structures of the possible products and so the fragmentation reaction schemes. We use the DFT method with B3LYP [2, 3] functional together with 6-311++G(2df,2pd) one particle basis set for optimizing the geometries of the calculated compounds. The optimal ground state structures of all fragments are then used as inputs for the complex energy computational method G3MP2 [4]. Multiple ab initio calculations are performed within this method including an empirical correction in the final step. As the consequence more reliable results are obtained as on B3LYP level comparing to experiment.

We found two theoretical studies concerning about the energetically lowest conformers of gas-phase leucine [5] and isoleucine [6]. Only the most stable conformers from this works were decided to use for our calculations (Fig.1), both are characterized with a weak interaction of one hydrogen from amino group with the carboxylic oxygen (HN-H···O=COH).

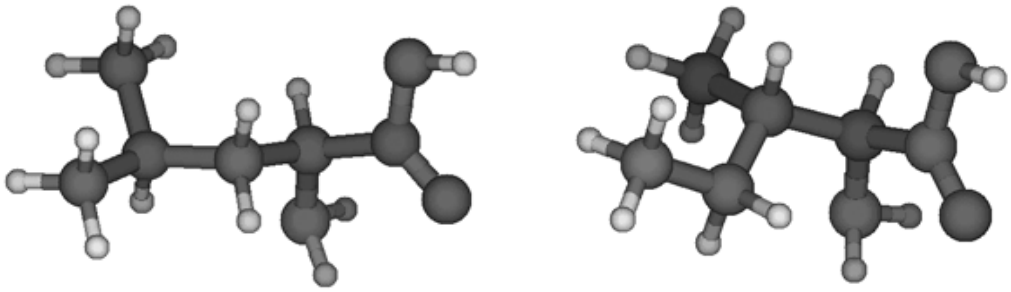

Fig.1: Energetically lowest conformers of neutral molecules of leucine (left) and isoleucine (right) amino-acids, taken from [4] and [5] respectively.

We show that the most abundant species form the spectrum refer to the hydrogen atom cleavage from the carboxylic group (the right hand side groups of both isomers on figure 1). Also another extra dissociations from carbon and nitrogen atoms are taken into account during calculations, but these could refer to energetically higher processes. The anionic channels with 115 m/z and 114 m/z can be associated with $(M\text{-}NH_2)^-$/$(M\text{-}O)^-$/$(M\text{-}CH_4)^-$ and $(M\text{-}OH)^-$/$(M\text{-}NH_3)^-$/$(M\text{-}CH_4\text{-}H)^-$ ions, respectively. There are typical ions for aliphatic amino acids $COOH^-$, OH^-, CN^- and 112 m/z. The 112 m/z ions may have two different structures and formed via two reactions: i) elimination water molecule and H atom from transient anions or ii) loss of ammonia and hydrogen molecule. Evidently, by analogue to 112 m/z ions, the ions 113 m/z are generated and have follow structures $(M\text{-}H_2O)^-$ or $(M\text{-}NH_3\text{-}H)^-$. Also mass-spectrum for both molecules demonstrated the peak for 74 m/z, which is probably formed by loss of side aliphatic chain and ascribed as $NH_2CHCOOH^-$. In contrast to valine [1], we have not obtain $(M\text{-}COOH)^-$ ions in leucine or isoleucine spectrum. However, we have detected 84 and 82 m/z anions and tentatively attribute these fragment ions to $(M\text{-}COOH\text{-}H_2)^-$ and $(M\text{-}COOH\text{-}2H_2)^-$, respectively, although another structure of these ions cannot be ruled out.

This work was supported by the Slovak Research and Development Agency, Project No. APVV-LPP-143-06. The partial support was from Russian Foundation for Basic Research (Grant numbers 05-03-97911-p_agidel_a, 06-03-32412-a).

[1] P. Papp, J. Urban, Š. Matejčík, M. Stano, O. Ingolfsson, J. Chem. Phys. **125**, 204301 (2006).
[2] C. T. Lee, W. T. Yang, and R. G. Parr, Phys. Rev. B **37**, 785 (1988).
[3] A. D. Becke, Phys. Rev. A **38**, 3098 (1988).
[4] L. A. Curtiss, K. Raghavachari, P. C. Redfern, V. Rassolov, and J. A. Pople, J. Chem. Phys. **109**, 7764 (1998).
[5] E. J. Cocinero, A. Lesarri, J.-U. Grabow, J. C. Lopez, J. L. Alonso, ChemPhysChem. **8**, 599 (2007)
[6] A. Lesarri, R. Sanchez, E. J. Cocinero, J. C. Lopez, J. L. Alonso, J. Am. Chem. Soc. **127**, 12952 (2005)

About vibronic origin of the strong non-adiabatic effects and unexplored possibilities to control chemical transformations on interphases using gas-phase electronic excitation

Victor V. Petrunin

Physics and Chemistry Department, SDU University of Southern Denmark, 5230 Odense, Denmark

It will be argued that in the process of chemical adsorption/desorption on a surface, a molecule with several electrons involved in formation of chemical bonds will always pass extended regions of degeneracy with electronically excited molecular configurations. Such degeneracy allows a ”vibronic” coupling mechanism between the ground and the electronically-excited states; a process similar to Inverse Electronic Relaxation may start to play a significant role. Conditions at which the above-mentioned phenomenon can appear as a particularly strong nonadiabatic effect will be examined and links drawn to experimental observations made on several systems as well as to theoretical attempts to account for these effects.

Particularly, the observations reporting a strong dumping of internal vibrations in molecules [1,2,3] will be discussed and reconsidered with an attempt to implement the new ideas. In the model proposed, dissipation of the energy from “hot” coordinate(s) of the system is resonantly-enhanced by excited electronic configuration; the mechanism may lead to preferential dissipation of large energy quanta in form of excitons, rather than to direct generation of electron-hole pairs commonly discussed in the connection to non-adabatic effects within the “friction force” and “hole diving” models . It will be argued that experiments with electronically excited species can provide vital information for understanding of the very nature of passways of surface chemical reactions and of the corresponding reaction dynamics effects.

The topology of the potential energy surfaces, which follows from the presented general consideration, strongly suggests an unexplored previously possibility to initiate elementary chemical transformations on interfaces via electronic excitation of gas-phase molecules. The principal advantages of the new approach over photochemistry within gas phase and over photoexcitation within molecular aggregates/adsorbates will be emphasized.

Finally, experimental results demonstrating the first surface chemical reaction with electronically excited molecules and a new experimental approach, capable of producing macroscopic fluxes of excited reagents, will be presented [4]. We will report a quantum yield

close to 1 for dissociative adsorption of electronically excited SO_2 molecules on a surface leading to formation of molecular sulphur.

[1] L. Diekhöner, L. Hornekær, H. Mortensen, E. Jensen, A. Baurichter, V.V. Petrunin, and A.C. Luntz J.Chem.Phys.**117**, 5018 (2002).

[2] H. Mortensen, E. Jensen, L. Diekhöner, A. Baurichter, A.C. Luntz, and V.V.Petrunin J.Chem.Phys.**118**, 11200 (2003).

[3] J.D.White, J.Chen, D.Matsiev, D.J.Auerbach, and A.M.Wodtke J.Chem.Phys. **124**, 064702 (2006) and refences herin.

[4] J. J. Madhukeswara and V.V. Petrunin Chem. Phys. Lett, **445**, 309 (2007).

Sticking and hot-atom relaxation in dissociative chemisorption of H2 on Ni(100)

I. Pino
Chemistry Department, University „Federico II“ of Naples, Italy

G.F. Tantardini
Chemical Physics and ElectrochemistryDepartment, University of Milan, Italy

Dissociative chemisorption of H_2 molecules on a clean Ni(100) surface has been studied theoretically with classical and quasi-classical dynamics. In our model metal atoms are allowed to move in an Embedded-Diatomics-In-Molecules description and generalized Langevin oscillators are used at the bottom of a 5x5x5 simulation slab in order to describe energy dissipation to the bulk. We focus on the sticking coefficient as well as on the relaxation of H adatoms following molecular dissociation. The latter have hyperthermal energy and may considerably move on the surface before finding the final adsorption site (see Fig.1). This behaviour is analogous to what happens in other gas-surface processes[1]. Though the adopted interaction potential does not allow a rigorous comparison with existing experimental results, the aim of the present study is to provide a picture of the whole dissociative chemisorption process, in the light of recent results reporting fast hot-atom relaxation on a different metal surface[2] .

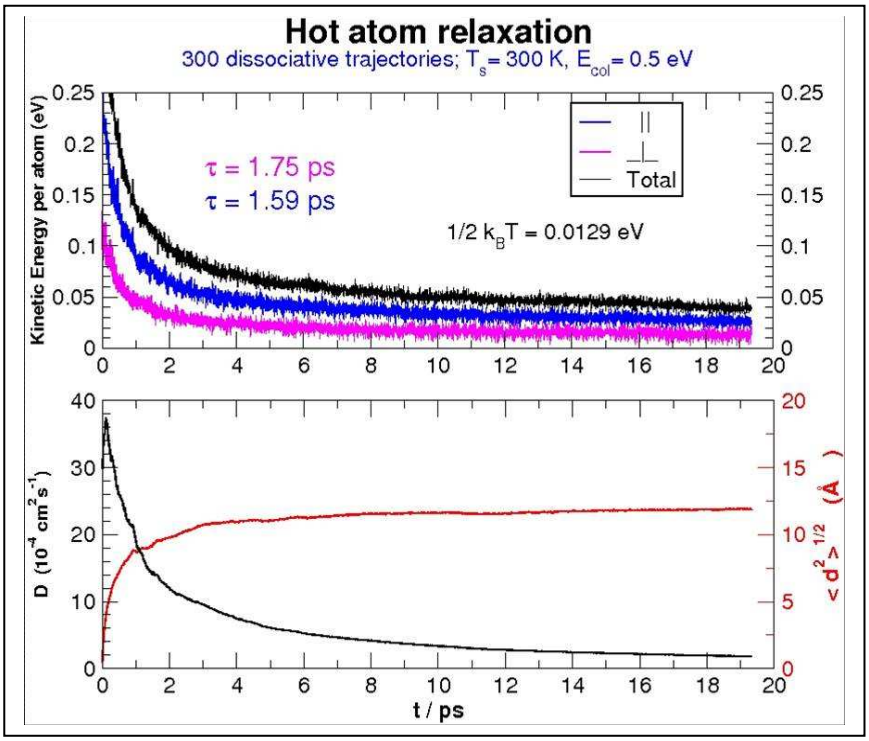

Figura 1.

Upper panel: calculated parallel and perpendicular components of the average kinetic energy per atom of H adatoms on a Ni(100) surface at T_s=300 K following dissociation of a H_2 beam colliding perpendicular to the surface with a collision energy of 0.5 eV.

Lower panel: root mean square displacement of H atoms from the impact and dissociation sites (curve 1 referred to right axis) and diffusion coefficient (curve 2 referred to left axis) as a function of time.

[1] R. Martinazzo, S. Assoni, G. Marinoni, G.F. Tantardini, J. Chem. Phys. **120**, 8761 (2004).
[2] N. Pineau, H.F. Busnengo, J.C. Rayez, A. Salin J. Chem. Phys. **122**, 214705 (2005).

Photolysis of hydrogen halides on water clusters

V. Poterya and M.Fárník
J.Heyrovský Institute of Physical Chemistry AS CR, Dolejškova 3, 18223 Prague 8, Czech Republic

M. Ončák and P. Slavíček
Department of Physical Chemistry, Institute of Chemical Technology, Technická 5, Prague 6, Czech Republic

U. Buck
Max-Planck-Institut für Dynamik und Selbstorganisation, Bunsenstr. 10, Göttingen

In this contribution we focus on photochemistry of hydrogen halide molecules HX (X=Br, Cl) on large water clusters. The acid solvation on particle surfaces, such as those of ice crystals or liquid aerosols, attracted a great interest, because of applications in atmospheric reactions leading to the stratospheric ozone depletion [1]. Therefore a great effort has been devoted to elucidate these processes at the molecular level.

We investigate these processes in a molecular beam experiment [2]. The water cluster beam $(H_2O)_n$, $n\approx500$, is produced by a supersonic expansion of neat water vapor through a conical nozzle. The clusters are doped with the HX molecules in a pick-up cell. Then the clusters enter a vacuum chamber with a time-of-flight (TOF) spectrometer. Here the molecules are photolysed with a 193 nm laser and the H-fragments are successively ionized by (2+1) REMPI process with 243 nm laser. The TOF spectra of H-fragment atoms provide information about the photodissociation process. To determine the origin of the H-atoms in $HX(H_2O)_n$ photolysis, the spectra with deutherated species DX and D_2O were measured.

The H-fragment signals originates from the presence of the hydrogen halide molecule on the cluster, however, it is not simply a signal due to the direct photolysis of the HX molecule on the cluster. This indicates an exchange of hydrogen atoms between the hydrogen halide and the water cluster via generation of the hydronium H_3O molecule [3]. The observed hydrogen fragment originates from the dissociation of the hydronium.

Figure 1 shows the two slightly different ways of photochemical production of the hydronium: (I) HBr molecule dissociates on water cluster generating the ion pair, which is then excited with the 193 nm laser radiation into an excited state. Subsequently, this state can relax, generating the neutral hydronium molecule H_3O. The H-atom is then emitted from the hydronium. (II) Alternatively, intact HBr molecule is dissociated by the 193 nm photon. The H-fragment reacts with the neighboring H_2O molecule to create the excited hydronium. It can then

relax to the ground state H_3O as in the former case (I), which results in H-atom dissociation from the hydronium.

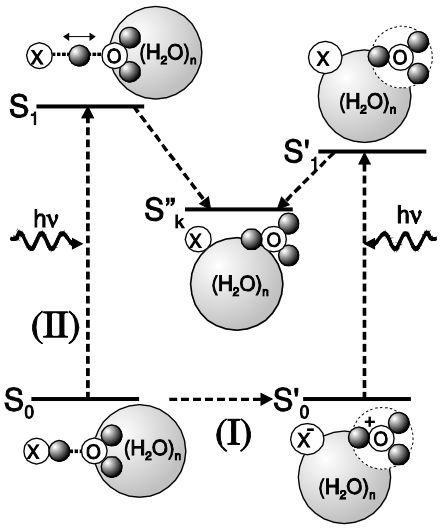

Fig. 1: Two alternative pathways of $HX(H_2O)_n$ photochemistry

The present model has recently been supported by theoretical calculations in our group, and by futher experimental evidence in measuring the relative photodissociation cross sections for HBr vs. HCl molecules on the $(H_2O)_n$ clusters. These new results will be discussed in our presentation.

Acknowledgement: The present work has been supported by the special program "Nanotechnology for society" of the Czech Academy of Sciences KAN400400461, and by the Grant Agency of the Czech Republic 203/06/1290.

[1] M.J. Molina, T.L. Tso, L.T. Molina, F.C.-Y. Wang, Science. **238**, 1253 (1987).

[2] V. Poterya, M. Fárník, P. Slavíček, U. Buck, V. Kresin, J. Chem. Phys. **126**, 071101 (2007).

[3] A.L. Sobolewski, W. Domcke, Phys. Chem. Chem. Phys. **9**, 3818 (2007).

Anions of Aromatic Nitrate and the NO – Abstraction Reaction: Calculated Energetics

Andreas Mauracher, Michael Probst, Stefan Denifl, Natcha Injan†, Jumras Limtrakul†,Tilmann Märk and Paul Scheier

Institute of Ion Physics and Applied Physics, University of Innsbruck, Technikerstraße 25, 6020 Innsbruck, Austria
†*Center of Nanotechnology, Kasetsart University, Bangkok 10900, Thailand*

Dissociative Electron Attachment (DEA) to aromatic nitrates is an interesting process and has been studied intensively experimentally (see for example [1]). It is not only a model process for DEA but has potential practical applications [2]. It is also a very complicated process [1] on the atomic level and many details are still obscure. The simplicity of aromatic nitrates makes them also an interesting subject for accurate quantum chemical calculations. We give an overview of our computational work and discuss the energetic features of some important species. The reaction pathway derived for the probably most important DEA reaction, the abstraction of NO, is discussed.

Aromatic nitrates – mononitrobenzene (MNB)

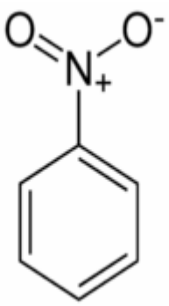

The prototypical aromatic nitrate is nitrobenzene. Like other nitrobenzenes it can be produced by the reaction of nitric acid with benzene. This process is called electrophilic nitration since a NO_2^+ ion is thought to be the intermediate reacting with the electronic system of benzene [3]. Contrary to the arguments often used to explain organic chemical reactions, there is little conjugation in nitrobenzene (little interaction of the benzene π system with p-orbitals of the NO_2 group) and not much energy is required to rotate the NO_2 group although the most stable conformation is planar [4] except if there is steric hindrance like in o-DNB. The conformations where NO_2 and C_6H_5 are perpendicular are typically 0.1-0.3 eV higher in energy. Aromatic nitrates have a positive electron affinity. As for most comparable closed-shell molecules, the ubiquitous H-abstraction reaction proceeds more easily from the anion and the EAs of the molecules without hydrogen are rather large, for example 2.25, 2.10 and 2.15 eV for the o,m,p - isomers of MNB.

Aromatic nitrates – dinitrobenzene (DNB)

A bit surprisingly as well, the ortho, meta and para (o,m,p) isomers of DNB are not very different in many of their properties. One trivial exception are the dipole moments where the para-isomer has no dipole moment due to its symmetry. In the following table they are shown together with IP's and relative energies:

	o-DNB	m-DNB	p-DNB
Energy neutral	0.00	-3.77	-3.76
Energy anion	-1.71	-5.10	-5.29
EA	1.71	1.33	1.53
dipole moment	5.0	5.7	0.0

The high relative energy of o-DNB is a consequence of the repulsion between the nitro-groups. The energies are (all in eV) were calculated with the G2(MP2) method, a quantum chemical extrapolation scheme that is normally accurate to about 0.1 eV. One important fact is also the relatively large positive electron affinity mentioned before – all anions are thermodynamically stable. The nitrate region of the molecules is always the negative one. This is very similar for all isomers (and also for toluenes etc.) and is shown here for the example of m-DNB: A positive electrostatic potential is painted dark and a negative is shown in lighter grey tones. Other properties like BDEs will be discussed in the presentation.

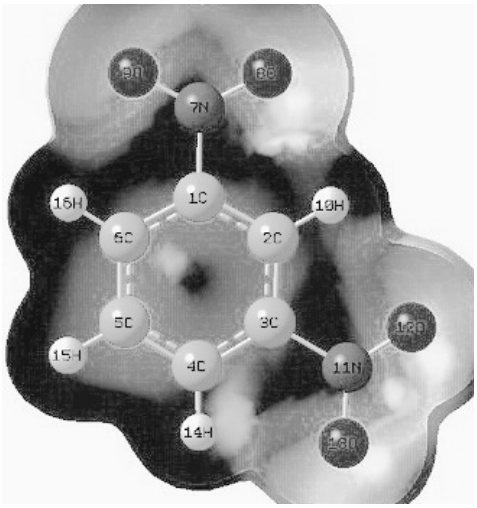

NO abstraction: $\Phi\text{-}NO_2^- \rightarrow \Phi\text{-}O^- + NO$

One of the intriguing experimental findings is a reaction of one molecule with one electron at 0 eV that leads to the production of NO. We tried to understand the details of this process. This is normally quite demanding and a good example of an elaborate exploration is [5]. We tried something similar with MNB anion as the simplest aromatic nitro-compound that undergoes the NO – loss reaction.

If the reactants and products are known, one can search for the reaction coordinate with the lowest barrier. This is, however, practically only possible for very simple reactions. For the NO-loss reaction we had to made the assumption that before the OH loss the Φ-ONO isomer (phenylnitrite) is formed. This is probably reasonable since the reaction directly from $\Phi\text{-}NO_2^-$ would require the simultaneous breaking of two bonds. The reaction profile was then calculated by locating the transition states. It is shown on the next page. Only the isomerisation from $–NO_2$ to –ONO has a real transition state because the Φ-ONO isomer subsequently can lose NO easily. Since the calculation of reaction pathways is much more difficult than the calculation of properties of equilibrium structures, we could until now only calculate the reaction pathways at the HF/CEP-31G and B3LYP/6-31G* levels of theory. The one shown is for HF/CEP-31G. The B3LYP/6-31G* results are similar with the barrier being ~3.5 eV and the reaction exothermic by 1.7 eV. This indicates that the calculated barrier height is not very accurate. The results should be qualitatively correct, though, and the profile exhibits some interesting features: (a) this barrier between the nitrate and benzylnitrite isomers is rather high and cannot be

Figure: Structure and relative energies of the molecules involved into NO abstraction from nitrobenzene anion, together with the reaction coordinate.

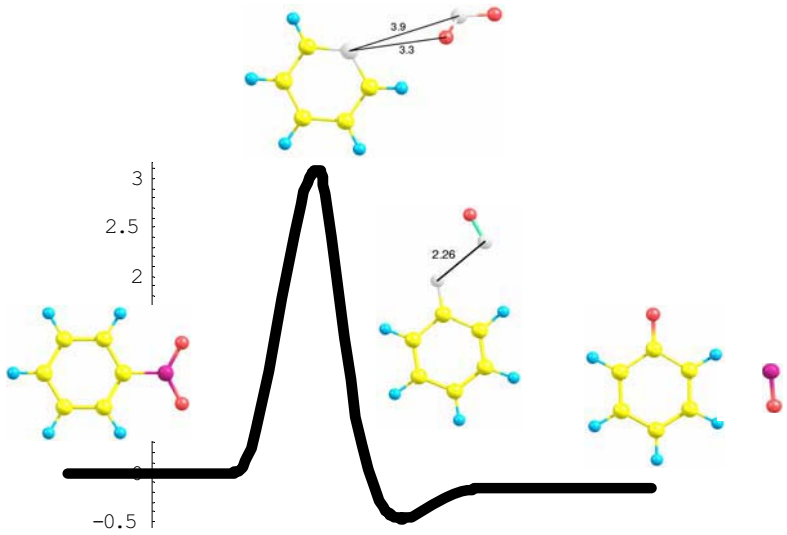

overcome for Φ-NO_2 by the EA alone. It might be much lower, though, for substituted nitrobenzenes. (b) The transition state is nonplanar and unsymmentric. (c) Φ–ONO^- should be a short-lived intermediate since it carries the energy when the reaction proceeds downhill the transition state.

All methods of calculation (for the overall energy balance of the NO – loss accurate standard thermochemistry can also be employed) agree with the experimental results in that the overall reaction is exothermic.

---

[1] Sulzer, Philipp; Mauracher, Andreas; Denifl, Stephan; Probst, Michael; Märk, Tilmann D.; Scheier, Paul; Illenberger, Eugen; Int. J. Mass Spectrometry (2007), 266 (1-3), 138-148.

[2] Sulzer, Philipp; Mauracher, Andreas; Denifl, Stephan; Zappa, Fabio; Ptasinska, Sylwia; Beikircher, Manuel; Bacher, Arntraud; Wendt, Nina; Aleem, Abid; Rondino, Flaminia; Matejcik, Stefan; Probst, Michael; Märk, Tilmann D.; Scheier, Paul.; Anal. Chem. (2007), 79(17), 6585-6591

[3] Esteves, Pierre M.; Walkimar de Carneiro, Jose; Cardoso, Sheila P.; Barbosa, Andre G. H.; Laali, Kenneth K.; Rasul, Golam; Prakash, G. K. Surya; Olah, George A. J.Am.Chem.Soc. (2003), 125(16), 4836-4849.

[4] Politzer, Peter; Lane, Pat; Jayasuriya, Keerthi; Domelsmith, Linda N, J.Am.Chem.Soc. (1987), 109(7), 1899-901.

[5] Il'ichev, Yuri V.; Wirz, Jakob, *;* J. Phys. Chem. A (2000), 104(33), 7856-7870.

Photodissociation Spectroscopy of Cationic Porphyrins in the Gas Phase. Influence of the Complexation with DNA. Comparison with Solution Phase.

F. Rosu, E. De Pauw, and V. Gabelica
Mass Spectrometry Laboratory, Université de Liege, Liège, Belgium

R. Antoine and P. Dugourd
LASIM, Université Lyon 1, Lyon, France

We recently started exploring the gas-phase reactivity of multiply charged DNA single strands, and double strands anions upon UV irradiation around 260 nm [1-3]. To our surprise, we found out that, instead of fragmentation, electron detachment was the major reaction pathway. Double stranded DNA and quadruplex DNA multiply charged anions coupled to chromophores were subjected to UV-Vis photoactivation in a quadrupole ion trap mass spectrometer. The chromophores included noncovalently bound porphyrins which were activated with visible light.

Free Ligand (positive ions):

Wavelength dependence of dissociation yield of the Porphyrins (TmPyP4, A2cis and A2trans) alone was compared to the absorption spectra in solution. In the gas phase, all three porphyrins show clearly two bands, at 435 nm and 457 nm. In aqueous solution there is only one band (usually called Soret band, or B band), at 408 nm for A2cis and A2trans, and at 424 nm for TMPyP4. The porphyrin absorption is blue-shifted by H_2O. The Observation of two bands for porphyrins in gas phase is unprecedented (Figure 1).

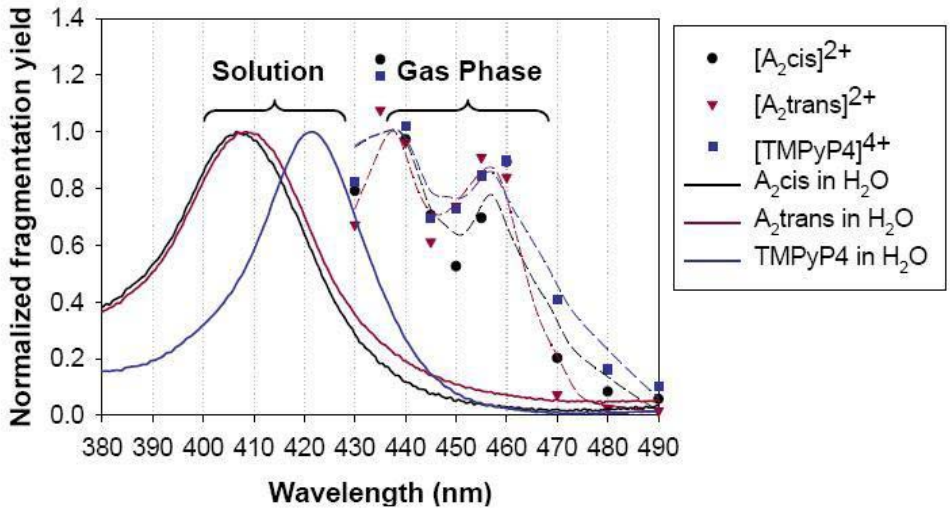

Figure 1: Solution absorption spectra of porphyrin TmPyP4, A2cis and A2trans (solid line). Gas phase action spectra of the porphyrins (dash line).

Ligand-DNA complex (negative ions):

In solution, a red shift is detected upon porphyrin complexation to DNA. Similar result (red shift) is observed in the gas phase. The influence of the environment polarity on the absorption spectra of the porphyrin is described. Spectrum is blue-shifted as the polarity

increases (confirms gas phase observations). Upon complexation to DNA, the solvent blue-shift effect is reduced when ligand interacts with the DNA rather than with the solvent.

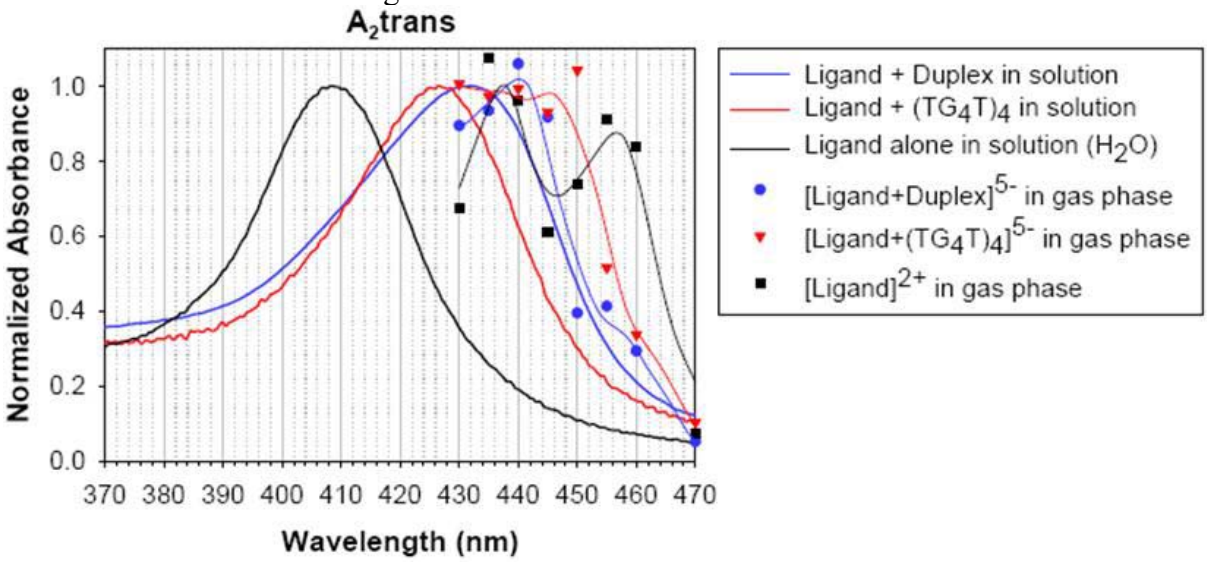

Figure 2: Solution absorption spectra of porphyrin A2trans and the A2trans-Duplex or A2trans-quadruplex complexes (solid line). Gas phase action spectra of the A2trans–Duplex and A2trans-quadruplex (dash line).

Methods:

The experiments are performed on LCQ and LTQ quadrupole ion trap mass spectrometers (ThermoFinnigan, San Jose, CA), which are coupled to pulsed UV lasers (OPO tunable laser or fixed wavelength solid-state laser). The mass spectrometers are modified to allow the injection of UV and visible lights into the ion traps. An electromechanical shutter triggered on the RF signal of the ion trap synchronizes the laser irradiation with the MS/MS events. Precursor ions were first isolated in the ion trap and then irradiated with UV or visible light. Mass spectra obtained after irradiation (MS2) were recorded.

References

[1] V. Gabelica, T. Tabarin, R. Antoine, F. Rosu, I. Compagnon, M. Broyer, E. De Pauw, P. Dugourd, Anal. Chem. **78**, 6564 (2006)
[2] V. Gabelica, F. Rosu, T. Tabarin, C. Kinet, R. Antoine, M. Broyer, E. De Pauw, P. Dugourd, J. Am. Chem. Soc. **129**, 4706 (2007).
[3] V. Gabelica, F. Rosu, E. De Pauw, R. Antoine,T. Tabarin, M. Broyer, P. Dugourd, J Am. Soc. Mass Spectrom. **18**, 1990 (2007)

State-Resolved Reactivity of Vibrationally Excited CH_4 on Pt(110) (2x1)

M. Sacchi, R. Bisson, B. L. Yoder, T. T. Dang, and R.D. Beck
Laboratoire Chimie Physique Moléculaire,
Ecole Polytechnique Fédérale de Lausanne,
CH-1015 Lausanne, Switzerland

The key step in technologically important processes as steam-reforming or partial oxidation of methane is the dissociative adsorption of methane onto metal surfaces. The interaction between CH_4 and Pt(110) has been the object of a wide number of both theoretical and experimental studies because the corrugated Pt(110) surface is a simplified model of real catalysts. Nevertheless, no previous experimental work has been able to measure the contribution of different vibrational modes for promoting the chemisorption reaction. With our experimental apparatus, we can prepare methane in selected quantum states and study the effect of the vibrational energy onto the reaction probability. In this work, we have measured quantum state resolved sticking coefficients of CH_4 on the Pt(110) (2x1) surface (Figure 1). Using a tunable pulsed infrared laser setup[1], we have excited CH_4 to the vibrational states $2\nu_3$, $\nu_1+\nu_4$ and $2\nu_2+\nu_4$, containing different amounts of vibrational quanta of stretching and bending. The label ν_1 indicates the symmetric stretch of CH_4, ν_3 the antisymmetric stretch, ν_2 the symmetric bend and ν_4 the bending mode of F2 symmetry . Our experimental apparatus is composed of a pulsed molecular beam source[2] in combination with a UHV chamber, we have studied the dependence of the reaction probability as a function of the kinetic energy of the molecules incident on the surface. The results (Figure 2) show that the chemisorption reaction is strongly activated by the incident translational energy of the molecules in the energy range from 4 to 64 kJ/mol.

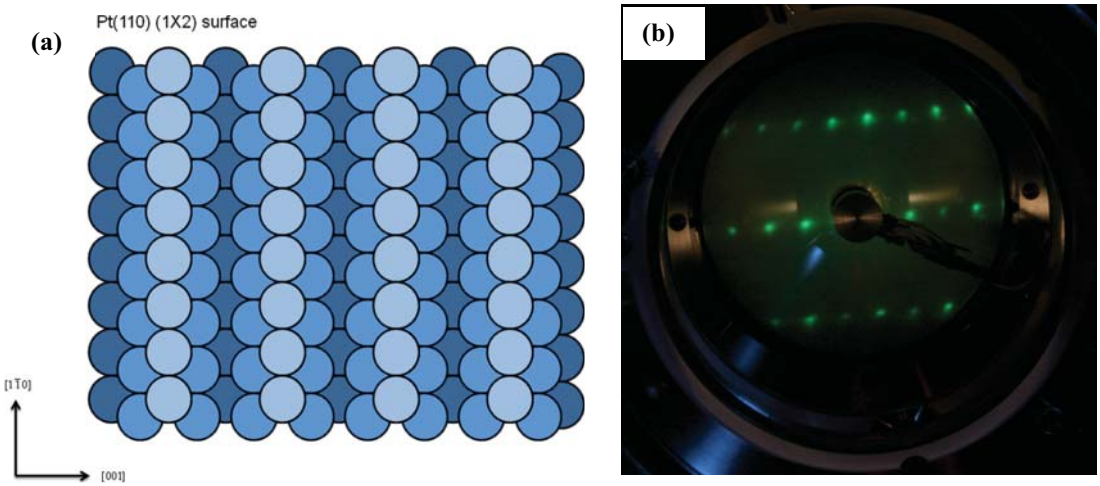

Figure 1 (a) Schematic illustration of the Pt(110) (2X1) surface. The different circle colors are used to indicate the top first, second and third layer of Pt atoms. (b) LEED pattern of the Pt(110) (2X1) surface after cleaning.

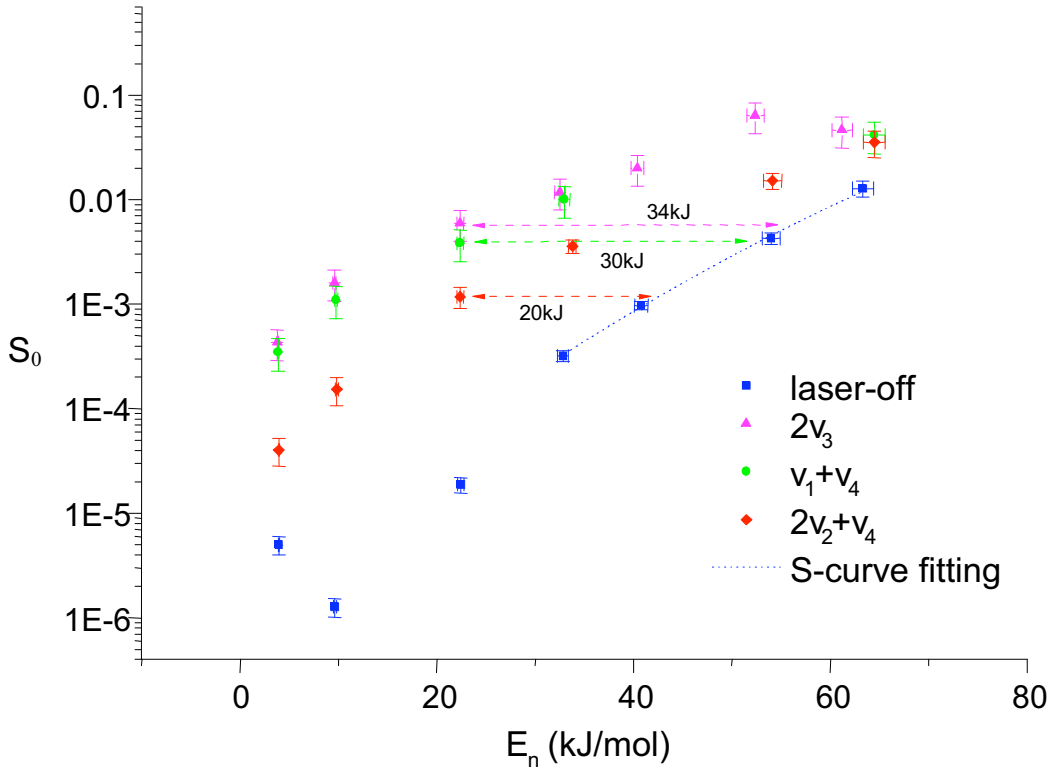

Figure 2 Sticking coefficients as a function of incident kinetic energy (normal incidence) for dissociative chemisorption of CH_4 on Pt(110) (2X1) (T_s = 400K). (■) Laser-off data, (▲) $2\nu_3$, (●) $\nu_1+\nu_4$, (♦) $2\nu_2+\nu_4$. The horizontal dash arrows indicate the amount of normal kinetic energy which produces the same increase in reactivity as the vibrational excitation. The dotted blue curve is a S-curve fitting of the laser-off data from 33 to 64 kJ, the agreement between the experimental data point and the fitting curve is good in this range of kinetic energy since only the direct-adsorption pathway is dominant.

We interpret these results as evidence that the chemisorption of CH_4 on Pt(110) (2x1) occurs by a direct adsorption mechanism with a high energy barrier for E_n > 10 kJ/mol. At a translational energy below 10 kJ/mol, the sticking coefficient of the unexcited molecules increases with decreasing incident energy, indicative of a precursor-mediated adsorption pathway[3]. Our measurements also show that vibrational excitation enhances the dissociation probability of methane on Pt(110), similar to what has been found in previous state-resolved studies for Pt(111). The reactivity enhancement relative to the ground state varies considerably with the incident kinetic energy. For example, at Ek = 33 kJ/mol, the sticking coefficient of the $2\nu_3$ and $\nu_1+\nu_4$ state is ~30 times higher than the correspondent laser-off measurement, while the excitation of the $2\nu_2+\nu_4$ mode only enhances the ground-state reactivity of a factor of 10, while, at 10 kJ/mol, we observe the maximum vibrational enhancement in the reaction probability up to 3 order of magnitude.

Within the kinetic energy range we have used for our measurements, we observe that the excitation of the modes $2\nu_3$ and $\nu_1+\nu_4$ produces the same increase in reaction probability

(Figure 2), nevertheless, since these two modes have different energies (71.4 kJ for the $2\nu_3$ mode, and 50.5 kJ for the mode $\nu_1+\nu_4$), the $\nu_1+\nu_4$ state has higher efficacy than the $2\nu_3$ mode (Table 1).

Table 1 The vibrationaly efficacy[4] is a parameter that compare the effect of vibrational and translational energy on the reaction probability. The vibrational efficacies of the different states on Pt(110) are calculated at kinetic energy of 22 kJ/mol.

State	***Vibrational Energy (kJ/mol)***	***Vibrational Efficacy***
$2\nu_3$	71.4	48%
$\nu_1+\nu_4$	50.5	60%
$2\nu_2+\nu_4$	52.2	39%

The vibrational efficacy that we have measured for the mode $2\nu_3$ on Pt(110) is similar to what was reported by Higgins et al.[5] on the less corrugate Pt(111) surface, this result can point to a similarity in the transition state geometry of methane on these two surfaces. In fact, DFT calculations performed by Psofogiannakis et al. [8] on Pt(111) and by Anghel et al. [7] on Pt(110) shown that the dissociating bond is similarly stretched in the TS configuration, 1.38 Å for the Pt(111) and 1.48 Å for the Pt(110) respectively, with the leaving H atom onto the bridge position between two adjacent Pt atoms (Figure 3).

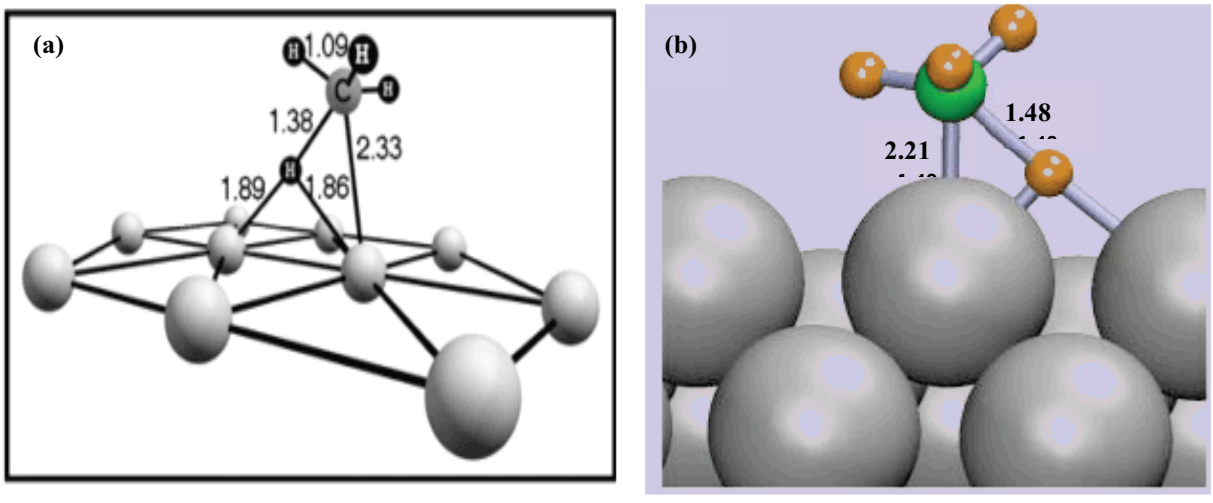

Figure 3 (a) TS structure on Pt(111) (Psofogiannakis et al. [8]). (b) TS structure on Pt(110) (2x1) (Anghel et al. [7]). All the bonds lengths and distances in the figure are in Å.

In conclusion, we show that the vibrational energy is not as effective as the translational energy in promoting the dissociation of CH_4 on Pt(110), the fact that the dissociation

probability doesn't scale with the total energy of the molecule cannot be explained by statistical models[6] of gas/surface interaction. Furthermore, we probed how different vibrational modes effect the reactivity, and we observe that bending plus stretching ($\nu_1+\nu_4$) mode has an higher efficacy than both the pure bending ($2\nu_2+\nu_4$) and the pure stretching ($2\nu_3$) mode (see Table 1). Observing that the pure bending vibrational mode $2\nu_2+\nu_4$ is not as effective as the pure stretching mode $2\nu_3$, we can deduce that the role of the vibrational activation cannot be explained by a "deformation model" mechanism (Lee et al.[7]) because in this case $2\nu_2+\nu_4$ will be more efficient than $2\nu_3$. We can understand why the $\nu_1+\nu_4$ mode is the most efficient only analyzing the geometry of the transition state, in fact, recent ab-initio calculations[8] have shown that the reaction pathway for the dissociation reaction of CH_4 on Pt(110) (2X1) "*involve simultaneous stretching of a C-H bond and deformation of methane bond angles"*. Our state-resolved measurements confirm that, on Pt(110), the combination of bending plus stretching vibrational excitation ($\nu_1+\nu_4$) is the most efficient in promoting the reaction.

References

1 M. P. Schmid, P. Maroni, R. D. Beck, and T. R. Rizzo, J. Chem. Phys. **117** (19), 8603 (2002).

2 M. P. Schmid, P. Maroni, R. D. Beck, and T. R. Rizzo, Rev. Sci. Instr. **74** (9), 11 (2003).

3 A. V. Walker and D. A. King, Phys. Rev. Lett. **82** (25), 4 (1999).

4 R. R. Smith, D. R. Killelea, D. F. DelSesto, and A. L. Utz, Science **304**, 4 (2004).

5 J. Higgins, A. Conjusteau, G. Scoles, and S. L. Bernasek, J. Chem. Phys. **114** (12), 5277 (2001).

6 H. L. Abbott, A. Bukoski, and I. Harrison, J. Chem. Phys. **121** (8), 3792 (2004).

7 M. B. Lee, Q. Y. Yang, and S. T. Ceyer, J. Chem. Phys. **87** (5), 2724 (1987).

8 A. T. Anghel, D. J. Wales, S. J. Jenkins, and D. A. King, Physical Review B **71**, 4 (2005).

Biomolecules in the gas-phase. Myth or reality ?

G.Grégoire, F.Lecomte, C.Desfrançois and J.P.Schermann

Laboratoire de Physique des Lasers, Institut Galilée,
Université Paris 13, 93430, Villetaneuse, France

The study of biomolecules isolated in the gas-phase is sometimes considered as a discipline close to mythology. It is then argue that the only relevant studies should be conducted in aqueous solution while, nevertheless, structures determined from crystals are highly praised. In a cell, biomolecules are, in fact, embedded in a crowded medium and realistic experiments should be conducted in rather highly concentrated and inhomogeneous solutions of proteins. However, in some cases, biomolecular systems are specifically recognized by their receptors in hydrophobic pockets and are then in presence of a very small number of water molecules in a medium possessing a small dielectric constant. Gas-phase conditions are then no longer that far from reality.

Acetylcholine is a neurotransmitter and the study of its interactions with its receptor is crucial for the design of drugs fighting Alzheimer or Parkinson diseases. This very flexible molecule has two important agonists, nicotine and muscarine, that possess very different chemical composition but identical or similar functional groups called pharmacophores. Those groups are a positively-charged quaternary ammonium and a hydrogen bond acceptor acting in a highly hydrophobic environmentt (“aromatic box”). What really matter for biomolecular recognition and thus bioactivity are structural arrangements of those pharmacophores. A combination of spectroscopic studies of those molecules conducted in the infrared region either in the gas-phase or in solution and their theoretical interpretation with explicit water molecules allows following the changes in structure and pharmacophoric activity of acetylcholine, nicotine and muscarine induced by the presence of solvent.

Reactivity of zirconium in the presence of mixed clusters containing polar solvent molecules

S. Soorkia, J-M. Mestdagh and B. Soep
Laboratoire Francis Perrin, CEA, 91191 Gif sur Yvette Cedex, France

A transition metal is an element found in the *d*-block of the periodic table and is more precisely defined as a metal having an incomplete *d* subshell. As such, transition metal elements have more electronic configurations compared to metals of the *s*-block because there are more subshells available to accommodate the valence electrons. The arrangement of electrons in the atomic orbitals gives rise to a variety of high-spin and low-spin states each of which is potentially a different chemical [1]. Hence, we can expect that a transition metal element in a specific electronic configuration has a specific reactivity. The zirconium atom is a second row transition metal element and the particularity of these elements is that the *4s* and *5d* orbitals are of comparable size and energy [2]. As a consequence, these orbitals can both be involved in a chemical reaction. We are interested in the reactivity of a zirconium atom associated with a simple functional molecule in a van der Waals complex formed in a supersonic expansion in the model reaction Zr + CH_3F.

A laser ablation/molecular beam experimental setup was used to put into contact Zr atoms with CH_3F molecules seeded in a carrier gas. A frequency doubled dye laser at 212 nm and a fluorine excimer laser at 157 nm were used to ionize separately with one photon the species present in the molecular beam.

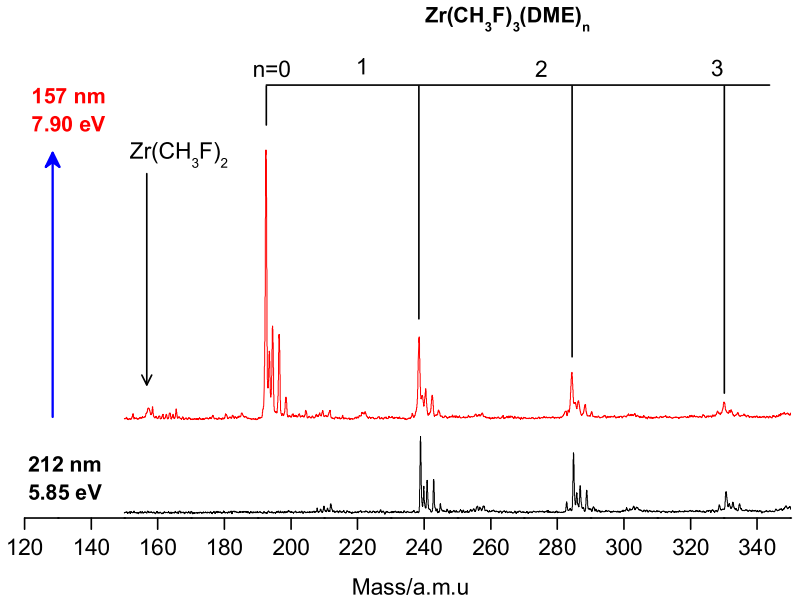

FIG. 1 – One photon mass spectrum at 5.85 eV (bottom) and 7.90 eV (top) of species present in the molecular beam seeded with CH_3F and CH_3OCH_3 (DME) acting as solvent molecules.

We have brought into evidence different products in the supersonic expansion : van der Waals complexes of the type $Zr - (CH_3F)_n$ and other products, most probably insertion compounds depending on the conditions of generation and solvation. If a mixture of CH_3F molecules seeded in pure He is used, van der Waals complexes are detected at 5.9 eV which is below the ionization potential of a Zr atom (6.63 eV). We can estimate the Zr^+ ion to be stabilized by at least 0.8 eV with a CH_3F molecule. On the other hand, when dimethylether molecules (CH_3OCH_3) acting as solvent molecules is added together with a fraction of Ar as carrier gas, compounds of the type $Zr - (CH_3F)_3(CH_3OCH_3)_n$ are detected (see figure 1). Surprisingly, the first mass peak of this series which corresponds to $Zr - (CH_3F)_3$ is detected with the 157 nm laser. This corresponds to a high ionization potential (> 8 eV),while for a zirconium van der Waals complex, the ionization potential should be lower than 5.9 eV (see figure 2).

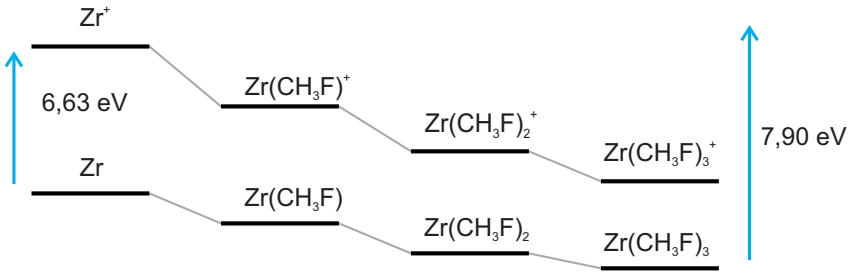

FIG. 2 – Evolution of the ionization potentiel of $Zr - (CH_3F)_n$ vdW complexes.

By comparison with a DFT calculation on the insertion compound $F - Mg - CH_3$, one would expect the ionization potential to be around 10 eV. On this basis, we can assume that the ionization potential of $F - Zr - CH_3$ should be lowered by at least 2 eV if solvated by two molecules. Hence we would be detecting the inserted compound in its minimal configuration, that is stabilized and solvated by two CH_3F (see figure 3). This would be the first time that such isolated inserted reaction products be detected in a molecular beam.

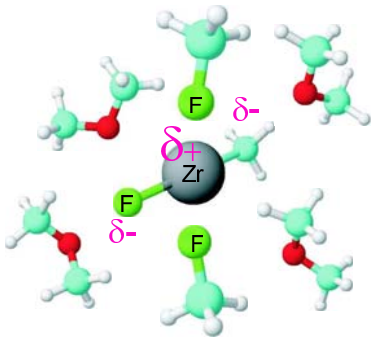

FIG. 3 – Stabilization of $F - Zr - CH_3$ by two CH_3F molecules and CH_3OCH_3 solvent molecules.

[1] James C. Weisshaar, Acc. Chem. Res. **26**, 213 (1993)
[2] P. E. M. Siegbahn, Theor. Chim. Acta. **86**, 219 (1993).

Quantities, Units and Symbols in Physical Chemistry

Jürgen Stohner[1,2] and Martin Quack[1]
[1] *ETH Zürich, Physical Chemistry, Wolfgang-Pauli-Str. 10, CH 8093 Zürich, Switzerland*
[2] *Zürich University for Applied Sciences, Technikumstr. 9, CH 8401 Winterthur, Switzerland*

Abstract
We provide a very brief collection of useful rules and recommendations treated in much detail in the International Union of Pure and Applied Chemistry (IUPAC) publication with the above listed title and which is also known as the 'Green Book'. The 2007 new edition has jointly been published by IUPAC and The Royal Society of Chemistry (RSC).

1 Introduction

The so called IUPAC (International Union of Pure and Applied Chemistry) 'Green Book' has a long history going back to 1969 where the *Manual of Symbols and Terminology for Physicochemical Quantities and Units* was first published by M. L. McGlashan, the Chairman of the IUPAC Physical Chemistry Division. The first edition of the Green Book as we know it now has been published in 1988 and the third, revised and enlarged edition was published recently by IUPAC and RSC [1].

The intention of the Green Book ever since its appearance was not to present a list of recommendations as commandments, but rather, its aim was and still is to help the user in what may be called a 'good practice of scientific language'. Many well established conventions are used in science and technology, but mixing conventions can lead to misunderstandings or even cause severe errors. One of those errors, caused by confusion of metric and imperial units, led to the loss of the NASA Mars Climate Orbiter (MCO) in 1999, worth about 200 Million USD of equipment and a non-quantified loss of scientific data and work. The reason for the loss of MCO was that although NASA used metric units (N s), the European partner used imperial units (lbf s) sending the satellite off course [2]. Another incident concerned the construction of a bridge in Laufenburg (Hochrheinbrücke, 2003/4) between Switzerland and the southern part of Germany. Whereas Germany measures its altitude relative to North Sea level, Switzerland uses the Mediterranian Sea (see Table below); both reference levels differ by 27 cm.

Country	Description	Reference Level (town)
Austria	meter über Adria (m ü. Adria)	Trieste
France	mètres d'altitude (m)	Marseille
Germany	meter über Normalnull (m ü. NN)	Amsterdam
Great Britain	metres above sea level (m ASL)	Newlyn
Italy	metri sul livello del mare (m s.l.m.)	Genua
Switzerland	meter über Meer (m ü. M.)	Marseille

This was known to the engineers, unfortunately the correction was performed in the wrong way introducing a difference in height by 54 cm. It was stated that the correction could be made without financial adjustments (because the insurance of the engineering company

covered the additional costs). One can estimate enormous daily economic losses due to the use of inadequate units worldwide under a variety of circumstances.

These examples show that it is worth caring about units as well as their proper usage.

2 Symbols and Units for Quantities and Operators

Symbols for physical quantities should be single-lettered using the Latin or Greek alphabet. The letters may be capital or lower case but should be printed in italic (slanted) type. Subscripts and superscripts may be added for clarity. All subscripts and superscripts are printed in Roman type (upright) except when these are symbols for physical quantities and therefore printed in italic type. Symbols for units should always be printed in Roman type. Similarly, symbols for chemical elements, elementary particles and mathematical operators (e.g. sin, exp, ln, $\mathrm{d}/\mathrm{d}x$, etc.) are also printed in Roman type (see Sections 1.3 and 1.6 in [1]).

3 Base Quantities and the SI as a Coherent System of Units

The International System (SI) consists of seven base quantities and their corresponding units (see Sections 1.2, 3.3 and 3.8 in [1]):

> metre (symbol: m), kilogram (symbol: kg), second (symbol: s), ampere (symbol: A), kelvin (symbol: K), mole (symbol: mol), and candela (symbol: cd).

A *coherent system* of units is such that equations between numerical values of physical quantities can be written exactly as the corresponding equations between the physical quantities itself. This coherent system therefore avoids numerical factors between units and is especially useful for so-called dimensional checking. The SI is such a coherent system of units. The coherence is lost, however, when prefixes are used.

4 Physical Quantities and Quantity Calculus

The value of a *physical quantity* Q can be written as a product of a *numerical value* $\{Q\}$ and a *unit* $[Q]$

$$Q = \{Q\}\,[Q] \tag{1}$$

Equations between quantities do not depend on the choice of units, however, equations between numerical values do depend on the choice of units. Physical quantities, numerical values, and units may be manipulated by algebraic rules ('quantity calculus'). The wavelength λ of one of the yellow sodium lines, for example, can be written in various equivalent ways:

$$\lambda = 5.896 \times 10^{-7}\ \mathrm{m} = 589.6\ \mathrm{nm} \tag{2a}$$

$$\lambda/\mathrm{m} = 5.896 \times 10^{-7} \tag{2b}$$

$$\lambda/\mathrm{nm} = 589.6 \tag{2c}$$

Conversion between different units of energy E can be achieved by using quantity calculus:

1 cm^{-1} is converted to eV (electronvolt)

$$(1\ \mathrm{cm}^{-1})\ hc\left(\frac{e}{e}\right) \mathrel{\widehat{=}} \frac{(1.986\,445\,501 \times 10^{-25}\ \mathrm{J}) \times 10^2\ e}{1.602\,176\,487 \times 10^{-19}\ \mathrm{C}} \mathrel{\widehat{=}} 1.239\,842 \times 10^{-4}\ \mathrm{eV} \qquad (3a)$$

and 1 kcal mol^{-1} is converted to cm^{-1}

$$\begin{aligned} \frac{(1\ \mathrm{kcal\ mol^{-1}})}{hcN_\mathrm{A}} &\mathrel{\widehat{=}} \frac{4.184 \times (1\ \mathrm{kJ\ mol^{-1}})}{hcN_\mathrm{A}} \\ &\mathrel{\widehat{=}} \frac{4.184 \times (10^3\ \mathrm{J\ mol^{-1}})}{(1.986\,445\,501 \times 10^{-25}\ \mathrm{J}) \times 10^2\ \mathrm{cm} \times (6.022\,141\,79 \times 10^{23}\ \mathrm{mol^{-1}})} \\ &\mathrel{\widehat{=}} 349.7551\ \mathrm{cm}^{-1} \end{aligned} \qquad (3b)$$

In a table or graphical representation, it is desirable to display numerical entries by dividing the quantities by their corresponding units:

$$\ln(p/\mathrm{MPa}) = a + b/T = a + b'(10^3\ \mathrm{K}/T) \qquad (4)$$

T/K	$10^3\ \mathrm{K}/T$	p/MPa	$\ln(p/\mathrm{MPa})$
216.55	4.6179	0.5180	−0.6578
273.15	3.6610	3.4853	1.2486
304.19	3.2874	7.3815	1.9990

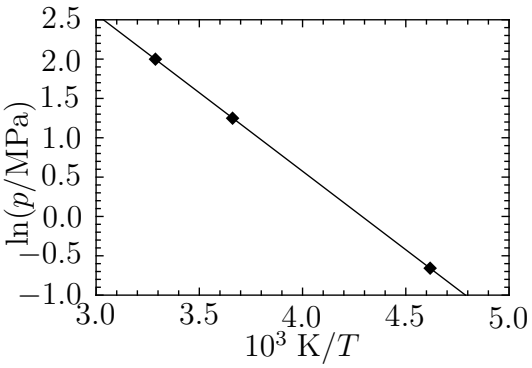

Algebraically equivalent forms may be used in place of $10^3\ \mathrm{K}/T$, such as kK/T or $10^3\ (T/\mathrm{K})^{-1}$. In eq. (4) one can see by writing the first few terms of a series expansion

$$\ln x \approx 2\left(\frac{x-1}{x+1} + \frac{(x-1)^3}{3(x+1)^3} + \cdots\right) \qquad (5)$$

that omitting the unit of the logarithm's argument would imply that one subtracts a number from a pressure. It is therefore mandatory to write $\ln(p/\mathrm{MPa})$ instead of $\ln(p)$.

5 Units outside the SI

There are non-SI units which are accepted for use with the SI: min (minute), h (hour), d (day), eV (electronvolt), Da (Dalton; this is equivalent to u, 1 Da = 1 u), u (unified atomic mass unit), and some more (see Section 3.7 in [1]). The year (symbol a) is not among those units, because the Julian year is defined in terms of days as 365.25 d, the Gregorian year as 365.2425 d, and the Mayan year as 365.2420 d (see Section 7.2 in [1]).

One should avoid using non-SI units from the following unit systems: the esu (electrostatic unit system), the emu (electromagnetic unit system), the Gaussian, and the atomic unit system. However, equations relating these still widely used unit systems to the SI are listed in Chapter 7 of [1] which also makes extensive use of quantity calculus to help converting between those systems of units.

Sometimes, quantities of dimension one (frequently called 'dimensionless' quantities) are written in mathematical equivalent forms denoted by special symbols (e.g. % for percent, 10^{-2}) or abbreviations (ppm, parts per million, 10^{-6}). These are often ambiguous, for example ppt could mean parts per thousand (10^{-3}) or parts per trillion. The latter is also ambiguous since a trillion can either be 10^{12} (American system of names) or 10^{18}. Similarly, the frequently used ppb (parts per billion) is ambiguous since a billion can either be 10^{9} (American system) or 10^{12} (European system). Since those quantities of dimension one can always be replaced by a proper fractional expression and ambiguities must be avoided, their use is deprecated (see Section 3.10 in [1]).

Calories should not be used, because there are different calories: $\mathrm{cal_{th}}$ (thermochemical calorie, 4.184 J), $\mathrm{cal_{IT}}$ (international calorie, 4.1868 J), and the $\mathrm{cal_{15}}$ (15 °C calorie, approximately 4.1855 J). It is often not clear which conversion was used in a given context. Many more examples can be found in Section 7.2 of [1].

6 Summary and Outlook

We have given here a very short overview of various topics covered in the 2007 edition of the Green Book which are relevant for everyday life of scientists because they facilitate cross-border communication among various disciplines in chemistry and physics.

The present edition has new sections (e.g. on uncertainty). The most recent fundamental physical constants and atomic masses are tabulated. The symbol as well as the subject index has considerably been extended to facilitate the usage of the Green Book. A table of numerical energy conversion factors is given and the most recent IUPAC perdiodic table of the elements is given on the inside back cover.

The definitions of the seven SI base units are subject to changes as experimental methods lead to an increase in precision and accuracy. This led already to a redefinition of the second by counting the periods of the radiation corresponding to the transition between the two hyperfine levels of the ground state of the caesium 133 atom. In 1967/68 it replaced the then adopted definition of the second as the fraction 1/31 556 925.9747 of the tropical year for 1900 January 0 at 12 hours ephemeris time. Today, for example, one wishes to redefine the kilogram (along with the ampere, the kelvin and the mole) in terms of fundamental physical constants. Presently, the definition of the kilogram still relies on a definition, that goes back to the French Revolution using a prototype (see [3] and references therein).

Comments and suggestions on the IUPAC Green Book can be mailed to just@ir.phys.chem.ethz.ch and Martin@Quack.ch.

[1] E.R. Cohen, T. Cvitas, J.G. Frey, B. Holmström, K. Kuchitsu, R. Marquardt, I. Mills, F. Pavese, M. Quack, J. Stohner, H.L. Strauss, M. Takami, A.J Thor, *Quantities, Units and Symbols in Physical Chemistry*, 3rd edition, IUPAC & The Royal Society of Chemistry, Cambridge (2007); ISBN 978-85404-433-7.

[2] The report can be found at ftp://ftp.hq.nasa.gov/pub/pao/reports/1999/MCO_report.pdf.

[3] T. Feder, *Physics Today*, p. 32, April 2006; I.M. Mills, P.J. Mohr, T.J. Quinn, B.N. Taylor, E.R. Williams, *Metrologia*, **42**, 71 (2005); I.M. Mills, *Mol. Phys.*, **103**, 2989 (2005).

XPS surface analysis of poly-L-arginine hydrochloride

Agnieszka Stypczynska[1,2], Sylwia Ptasinska[1], Tony Nixon[3], Janusz Rak[2] and Nigel J. Mason[1]

[1] Department of Physics and Astronomy, The Open University, Walton Hall, Milton Keynes, MK7 6AA, United Kingdom
[2] Department of Chemistry, University of Gdansk, 18/19 Sobieskiego, 80-952 Gdansk, Poland
[3] Systems Department, Technology Faculty, The Open University, Walton Hall, MK7 6AA, United Kingdom

This work reports an analysis of changes in the photoemission parameters of poly-L-arginine hydrochloride deposited on a silicon wafer. X-ray photoelectron spectroscopy (XPS) has been used to analyze the chemical and coordination state of the studied peptide. XPS is a surface sensitive technique used to determine atomic compositions and provide information about the types of bonding that occurs within various compounds. It not only permits the elemental analysis to be carried out but also the chemical state of particular atoms and their concentrations to be determined.

The XPS spectra were recorded using a Kratos XSAM 800 instrument that consists of an X-ray source, an electrostatic energy analyzer for the photoelectrons and an electron detector. The analysis and detection of photoelectrons requires that the sample be placed in a high-vacuum chamber (10^{-7}-10^{-8} mbar). Ultrahigh vacuum is necessary to get results free of and background signal from hydrocarbons introduced by the pumping system.

Poly-L-arginine hydrochloride was irradiated by Mg Kα X-ray and the photoelectron current was recorded as a function of time (from 0 to 5h). Through the XPS method, we are able to derive an elemental analysis and make detailed scans of O (1s), N (1s), C (1s) and Cl (2p) peaks in the constituent compound (Fig. 1). We have observed changes in the photoelectron spectra as a function of irradiation time for some of elements. Such changes are due to chemical modifications of the system under study, e.g. free radical formation or mass loss. Further details will be presented at the conference.

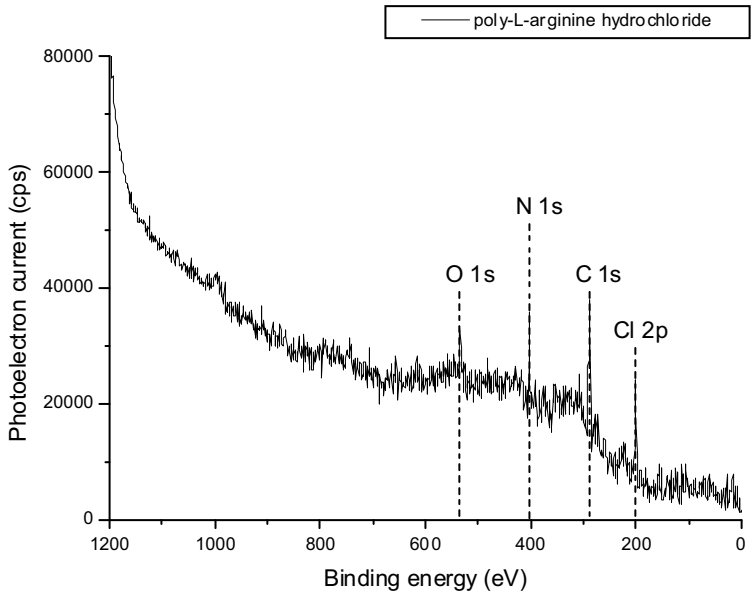

Fig. 1: XPS wide spectrum of a pristine poly-L-arginine hydrochloride sample

Are intermolecular potentials responsible for discrepancies between theoretical and experimental spectra of molecules embedded in helium nanodroplets?

Krzysztof Szalewicz
University of Delaware

Investigations of molecules embedded in superfluid helium nanodroplets led to some of the most important discoveries in physics and chemistry during the past decade. This work has been supplemented by experiments on He_n-molecule clusters with a controlled value of n. Recently, clusters with n as large as 80 have been observed. These experiments are very important since the observations can be directly compared with the results of quantum dynamics calculations on exactly the same systems. Although generally theory agrees with experiment and explains the observed dependencies on n, the quantitative agreement is only to about one digit as the discrepancies are often of the order of 20%. The natural suspect for the discrepancies are inaccuracies of the interaction potentials. Some investigations of this issue will be presented. Other possible reasons for the discrepancies will also be discussed.

Multi-mass imaging using a fast frame-transfer CCD camera

Claire Vallance, Alexander Johnsen, and Mark Brouard
Department of Chemistry, University of Oxford, Oxford, UK

Velocity-map imaging has been used with great success in the field of small-molecule reaction dynamics to study both molecular photofragmentation and a range of photoinitiated bimolecular events. A velocity-map imaging apparatus generally consists of a time-of-flight mass spectrometer fitted with a position sensitive detector and employing a velocity-mapping electrostatic lens in place of the more usual Wiley-McLaren ion optics. By adjusting the electrode potentials, the lens may be tuned such that either the positions or the velocities of the ions at their point of formation are projected in two dimensions onto the detector

A standard imaging detector converts the spatial distribution of ions striking the front face of a pair of microchannel plates into an optical image on a phosphor screen located behind the rear face. A CCD camera focused on the phosphor captures the images for processing and storage. Typically, a single photofragment or reaction product is selected for imaging by time-gating either the microchannel plates or an image intensifier located in front of the camera, such that a signal is only detected when the chosen mass arrives at the detector. For small molecule studies, characterisation of a single fragment is often sufficient to obtain a fairly complete picture of the dynamics of a photoinitiated process. However, larger molecules often have much more complex dissociation dynamics and may separate into numerous fragments. In these cases, characterisation of a single product is often insufficient, and the ability to record images of several fragments simultaneously becomes highly desirable. Previously, there have been two techniques developed to perform 'multimass imaging', both of which rely on spatial separation of the images at the detector through the application of static or pulsed electric or magnetic fields. The technique developed by Suits et al [1] employs a pulsed deflection field to achieve spatial separation of ions of different masses transverse to the time-of-flight axis, and has been used to study the dissociation dynamics of the ethylene cation, $C_2H_4^+$ [2,3]. While this is a promising approach, it does have the disadvantage that the mass resolution and mass range, as well as the spatial resolution of individual images, are limited significantly by the combination of the detector size and the maximum speed of the nascent fragment ions, which determines the individual image sizes. A second technique, developed in the group of Y. T. Lee [4] and based on a radial cylindrical energy analyser, yields the speed distributions for ions of different masses, but no angular information. This latter technique has, however, been used with great success in studying the dissociation dynamics of a wide range of organic species [5].

We propose a new method of multimass imaging in which the multimass modality is achieved by employing a programmable ultrafast frame-transfer CCD camera, clocked to the arrival times of the various masses, in the detection step. Using our method, images for different masses are separated in time rather than in space, allowing the use of a completely standard velocity-map imaging setup with no additional fields required. In principle, the method has the potential to offer essentially unlimited mass channels, mass range and spatial resolution. Our prototype camera is capable of recording up to 16 images per event at user-defined times with a time resolution of 5 ns and a spatial resolution of 64x64 pixels. After each trigger

cycle, the stored images are transferred from the chip to a PC at standard data rates for processing and permanent storage. After a brief description of the CCD chip architecture, we will present some of our proof of concept work on the technique and outline some of the potential applications for the new technology in the areas of both velocity-map imaging of gas phase samples and spatial map imaging of surfaces.

[1] M.H. Kim, B.D. Leskiw, L. Shen, and A.G. Suits, Int. J. Mass Spectrom., **252**, 73 (2006).
[2] M.H. Kim, B. D. Leskiw, and A. G. Suits, J. Phys. Chem., **109(35)**, 7839 (2005).
[3] M. H. Kim, B. D. Leskiw, L. Shen, and A. G. Suits, J. Phys. Chem. A, **111(31)**, 7473 (2007).
[4] S.T. Tsai, C K. Lin, Y.T. Lee, and C.K. Ni, Rev. Sci. Instrum., **72**, 1963 (2001).
[5] See for example: C. K. Ni and Y. T. Lee, Int. Rev. Phys. Chem., **23(2)**, 187 (2004) and references therein.

Molecular dynamics study of the photodesorption of CO ice

Junko Takahashi
Leiden Observatory, University of Leiden, NL 2300 RA Leiden
and
Marc C. van Hemert
Leiden Institute of Chemistry, University of Leiden, NL 2300 RA Leiden

We have used a molecular dynamics simulation to analyze the photodesorption process of CO ice in interstellar space. At the densities and temperatures found in star-forming regions all molecules other than H_2 should stick on dust grains on timescales shorter than the cloud lifetimes. Yet gaseous CO is detected in these clouds. Thermal desorption is negligible and thus photodesorption has been suggested as a possible mechanism for formation of CO in the gasphase.[1]
We have constructed a force field by performing *ab initio* coupled cluster calculations for the CO dimer on a large grid of orientations and intermolecular distances. We also have taken into consideration the intramolecular distance of the CO molecules. In order to be able to use the computed potential energy surface, consisting of some 15000 data points, various forms of fits have been tested. All fits were combinations of Lennard-Jones parameters with site point charges. It will be shown that the intramolecular distance dependence of the interaction can be well represented by the intramolecular distance dependence of the point charges only.
For the dynamics calculations it is supposed that the photon energy is converted into ground state vibrational energy of a single, selected, CO molecule and that this conversion takes place on a time scale shorter than the molecular dynamics time step. We follow the evolution of the energy in a CO cluster consisting of a few hundred molecules. We repeat the dynamics for a number of excitation energies and selected molecules. We find that it takes quite some time before the initial vibrational energy is spread over the cluster and ultimately leads to desorption of a surface molecule.
In the poster we will show cuts of the interaction potential, both in the ab initio and in the fitted form. We will also show time traces of various observables of the molecular dynamics runs.

[1] K.I. Öberg, G.W. Fuchs, Z. Awad, H.J. Fraser, S. Schlemmer, E.F. van Dishoeck and H. Linnartz, The Astrophysical Journal, **662**:L23-26 (2007).

The role of the partner X in the enhanced UV-photochemistry of van der Waals clusters O_2-X (X=CH_3I, C_3H_6, C_5H_8, C_6H_{12}, Xe)

Konstantin V. Vidma, Dmitri A. Chestakov, David H. Parker

Institute for Molecules and Materials, Radboud University Nijmegen, Toernooiveld 1, 6525 ED Nijmegen, The Netherlands

Alexey V. Baklanov, Georgii A. Bogdanchikov

Institute of Chemical Kinetics and Combustion, Institutskaja Street 3, Novosibirsk 630090 Russia

and Novosibirsk State University, Pirogova St. 2, Novosibirsk 630090, Russia

Introduction

Small van der Waals clusters are the systems of intermediate level of complexity between the individual molecules and the condensed medium. Investigation and understanding of the mechanism of photochemical processes in such clusters is crucial for understanding of photochemical properties of molecules in the presence of environment and photochemical properties of condensed media.

In the present study the UV photodissociation of van der Waals clusters O_2-X has been investigated (O_2 – is molecule of oxygen and X – is a molecule-partner). A number of different molecules such as CH_3I, C_3H_6, C_5H_8, C_6H_{12}, Xe were used as a molecule-partner.

UV-photoabsorption and UV-photochemistry of oxygen molecules are known to be very strongly dependent on the presence of the environment.

In the wavelength region of 200-300 nm the individual molecule of oxygen has a weak absorption band that is called Herzberg band. This band corresponds to the transitions to three excited states (Herzberg states of O_2). All those transitions are optically forbidden and therefore the absorption cross-section in this region is very small ($<2\cdot10^{-23}$ cm^2) [5].

But if molecule of oxygen have one or several partners nearby than the absorption in this region increases dramatically [6, 7]. This effect has been observed in many spectroscopic studies for O_2 molecules solved in liquid, frozen in solid matrix and for O_2 molecules during collisions with other molecules in the gas phase. For some sort of partners or environment the increasing in absorption cross-section per molecule of O_2 was observed to be of 6-7 orders of magnitude.

The phenomenon of enhanced UV absorption of oxygen plays important role in the chemistry of upper atmosphere, because it provides the enhanced production of highly reactive O atoms that drive many photochemical processes in the atmosphere including the process of ozone formation.

Despite of the great interest to the effect of enhanced UV absorption in O_2 the mechanism of this phenomenon has not yet been totally understood.

In the present study we used van der Waals clusters O_2-X as a model system for investigation of the detailed mechanism of the enhanced absorption and subsequent photochemical processes.

Experiment

Clusters O_2-X were prepared in the pulsed supersonic molecular beam. The number of different molecules X were used as partners of O_2 (X= CH_3I, C_3H_6, C_5H_8, C_6H_{12}, Xe). Clusters were excited by the laser pulse with tunable wavelength (222-277 nm). The products arising in the photodissociation were detected with using of velocity map imaging technique [8] that provides the information about speed and angular distribution of recoil of

nascent photofragments. Most attention has been paid to the channel of formation of O atoms in ground $^3P_2$ state. Those atoms were selectively ionized by the second laser pulse with the wavelength 225.656 nm, that corresponds to (2+1) resonantly enhanced multiphoton ionization (REMPI) of O($^3P_2$) atoms.

Results and discussion

For all clusters O_2-X the dramatic enhancement in the yield of O atoms in comparison with photodissociation of individual molecules of O_2 has been observed:

1. $O_2 + h\nu \rightarrow O + O$ very weak signal
2. $O_2\text{-}X + h\nu \rightarrow O + \ldots$ >330 times stronger signal

The enhanced signal of O atoms consisted of several different channels (FIG.1). Each channel corresponds to the specific speed and anisotropy of recoil of O atoms. All those channels are different from the channels arising in the photodissociation of individual molecules O_2 and much stronger as well. The energy, anisotropy and wavelength dependency of those enhanced channels gave the valuable information about the mechanism of the enhanced absorption and the mechanism of subsequent fragmentation of clusters.

Obtained results enable us to make a conclusion that the enhancement in the absorption in clusters O_2-X in comparison with individual O_2 occurs due to the influence of charge transfer state (CT state) of clusters O_2-X. This state is characterized by transfer of electron from partner X to molecule O_2. Enhanced absorption corresponds either to direct transitions to CT state, or to the transitions to the Herzberg states of oxygen, that become much more efficient due to the admixture of CT state.

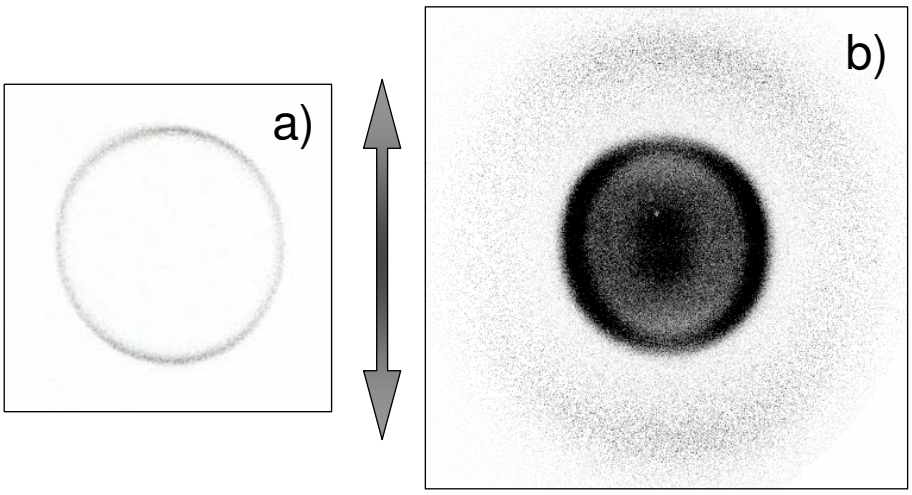

Fig. 1. These two velocity map images demonstrate the dramatic difference in the intensity, speed and angular distributions of oxygen atoms O($^3P_2$) arising in the photodissociation of individual molecules O_2 and clusters O_2-CH_3I. Excitation wavelength 225.656 nm. The arrow between the images indicate the direction of polarization of excitation laser.

a) Image arising as a result of photoexcitation of individual molecules O_2.
b) Image arising as a result of photoexcitation of clusters O_2-CH_3I.

Properties of observed channels of formation of O atoms enabled the possibility to identify several new photochemical pathways following the enhanced absorption. Those pathways give rise particularly to the formation of such interesting products as superoxide anion O_2^-, and different forms of singlet molecular oxygen $O_2(a\ ^1\Delta_g)$ and $O_2(b\ ^1\Sigma^+_g)$.

Acknowledgement

The financial support of this work by the Netherlands Organization for Scientific Research (NWO), Russian Foundation for Basic Research (Grant N 06-03-32542) and Siberian Branch of RAS (Interdisciplinary grant № 62) is gratefully acknowledged.

Reference

1. A.V. Baklanov, G.A. Bogdanchikov, K.V. Vidma, D.A. Chestakov, D.H. Parker, *J. Chem. Phys.* **126**, 124316 (2007).
2. G. DeBoer and M. A. Young, *J. Chem. Phys.* **106**, 5468 (1997).
3. G. DeBoer, A. P. Prince, and M. A. Young, *J. Chem. Phys.* **115**, 3112 (2001).
4. B. F. Parsons and D. W. Chandler, *J. Phys. Chem. A* **107**, 10544 (2003).
5. D. H. Parker, *Acc. Chem. Res.* **33**, 563 (2000).
6. A. J. Blake and D. G. McCoy, *J. Quant. Spectrosc. Radiat. Transf.* **38**, 113 (1987).
7. S. Koda and K. Sugimoto, *J. Photochem. Photobiol. C* **4**, 215 (2003).
8. A.T.J.B. Eppink and D.H. Parker, Rev. Sci. Instrum. **68**, 3477 (1997).

H_2 (v = 1) Scattering on Metal-Film Schottky Surface: Is the Born-Oppenheimer approximation valid?

Bruce Yoder and Rainer D. Beck
Laboratoire de Chimie Physique Moléculaire,
Ecole Polytechnique Fédérale de Lausanne,
Lausanne, Switzerland

Hermann Nienhaus
Universität *Duisburg-Essen,*
Duisburg, Germany

More than 90 percent of the chemical industry's production processes employ catalysis. The production of industrial catalysts constitutes a $10+ billion industry.[1] It is, therefore, of great interest to understand the chemical processes that take place at the catalyst-reactant interface. In the Laboratoire de Chimie Physique Moleculaire (LCPM-EPFL), we have the necessary tools to address fundamental surface science questions experimentally.[2, 3] The detailed, state resolved data from our experiments enables stringent test of theoretical models. With evolving models of catalytic systems, we gain a better understanding of the chemistry taking place during catalysis. In favorable cases, theoretically modeled catalytic systems have been able to predict improvements to existing catalysts used in industrial process.[4, 5]

To date, the Born-Oppenheimer approximation is used in most theoretical approaches to model surface reactions, but may be an unreasonable assumption. In the experiments proposed here, we intend to study the validity of the Born-Oppenheimer approximation being applied to chemical processes occurring at metal surfaces.[6] Specifically, we will use a beam of vibrationally excited molecular hydrogen impinging on an ultrathin palladium film deposited onto a semiconductor to detect electrical current generation upon the deexcitation of state-selected hydrogen on a palladium surface. If electronic excitations in the metal occur during the interaction, electrons could travel ballistically through the metal film and cross the Schottky barrier (if they possess enough energy) to be detected as electrical current.

Recently, Luntz and coworkers have shown good qualitative agreement between vibrational deexcitation of H_2 (D_2)/Cu scattering experiments and reduced dimensionality quasiclassical nonadiabatic calculations.[7] This work predicts the feasibility of our plan to experimentally detect nonadiabatic effects.

Two laser schemes will be employed in this experiment. Vibrational excitation will be performed by stimulated Raman pumping which will excite H_2 molecules in the molecular beam to the v=1 state. The fraction of vibrationally excited H_2 in the beam will be probed by resonance enhanced multiphoton ionization (2+1 REMPI). For our experiments, we have chosen to use H_2 (v=0, *J*=1) or *ortho*-hydrogen as a starting point because *J*=1 is the rotational level with the highest population in the cold molecular beam due to nuclear spin statistics of hydrogen.

This research project is be a collaborative effort with Professor Hermann Nienhaus from Gerhard-Mercator-Universität Duisburg in Germany. We intend to use Schottky diode surfaces that has been developed in his laboratory to detect electrical current produced upon the deexcitation of hot hydrogen on palladium.[8,9,10] If we are able to detect electrical current while impinging vibrationally excited hydrogen on the metal film, it would demonstrate the existence of electronic excitations in the metal, see Figure 1.

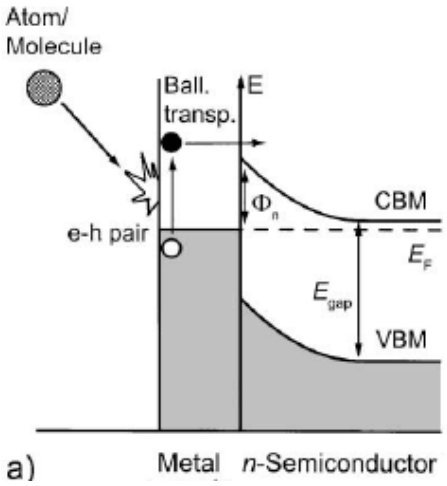

Figure 1: Detection schematic of "hot electrons" with thin metal film-semiconductor diodes. An e-h pair is created upon chemical reaction, and excited electron can travel ballistically through the metal film, traverse the Schottky barrier (if it possesses energy in excess to the barrier) and be detected as electrical current.[10]

In regards to the breakdown of the Born-Oppenheimer approximation, some experimental work has been conducted.[11] There exists indirect evidence that chemical dynamics and reaction rates at a metal surface may be influenced by electronically

nonadiabatic couplings of the metal to an impinging gas molecule.[12,13] It is reasonable to believe that some systems will be electronically adiabatic, while others will not.

Based on the calculations of Luntz *et al*., we may expect a detectable current generated from the deexcitation of vibrationally "hot" hydrogen impinging on a palladium surface. If in fact we do observe such a current for this system, it would constitute the first direct evidence for electronically nonadiabatic energy dissipation for H_2, as well as, provide detailed experimental data for comparison to the highest-level theoretical calculations available. This information will be useful in the construction of more accurate theoretical models of gas-surface interactions.

References:

1. NIST, Advanced Technology Program: Catalysis and Biocatalysis Technologies. In 2005.
2. R. D. Beck, P. M., D. C. Papageorgopoulos, T. T. Dang, M. P. Schmid, T. R. Rizzo, *Science* **2003,** 302, (5642), 98-100.
3. P. Maroni, D. C. P., M. Sacchi, T. T. Dang, R. D. Beck, T. R. Rizzo, *Phys.Rev.Lett.* **2005,** 94, (24), 246104.
4. J. R. Kitchin, J. K. N., M. A. Barteau, J. G. Chen, *Phys. Rev. Lett.* **2004,** 93(15), 156801.
5. J. Greeley, J. K. N., *Surf. Science* **2005,** 592, (1-3), 104-111.
6. M. Born, E. O., Born Oppenheimer approximation. *Ann. Physik* **1927,** 84, 457.
7. A. C. Luntz, M. P., G. O. Sitz, *J. Chem. Phys.* **2006,** 124, (9), 091101.
8. Nienhaus, H., *Surf. Sci. Rep.* **2002,** 45, 1-78.
9. H. Nienhaus, S. J. W., B. Gergen, E. W. McFarland, *Sensors and Actuators B-Chemical* **2002,** 87, (421-424).
10. B. R. Cuenya, H. N., E. W. McFarland, *Phys. Rev. B* **2004,** 70, (11), 115322.
11. A. M. Wodtke, J. C. T., D. J. Auerbach, *Inter. Rev. Phys. Chem.* **2004,** 23, (4), 513-539.
12. A. M. Wodtke, Y. H. H., D. J. Auerbach, *Chem. Phys. Lett.* **2005,** 414, (1-3), 138-142.
13. J. D. White, J. C., D. Matsiev, D. J. Auerbach, A. M. Wodtke, *J. Chem. Phys.* **2006,** 124(6), 064702.

Index